

Mineral Ores as Disposable Catalysts in Coal Liquefaction

V. K. Mathur* & V. Venkataramanan

Department of Chemical Engineering
University of New Hampshire
Durham, New Hampshire 03824

INTRODUCTION

Coal constitutes the largest single fossil fuel resource in the U.S. Until the last few years, its use did not increase with increased fuel demands because of environmental restrictions and the ready availability of petroleum and natural gas. Now that the demand for liquid and gaseous fuels has surpassed the nation's capability to supply them without excessive imports, use of coal must increase both in power plants and as a means of producing petroleum and natural gas.

Reduced American reliance upon imported energy supplies hinges on the use of more domestic coal, through direct burning in the short-term, and through gasification and liquefaction in the long term. Although it is not yet economically feasible to convert coal into synthetic gasoline, jet fuel or diesel fuel oil, the technical feasibility of such a process has been proved. A number of liquefaction systems have been developed through the pilot plant stage, covering a wide range of alternative technologies.

However, there are a number of problems associated with the production of liquid fuels from coal -- loss of expensive catalyst, high pressure equipment, and environmental pollution -- that remain unsolved. But the basic problem is economic, mainly due to the high cost of hydrogen, high pressure equipment, and catalysts. Hydrocarbons, including natural gas, LPG, naphtha, etc., are the principal process raw materials for the manufacture of hydrogen these days. The high cost of these raw materials for the manufacture of hydrogen is one of the reasons for the synthetic liquid fuel from coal to be more expensive than natural crude oil (1). However, production of hydrogen from coal which is a proven technology will make the coal liquefaction more attractive. Secondly, by using highly active catalysts, hydrogenation pressure has been cut down to 2000 - 3000 psig (13,790-20,685 kPa) which would considerably reduce the cost of commercial reactors.

The greatest problem in the direct hydrogenation yet to be solved is the use of commercial catalysts which are expensive, with short life and cannot be recovered or regenerated. The answer to this problem is to find a low cost disposable catalyst(s). Our work and that of others have well established that cobalt and molybdenum are good catalysts for hydrogenation and hydrodesulfurization of coal, whereas nickel and molybdenum are effective for coal hydrodenitrogenation. The most inexpensive source of these metals is their ores where they are present mostly as sulfides or oxides. Use of these ores in coal liquefaction as disposable catalysts must be explored.

The object of this study was to investigate the hydrogenation of coal-SRC-11 oil slurry using disposable ore catalysts (DOC) at the SRC-11 process operating conditions with special reference to maximizing liquefaction and minimizing viscosity of the product oil. All experiments were conducted at 425°C and 2000 psig (13,790 kPa) hydrogen pressure for a period of half an hour.

*Correspondence concerning this paper should be addressed to this author.

LITERATURE REVIEW

There is considerable published work on the various aspects of coal liquefaction. One of the authors of this paper has presented detailed literature reviews for coal hydrogenation and hydrodesulfurization in his papers (2,3).

Hydrodenitrogenation (HDN) is of interest and importance for the synthetic fuels industry for minimizing NO_x formation during the combustion of coal-derived oil. This oil contains unacceptably high levels of nitrogen. So far, nitrogen removal has not received nearly as much attention as has desulfurization because sulfur, a severe catalyst poison and a serious atmospheric pollutant, has historically been the primary concern in processing petroleum feedstocks. Research work on hydrodenitrogenation using hydrogen or syngas is limited (4,5,6,7,8,9).

Rationale for the Use of Ores as Catalysts: Coal liquefaction takes place through metal -- catalyzed reactions. It is also reported that metallic catalysts in general are not expected to survive as metals in a coal liquefaction environment at sulfur levels exceeding 1%. It has been shown that all metals can form bulk sulfides under these conditions, and therefore the true catalyst would be a mixed sulfide and not a bimetallic system (9). In the presence of hydrogen at 380-440°C and pressures between 2000-3000 psig, (13,790-20,685 kPa), the metallic oxides are expected to be reduced to metals or get converted to sulfides or oxysulfides. Further, it has been well demonstrated (10,11) that mineral matter, particularly pyrite, in coal acts as a catalyst during hydrogenation. Inclusion of these ores individually or as mixtures of various ores, providing Co, Mo, and Ni, etc. should catalyze hydrogenation, hydrodesulfurization, and hydrodenitrogenation of coal.

Some of these metals are present in their ores in low concentration and may have to be beneficiated to increase their content by removing the inert material. Concentrate containing cobalt four to eight times higher than that of the ore can be obtained by flotation technique alone (12,13). Other ore dressing techniques can also be used. Since the equipment and operation of ore dressing are relatively inexpensive, the cost of the upgraded ore will still be comparatively low.

Lastly, it may be possible to recover these metals from the waste unconverted coal-ash-DOC mixture or ash-DOC mixture (rejects from SRC-II gasifier) by conventional metallurgical processes making the use of these ores as catalysts all the more attractive.

OCCURRENCE OF MINERAL ORES

Our research work (2,3,14,15) as well as a literature review reveal that cobalt and molybdenum are eminently suited catalysts for hydrogenation and hydrodesulfurization of coal, whereas nickel and molybdenum are good for hydrodenitrogenation. Other metals like iron, copper, tin, zinc, platinum, and tungsten have also been found to be effective in coal liquefaction (16). Further, it has also been demonstrated that the mineral matter in coal acts as a catalyst in coal liquefaction (4). The most inexpensive source of these metals is their ores where they are present mostly as sulfides or oxides.

Cobalt is usually recovered as a by-product in the mining of copper, nickel, and silver ores, and in some localities as a by-product of iron, chromium, lead, zinc, uranium, or manganese. The copper ores of Zaire and Zambia, Africa contain as high as three to four percent of cobalt. The ores of Sudbury district of Ontario, Canada have a cobalt content of 0.07%. The small nodules on the ocean floor contain 1.6% nickel and 0.21% of cobalt along with manganese, copper, and other metals. The presence of arsenic in some of the ores of cobalt should not be considered as a drawback since it is reported that arsenic assists coal liquefaction (16).

About 66% of molybdenum is produced mainly from the ore molybdenite (MoS_2). The remainder is obtained as a by-product of copper from copper minerals by selective flotation, and from tungsten and uranium ores.

Nickel occurs as nickel-copper sulfides, nickel silicates, or laterites. Pentlandite, $(\text{NiFe})_9\text{S}_8$ occurs in association with chalcopyrites (CuFeS_2). It is also available as a by-product in copper production.

MATERIAL, APPARATUS AND EXPERIMENTAL PROCEDURE

The major materials used in this study consisted of bituminous coal, SRC distillate and disposable ore catalysts. The hydrogenation reaction was carried out in an internally stirred autoclave. Hydrogen gas at high pressure was supplied to the autoclave by a compressor.

Bituminous coal from Blacksville mine, Pittsburgh Bed was used in this study. Proximate and ultimate analyses of the coal are presented in Table I. The vehicle oil used was SRC-II heavy distillate.

The hydrogenating catalyst ores were obtained from mining companies. The details of these ores are presented in Table II. The operating variables are shown in Table III.

Table III
Operating Variables for Coal Liquefaction Using
Disposable Catalysts

| | |
|------------------|--|
| Coal | Blacksville Mine #2 Pittsburgh Bed #8 |
| Solvent | SRC-II (232 - 454°C) |
| Gas | Hydrogen |
| Temperature | 425°C |
| Pressure | ~ 2000 psig (13,790 kPa) |
| Time of Reaction | 30 minutes |

Apparatus

The hydrogenation reaction was carried out in a stainless steel liner placed in a high pressure internally stirred autoclave of one liter capacity. The experiments were carried out at the stirrer speed of 1500 rpm. The autoclave was provided with a cooling coil through which water could be passed to reduce the reaction temperature if so desired. The autoclave had an electric furnace around the vessel to heat it. The temperature was controlled by a proportional temperature controller. The temperature of the reaction mass was continuously monitored by a temperature recorder. In addition, the autoclave was provided with a thermowell, a pressure gauge, a vent, a sampling valve and a safety rupture disc. A compressor was used to pressurize the autoclave.

TABLE I

Proximate and Ultimate Analyses of Coal Sample

Proximate Analysis

| | As Recd. | Moist. Free | Moist., Ash Free |
|--------------|----------|-------------|------------------|
| | % | % | % |
| Moisture | 1.2 | N/A | N/A |
| Volatile | 35.8 | 36.2 | 41.0 |
| Fixed Carbon | 51.5 | 52.1 | 59.0 |
| Ash | 11.5 | 11.7 | N/A |

Ultimate Analysis

| | As Recd. | Moist. Free | Moist., Ash Free |
|----------|----------|-------------|------------------|
| | % | % | % |
| Hydrogen | 5.0 | 4.9 | 5.5 |
| Carbon | 72.0 | 72.9 | 82.5 |
| Nitrogen | 1.0 | 1.2 | 1.4 |
| Sulfur | 2.7 | 2.7 | 3.1 |
| Oxygen | 7.7 | 6.7 | 7.6 |
| Ash | 11.5 | 11.7 | N/A |
| Btu/lbm | 12,892 | 13,052 | 14,776 |

TABLE II
Analyses of Catalysts Used
(Major Constituents)

| | | % |
|---|------------------|------|
| Limonite | Si | 16.4 |
| | Fe | 20.2 |
| | Cr | 0.5 |
| | Ni | 2.2 |
| | Mg | 9.8 |
| Falconbridge nickel ore lumps (FNOL) | Al | 1.4 |
| | Al | 2.0 |
| | Ca | 2.7 |
| | Cu | 1.0 |
| | Fe | 39.6 |
| Molybdenum Oxide concentrate | Mg | 0.9 |
| | Ni | 3.2 |
| | S | 15.3 |
| | Si | 5.9 |
| | Mo | 55.9 |
| Molybdenum sulfide concentrate | Al | 0.5 |
| | Ca | 0.5 |
| | Cu | 0.5 |
| | Fe | 3.6 |
| | Mg | 0.6 |
| Iron pyrites | Si | 3.2 |
| | Mo | 49.8 |
| | Si | 2.6 |
| | S | 23.5 |
| | Fe | 0.7 |
| Rare earth | Ca | 0.6 |
| | FeS ₂ | 80.0 |
| | Al | 5.2 |
| | Ca | 1.9 |
| | Fe | 2.5 |
| Harshaw Co-Mo (0402T) | K | 3.9 |
| | Si | 27.0 |
| | Mg | 0.8 |
| | S | 0.6 |
| | Si | 2.1 |
| Bastnasite | Co | 1.9 |
| | Mo | 8.6 |
| | Al | 37.4 |
| | Cr | 7.6 |
| | Al | 0.8 |
| | Fe | 2.4 |
| | K | 0.6 |
| | Mg | 1.7 |
| | Mo | 0.5 |
| | S | 0.5 |
| | Si | 5.3 |

Experimental Procedure

Each of the experimental runs consisted of two cycles. In the first cycle, SRC-II oil was used as the vehicle oil while in the second cycle, the product oil from the first cycle was used instead. This procedure was followed so that the experimentation was done under similar conditions as would exist in a commercial-scale operation, where a part of the coal-derived oil would be recycled as the vehicle oil. The results of this study, thus, would be more useful in the commercialization of this technology. Since the percent of coal-derived oil was higher in the product oil obtained in the second cycle than in the first, the effect of the catalyst would be better reflected in the second rather than in the first cycle of liquefaction.

First Cycle Liquefaction: Coal as received was crushed and pulverized in a micromil to pass through 200 mesh screen. Forty grams of this crushed coal was taken in the liner. About 83.6 gms of SRC-II oil (in approximately 1:2.1 ratio) was then added to the liner. Pre-determined amount of the catalyst or an ore, of -200 mesh size, was next added to the contents of the liner. The stirrer assembly was fitted onto the autoclave and securely bolted. After making sure that there was no leakage, the autoclave was purged with hydrogen three or four times to drive out any air and keep the contents of the liner in a total hydrogen atmosphere. The autoclave was then pressured to a pre-determined value depending upon the room temperature, so that a pressure of about 2000 psig (13.79 MPa) was reached at 797°F (425°C) reaction temperature. The heating was initiated thereafter. Throughout this study, the experimental parameters were set at the SRC-II pilot plant operating conditions as presented in Table III. It usually took 65-70 minutes to heat the autoclave and its contents from room temperature to 797°F (425°C). The reaction was then allowed to proceed for 30 minutes. The temperature was maintained at 797°F (425°C) during this period by controlling the furnace temperature. After 30 minutes, the reaction was arrested by turning off the power to the furnace and cooling the contents down rapidly by passing cold water through the cooling coil. The autoclave was allowed to cool down to the room temperature by leaving it overnight. The liquefied products were then taken out of the autoclave and hot filtered (17) to remove unconverted coal, ash and catalyst. The filtered oil and residue were weighted and percent conversion and liquefaction calculated. Viscosity of the product oil was determined using a Brookfield Viscometer.

Second Cycle Liquefaction: The same procedure was repeated using product oil from the first cycle as the vehicle oil in place of SRC-II oil.

DISCUSSION OF RESULTS

The main objective of this investigation was to study the effects of ores and ore concentrates containing primarily cobalt, molybdenum, and nickel, as disposable catalysts in coal liquefaction. Experiments were also conducted using a commercial catalyst (Harshaw Chemicals, 0402T) and no catalyst at all to compare the results. Since iron pyrite has been reported to be a good disposable catalyst, experiments were also conducted using pyrite individually as well as in admixture with a nickel ore. The chemical analyses of the mineral ores, concentrates, and commercial catalyst are presented in Table II. The percent conversion, percent oil yield, and viscosity, of the product oils are presented in Table IV.

Percent conversion and liquefaction of coal are defined as follows:

$$\text{Percent Conversion} = \frac{(\text{Original Cost (macf)} - \text{Toluene Insolubles (macf)}) \times 100}{\text{Original Coal (macf)}}$$

TABLE IV
Effect of Catalyst on Liquefaction of Coal

| SN | Cycle | Catalyst used | Catalyst based on Coal(maf) | Coal Vehicle Oil | Conversion % | Liquefaction % | Product Oil Viscosity, cp at 60°C | Conversion minus Liquefaction % |
|----|-------|---------------|-----------------------------|------------------|--------------|----------------|-----------------------------------|---------------------------------|
| | | | | | | | | |
| 1 | I | ----- | ----- | 2.10 | 83.96 | 70.73 | 20.8 | 13.23 |
| 2 | II | ----- | ----- | 2.10 | 60.20 | 43.24 | 81.0 | 16.96 |
| 3 | I | Co-Mo | 2.49 | 2.09 | 84.45 | 74.17 | 17.9 | 10.28 |
| 4 | II | Co-Mo | 2.55 | 2.09 | 80.50 | 68.16 | 57.4 | 12.34 |
| 5 | I | Co-Mo | 5.04 | 2.10 | 80.13 | 69.30 | 15.6 | 10.83 |
| 6 | II | Co-Mo | 5.05 | 2.09 | 76.13 | 63.57 | 47.0 | 12.56 |
| 7 | I | MoO Conc. | 2.48 | 2.09 | 82.72 | 75.60 | 23.4 | 7.12 |
| 8 | II | MoO Conc. | 2.59 | 2.09 | 76.82 | 63.00 | 55.2 | 13.82 |
| 9 | I | MoS Conc. | 2.51 | 2.09 | 83.61 | 73.31 | 23.9 | 10.30 |
| 10 | II | MoS Conc. | 2.51 | 2.10 | 70.15 | 59.57 | 62.6 | 10.58 |
| 11 | I | Limonite | 2.49 | 2.13 | 83.02 | 73.31 | 21.6 | 9.71 |
| 12 | II | Limonite | 2.50 | 2.09 | 70.43 | 58.71 | 66.0 | 11.72 |
| 13 | I | Rare Earth | 2.51 | 2.09 | 87.33 | 75.60 | 20.3 | 11.73 |
| 14 | II | Rare Earth | 2.52 | 2.10 | 70.16 | 56.42 | 74.2 | 13.74 |
| 15 | I | Bastnesite | 2.52 | 2.19 | 83.33 | 71.31 | 19.3 | 12.02 |
| 16 | II | Bastnesite | 2.51 | 2.10 | 75.30 | 57.85 | 75.0 | 17.45 |
| 17 | I | FNOL | 2.52 | 2.09 | 88.76 | 73.02 | 22.4 | 15.74 |
| 18 | II | FNOL | 2.52 | 2.10 | 73.02 | 54.12 | 74.2 | 18.90 |
| 19 | I | Iron Pyrite | 2.52 | 2.14 | 83.37 | 71.59 | 18.4 | 12.32 |
| 20 | II | Iron Pyrite | 2.53 | 2.10 | 71.61 | 59.28 | 60.4 | 12.90 |
| 21 | I | Iron Pyrite | 2.51 | 2.30 | 85.58 | 72.45 | 19.7 | 13.66 |
| 22 | II | Iron Pyrite | 2.58 | 2.33 | 80.19 | 68.19 | 54.8 | 12.50 |

Percent Liquefaction = Oil Products x 100/Original Coal (macf)
where macf = moisture, ash, catalyst free.

Effect of Mineral Ores

Liquefaction of coal was conducted using molybdenum sulfide concentrate, molybdenum oxide concentrate, Falconbridge nickel ore lumps (FNOL), bastnasite, rare earth ore, limonite, and iron pyrite. Table IV lists the results of these experiments.

As can be seen, increasing the concentration of the commercial Co-Mo catalyst from 2.5% to 5.0% based on coal (maf), did not bring about any significant change in the percent conversion, liquefaction, or the product oil viscosity. Hence, experiments with all the mineral ores were conducted at 2.5% concentration.

The results of the first cycle liquefaction, namely, the percent conversion, liquefaction, and the product oil viscosity did not show any appreciable change with the catalysts used. As was discussed earlier, the product oil from the first cycle liquefaction contained only 15% coal-derived oil, and therefore, did not cause any appreciable change in the overall viscosity of the product oil.

On the contrary, since there was about 30% coal-derived oil in the second cycle product oil, the amount and viscosity of the former had a greater effect on the overall viscosity of the product oil. Therefore, the catalytic effect of these mineral ores were better reflected in the results of the second cycle liquefaction than in the first.

Referring to Table IV, it was also seen that the percent conversion and liquefaction and the viscosity of the product oil in the second cycle of liquefaction obtained using the mineral ores were much better than those obtained using no catalyst. The percent conversion using these mineral ores was in the range of 70-80% as against 60% without any catalyst. The percent liquefaction was in the range of 54-68% as compared to 43% obtained without any catalyst. The product oil viscosity also showed a marked improvement.

Molybdenum oxide concentrate, when used as a catalyst, gave 76.82% conversion and 63.00% liquefaction, which compares well with 80.50% conversion and 68.16% liquefaction obtained using 2.5% commercial Co-Mo catalyst. However, the viscosity of the product oil was 66.2 cp as compared to 57.4 cp obtained using the commercial Co-Mo catalyst. Therefore, the performance of molybdenum oxide concentrate as a catalyst in coal liquefaction was found to be only slightly lower than that of the commercial Co-Mo catalyst. The lower cost of molybdenum oxide concentrate as compared to the commercial Co-Mo catalyst, should more than compensate for its lower catalytic activity.

The 70.15% conversion and 59.57% liquefaction obtained using molybdenum sulfide concentrate as catalyst were lower than that obtained using molybdenum oxide concentrate. However the viscosity of the product oil was 60.3 cp as against 66.2 cp that molybdenum oxide concentrate yielded. The decrease in the percent liquefaction could have resulted in a decrease in the viscosity of the product oil.

Rare earth, bastnasite, limonite, and Falconbridge nickel ore lumps (FNOL) gave percent conversion and liquefaction ranging from 70-75% and 54-58%, respectively. The viscosity of the product oils obtained ranged from 66-75 cp, indicating that the quality of the product oil was inferior to that obtained using molybdenum oxide and molybdenum sulfide concentrates. The difference between the percent conversion and liquefaction (vide, Table IV) also showed that bastnasite and FNOL converted more of the coal to gas than the other mineral ores tested in this study.

Hence, it could be inferred that these mineral ores at 2.5% concentration exhibited less catalytic activity for coal liquefaction.

Iron Pyrite, a by-product of coal-mining operation gave 71.64% conversion and 59.28% liquefaction. Also, it yielded a product oil of viscosity 60.4 cp which was lower than that obtained using molybdenum oxide concentrate. This lower viscosity in the case of iron pyrite could be due to less coal-derived oil produced because of the lower percent liquefaction achieved. Also, the conversion and liquefaction obtained using iron pyrite were lower than the 80.50% conversion and 68.15% liquefaction achieved using the commercial Co-Mo catalyst. Iron pyrite yielded a product oil viscosity of 60.4 cp as compared to 57.4 cp obtained using the commercial Co-Mo catalyst.

Effect of Mixture of Mineral Ores on Liquefaction

Addition of limonite to the iron pyrite was found to considerably improve the liquefaction obtained using the pyrite alone. A 1:1 mixture of iron pyrite and limonite increased the percent conversion and liquefaction to 80.74% and 68.16%, respectively, as compared to 71.64% and 59.28% obtained using the pyrite alone. The viscosity of the product oil improved to 54.8 cp from 60.4 cp. Thus, a mixture of iron pyrite and limonite worked equally well, if not better, as the commercial Co-Mo catalyst in the coal liquefaction process.

CONCLUSIONS

The results of this study showed that ores containing metals such as cobalt, molybdenum, and nickel were catalytically active for the liquefaction of coal; the molybdenum oxide showed the best results. The reactivity of iron pyrite was found to increase when used in admixture with limonite. This increase in activity is specially noteworthy since iron pyrite is available in large amount, and at present is considered to be the best available disposable catalyst.

ACKNOWLEDGEMENT

The authors wish to express their appreciation to Falconbridge Nickel Mines, Ltd. Ontario, Canada, Climex Corporation, New York, and Moly Corp. Inc. Washington, Pa., and Harshaw Chemicals for providing ores and commercial catalyst. Our thanks are also due to Pittsburgh Energy Technology Center, Pittsburgh, Pa. for making SRC-II heavy distillate available to us.

REFERENCES

1. Katell, S., L.G. White, "Clean Fuels from Coal are Expensive," *Hydrocarbon Processing*, 8, 83, 1976.
2. O'Leary, M.J., D.C. Stetson, V.K. Mathur, "Catalytic Liquefaction of Coal," *Coal Processing Technology*, Vol. V., 1979.
3. Mathur, V.K., "Coal Power, Its Promises and Problems," A series of energy sources, their promises and problems, published by the Center for Industrial and Institutional Development, University of New Hampshire, Durham, NH, Feb. 1980.
4. Calderwood, W., "Catalytic Hydrodenitrogenation of Coal Using CO-Steam and Hydrogen," Internal Report, Department of Chemical Engineering, University of New Hampshire, 1979.

5. Thakkau, V.P., "Kinetics of the Hydrodenitrogenation of Nitrogen Compounds in a Coal-Derived Oil," Ph.D. Thesis, Colorado School of Mines, 1978.
6. Smith, W.M., T.C. Landron, G.E. Phillips, "Hydrogenation of Shale Oil," Ind. Eng. Chem., 44, 586, 1952.
7. Staubs, D.W., R.L. Miller, H.F. Silver, R.J. Hurtubise, "The Effect of Solvent Refined Coal Denitrification," Ind. Eng. Chem. Proc. Design and Dev., Vol. 18, 4,667,1979.
8. Satterfield, C.N., M. Modell, R.A. Hites, C.J. Declerck, "Intermediate Reaction in the Catalytic Hydrodenitrogenation of Quinoline," Ind. Eng. Chem. Proc. Design and Dev., 17, 141, 1978.
9. Cusumano, J.A., R.A. Dalla Betta, R.B. Levy, "Catalysis in Coal Conversion," Academic Press, 1978.
10. Jackson, D.M., B.K. Schmid, "Commercial Scale Development of the SRC-II Process," Presented at the Fifth Annual International Conference on Commercialization of Coal Gasification, Liquefaction and Conversion to Electricity, University of Pittsburgh, PA, Aug. 1978.
11. Ellington, R.T., Liquid Fuels from Coal, Academic Press, New York, p. 45, 1977.
12. Mineral Facts and Problems, Bureau of Mines Bulletin No. 667, U.S. Department of the Interior, 1976.
13. Brobst, D.A., W.P. Pratt (ed.), U.S. Mineral Resources Geological Survey Professional Paper 820, U.S. Department of Interior, 1973.
14. Stetson, D.C., "Catalytic Liquefaction of Coal Using Carbon Monoxide and Steam," M.S. Thesis, University of New Hampshire, 1977.
15. Guttal, V., "Catalytic Desulfurization of Coal Using CO and Steam," M.S. Thesis, University of New Hampshire, 1979.
16. Weller, S., M.G. Pelepetz, S. Frierman, H.H., Storch, "Coal, Hydrogenation Catalysts," Ind. Eng. Chem., Vol. 42,2,330, 1950.
17. Venkataramanan, V., "Liquefaction of Coal Using Disposable Catalysts," M.S. Thesis, University of New Hampshire, 1981.

EFFECT OF ORGANOMETALLIC CATALYSTS ON COAL LIQUEFACTION AND PRODUCT DISTRIBUTION

Ram K. Sharma and Gary Moffett

Department of Physical Sciences, Eastern New Mexico University,
Portales, New Mexico 88130

INTRODUCTION

Coal hydrogenation remains an attractive and potentially useful source of liquid fuels. There have been a number of studies on the comparative effectiveness of various catalysts and the results have been reviewed from time to time (1-5). A significant finding which has emerged from such studies is the importance of catalyst distribution. For example, in the hydrogenation of Rock Springs coal, nickelous chloride was found to be an ineffective catalyst when added as a powder, however, it was quite effective when it was impregnated on coal (6).

Because of their compatibility with the pasting oil which is used to slurry coal in hydrogenation studies, organometallic compounds would seem to be able to disperse better and therefore might be expected to be more effective catalysts.

Coal can be regarded as a highly cross linked "polymer" in which condensed aromatic rings are linked to one another through hydroaromatic or heteroatom linkages (7,8). On heating, weak bonds break leading to free radicals which can be stabilized by transfer of hydrogen to give soluble products or they may recombine to form insoluble chars (9). The hydrogen which is transferred to the radical could come from coal itself, donor solvent or molecular hydrogen. It is possible that some organometallics might be able to generate an intermediate under liquefaction conditions which might be an effective hydrogen transfer agent (10).

A few reports on the use of organometallics in coal liquefaction have been published. It appears that at temperatures less than 350°C such catalysts are ineffective (11). However, at higher temperatures some organometallics were found to aid coal liquefaction (12). Metal naphthenates of molybdenum, nickel, tin, iron and cobalt produced conversions exceeding 80 percent at 500°C, zero time at temperature (4).

In the present study we have assayed the catalytic activity of a variety of organometallic compounds in the liquefaction of two New Mexico coals. We have also examined their effect on the proportion of asphaltene and oil produced.

EXPERIMENTAL

Parr 4022 pressure reactor with 1 liter T316 stainless steel bomb, 2250 watt heater and 0-600°C automatic temperature controller was used in all hydrogenation experiments. In order to avoid catalyst memory effects, the reactants were placed in a glass vessel (liner) which fitted snugly inside the bomb.

A sub-bituminous coal from Navajo Mine (South Barber Seam 8) and a bituminous high volatile coal from York Canyon seam in Raton Formation were used in our studies. Ultimate analysis of the coals is given in Table 1.

Into the glass container 15g of -60 mesh coal, catalyst (1% of maf coal) and 45g tetrahydronaphthalene (THN) were placed. The container was put in the steel bomb and the bomb was pressurized with hydrogen to 1500 psi after flushing to remove air. It was then heated to the designated temperature and kept at that temperature for the selected reaction time. The reactants were kept mixed by the rocking motion of the pressure reactor. After the reaction, the bomb was cooled to room temperature and contents flushed with benzene and filtered. The filter-cake was extracted in a soxhlet extractor for 24 hours, dried and weighed to obtain the weight of unreacted coal and ash. After distilling off benzene from the filtrate and the soxhlet extract, pentane was added to precipitate asphaltene which was filtered and dried to a constant weight at 50°C at 3mm in a vacuum oven.

After distilling pentane from the filtrate through a vigreux column, as much of THN as possible was removed by distillation under vacuum (16mm) and an oil bath temperature of 120°C. A weighed amount of methyl naphthalene (MNI) was added to the residue which was thinned with chloroform and analyzed by gas liquid chromatography.

From the areas of the peaks of THN and MN the amount of THN present was calculated using a correction factor determined previously from a mixture of known amounts of THN and MN. Difference in the weight of the vacuum distillation residue and the amount of THN gave the amount of oil present.

The results were calculated as follows:

Percent Conversion = (maf coal - unreacted coal) X 100 / maf coal

Percent yield asphaltene = wt. of asphaltene X 100 / coal converted

Percent yield oil = wt. of oil X 100 / coal converted

Percent conversion asphaltene = wt. of asphaltene X 100 / maf coal originally present

Percent conversion oil = wt. of oil X 100 / maf coal originally present

RESULTS AND DISCUSSION

Effect of Catalysts on Coal Conversion: For the Navajo Mine coal (Table 2) organometallic compounds of palladium, rhenium, iridium, molybdenum, rhodium, iron, cobalt, tin and nickel were found to be effective catalysts. Organometallic compounds of germanium, tungsten, gallium, arsenic had moderate catalytic activity whereas the organometallic compounds of copper, lead, zinc and manganese had marginal or no catalytic activity.

For the York Canyon Mine coal (Table 3) organometallic compounds of iridium, rhodium, molybdenum and nickel showed good catalytic activity. Organometallic compounds of germanium, nickel, gallium and antimony were found to be moderately active whereas compounds of arsenic, copper, lead, manganese, chromium and zinc had no or marginal catalytic activity.

Of the other catalysts tested, stannous chloride was found to be an excellent catalyst in agreement with other reports in literature and was used as a standard of comparison. Ammonium molybdate on the other hand was found to have marginal catalytic activity.

Effect of Catalysts on Product Distribution: Hydroliquefaction of coal is the net result of a complex series of parallel or sequential reactions including hydrogenation, thermal fragmentation, disproportionation and stabilization of free radicals etc. It was thought that different catalysts would affect many of the above reactions to varying degrees and thus change the proportion of asphaltene, oil and gas produced.

In our experiments the product of liquefaction was partitioned into asphaltene and oil and the amount of each was determined by the procedures described in the experimental section. Percent of the product found as asphaltene and oil are shown in Table 4.

In uncatalyzed hydrogenation of York Canyon Mine coal the ratio of asphaltene to oil produced is 1.7 whereas for most of the active catalysts the ratio is 1.8-2.5. Thus many of the catalysts produce slightly more asphaltene than the uncatalyzed hydrogenation. Also the sum of asphaltene and oil yield is nearly 100 percent. This indicates that very little gaseous products are formed in hydrogenations at 380°C for 6 hours.

These results can be accommodated in the free radical mechanism of coal liquefaction. At high temperature coal substance fragments into free radicals which are stabilized by transfer of hydrogen to yield asphaltene, oil and gaseous products. In the absence of a catalyst some of these radicals may combine to produce insoluble char. In the presence of a catalyst, more of these radicals are stabilized by hydrogen transfer to produce soluble products.

Effect of Reaction Time and Temperature: York Canyon Mine coal was hydrogenated for various lengths of time in the absence and also in the presence of molybdenum hexacarbonyl as a catalyst. The results show (Fig. 1) that the amount of asphaltene increases, reaches a maximum and then decreases with time. The increase in asphaltene in the initial stages of the reaction and its decrease in the later stages is faster in the catalyzed than in the uncatalyzed hydrogenation. Thus a catalyst not only helps to liquefy coal, it also helps to convert asphaltene into oil.

Paralleling above results, the amount of oil produced (Fig. 1) also increases with time and the increase is faster in the presence of a catalyst than in its absence.

The effect of temperature on the product distribution in some catalyzed and

uncatalyzed hydrogenations is shown in Fig. 2. As noted before, more asphaltene is produced in the early stages of the reaction in the catalyzed than in the uncatalyzed process. In the later stages of the reaction asphaltene is converted faster into oil and gaseous products in the catalyzed than in the uncatalyzed reactions. Molybdenum hexacarbonyl appears to be a better catalyst in this respect than stannous chloride.

The sum of the percent of product found to be asphaltene and oil (Table 5) decreases with time and with increase in temperature. This indicates that asphaltene and oil are being converted into gaseous products at higher temperatures and longer reaction times. Comparison of the catalyzed with the uncatalyzed hydrogenations shows that more gaseous products are formed in the former than in the latter case, and again molybdenum hexacarbonyl is more effective in this respect than stannous chloride.

ACKNOWLEDGEMENT

We are grateful for the support of this work from the New Mexico Energy and Minerals Department and the New Mexico Energy Institute at The University of New Mexico.

REFERENCES

1. T.E. Warren, K.W. Bowles and R.E. Gilmore, *Ind. Eng. Chem., Anal. Ed.* 11, 415 (1939).
2. S. Weller, M.G. Pelipetz, S. Friedman and H.H. Storch, *Ind. Eng. Chem.*, 42, 330 (1950).
3. S. Weller, In "Catalysis"; Emmet, P.H., Ed.; Reinhold Publishing Corporation, New York, 1956; Vol. IV, Chapter 7.
4. C.O. Hawk and R.W. Hiteshue, *U.S. Bur. Mines. Bull.* 622 (1965).
5. W.R.K. Wu and H.H. Storch, *U.S. Bur. Mines. Bull.* 633 (1968).
6. S. Weller and M.G. Pelipetz, *Ind. Eng. Chem.*, 43, 1243 (1951).
7. P.H. Given, *Fuel*, 31, 147 (1960).
8. D.D. Whitehurst, T.O. Mitchell and M. Farcasiu, "Coal Liquefaction", Academic Press, New York, 1980, p. 20.
9. W.H. Wiser, G.R. Hill and N.J. Kertamus, *Ind. Eng. Chem., Process, Design and Development*, 6, 133 (1967).
10. S. Friedman, S. Metlin, A. Svedi, and I. Wender, *J. Org. Chem.*, 24, 1287 (1959).
11. N. Holy, T. Nalesnik and S. McClanahan, *Fuel*, 56, 47 (1977).
12. M.V. McCabe and M. Orchin, *Fuel*, 55, 266 (1976).

TABLE 1 Ultimate Analysis of Coals
Navajo Mine (South Barber Seam #) Coal

| | wt% |
|----------------|--------------|
| Moisture | 8.62 |
| Carbon | 57.00 |
| Hydrogen | 3.07 |
| Nitrogen | 1.17 |
| Sulfur | 0.74 |
| Ash | 15.77 |
| Oxygen (diff.) | <u>13.65</u> |
| | 100.00 |

York Canyon Mine Coal

| | wt% |
|----------------|-------------|
| Moisture | 1.57 |
| Carbon | 63.89 |
| Hydrogen | 4.42 |
| Nitrogen | 1.35 |
| Sulfur | 0.44 |
| Ash | 22.30 |
| Oxygen (diff.) | <u>6.05</u> |
| | 100.00 |

TABLE 2 Effectiveness of Catalysts in the Hydrogenation of Navajo Mine Coal
Hydrogen pressure initial (cold): 1500 psi; Catalyst: 1% maf coal;
Time: 6 hours; Solvent: Tetrahydronaphthalene; Temperature: 350°C.

| No. Catalyst | Percent Conversion |
|--------------------------------|--------------------|
| 1. None | 61 |
| 2. $(C_2H_5)_2Ni$ | 68 |
| 3. $Co(C_2H_5O)_2$ | 74 |
| 4. $CoCl_2 \cdot 6H_2O$ | 73 |
| 5. $Cu(C_2H_5O)_2$ | 67 |
| 6. $Fe(C_2H_5O)_2$ | 75 |
| 7. $FeCl_3 \cdot 6H_2O$ | 67 |
| 8. $Ga(C_2H_5O)_2$ | 69 |
| 9. $(C_2H_5)_2Fe$ | 69 |
| 10. $[Ir(CO)_2Cl]_x$ | 83 |
| 11. $Mn(C_2H_5O)_2$ | 63 |
| 12. $Mo(CO)_6$ | 79 |
| 13. $(Ni)_6O_{10} \cdot 2H_2O$ | 66 |
| 14. $Ni(C_2H_5O)_2$ | 73 |
| 15. $NiCl_2 \cdot 6H_2O$ | 67 |
| 16. $Pb(C_2H_5O)_2$ | 66 |
| 17. $(C_2H_5)_4Pb$ | 63 |
| 18. $Pd(C_2H_5O)_2$ | 84 |
| 19. $Re_2(CO)_{10}$ | 84 |
| 20. $Rh(C_2H_5O)_2$ | 82 |
| 21. $SnCl_2 \cdot 2H_2O$ | 75 |
| 22. $(C_2H_5)_2Sn$ | 73 |
| 23. $(C_2H_5)_3SnH$ | 67 |
| 24. $W(CO)_6$ | 68 |
| 25. $Zn(C_2H_5O)_2$ | 64 |
| 26. $ZnCl_2$ | 65 |

TABLE 3 Effectiveness of Catalysts in the Hydrogenation of York Canyon Mine Coal

Hydrogen pressure initial: 1500 psi; Catalyst: 1% maf coal; Solvent: Tetrahydrofuran; Temperature: 350°C; Time: 6 hours

| No. | Catalyst | Percent Conversion |
|-----|--|--------------------|
| 1. | None | 44 |
| 2. | $\text{SnCl}_2 \cdot 2\text{H}_2\text{O}$ | 72 |
| 3. | $(\text{C}_6\text{H}_5)_3\text{As}$ | 53 |
| 4. | $\text{Co}(\text{C}_5\text{H}_5)_2$ | 63 |
| 5. | $\text{Co}_2(\text{CO})_8$ | 74 |
| 6. | $\text{Cu}(\text{C}_6\text{H}_5)_2(\text{C}_6\text{H}_5)_2(\text{COO})_2$ | 53 |
| 7. | $\text{Cr}(\text{C}_6\text{H}_5)_2\text{O}_2$ | 47 |
| 8. | $\text{Cr}(\text{CO})_6$ | 48 |
| 9. | $\text{Fe}(\text{C}_5\text{H}_5)_2$ | 54 |
| 10. | $\text{Fe}(\text{C}_5\text{H}_5)_2 \cdot \text{I}_2 \cdot \text{I}_2(0.5\%)$ | 76 |
| 11. | $\text{Fe}(\text{CO})_5$ | 58 |
| 12. | $\text{Ga}(\text{C}_5\text{H}_5)_2$ | 61 |
| 13. | $\text{Ge}(\text{C}_6\text{H}_5)_4$ | 64 |
| 14. | $\text{I}_2(0.5\%)$ | 72 |
| 15. | $\text{In}(\text{C}_5\text{H}_5)_2$ | 59 |
| 16. | $\text{Ir}(\text{CO})_2\text{Cl}$ | 77 |
| 17. | $\text{Mn}(\text{C}_6\text{H}_5)(\text{C}_6\text{H}_5)_2(\text{COO})_2$ | 47 |
| 18. | $\text{Ni}_2\text{Nb}_2\text{O}_7 \cdot 2\text{H}_2\text{O}$ | 46 |
| 19. | $\text{Mo}(\text{CO})_6$ | 73 |
| 20. | $\text{Mo}(\text{CO})_6 \cdot \text{I}_2(0.5\%)$ | 80 |
| 21. | $\text{Ni}(\text{C}_5\text{H}_5)_2$ | 67 |
| 22. | $\text{Pd}(\text{C}_6\text{H}_5)_2(\text{COO})_2$ | 49 |
| 23. | $\text{Pd}(\text{C}_5\text{H}_5)_2$ | 72 |
| 24. | $\text{Re}_2(\text{CO})_{10}$ | 74 |
| 25. | $\text{Rh}(\text{C}_5\text{H}_5)_2$ | 75 |
| 26. | $\text{Ru}_3(\text{CO})_{12}$ | 46 |
| 27. | $\text{Sb}(\text{C}_6\text{H}_5)_3$ | 58 |
| 28. | $\text{Sn}(\text{C}_6\text{H}_5)_4$ | 74 |
| 29. | $\text{W}(\text{CO})_6$ | 43 |
| 30. | $\text{Zn}(\text{C}_6\text{H}_5)_2$ | 43 |

TABLE 4 Effect of Catalysts on the Percent Yield of Asphaltene and Oil from York Canyon Mine Coal.

| No. | Catalyst | %Conversion | %Yield Asph. | %Yield Oil | %Yield Asph-Oil | %Asph. Oil |
|-----|---|-------------|--------------|------------|-----------------|------------|
| 1. | None | 48 | 64 | 58 | 102 | 1.7 |
| 2. | $\text{Co}_2(\text{CO})_8$ | 74 | 69 | 29 | 98 | 2.4 |
| 3. | $\text{Cr}(\text{C}_6\text{H}_5)_2$ | 50 | 41 | 59* | --- | 0.7 |
| 4. | $\text{Fe}(\text{C}_5\text{H}_5)_2$ | 48 | 66 | 53 | 99 | 2.0 |
| 5. | $\text{Fe}(\text{C}_5\text{H}_5)_2 \cdot \text{I}_2(0.5\%)$ | 76 | 65 | 36 | 101 | 1.8 |
| 6. | $\text{Ga}(\text{C}_5\text{H}_5)_2$ | 61 | 70 | 36 | 106 | 1.9 |
| 7. | I_2 | 72 | 61 | 41 | 102 | 1.5 |
| 8. | $\text{In}(\text{C}_5\text{H}_5)_2$ | 59 | 31 | 68* | --- | 0.4 |
| 9. | $\text{Ir}(\text{CO})_2\text{Cl}$ | 77 | 65 | 34 | 99 | 1.9 |
| 10. | $\text{Mo}(\text{CO})_6$ | 75 | 68 | 32* | --- | 2.1 |
| 11. | $\text{Mo}(\text{CO})_6 \cdot \text{I}_2(0.5\%)$ | 80 | 71 | 32 | 103 | 2.2 |
| 12. | $\text{Ni}(\text{C}_5\text{H}_5)_2$ | 64 | 73 | 29 | 102 | 2.5 |
| 13. | $\text{Pd}(\text{C}_5\text{H}_5)_2$ | 73 | 61 | 36 | 97 | 1.7 |
| 14. | $\text{Re}_2(\text{CO})_{10}$ | 73 | 64 | 36 | 100 | 1.8 |
| 15. | $\text{Rh}(\text{C}_5\text{H}_5)_2$ | 75 | 46 | 54* | --- | 0.9 |
| 16. | $\text{Ru}_3(\text{CO})_{12}$ | 75 | 61 | 37 | 98 | 1.6 |
| 17. | $\text{SnCl}_2 \cdot 2\text{H}_2\text{O}$ | 73 | 72 | 30 | 102 | 2.4 |

* values of percent yield oil were obtained as follows:

$$100 - \% \text{ yield asphaltene} = \% \text{ yield oil}$$

TABLE 5 Effect of Time and Temperature on the Sum of the Percent Yield of Oil and Asphaltene in the Hydrogenation of York Canyon Mine Coal.

| Temp., °C | PERCENT YIELD (OIL + ASPHALTENE) | |
|------------|----------------------------------|--------------------------|
| | None | $\text{Mo}(\text{CO})_6$ |
| 350-400 hr | 580-600 | 580-600 |
| 350-400 hr | 580-600 | 580-600 |
| Time hr | | |
| 1 | - 100-110 | - 95-9* |
| 6 | 102-91-89 | 100-91-85 |
| 24 | 92-86-78 | 90-78-59 |

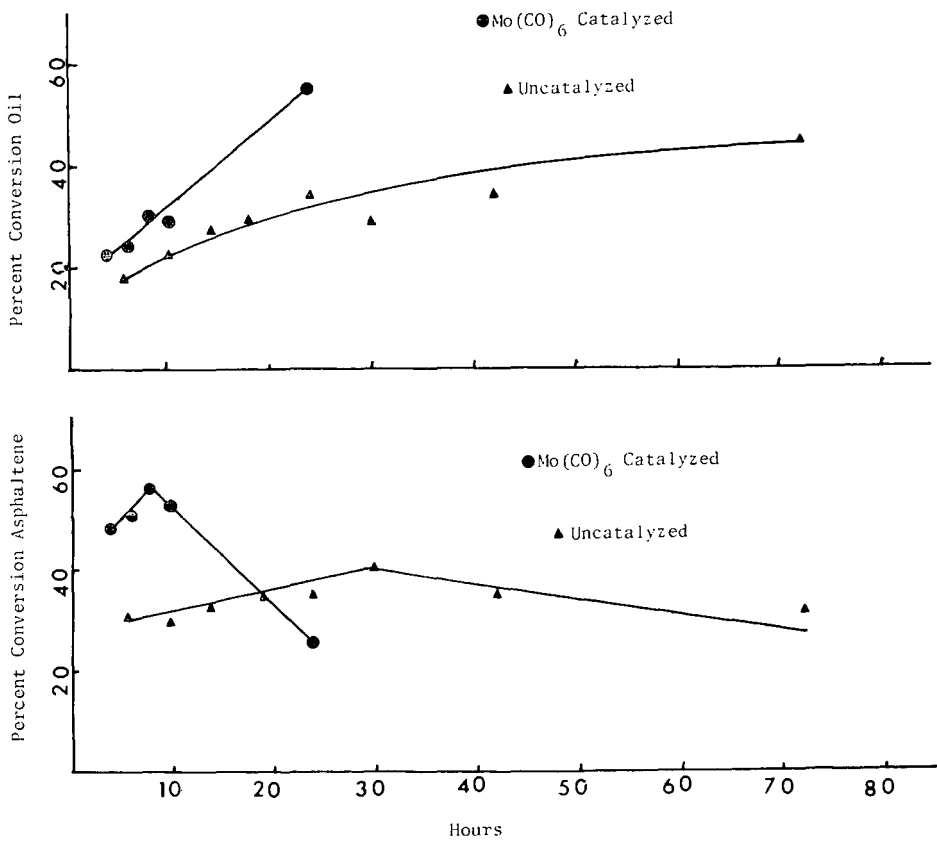


Fig. 1 Percent Conversion Asphaltene and Oil in the Hydrogenation of York Canyon Mine Coal.

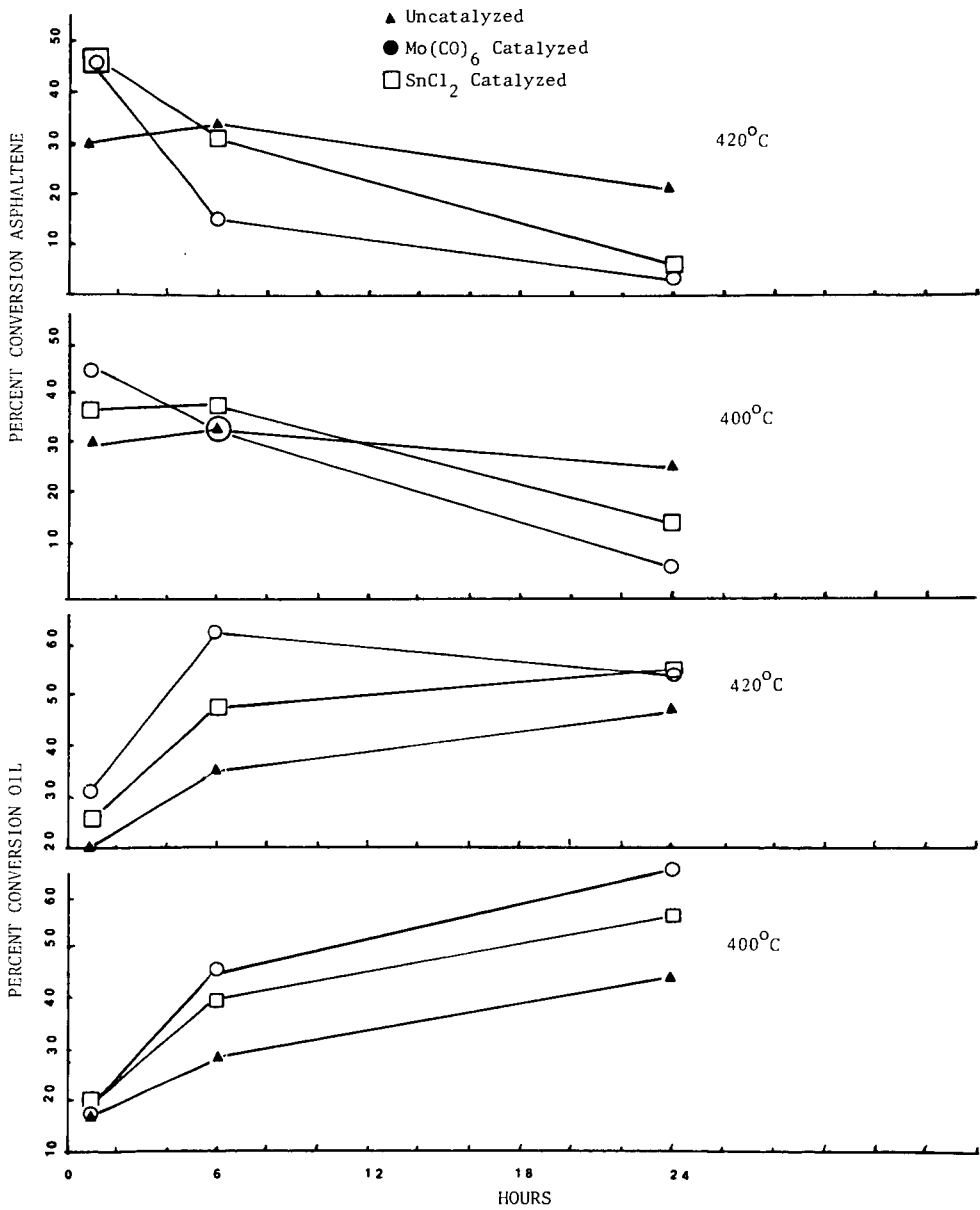


Fig. 2 Effect of Temperature and Reaction Time on the Percent Conversion Oil and Asphaltene.

SRC II PROCESSING OF WESTERN COALS WITH ADDED PYRITE

B. F. Alexander and R. P. Anderson

The Pittsburg & Midway Coal Mining Co.
P. O. Box 2970
Shawnee Mission, KS 66201

I. INTRODUCTION

A. History of the P&M Merriam Laboratory in Coal Liquefaction

The P&M Merriam Laboratory began a bench scale investigation of solvent refining of coal in 1962. Early work was to verify design concepts and operability for a one ton per day process development unit (PDU) in Kansas City which was built during 1963 and operated during much of 1964⁽¹⁾.

In 1967, bench scale studies resumed at Merriam, primarily to support the design effort for the 50 ton per day pilot plant at Ft. Lewis, Washington which operated from 1974 until 1981. Work has continued on a large variety of coal liquefaction problems since 1967 under sponsorship of the Office of Coal Research, Energy Research and Development Administration and the Department of Energy⁽²⁾.

B. Current Activities

The experiments described in this paper were conducted at the Merriam Laboratory during 1980 and 81. They were begun under DOE Contract 79ET14800 during a study on the relationship between coal properties and liquefaction behavior. Additional work was carried out during the current contract (81PC40005) to investigate SRC processing characteristics with disposable catalysts using alternate coals from different regions.

C. Previous Work

Earlier studies had shown subbituminous coals to be of low reactivity in SRC processes (3,4,5). The low reactivity of these coals was believed to be due primarily to a lack of iron to act as an in-situ catalyst. This was verified in the current work for a variety of coals from the Rocky Mountain and Great Plains Provinces where operation without added catalyst was not possible at normal SRC II conditions. Addition of moderate amounts of pyrite (4-5 wt % FeS₂, based on coal) resulted in trouble free operation, however, and attractive yields of high quality oils.

D. Factors Affecting the Results

The specific yields and product quality obtained in these experiments depended on the coal, source and level of pyrite added and on liquefaction conditions. Each of these factors will be discussed below.

II. EXPERIMENTAL

A. Bench Scale Unit

All of the experiments were conducted at Merriam using the bench scale unit depicted in Figure 1. This unit has been in operation since 1978 and allows for recycle of solid and liquid phases⁽⁶⁾. It has produced results which match closely those obtained in larger scale operations.

Coal was mixed with recycled solvent and recycled unfiltered coal solution and charged at 1800 or 2250 psig with a Hills-McCanna pump. Pure hydrogen was added at

the base of the preheater. The slurry passed through a 310 cm³ preheater, where the temperature was raised to 400°C, and 1 liter dissolver. The dissolver was housed in a 6-zone air furnace which allowed close temperature control and either an isothermal (at 450°C and 465°C) or simulated adiabatic (457°C average) profile. The dissolver effluent was separated into five streams by a system of four equilibrium flash vessels operated at reactor pressure as well as an atmospheric flash and distillation column.

B. Run Conditions

The conditions used in these runs are shown in Table I. This rather generous pressure of 2250 psig, used in all of the runs except one, was chosen initially to allow operation with a wide variety of coals. The runs with added pyrite were continued until steady state was achieved. The runs without added pyrite were conducted by lining out first with pyrite in the feed and then dropping pyrite out. Yields were determined at the point at which operation could no longer be sustained.

The coals used in this series of experiments are listed in Table II. Two were subbituminous, one high volatile C bituminous and two borderline between these two classifications. A low-iron Pittsburgh seam coal is included for comparison.

Four different pyrites were used with the properties shown in Table III. The Matheson, Coleman & Bell pyrites were mined in Georgia as a discrete mineral. They were ball milled and passed through a 140 mesh screen before use. The Robena pyrites were obtained from the coal cleaning operation of the U. S. Steel Robena Mine, Green County, Pennsylvania. They were finely ground by The Jet Pulverizer Company, Palmyra, New Jersey.

III. RESULTS

A. Effect of Coal Source

1. Sensitivity of Various Coals to Pyrite Addition

The primary difference in the SRC II processing of western coals with and without pyrite is that with pyrite they can be run, without pyrite they can not! Beyond that, there are dramatic changes in the yield patterns, as shown in Table IV. The changes shown are minimum values computed at the time when operation could no longer be sustained without additive. If the runs without additive could be lined out, the differences would be even greater.

With the western coals, total oil yield was 15 to 22 wt % (based on MAF coal) higher when pyrite was added and SRC yield from 9 to 12 wt % lower, with Belle Ayr Mine coal being the most responsive. For two of the coals, IOM yield decreased (total conversion increased) by 6 wt % and for Belle Ayr by 12 wt %. There were small variations in hydrocarbon gas yields, with two higher and two lower with additive. Hydrogen consumption increased by varied amounts.

The Blacksville No. 2 coal, a relatively low iron, low reactivity eastern bituminous coal, is included for comparison. The response in total oil, SRC and IOM yields to pyrite addition was about an order of magnitude less than with the western coals.

With Kaiparowits coal, a higher hydrogen level (8.6 vs 7.8 wt %) was achieved in the heavy distillate (>288°C) from the catalyzed run. With McKinley and Edna coals, however, the hydrogen levels actually decreased when catalyst was added, due to the large increase in conversion of material into the upper end of the heavy distillate boiling range. With all the western coals, the fusion point of the distillation residue was significantly lower with added pyrite and its solubilities in hexane and toluene considerably higher (lower preasphaltene content).

There were essentially no differences in elemental analyses for any of the products from the Blacksville No. 2 coal runs made with or without added pyrite.

2. Comparison of Coals with Added Pyrite

The yields and hydrogen consumptions resulting from the SRC II processing of five different coals at 450°C average dissolver temperature, 2250 psig and 1.0 hour residence time with added pyrite are compared in Table V.

The western coals yielded 49-57 wt % total oil (MAF coal basis) compared to approximately 44 wt % with Powhatan coals (at 457°C and 1800 psig) which are more typical of those used in development of the SRC II process. Kaiparowits and Edna Mine coals were at the high end of the range while Belle Ayr and McKinley were at the lower end.

SRC yields also varied widely, from 18-27 wt %, IOM yields from 2.8-4.6 wt %, hydrocarbon gas yields from 12-15 wt % and hydrogen consumption from 4 1/2 to 6 1/2 wt %. This compares to about 28 wt % SRC and 6 wt % IOM (MAF basis) in a conventional SRC II process with Powhatan coal. It is interesting to note that the hydrocarbon gas and hydrogen consumptions are quite low relative to oil yield compared to those for Powhatan coals. These typically yield 16 wt % hydrocarbon gas and consume a little over 5 wt % hydrogen (again, on a MAF basis).

B. Effect of Pyrite Source and Level in the Feed Slurry

1. Effect of Pyrite Source

The results of processing Belle Ayr coal with three different pyrite samples are compared in Table VI.

The Robena Pyrite II produced a much greater effect than the other two pyrite samples even though only about half as much was added and the total solids level in the feed slurry was about 5 wt % lower than in the other runs. Total oil yield was 11.3 wt % higher based on MF coal, than with Matheson, Coleman and Belle (MCB) pyrite while SRC, IOM and hydrocarbon gas yields were lower by 3.9, 5.0 and 1.3 wt %, respectively.

Addition of MCB pyrite results in a slightly higher total oil yield and slightly lower SRC yield than the Robena Pyrite III although total conversion to pyridine soluble material was less.

Hydrogen consumptions were nearly the same during these three runs.

There were no clear trends in the heavy distillate and distillation residue elemental analyses. The residue from the run with Robena Pyrite II had the lowest fusion point and highest solubilities in hexane and toluene (lowest preasphaltene content) while that from the run with MCB Pyrite II had the highest fusion point and lowest solubilities.

The conditions for these three experiments were identical except for the pyrite sample (and level) and feed slurry solids level. The Robena Pyrite II and III samples were obtained from a coal cleaning operation while the MCB pyrite was mined as a discrete mineral. The pyrite analyses differ somewhat, as shown in Table III.

As mentioned earlier, the MCB pyrite was ball milled, the Robena II was jet pulverized in air, and the Robena III was jet pulverized in a nitrogen atmosphere. The activity of the additive appears to correlate with surface area, perhaps as an indicator of differing surface structure. This conclusion is based on a small number of samples, however, and Sandia has reported that there is no correlation between surface area and pyrite activity(7).

2. Effect of Pyrite Level in the Feed Slurry

The effect of iron level in the feed slurry on yields was determined in run DOE 350R. The yields were calculated during steady-state operation with added pyrite and at 7 points after the additive was dropped from the formulation. It was found that yields plotted against total iron in the feed slurry on a logarithmic scale gave an essentially linear relationship, as shown in Figure 2.

The addition of 1 wt % pyrite to the feed in run DOE 350RA resulted in an iron level of about 2.5% in the equilibrated feed slurry. When pyrite addition was stopped in run DOE 350RC, the iron level in the slurry dropped to about 0.35 wt % before the run was terminated by a plug in the preheater. As iron concentration decreased over this range, total oil yield dropped from about 56 to 28 wt %, SRC yield increased from 14 to 28 wt % and IOM yield increased from 1.3 to 14 wt %. There was little effect on hydrocarbon gas yield.

The hydrogen level in the heavy distillate also dropped off significantly (from 8.5 to 7.7 wt %) as iron was worked out of the system. There was also a significant increase in distillation residue fusion point (from about 110 to 190°C).

C. Effect of Liquefaction Conditions

1. Temperature Effect

The effect of increasing the average dissolver temperature from 450 to 465°C with three different coals and added pyrite is shown in Table VII. In each case there was a significant increase in hydrocarbon gas yield and hydrogen consumption at the higher temperature, as expected. There were also decreases in oil and SRC yields and increases in IOM yields. From these results it is apparent that the optimum temperature for processing these coals with added pyrite is closer to 450°C than 465°C.

In each case, there were lower hydrogen levels in the heavy distillate and distillation residue at the higher temperature. Other product analyses were generally unaffected.

2. Combined Temperature/Pressure Effect

The results of processing Edna Mine coal at 450°C and 2250 psig or 457°C and 1800 psig are compared in Table VIII.

The results of run DOE 427RA are qualitative since the run was ended after three days due to increasing slurry viscosity. The higher reactivity in run DOE 427RB is still apparent, however.

The total oil yield was higher and the IOM yield lower at 450°C and 2250 psig. If run DOE 427RA could have been lined out, the differences would probably be more pronounced. The gas yield was higher at the higher temperature, as expected, and not much difference was observed in SRC yields and hydrogen consumptions.

Work is planned at Merriam to find the optimum conditions for processing western coals with added pyrite, and specifically to isolate the temperature and pressure effects. It is likely, however, that at least some of the improvement was due to the increased pressure.

3. Effect of Slurry Recycle

The scope of this paper has been limited to SRC II mode operation. It is interesting, however, to make at least one comparison to SRC I operation to determine the effect of recycling the added pyrite. This includes the effect of the higher

resulting iron concentration in the feed slurry as well as any changes that take place in the pyrite as it passes through the system.

Pyrite addition was highly beneficial in both modes of operation with Belle Ayr coal. Even with added pyrite, however, the SRC I studies with this coal indicated an unsatisfactory level of reactivity. Under the conditions used, 31 minutes residence time, 450°C, 1500 psig, 39 wt % coal concentration and 1 wt % pyrite addition, there was a 5 wt % deficiency of recycle solvent and overall conversion was poor as indicated by a 17 wt % insoluble organic matter yield. Thus, the SRC I studies would indicate that this coal was of low reactivity even with 1 wt % added pyrite.

As mentioned previously, dramatically different results were obtained in the SRC II mode (run DOE 350). With 1 wt % added pyrite (450°C, 2250 psig and 1 hr residence time), the Belle Ayr coal was one of the most reactive coals ever investigated at the Merriam Laboratory. Oil yield was 56 wt % (MF coal basis) and total organic residue yield (SRC + IOM) was only 15 wt %.

IV. CONCLUSIONS

1. Low iron, low rank coals can not be processed at normal SRC II conditions without added catalyst.
2. Addition of moderate amounts of pyrite (4-5 wt %, based on coal) results in attractive yields of high quality products and generally trouble-free operation.
3. Pyrites from different origins and those from the same origin obtained at different times may have varying activity. The factors influencing the catalytic activity of pyrite are not well understood, but in our studies activity generally increased with increasing surface area.
4. The yields from Belle Ayr coal at SRC II conditions vary with the logarithm of the iron concentration in the feed slurry over a wide range of the variables.
5. The optimum conditions for liquefaction probably vary with the coal and catalyst. The optimum temperature for the coals in this study was closer to 450°C than 465°C and yields can be expected to improve as hydrogen pressure is increased. Operating in the SRC II mode enhances the effect of added pyrite on coal reactivity.

REFERENCES

- (1) "Solvent Processing of Coal to Produce a Deashed Product," R&D Report No. 9, Kloepper, et al, Gulf Oil Corp., Merriam, Kansas; NTIS #PB167-809.
- (2) "Exploratory Research on Solvent Refined Coal Liquefaction," Quarterly Technical Progress Report for the Period April 1, 1979 through June 30, 1979; The Pittsburg & Midway Coal Mining Co., July 1980, FE/14800-10.
- (3) "Development of a Process for Producing an Ashless, Low-Sulfur Fuel from Coal," Interim Report #6 (Vol. II-Laboratory Studies; Part 1-Autoclave Experiments); The Pittsburg & Midway Coal Mining Co., 1975, GPO #163.10:53/INT 6, NTIS #PB236-305.
- (4) "Development of a Process for Producing an Ashless, Low-Sulfur Fuel from Coal," Interim Report #7 (Vol. II-Laboratory Studies; Part 2-Continuous Reactor Experiments Using Anthracene Oil Solvent); The Pittsburg & Midway Coal Mining Co., September 1977, FE-496-T4.

- (5) "Solvent Refined Coal (SRC) Process," Quarterly Technical Report for the Period April 1, 1977 through June 30, 1977; The Pittsburg & Midway Coal Mining Co., December 1977, FE-496-141.
- (6) "Solvent Refined Coal (SRC) Process," Quarterly Technical Report for the Period April 1, 1978 through June 30, 1978; The Pittsburg & Midway Coal Mining Co., May 1979, FE-496-157.
- (7) "The Relationship Between Properties of Iron Sulfides and Their Catalytic Activity," paper presented by F. V. Stohl and B. Granoff, Sandia National Laboratories, Albuquerque, NM, at the Disposable Catalysts for Synfuel Production Symposium at the 1981 AIChE Meeting at Houston, Texas, April 5-9, 1981.

TABLE I
RUN CONDITIONS

| | |
|---------------------|--|
| AVERAGE DISSOLVER | |
| TEMPERATURE: | 450, 465°C (ISOTHERMAL) OR 457°C (SIMULATED ADIABATIC) 450°C INLET, 460°C OUTLET |
| PRESSURE: | 1800 OR 2250 PSIG |
| RESIDENCE TIME: | 1.0 HOUR |
| COAL CONCENTRATION: | 30 WT % IN SLURRY |
| HYDROGEN FLOWRATE: | 4 WT %, BASED ON SLURRY (52 MSCF/TON OF COAL) |
| MODE: | SRC II (RECYCLE OF UNFILTERED COAL SOLUTION) |

TABLE II
COALS

| MINE | STATE | SEAM | RANK |
|--------------------------|-------|---------------------|----------------|
| BELLE Ayr | WY | WYODAK- ANDERSON | SUBBITUMINOUS |
| (KAIPAROWITS PLATEAU) | UT | RED | HVC BITUMINOUS |
| ENERGY | CO | WADGE | SUB A/HVC BIT. |
| McKINLEY | NM | * | SUBBITUMINOUS |
| EDNA | CO | WADGE | SUB A/HVC BIT. |
| BLACKSVILLE | WV | PITTSBURGH | BITUMINOUS |

* YELLOW, FUCHSIA, BLUE AND GREEN SEAMS ARE MINED.

TABLE III
PYRITES

| | MCB* PYRITE | MCB* PYRITE | ROBENA PYRITE | ROBENA PYRITE |
|-------------------------------------|----------------|----------------|------------------|------------------|
| WT % | | | | |
| Fe | 43.61 | 41.65 | 30.20 | 38.75 |
| S | 53.01 | 50.11 | 34.38 | 41.36 |
| C | 0.09 | 0.10 | 5.81 | 5.42 |
| H | 0.04 | 0.09 | 0.69 | 0.40 |
| MOLE RATIO S/Fe | 2.12 | 2.10 | 1.99 | 1.86 |
| PURITY, WT % BASED ON Fe | 94 | 89 | 65 | 83 |
| AVERAGE PARTICLE SIZE, μ M | | | | |
| BY COULTER COUNTER | -- | 12 | 1.7 | 3.5 |
| BET SURFACE AREA, M ² /G | 2.0 | 1.1 | 5.9 | 2.6 |

* MATHESON, COLEMAN AND BELL

TABLE IV
SENSITIVITY OF VARIOUS COALS TO PYRITE ADDITION

| CONDITIONS* | DOE 431RA/ 350RC-5 | DOE 401R/ 353RC | DOE 422RA/ 422RB | DOE 424RA/ 424RB | DOE 402R/ 403R |
|---|--------------------------|-----------------------|------------------------|------------------------|----------------------|
| COAL | BELLE AYR | Kaipar- OWITS | MC- KINLEY | EDNA | BLACKS- VILLE |
| CHANGE IN MAF YIELDS** | | | | | |
| C1-C4 | + 1.8 | + 0.2 | - 0.9 | - 2.3 | - 0.1 |
| TOTAL OIL | +22.0 | +16.7 | +20.3 | +14.9 | + 2.6 |
| SRC | -12.2 | - 9.0 | -10.5 | - 9.1 | - 0.7 |
| IOM | -12.0 | - 6.1 | - 6.0 | - 1.8 | + 0.3 |
| CHANGE IN MAF HYDROGEN CONSUMPTION** | + 0.1 | + 1.3 | + 2.2 | + 1.8 | + 0.7 |

* ALL AT 450°C, 2250 PSIG, 1.0 HOUR RESIDENCE TIME WITH 30 WT % COAL IN THE SLURRY AND 4 WT % HYDROGEN, BASED ON SLURRY.

** RUN WITH 1.86 WT % PYRITE III IN THE SLURRY COMPARED TO RUN WITHOUT ADDED PYRITE AT POINT WHERE OPERATION CEASED.

TABLE V
PROCESSING OF VARIOUS COALS WITH ADDED PYRITE

| CONDITIONS* | DOE 431RA | DOE 401R | DOE 422RA | DOE 424RA | DOE 402R |
|--|--------------|------------------|---------------|--------------|------------------|
| COAL | BELLE AYR | KAIPAR- OWITS | MC- KINLEY | EDNA | BLACKS- VILLE |
| <u>YIELDS, WT % MAF COAL</u> | | | | | |
| C ₁ -C ₄ | 12.7 | 11.8 | 12.4 | 14.8 | 13.0 |
| TOTAL OIL | 49.5 | 56.8 | 49.3 | 53.9 | 42.9 |
| SRC | 21.3 | 17.8 | 26.5 | 21.4 | 36.3 |
| IOM | 2.9 | 2.8 | 4.6 | 4.1 | 6.1 |
| <u>HYDROGEN CONSUMPTION, WT % MAF COAL</u> | 4.5 | 5.4 | 5.1 | 6.3 | 4.8 |

- * ALL AT 450°C, 2250 PSIG, 1.0 HR RESIDENCE TIME WITH 30 WT % COAL AND 1.86 WT % ROBENA PYRITE III IN THE SLURRY AND 4 WT % HYDROGEN, BASED ON SLURRY.

TABLE VI
EFFECT OF PYRITE CHARACTERISTICS

| CONDITIONS* | DOE 350RA | DOE 380RA | DOE 380RB |
|---|--------------|--------------|--------------|
| PYRITE | ROBENA II | MCB II | ROBENA III |
| ADDITION LEVEL, WT % COAL** | 2.15 | 4.18 | 4.26 |
| TOTAL SOLIDS IN FEED SLURRY | 44.6 | 50.7 | 49.8 |
| <u>YIELDS, WT % MF COAL</u> | | | |
| C ₁ -C ₄ | 10.8 | 12.1 | 13.0 |
| TOTAL OIL | 55.9 | 44.6 | 41.6 |
| SRC | 13.5 | 17.4 | 19.0 |
| IOM | 1.3 | 6.3 | 5.2 |
| <u>HYDROGEN CONSUMPTION, WT % MF COAL</u> | 5.4 | 5.1 | 4.8 |

- * FOR ALL: 449-450°C, 2250 PSIG AND 1 HOUR RESIDENCE TIME WITH 30 WT % BELLE AYR COAL IN THE SLURRY AND 4 WT % HYDROGEN, BASED ON SLURRY.

- ** AS PURE FeS₂.

TABLE VII
EFFECT OF TEMPERATURE ON PROCESSING
WESTERN COALS WITH ADDED PYRITE

| <u>CONDITIONS*</u> | <u>DOE</u> <u>350RA/B</u> | <u>DOE</u> <u>353RA/B</u> | <u>DOE</u> <u>355RA/B</u> |
|---|------------------------------|------------------------------|------------------------------|
| COAL | BELLE AYR | KAIPAR- OWITS | ENERGY |
| PYRITE | ROBENA II | MCB I | MCB I |
| <u>CHANGE IN MAF YIELDS**</u> | | | |
| C1-C4 | +3.5 | +4.4 | +3.3 |
| TOTAL OIL | -4.3 | -1.7 | -2.5 |
| SRC | -2.2 | -4.6 | -9.5 |
| IOM | +2.0 | +0.7 | +6.2 |
| <u>CHANGE IN MAF HYDROGEN</u> <u>CONSUMPTION**</u> | +0.9 | +1.0 | +0.2 |

- * ALL AT 2250 PSIG AND 1 HOUR RESIDENCE TIME WITH 30 WT % COAL AND 1.0 WT % ADDED PYRITE IN THE SLURRY; 4 WT % HYDROGEN, BASED ON SLURRY.
- ** RUN AT 465°C COMPARED TO ONE AT 450°C.

TABLE VIII
COMBINED EFFECTS OF TEMPERATURE AND PRESSURE
ON THE SRC II PROCESSING OF EDNA COAL
WITH ADDED PYRITE

| <u>CONDITIONS*</u> | <u>DOE 427RA</u> | <u>DOE 427RB</u> |
|---|------------------|------------------|
| AVERAGE DISSOLVER TEMP., °C | 457 | 450 |
| PRESSURE, PSIG | 1800 | 2250 |
| <u>YIELDS, WT % MF COAL</u> | | |
| C1-C4 | 14.4 | 12.2 |
| TOTAL OIL | 43.5 | 46.1 |
| SRC | 20.0 | 21.4 |
| IOM | 6.2 | 4.3 |
| <u>HYDROGEN CONSUMPTION,</u> <u>WT % MF COAL</u> | 4.9 | 5.1 |

- * ALL AT 1.0 HOUR RESIDENCE TIME WITH 30 WT % EDNA MINE COAL AND 1.86 WT % PYRITE IN THE FEED SLURRY; 4 WT % HYDROGEN, BASED ON SLURRY.

FIGURE 1
MERRIAM LABORATORY
BENCH SCALE COAL LIQUEFACTION UNIT

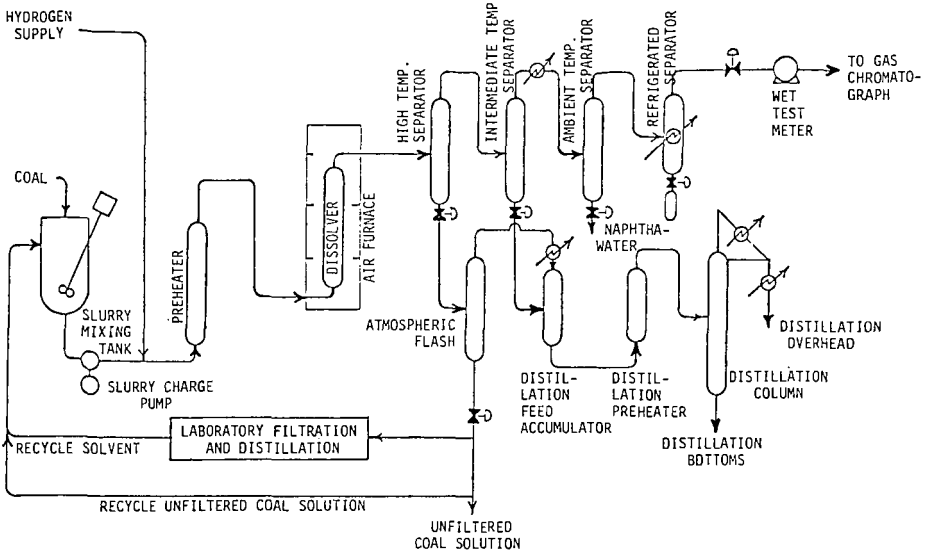
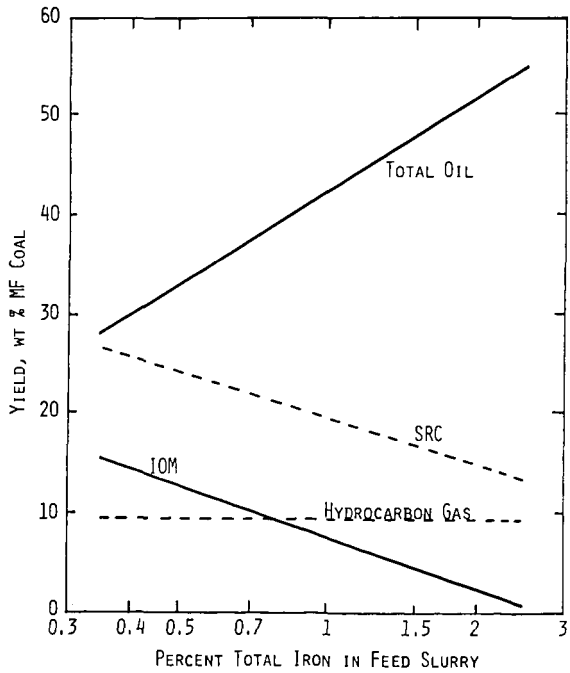


FIGURE 2
EFFECT OF IRON LEVEL ON YIELDS
RUN DOE 350RC



BATCH AUTOCLAVE TEMPERATURE-PRESSURE STUDIES ON THE
DIRECT CATALYTIC LIQUEFACTION OF VICTORIAN BROWN COAL

P.J. Cassidy, F.P. Larkins and W.R. Jackson

Department of Chemistry, Monash University
Clayton, 3168 Victoria, Australia

INTRODUCTION

Victorian brown coal is a low rank, low ash lignite with an elemental composition similar to North Dakota lignite (see Table 1).

Table 1: Comparison of Victorian Brown Coal and North Dakota Lignite

| | <u>As Received</u> | | <u>Daf basis</u> | | | |
|-------------------------------|-----------------------|----------|------------------|----------|----------|----------|
| | <u>H₂O</u> | <u>C</u> | <u>H</u> | <u>O</u> | <u>N</u> | <u>S</u> |
| Victorian Morwell Coal (1) | 62.5 | 69.3 | 5.0 | 24.5 | 0.6 | 0.6 |
| North Dakota Lignite (2) | 25.0 | 69.4 | 4.3 | 23.1 | 0.7 | 2.5 |

Previous batch autoclave studies^{3,4} using hydrogen gas with tetralin as the vehicle have confirmed that brown coal is suitable for direct catalytic hydrogenation giving high yields of liquid products. Furthermore, brown coal is an excellent ion-exchange medium primarily because a significant amount of the bound oxygen is present in carboxylic ($\sim 2.6 \text{ mol kg}^{-1}$) and phenolic ($\sim 3.2 \text{ mol kg}^{-1}$) functional groups.⁵ This property has been exploited to achieve high dispersion of metal catalysts throughout the coal.⁵

The work presented here is aimed at developing catalysts and reaction conditions which maximise the conversion to a low oxygen refinery feedstock. Product distribution dependences on reaction temperature (345-460°C : 6MPa H₂) and hydrogen pressure (1-10MPa : 385°C) using iron, tin and synergistic iron + tin (trace) catalysts are compared to those for untreated Morwell coal.

EXPERIMENTAL

Coal Preparation and Hydrogenation

The coal and catalysts were prepared for hydrogenation by the method of Jackson et al.³ The coal (3.0 g) was dried under nitrogen at 105°C to constant weight and slurried (1 : 1) with AR grade tetralin as the vehicle. The hydrogenations were performed in a 70 ml rocking autoclave heated to reaction temperature in 11 minutes. Reaction time was one hour at temperature after which the autoclave was quenched in an ice bath.

Catalyst concentrations used for the study were as follows:

| <u>Coal</u> | <u>Catalyst Concentration (mmol/kg daf coal)</u> | |
|----------------------------------|--|----------|
| untreated | Fe | 30 |
| iron treated | Fe | 300 ± 40 |
| tin treated | Sn | 200 ± 20 |
| synergistic iron-tin treated: | Fe | 300 ± 40 |
| | Sn | 20 ± 10 |

Product Analysis

Product gases (CO , CO_2 , CH_4 , C_2H_4 , C_2H_6 , C_3H_8 , C_3H_6 , $n\text{-C}_4\text{H}_{10}$, $i\text{-C}_4\text{H}_{10}$) were analysed by GLC using a standard gas mixture for calibration. Hydrogen was determined indirectly by difference. The liquid product was removed from the reaction using CH_2Cl_2 and the water produced was determined by azeotropic distillation. The insoluble material was Soxhlet extracted for 12-15 hours with CH_2Cl_2 and the residue dried at 105°C under nitrogen to determine the total conversion. The CH_2Cl_2 soluble material was further divided into asphaltene (insoluble in light petroleum) and oil (soluble in light petroleum). Elemental analyses for C, H, O, N, S were performed by the Australian Analytical Laboratories. The direct analysis for oxygen was cross checked by difference (Equation 1)

$$\text{wt\% O} = 100 - \% \text{C} - \% \text{H} - \% \text{S} - \% \text{N} \quad (1)$$

Acidic oxygen was determined by non aqueous titration using the method of Brookes and Maher.⁶

TEMPERATURE DEPENDENCE

Total Conversion

The temperature dependences of the product distributions for untreated iron, tin and iron-tin treated coals at 6MPa initial hydrogen pressure are shown in FIGURES 1A-D. The total conversions are compared in FIGURE 2. The temperature range chosen for study was from $345\text{--}460^\circ\text{C}$. At temperatures below 345° conversion was too low for meaningful measurements and at temperatures above 460° decomposition of tetralin can become a significant problem.^{7,8}

The total conversion of untreated coal increases steadily from 37% to 63% between 345°C and 425°C then it levels out to 65% at 460°C . An iron based catalyst results in a rapid increase in total conversion from 37% at 345°C to 63% at 385°C after which it increases steadily to 72% at 460°C . The tin catalyst increases the conversion dramatically from 43% at 345°C to 73% at 385°C after which it increases regularly to 81% at 460°C . The iron-tin catalyst is not as efficient as the tin catalyst up to 385°C as the conversion is only 66% at 385°C . However, above 385°C the conversion rises sharply reaching 85% at 425°C after which it levels out with a maximum of 88% at 460°C . Above 400°C the products from the tin and iron-tin coals are increasingly unstable with increasing amounts of CH_2Cl_2 insoluble material being precipitated during product work up. The result is reduced total conversions at all temperatures compared with findings using a larger 1 litre autoclave.^{5,9,10} The results should therefore be viewed as internally consistent, but not directly comparable with work in larger autoclaves with different temperature profiles.

Conversion to Useful Liquid Products (Oil and Asphaltene)

Between 365 and 425°C the three catalysed coals offer significantly improved CH_2Cl_2 soluble liquid (oil + asphaltene) yields compared to untreated coal (FIGURE 3). At 345°C tin gives an 8% improvement while the iron-tin and iron catalysts offer no improvement over the untreated coal yield of 20% (daf coal) at that temperature. In the region $365\text{--}385^\circ\text{C}$ tin continues to be superior giving 4-5% more liquid product than the Fe-Sn, 10-14% better than Fe and 22% more than untreated coal. However, above 405°C the yield of liquid product from tin coal deteriorates significantly from 50% at 405°C to 42% at 460°C . This can be attributed to increased yields of hydrocarbon gases and significant repolymerisation of asphaltenes during product workup. (The total oil + asphaltene yield in these small scale experiments is only 0.5 to 1.5 g.) Above 385°C the Fe-Sn catalyst dramatically increases the yield of useful liquid products from 44% at 385°C to 57% at 425°C after which it decreases slightly to 55% at 460°C . This improvement in yield at higher temperatures is due

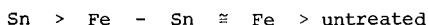
to the formation of a more stable product relative to the Sn catalyst system while the slight decrease at 460°C can be attributed to the increased production of hydrocarbon gases and some repolymerisation. The iron catalyst smoothly increases the liquid yield at 41% at 405°C and then levels out. The liquid yield from untreated coal increases steadily to 37% at 425°C after which there is little improvement.

The asphaltene temperature dependence (FIGURES 1A-D) is similar for the four coals with the yield increasing with temperature to a maximum of 405°C for untreated, iron and iron-tin coals and 385°C for tin treated coal after which it decreases regularly with increasing temperature. The iron-tin catalyst is clearly superior to the other three coals for producing oil (FIGURES 1A-D) at all temperatures except in the region of 400°C. The maximum oil production is 35-38% daf coal with the iron-tin catalyst between 425°-460°C. The oil production for the untreated, iron and tin coals is similar reaching a maximum of 30% daf coal at 460°C. The minor variations in the trend can be attributed to the formation and breakdown of the asphaltenes. The major effect of all the catalysts is to produce more asphaltenes at temperatures below 405°C which are degraded to oils at higher temperatures.

Oxygen Distribution in the Products as a Function of Reaction Temperatures

In developing useful catalysts for brown coal liquefaction one major objective is to achieve a high yield of low oxygen content liquid. It is important to know how the oxygen is distributed in the products and in what form (H₂O, CO₂, CO) it is removed from the coal system. The oxygen distributions for products from the four coals are shown in FIGURES 4A-D.

Generally raising the reaction temperature removes more oxygen, primarily as water. In all cases carbon monoxide production increases slightly with increased temperature while CO₂ formation appears to reach a maximum in the region of 385°C after which it decreases slightly for the three catalysed coals. There is no such maximum reached in the carbon dioxide produced from the untreated coal. As the majority of the carbon dioxide is formed at low temperatures (200-300°C) by decomposition of carboxyl groups, any variation on this level is probably a response to changes in the equilibrium of the water gas shift reaction. Tin is clearly the superior catalyst for removing oxygen from the coal products with the general order being



At 460°C tin has removed 98% of the oxygen, iron and iron-tin approximately 80% and untreated coal has lost only 67%. In fact little further oxygen is removed from untreated coal above 405°C. The distribution of acid oxygen in the CH₂Cl₂ insoluble residue is similar for all three catalysed reactions. The dramatic difference is that tin has removed significantly more non acidic oxygen from the residue at lower reaction temperatures. The oxygen content in the asphaltene is similar for the three catalysts, reaching a maximum in the region of 385°C and decreasing at higher temperatures. The oxygen level in the asphaltenes from untreated coal is almost invariant with reaction temperature. Tin is also the best catalyst for the removal of oxygen from the oil fractions at temperatures above 385°C while the iron and iron-tin catalysts have similar activity and are better than untreated coal. At temperatures below 385°C there is, in all cases, an increase in the oxygen level in the oil fraction as the reaction temperature decreases with the trend being most marked for the tin and iron-tin catalysts. This suggests that the catalysts are breaking carbon-oxygen bonds at low reaction temperature but do not have the ability to remove the oxygen completely from the system at low temperatures. It is a reasonable presumption that it is the trace of tin in the synergistic iron-tin catalyst which facilitates the improved bond breaking compared to the iron catalyst. Increasing the reaction temperature to 385°C is sufficient to remove this oxygen from the oil. The increase in total oxygen in the oil fraction

above 385°C for untreated, iron and iron-tin coals suggests that these catalysts have difficulty in removing oxygen from certain classes of oxygen containing functional groups. However, the ability of tin to catalyse the almost total removal of oxygen does lead to problems of product stability. Some of the derived products repolymerise even on standing in dichloromethane solution. It is possible that higher concentrations of reactive poly-enes are formed which are not hydrogenated in the absence of iron or other metals capable of catalysing liquefaction.

HYDROGEN PRESSURE DEPENDENCE

The hydrogen pressure dependence reactions were performed at 385°C for the four coals and at 425°C for the coals with iron-tin synergistic catalyst (see FIGURES 5 to 7). The most significant feature is that in all catalysed reactions the total conversion (FIGURE 5) increases with pressure until a critical pressure is reached above which increasing the hydrogen pressure has a reduced effect. For the iron and iron-tin catalysts at 385°C the critical pressure is 4MPa initial hydrogen while for the tin at 385°C and iron-tin at 425°C 6MPa is the critical hydrogen pressure. Furthermore increasing hydrogen pressure results in significantly more asphaltene being produced for the tin (385°C) and iron-tin (at 385°C and 425°C) catalysts (FIGURE 6) while it has little effect on oil production from both catalysed and non catalysed coals at 385°C (FIGURE 7). However, at 425°C the oil production from iron-tin coal shows a marked hydrogen pressure dependence (FIGURE 7) and these studies suggest that a suitable initial hydrogen pressure for obtaining high conversion in catalysed reactions is not very high e.g. an initial pressure of 6MPa for the iron-tin system for 425°C.

CATALYTIC EFFICIENCY - USEFUL CARBON/HYDROGEN VERSUS OXYGEN REMOVAL

While developing catalysts that remove oxygen from brown coal is a major objective it is also important to ensure that the maximum amount of carbon and hydrogen from the coal be carried through into the useful liquid products, i.e. oil and asphaltene. An additional view of conversion then is a measure of the percentage of carbon and hydrogen carried through to the useful products. Recognising that approximately 4% of the carbon is always lost from the system as carbon dioxide and carbon monoxide and that the coal contains ~25% oxygen, the maximum yield of carbon and hydrogen can only be 71% of the daf coal. Considered from this point of view the iron-tin catalyst converts 75% of the available carbon and hydrogen into liquid products at 425°C while the tin converts only 63%, iron 53% and untreated coal 46%.

FIGURE 8 compares the ability of the catalyst to remove oxygen and to convert the available carbon and hydrogen into useful products. The most efficient catalyst will be closest to the 45 degree line on the coordinate system. All of the coals lie to the left of the line which shows that all four of the reaction systems have a preference for the removal of oxygen relative to converting the carbon and hydrogen to useful products. This trend is particularly true for high temperature reactions where the shift to the left is associated with greater production of hydrocarbon gases and, in the case of tin catalysed reactions, significant repolymerisation of material which was initially soluble in methylene chloride. The exception is the iron-tin catalyst which lies very close to the line and at one point (corresponding to 425°C) actually shows a slight preference for converting the carbon and hydrogen into liquid products. In order of catalyst efficiency the four coals are ranked in order:

iron - tin > tin >> iron > untreated

CONCLUSION

The development of suitable catalysts and reaction conditions in the liquefaction of brown coal is a compromise of the ability of the catalyst to fulfill the following

requirements;

- Remove all of the organically bound oxygen
- Carry the maximum amount of carbon and hydrogen through to the liquid products
- Minimise production of hydrocarbon gases

Under the reaction conditions chosen for this study (6MPa initial hydrogen pressure and a low (1:1) hydrogen donor solvent to coal ratio) the synergistic iron-tin catalyst is superior to the other three coals. It achieves its objectives remarkably well at reasonably low reaction temperatures (425°C) and correspondingly low reaction pressure (14.6 MPa/2190 psi at 425°C). Under these conditions 75% of the available carbon and hydrogen is converted to liquid products and 5% to hydrocarbon gases. A large proportion (60%) of the liquid product is present as oil (X4 soluble) while 73% of all oxygen has been removed as CO₂, H₂O and CO. The tin catalyst is superior at removing oxygen (94% at 460°C) but produces more hydrocarbon gases and is less efficient at carrying the available carbon and hydrogen through to liquid products (63% at 425°C). It is possible that the tin requires higher hydrogen pressures to prevent repolymerisation of the unstable asphaltenes at these temperatures. At 425°C/6MPa hydrogen the iron catalyst is only 7% better than untreated coal for converting available carbon and hydrogen into useful liquids.

ACKNOWLEDGEMENTS

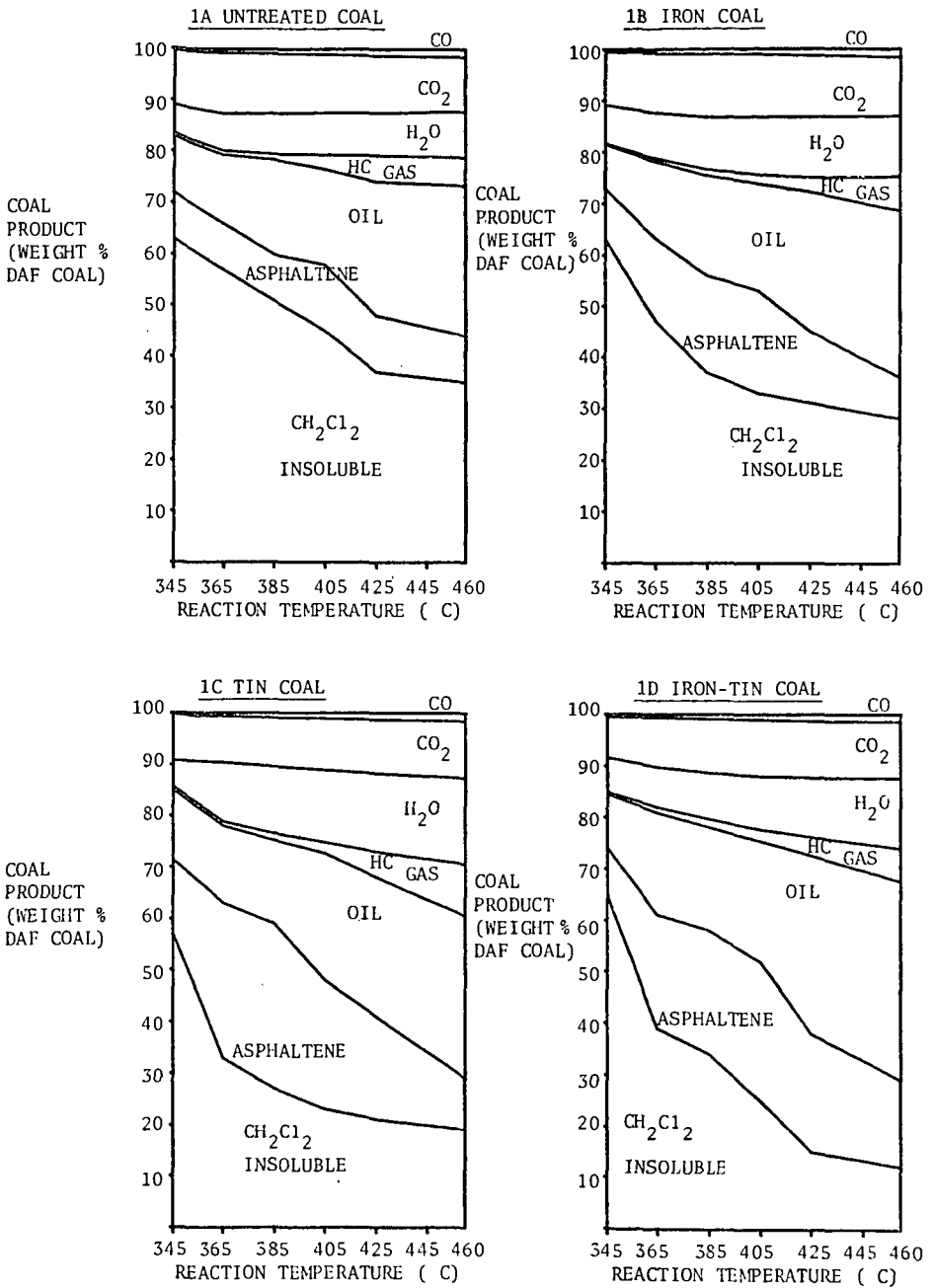
We gratefully acknowledge financial assistance for this work provided by the Victorian Brown Coal Council. The responsibility for the views expressed rest entirely with the authors. We also thank M. Marshall, D. Rash and P. Redlich for valuable discussions and assistance.

REFERENCES

1. State Electricity Commission of Victoria - Scientific Division Test Report CS/79/31 1979 Sheet 2.
2. H.R. Appell, R.D. Miller, E.G. Illig, E.C. Moroni, E.W. Steffgen, PETC/TR-79/1 1979 52.
3. W.R. Jackson, F.P. Larkins, M. Marshall, D. Nicolson and D. Rash, Fuel, 58, (1979) 156.
4. W.R. Jackson, F.P. Larkins, D. Rash and N. White, Fuel 58 (1979) 281.
5. M.R. Hatswell, W.R. Jackson, F.P. Larkins, M. Marshall, D. Rash and D.E. Rogers, Fuel 59 (1980) 442.
6. J.D. Brooks and T.P. Maher, Fuel 36 (1957) 51.
7. B.M. Benjamin, E.W. Hagaman, V.F. Raaen, and C.J. Collins, Fuel 58 (1979) 386.
8. J.M. Charlesworth, Fuel, 59 (1980) 859.
9. M. Marshall, W.R. Jackson, F.P. Larkins, M.R. Hatswell and D. Rash submitted for publication in Fuel.
10. F.P. Larkins, W.R. Jackson, M.R. Hatswell, S.J. Cochran, P.J. Cassidy, M. Marshall, D. Rash and P. Redlich, Proceedings of the International Conference on Coal Science Düsseldorf 7-9/9/1981 C12, pp. 392-397.

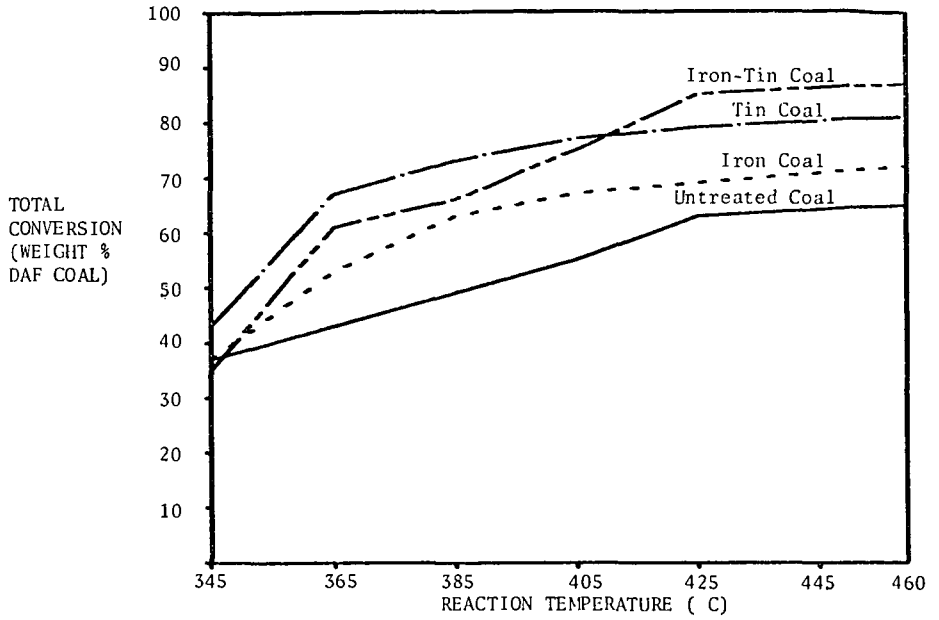
PRODUCT DISTRIBUTION vs REACTION TEMPERATURE

FIGURE 1.



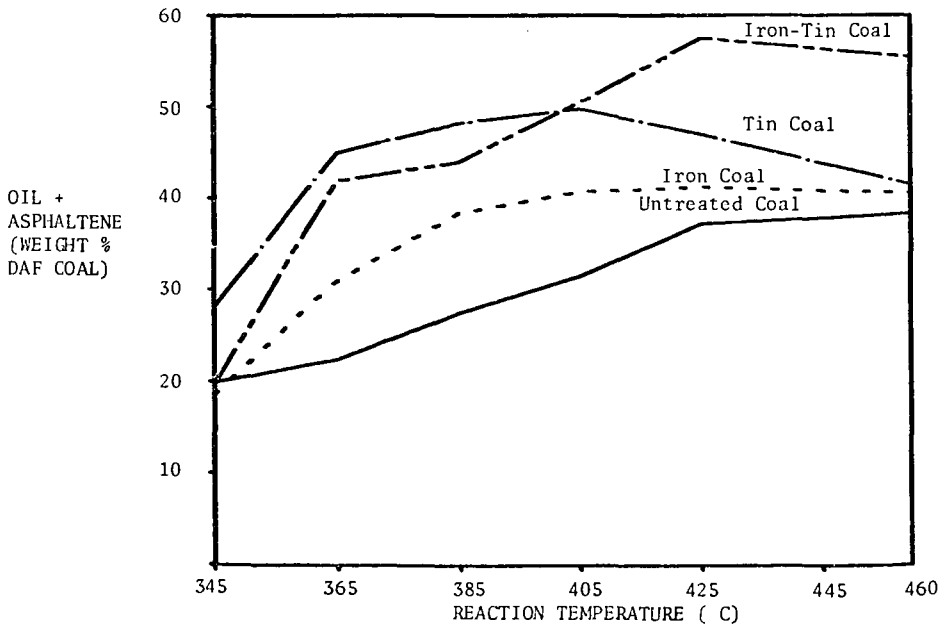
TOTAL CONVERSION vs REACTION TEMPERATURE

FIGURE 2.

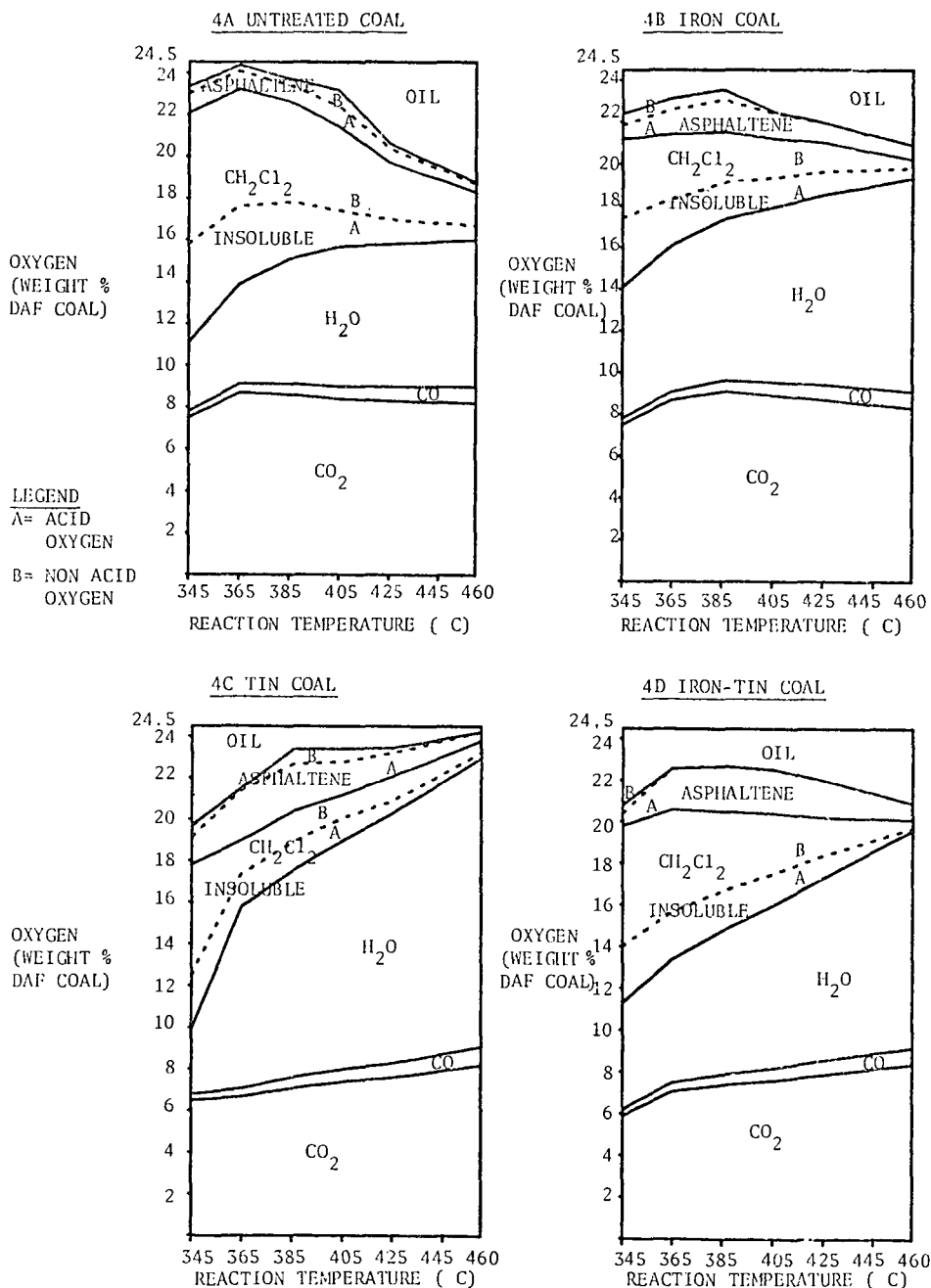


OIL + ASPHALTENE vs REACTION TEMPERATURE

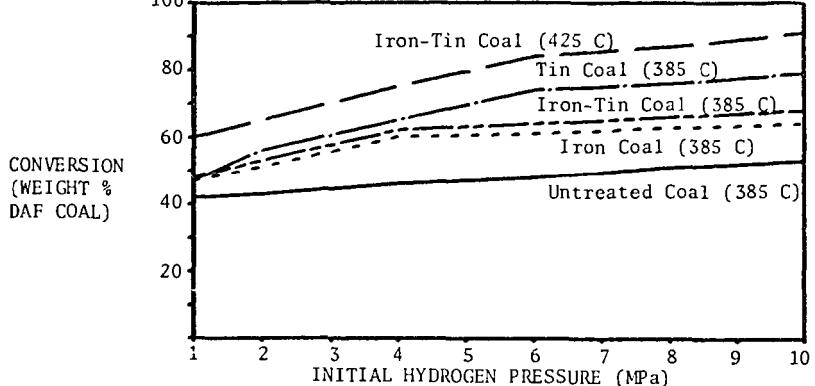
FIGURE 3.



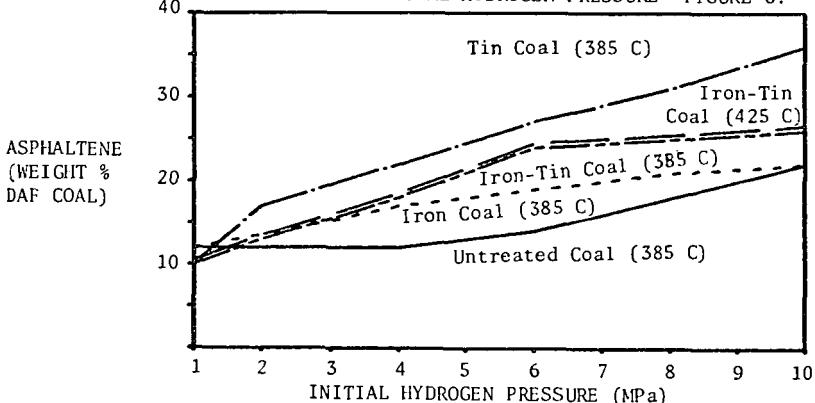
PRODUCT OXYGEN DISTRIBUTION vs REACTION TEMPERATURE FIGURE 4.



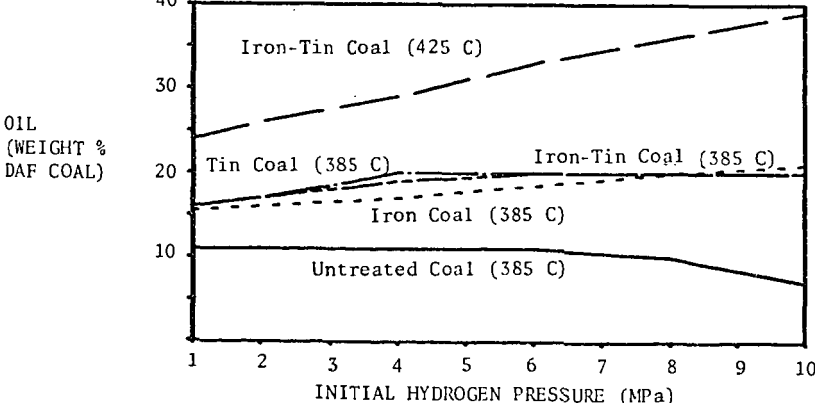
TOTAL CONVERSION vs INITIAL HYDROGEN PRESSURE FIGURE 5.



ASPHALTENES vs INITIAL HYDROGEN PRESSURE FIGURE 6.

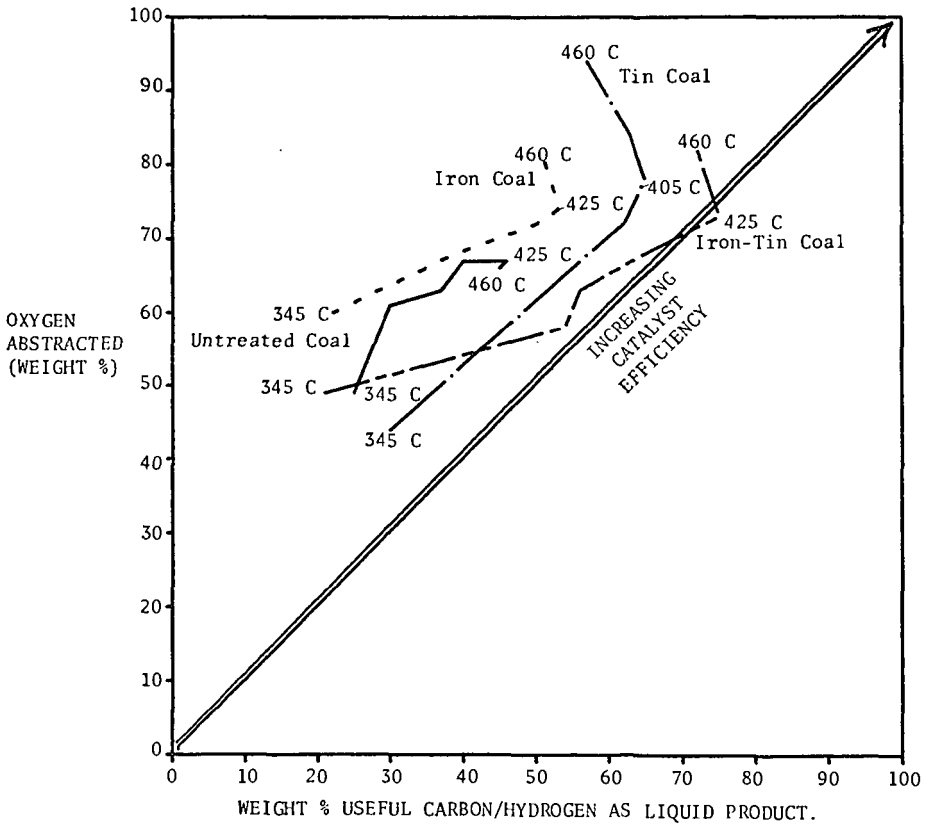


OIL vs INITIAL HYDROGEN PRESSURE FIGURE 7.



CATALYST EFFICIENCY

FIGURE 8.



Note: Temperatures quoted on the graph are the reaction temperatures for the areas of interest.

EFFECT OF CATALYST DISTRIBUTION IN COAL LIQUEFACTION

Diwakar Garg and Edwin N. Givens
Corporate Research and Development Department

Air Products and Chemicals, Inc.
P.O. Box 538, Allentown, PA 18105

Effect of the mode of catalyst addition was studied for the liquefaction of Eastern Kentucky Elkhorn #2 coal in a continuously stirred tank reactor. Particulate addition of iron as pyrite significantly catalyzed the coal liquefaction reaction. Both coal conversion and oil yield increased on addition of pyrite to the feed slurry; oil production increased by more than a factor of two both at 825° and 850°F. Pyrite Concentration had negligible effect on product distribution, but the mode of catalyst addition had a big impact on coal liquefaction. Impregnation of coal with one weight percent iron gave a similar product distribution as obtained with addition of 3.5 weight percent iron in the form of particulate pyrite. Significantly lower hydrocarbon gas make and hydrogen consumption were noted with impregnation over particulate addition. SRC sulfur content was marginally higher with impregnation. Solvent hydrogen content increased with particulate addition whereas it decreased with impregnation.

Introduction

The basic non-catalytic process for liquefaction of coal was developed by Bergius¹ in Germany circa 1912. In 1925 Brown-coal tar was catalytically hydrogenated for the first time with molybdenum oxide. This advance led to the development of the catalytic hydrogenation of coal.

A number of catalysts were studied and reported to give improved yield and product quality². Adding two percent molybdenum on coal as ammonium molybdate substantially increased the liquefaction performance. Subsequent experiments showed that 0.05 percent molybdenum gave a yield equal to that obtained with two percent when the alkalinity of coal was reduced. Because molybdenum was expensive and in short supply in Germany, it was replaced by iron catalyst. The Germans found that adding iron as iron sulfate to the feed slurry improved the liquefaction of coal². Bayermasse, an iron oxide-containing material obtained as by-product from aluminum manufacture was also shown to be active in coal liquefaction. In terms of iron content, twice as much Bayermasse as sulfate was needed to produce the same results in hydrogenation of coal. In certain cases the addition of sulfur to the system also improved the catalytic liquefaction effect of the iron². The iron to sulfur ratio in the liquefaction residue suggested that iron sulfide (FeS) was the ultimate form of the iron. With the advent of x-ray diffraction technique the FeS was found to be in the form of pyrrhotite³, $Fe_{1-x}S$.

Wright and Severson reported that the addition of iron as contained in the residues from coal liquefaction increased the hydrogen transfer capacity of anthracene oil.⁴ Seitzer⁵ magnetically separated the iron sulfur compound from coal liquefaction residues and used it as a catalyst in subsequent liquefaction reactions. He found that the magnetically separated material had, per

weight of iron, about the same catalytic effect as ferrous sulfate. Furthermore, he found that the magnetically separated material catalyzed the addition of hydrogen to the dissolved coal.

Moroni and Fischer⁶, who reviewed many papers in the area of coal mineral catalysis, concluded that pyrite was active in coal conversion. Neither the addition of the coal liquefaction residue nor the magnetically separated residue delineated whether pyrrhotite had better catalytic activity than pyrite. A significant amount of work has been done more recently to determine the true catalytic activity of pyrite and pyrrhotite. A detailed summary of literature on pyrite and pyrrhotite catalysis has been made by Garg and Givens.⁷

The distribution of catalyst in the coal appears to be a critical factor in coal conversion. The method of applying the catalyst to the coal affects the catalyst distribution. For example, iron sulfate was shown to be much more effective when impregnated than when mixed mechanically.^{2,8} Although prolonged mixing improved the effectiveness of the catalyst, the improvement was less than gained by impregnation. The method of impregnation is also quite important as was shown in one case in which an attempt to impregnate coal in-situ during hydrogenation gave poor results.⁸

A reduction in particle size of the pyrite, reported to play an important role in catalyzing the coal liquefaction reaction, improved the catalytic activity of the pyrite.⁹ Significantly more oil production was reported with the use of finely divided pyrite¹⁰ than with hand ground pyrite.¹¹

The contact between catalyst and coal can be increased either by adding finely divided catalyst (two to three micron size) or impregnating it on coal using a water soluble compound like iron sulfate or dispersing it at the molecular level in the reaction mixture by using thermally unstable organic compounds like iron naphthenate. In the present paper data are presented which show the catalytic activity of pyrite and impregnated iron sulfate in coal liquefaction. The effect of simple particulate addition of pyrite is compared to catalyst impregnation. The catalytic activity for the coal conversion reactions are related to the product distribution including hydrocarbon gas make, oil, asphaltene and preasphaltene yields, and degree of coal conversion. All of the data reported in this paper refer to results in a continuous 100 pounds per day coal process unit.

Experimental

Materials: Elkhorn #2 was a washed sample taken from a preparation plant in Floyd County, Kentucky. The coal sample was ground to 95% minus 200 mesh particles and dried in air. The coal was screened through a 150 mesh sieve prior to use. The detailed analysis of the screened coal is reported in Table 1.

A 550-850°F cut of SRC-II heavy distillate supplied by The Pittsburg and Midway Coal Mining Company was used as a process solvent. The chemical analysis of the process solvent is shown in Table 2. The solvent contained 93.8% pentane-soluble oils, 5.0% asphaltenes and 0.4% preasphaltenes.

The pyrite sample was received from an operating mine in southwestern Pennsylvania. The sample was dried at 110°C in nitrogen and then ground to 99.9% minus 325 U.S. mesh size in the presence of liquid nitrogen. The chemical analysis of the pyrite is given in Table 3. The sample was comprised of 75%

pyrite, 5% carbonaceous organic material and 20% magnetite, quartz, and other inorganic materials. The BET surface area of the pyrite was 1.0 m²/g and the material was relatively non-porous.

Iron sulfate (FeSO₄ · 7H₂O) was received from Textile Chemical Company, Reading, Pennsylvania. The chemical analysis of the iron sulfate is given in Table 4. The sample contained approximately 97% iron sulfate crystals.

Equipment: Process studies were done in a continuous 100 pound/day coal liquefaction unit equipped with a continuous stirred autoclave. The use of a stirred tank reactor insured that solvent vaporization matched that of an actual SRC-I dissolver and that coal minerals did not accumulate. Since there was no slurry preheater, all of the sensible heat had to be provided by resistance heaters on the reactor. Because of this high heat flux, the reactor wall was about 27°F hotter than the bulk slurry. Multiple thermocouples revealed that the slurry temperature inside the reactor varied by only 9°F from top to bottom. A detailed description of the reactor is presented elsewhere.¹²

The products were quenched to 320°F before flowing to a gas/liquid separator that was operated at system pressure. The slurry was throttled into the product receiver while the product gases were cooled to recover the product water and organic condensate. The product gases were then analyzed by an on-line gas chromatograph.

Procedure: Coal liquefaction runs were performed at 825 and 850°F, 2000 psig hydrogen pressure, 1000 rpm stirrer speed, hydrogen feed rate equivalent to 5.5 wt.% of the coal and a superficial slurry space velocity of 1.5 inverse hours. The coal concentration in the feed was 30 wt.%. Iron sulfate was impregnated on the coal by dissolving it in water and mixing it with coal. Impregnated coal sample was dried in nitrogen and ground to minus 200 mesh prior to use. The concentration of impregnated iron was 1.0 wt.% on the basis of coal. The concentration of pyrite was varied from 2.5 to 10 wt.% of feed slurry.

At least 10 reactor volumes of the product were discarded prior to collecting a product sample. A complete sample consisted of one 8-oz. sample of product slurry, one 1-liter sample of product slurry as back-up sample, a light condensate sample and a product gas sample.

The product slurry from the continuous reactor was solvent separated into four fractions: (1) pentane-soluble material (oil), (2) pentane-insoluble and benzene-soluble material (asphaltenes), (3) benzene-insoluble and pyridine-soluble material (preasphaltenes), and (4) pyridine-insoluble material. The latter contains insoluble organic material (IOM) and mineral residue. A detailed procedure for performing this separation will be reported elsewhere. The overall coal conversion is calculated as the fraction of organic material (moisture-ash-free coal) soluble in pyridine.

Results and Discussions

Effect of Pyrite on Coal Liquefaction - At 825 and 850°F, addition of pyrite increased the coal conversion from ~85 to ~92% (Table 5). The production of hydrocarbon gases, CO + CO₂, and water, marginally increased with pyrite. Oil production increased by more than a factor of two; 12 to 28% and from 8 to 27%

on addition of pyrite at 825 and 850°F, respectively. Production of preasphaltenes decreased and asphaltenes remained apparently unchanged. The additional converted coal and preasphaltenes with pyrite ended up in the oil fraction. Hydrogen consumption increased from 0.64 to 1.68% and from 0.53 to 2.41% on addition of pyrite at 825 and 850°F, respectively. Also, an additional amount of 0.5% hydrogen was consumed in reducing the added pyrite. X-ray diffraction analysis of coal liquefaction residue showed a complete conversion of pyrite to pyrrhotite. SRC sulfur content remained the same. Oil hydrogen content unchanged in the absence of pyrite but increased in its presence.

In summary, the addition of pyrite to coal during liquefaction improved conversion of coal and preasphaltenes, increased production of oil and hydrocarbon gases, promoted rehydrogenation of the process solvent and increased consumption of hydrogen. Increasing reaction temperature in the presence of pyrite increased conversion of preasphaltenes and increased production of hydrocarbon gases and hydrogen consumption. The conversion of coal and production of oil and asphaltenes marginally decreased with increasing temperature.

Effect of Pyrite Concentration on Coal Liquefaction - Conversion of coal and production of hydrocarbon gases remained the same upon increasing the pyrite concentration from 2.5 to 10 wt. percent. (Table 6, Figures 1 and 2). The production of CO + CO₂, water and oil shown in Table 6 and Figures 2 and 3 increased slightly as pyrite concentration increased. Asphaltenes remained the same and preasphaltenes decreased with increasing concentration of pyrite (Figure 4). Hydrogen consumption increased significantly as the pyrite concentration increased as shown in Table 6 and Figure 5. SRC sulfur content plotted in Figure 6 also marginally increased. Finally, increasing the concentration of pyrite from 2.5 to 10 wt.% of feed slurry had no significant effect on liquefaction of Elkhorn #2 coal.

Effect of Iron Impregnation on Coal Liquefaction - Conversion of coal was not significantly affected by impregnation at both 825 and 850°F. The production of hydrocarbon gases decreased considerably with iron impregnation while oil production increased by over a factor of two at both temperatures (Table 7). Asphaltene yield was unchanged but preasphaltene yield decreased considerably with iron impregnation. X-ray diffraction analysis of coal liquefaction residue showed a complete conversion of iron sulfate to pyrrhotite. Hydrogen consumption and SRC sulfur content were not significantly affected by iron impregnation. Oil hydrogen content was maintained without any additive but decreased with iron impregnation at both 825 and 850°F. Finally, iron impregnation significantly reduced the hydrocarbon gases and preasphaltenes production and increased the oil production.

Comparison of Iron Impregnated Versus Particulate Addition - The liquefaction of coal impregnated with one wt.% iron based on coal is compared with addition of 3.5 wt% particulate iron in the form of pyrite to coal-oil slurry. Conversion of coal was slightly lower with iron impregnation compared to pyrite addition. Iron impregnation gave significantly lower hydrocarbon gases production and hydrogen consumption (Table 8, Figures 7 and 8). Oil, asphaltenes and preasphaltenes production with iron impregnation were comparable to that obtained by pyrite addition. SRC sulfur content was marginally higher with iron impregnation. Oil hydrogen content was improved with pyrite, whereas it decreased with iron impregnation.

The above data emphasize the importance of the method of catalyst distribution in coal liquefaction. The effectiveness of a metal catalyst can be enhanced significantly by increasing the intimate contact between catalyst and coal. The mode of catalyst distribution therefore determines the amount of catalyst required for the reaction.

Conclusion

Addition of pyrite significantly catalyzes the coal liquefaction reaction. It improves coal conversion, increases oil and gases production, increases hydrogen consumption and rehydrogenates the process solvent. Changing the concentration of pyrite does not significantly alter the coal liquefaction reaction. Mode of catalyst addition is very important in coal liquefaction. The activity of a catalyst depends on the level of intimate contact of catalyst with coal. Therefore, the concentration of the metal catalyst can be greatly reduced without affecting product distribution by insuring efficient contact between catalyst and coal. The reduction in catalyst loading will eventually increase the overall throughput of the plant, drastically reduce the load in the solid-liquid separation unit, and improve the overall process economics.

References

1. Bergius, F., and Billwiller, J., German Patent 301,231, August 1, 1913.
2. Wu, W. R. K., and Storch, H. H., "Hydrogenation of Coal and Tar", U.S. Department of the Interior, Bureau of Mines Bulletin 633, 1968.
3. Given, P. H., Spackman, W., Davis, A., Walker, P. L. Jr., and Lovell, H. L., "The Relation of Coal Characteristics to Coal Liquefaction Behavior", Report No. 1 Submitted to NSF (RANN Division) by the Pennsylvania State University, 15 March 1974.
4. Wright, C. H., and Severson, D. E., ACS Division of Fuel Chem., Preprints, 1972, 16, 68.
5. Seitzer, W. H., "Miscellaneous Autoclave Liquefaction Studies," Final Report Prepared for EPRI by Suntech, Inc., under the contract EPRI AF-612 (RP-779-7), February, 1978.
6. Moroni, E. C. and Fischer, R. H., "Disposable Catalysts for Coal Liquefaction," Paper Presented at the 179th National Meeting of American Chemical Society, Houston, March, 1980.
7. Garg, D. and Givens, E. N., "Pyrite Catalysis in Coal Liquefaction," Paper Accepted for Publication in I&EC Process Design and Development.
8. Weller, S. W. and Pelipetz, M. G., Ind. Eng. Chem., 1951, 43, 1243.
9. Guin, J. A., Tarrer, A. R., Lee, J. M., Lo, L. and Curits, C. W., Ind. Eng. Chem. Process Des. Dev., 1979, 18, 371.
10. Anderson, R. P., "Low Cost Additives in the SRC Processes," Paper Presented at the Dept. of Energy Project Review Meeting on Disposable Catalysts in Coal Liquefaction held in Albuquerque, New Mexico, June, 1979.
11. Solvent Refined Coal (SRC) Process, Quarterly Technical Progress Report FE/496-155 Prepared for U.S. Dept. of Energy by The Pittsburg and Midway Coal Mining Co., Shawnee Missio, Kansas, March, 1979.
12. Skinner, R. W., and Givens, E. N., "Effects of Solvent Hydrogen Content in the SRC Process," Paper Presented at the 179th National Meeting of American Chemical Society, Houston, March, 1980.

TABLE 1
CHEMICAL ANALYSIS OF COAL SAMPLE

| | ELKHORN #2 WEIGHT % |
|---|------------------------|
| ULTIMATE ANALYSIS (AS RECEIVED) | |
| CARBON | 77.84 |
| HYDROGEN | 5.24 |
| OXYGEN | 7.20 |
| SULFUR | 1.08 |
| NITROGEN | 1.75 |
| PROXIMATE ANALYSIS (AS RECEIVED) | |
| ASH | 6.29 |
| MOISTURE | 1.55 |
| DISTRIBUTION OF SULFUR | |
| TOTAL SULFUR | 1.08 |
| SULFATE SULFUR | 0.04 |
| PYRITE SULFUR | 0.25 |
| ORGANIC SULFUR | 0.79 |

TABLE 3
ANALYSIS OF PYRITE

| | WEIGHT % |
|----------------------------------|----------|
| CARBON | 4.48 |
| HYDROGEN | 0.34 |
| NITROGEN | 0.61 |
| SULFUR | 41.34 |
| OXYGEN | 5.97 |
| IRON | 42.30 |
| OTHER IMPURITIES (BY DIFFERENCE) | 4.96 |
| TOTAL | 100.00 |

SURFACE AREA = 1.0 m²/g

TABLE 4
ANALYSIS OF IRON SULFATE

| | WEIGHT % |
|--------------------------------------|----------|
| FERROUS SULFATE, FeSO ₄ | 53.78 |
| IRON, Fe ₂ O ₃ | 0.06 |
| TITANIUM, TiO ₂ | 0.33 |
| MAGNESIUM SULFATE, MgSO ₄ | 1.80 |
| COPPER | 0.0004 |
| LEAD | 0.0005 |
| WATER OF CRYSTALLIZATION | 42.28 |
| TOTAL | 99.25 |

TABLE 2
ANALYSIS OF HEAVY DISTILLATE

| ELEMENT | WEIGHT % |
|---------------------------------|----------|
| CARBON | 89.44 |
| HYDROGEN | 7.21 |
| OXYGEN | 1.70 |
| NITROGEN | 1.10 |
| SULFUR | 0.55 |
| NUMBER AVERAGE MOLECULAR WEIGHT | 222 |

TABLE 5
LIQUEFACTION OF COAL IN THE PRESENCE AND ABSENCE OF PYRITE

| FEED COMPOSITION | 70% SOLVENT + 30% COAL | | 60% SOLVENT + 30% COAL + 10% PYRITE | |
|--------------------------------------|------------------------|-----------|-------------------------------------|-----------|
| | Fe CONC., WT. % COAL | TEMP., °F | Fe CONC., WT. % COAL | TEMP., °F |
| TEMP., °F | 825 | 850 | 825 | 850 |
| PRESSURE, PSIG | 2000 | 2000 | 2000 | 2000 |
| RESIDENCE TIME, MIN. | 35 | 39 | 37 | 39 |
| HYDROGEN TREAT RATE, MSCF/T | 18.9 | 23.0 | 19.9 | 22.5 |
| PRODUCT DISTRIBUTION, WT. % MAF COAL | | | | |
| HC | 5.2 | 7.0 | 5.7 | 10.6 |
| CO, CO ₂ | 0.7 | 0.6 | 0.9 | 1.2 |
| H ₂ S | 0.3 | 0.3 | 0.0 | 0.0 |
| OIL | 12.2 | 8.3 | 28.2 | 27.0 |
| ASPHALTENES | 21.2 | 21.6 | 24.3 | 22.3 |
| PREASPHALTENES | 44.2 | 43.4 | 29.6 | 25.6 |
| I.O.M. | 14.7 | 15.7 | 8.1 | 9.3 |
| WATER | 1.5 | 3.1 | 3.2 | 4.0 |
| CONVERSION, % MAF | 85.3 | 84.3 | 91.9 | 90.7 |
| HYDROGEN CONSUMPTION, * WT. % MAF | 0.64 | 0.53 | 1.68 | 2.41 |
| OIL HYDROGEN CONTENT, WT. % | | | | |
| START | 7.2 | 7.2 | 7.2 | 7.2 |
| FINISH | 7.2 | 7.2 | 7.5 | 7.5 |
| SRC SULFUR, % | 0.61 | 0.55 | 0.60 | 0.57 |

*HYDROGEN CONSUMPTION DOES NOT INCLUDE THE HYDROGEN REQUIRED FOR REDUCING FeS₂ TO FeS

TABLE 7
EFFECT OF IRON IMPREGNATION ON COAL LIQUEFACTION

| FEED COMPOSITION | NO | | YES | |
|--------------------------------------|----------------------|-----------|----------------------|-----------|
| | Fe CONC., WT. % COAL | TEMP., °F | Fe CONC., WT. % COAL | TEMP., °F |
| TEMP., °F | 825 | 850 | 825 | 850 |
| PRESSURE, PSIG | 2000 | 2000 | 2000 | 2000 |
| RESIDENCE TIME, MIN. | 35 | 37 | 33 | 41 |
| HYDROGEN TREAT RATE, MSCF/T | 18.9 | 19.9 | 20.6 | 27.3 |
| PRODUCT DISTRIBUTION, WT. % MAF COAL | | | | |
| HC | 5.2 | 7.0 | 3.5 | 4.4 |
| CO, CO ₂ | 0.7 | 0.6 | 0.6 | 0.5 |
| H ₂ S | 0.3 | 0.3 | 0.2 | 0.2 |
| OIL | 12.2 | 8.3 | 25.0 | 30.3 |
| ASPHALTENES | 21.2 | 21.6 | 19.1 | 20.8 |
| PREASPHALTENES | 44.2 | 43.4 | 35.8 | 27.5 |
| I.O.M. | 14.7 | 15.7 | 13.5 | 13.1 |
| WATER | 1.5 | 3.1 | 2.3 | 3.2 |
| CONVERSION, % MAF | 85.3 | 84.3 | 86.5 | 86.9 |
| HYDROGEN CONSUMPTION, * WT. % MAF | 0.64 | 0.53 | 0.40 | 0.60 |
| OIL HYDROGEN CONTENT, WT. % | | | | |
| START | 7.2 | 7.2 | 7.2 | 7.2 |
| FINISH | 7.2 | 7.2 | 7.1 | 7.0 |
| SRC SULFUR, % | 0.61 | 0.55 | 0.61 | 0.57 |

TABLE 8
IRON IMPREGNATION VERSUS PARTICULAR ADDITION

| FEED COMPOSITION | PYRITE | | IMPREGNATION | |
|--------------------------------------|----------------------|-----------|----------------------|-----------|
| | Fe CONC., WT. % COAL | TEMP., °F | Fe CONC., WT. % COAL | TEMP., °F |
| TEMP., °F | 850 | 100 | 850 | 100 |
| PRESSURE, PSIG | 2000 | 2000 | 2000 | 2000 |
| RESIDENCE TIME, MIN. | 35 | 38 | 38 | 41 |
| HYDROGEN TREAT RATE, MSCF/T | 24.2 | 22.2 | 24.2 | 27.3 |
| PRODUCT DISTRIBUTION, WT. % MAF COAL | | | | |
| HC | 10.2 | 9.9 | 10.2 | 4.4 |
| CO, CO ₂ | 0.9 | 0.9 | 0.9 | 0.5 |
| H ₂ S | 0.3 | 0.3 | 0.2 | 0.2 |
| OIL | 25.6 | 24.3 | 30.3 | 30.3 |
| ASPHALTENES | 22.3 | 18.6 | 22.3 | 20.8 |
| PREASPHALTENES | 28.2 | 32.3 | 28.2 | 27.5 |
| I.O.M. | 14.7 | 15.7 | 13.1 | 13.1 |
| WATER | 3.2 | 3.5 | 3.2 | 3.2 |
| CONVERSION, % MAF | 90.7 | 89.6 | 90.7 | 86.9 |
| HYDROGEN CONSUMPTION, * WT. % MAF | 1.75 | 1.81 | 1.75 | 0.80 |
| OIL HYDROGEN CONTENT, WT. % | | | | |
| START | 7.2 | 7.2 | 7.2 | 7.2 |
| FINISH | 7.3 | 7.5 | 7.3 | 7.0 |
| SRC SULFUR, % | 0.49 | 0.51 | 0.49 | 0.57 |

*HYDROGEN CONSUMPTION DOES NOT INCLUDE THE HYDROGEN REQUIRED FOR REDUCING FeS₂ TO FeS

TABLE 6
EFFECT OF PYRITE CONCENTRATION ON COAL LIQUEFACTION

| FEED COMPOSITION | 70% SOLVENT + 30% COAL | | 60% SOLVENT + 30% COAL + 10% PYRITE | |
|--------------------------------------|------------------------|-----------|-------------------------------------|-----------|
| | Fe CONC., WT. % COAL | TEMP., °F | Fe CONC., WT. % COAL | TEMP., °F |
| TEMP., °F | 850 | 850 | 850 | 850 |
| PRESSURE, PSIG | 2000 | 2000 | 2000 | 2000 |
| RESIDENCE TIME, MIN. | 35 | 39 | 37 | 39 |
| HYDROGEN TREAT RATE, MSCF/T | 24.2 | 22.2 | 22.5 | 22.5 |
| PRODUCT DISTRIBUTION, WT. % MAF COAL | | | | |
| HC | 10.2 | 9.9 | 10.6 | 10.6 |
| CO, CO ₂ | 0.9 | 0.9 | 1.0 | 1.2 |
| OIL | 25.6 | 24.3 | 27.0 | 27.0 |
| ASPHALTENES | 22.3 | 18.6 | 22.3 | 22.3 |
| PREASPHALTENES | 28.2 | 32.3 | 28.2 | 28.2 |
| I.O.M. | 14.7 | 15.7 | 8.1 | 9.3 |
| WATER | 3.2 | 3.5 | 4.0 | 4.0 |
| CONVERSION, % MAF | 90.7 | 89.6 | 90.7 | 90.7 |
| HYDROGEN CONSUMPTION, * WT. % MAF | 1.75 | 1.81 | 2.41 | 2.41 |
| OIL HYDROGEN CONTENT, WT. % | | | | |
| START | 7.2 | 7.2 | 7.2 | 7.2 |
| FINISH | 7.3 | 7.5 | 7.5 | 7.5 |
| SRC SULFUR, % | 0.49 | 0.51 | 0.57 | 0.57 |

*HYDROGEN CONSUMPTION DOES NOT INCLUDE THE HYDROGEN REQUIRED FOR REDUCING FeS₂ TO FeS

Figure 1
Variation in the Conversion of Coal
With the Concentration of Pyrite

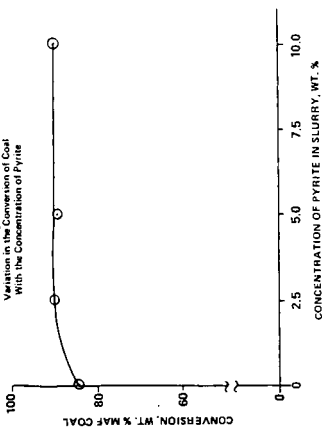


Figure 2
Variation in the Production of Gases and Water
With the Concentration of Pyrite

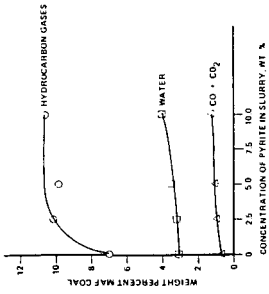


Figure 3
Variation in the Production of Oils
With the Concentration of Pyrite

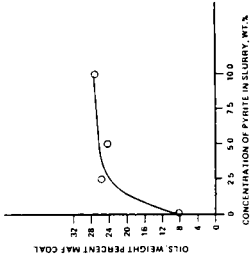


Figure 4
Variation in the Production of Asphaltenes and Preasphaltenes
With the Concentration of Pyrite

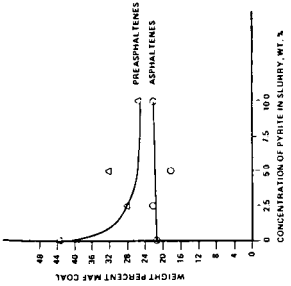


Figure 5
Variation of Hydrogen Consumption With the
Concentration of Pyrite

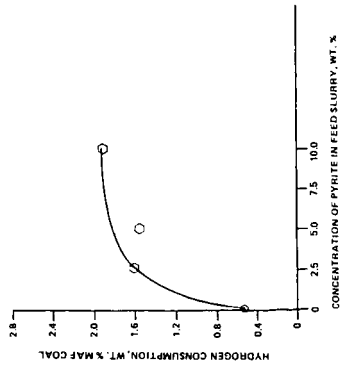


Figure 6
Variation of SRC Sulfur Content With the Concentration
of Pyrite

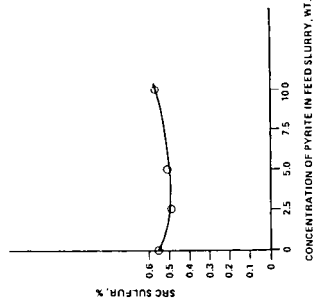


Figure 7
Iron Impregnation Versus
Particulate Addition

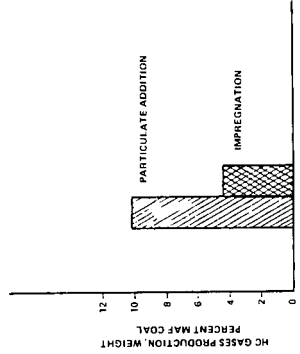
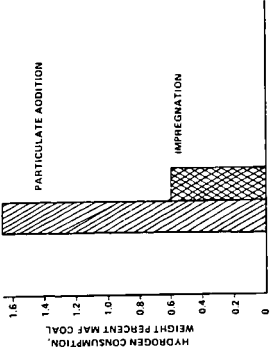


Figure 8
Iron Impregnation Versus
Particulate Addition



CATALYTIC HYDROPYROLYSIS OF COAL TO DISTILLATE OILS

Shaik A. Qader

Jet Propulsion Laboratory
California Institute of Technology
4800 Oak Grove Drive
Pasadena, California 91103

INTRODUCTION

Coal is predominantly aromatic in nature and deficient in hydrogen. It contains only about 4.5-5.0 percent hydrogen as compared to crude oils which contain 11-13 percent hydrogen. Coal therefore, can be converted to a crude oil type liquid either by removing carbon from it or by adding hydrogen to it. Pyrolysis processes come under the first category which produce large quantities of carbon rich char and small quantities of hydrogen rich tar. Under practical conditions of pyrolysis¹, tar yield varies between 20 and 25 percent with char yield of about 50 percent. Pyrolysis tars are poor in quality and require catalytic hydrotreatment for conversion to refined products.

The yield and quality of tar can be improved by carrying out coal pyrolysis under hydrogen pressure. In hydrolysis, hydrogen improves tar yield by stabilizing reactive fragments formed from coal during pyrolysis. In the absence of hydrogen, some of the reactive fragments undergo polymerization and condensation reactions forming char. Hydrogen also improves tar quality by promoting hydrocracking and hydrorefining of₂₋₈ tar during the pyrolysis process. In most of the hydrolysis work,²⁻⁸ light oils containing mostly BTX are produced in low yields of 10-20 percent. The hydrolysis processes operate at very high temperatures of 700-1000°C where the primary tar undergoes extensive hydrocracking forming BTX and gas.

The yield and quality of tar can be further improved by carrying out hydrolysis at medium temperatures of 500-600°C in the presence of a catalyst that promotes hydrogenation and hydrocracking reactions. Though work on pyrolysis and hydrolysis¹⁰ of coal was done¹ extensively, very little is known about catalytic hydrolysis. Schroeder¹¹ patented a catalytic hydrogenation process where he claimed that a bituminous coal impregnated with ammonium molybdate yielded 30-60 percent light oil at 800°C and 2000 psi pressure. Friedman et al¹² hydrogenated a New Mexico coal impregnated with one percent molybdenum in the form of ammonium molybdate in fixed and fluid beds. Most of the experimental work was done at 600-900°C under a pressure of 6000 psi. Most of the coal was converted to gas with a liquid yield of less than 20 percent. But high yield of coal liquid of up to 57 percent was obtained when the hydrogenation was carried out at 480°C under a pressure of 6000 psi. Steinberg and Fallon¹³ hydrolyzed a lignite impregnated with ammonium molybdate at 700°C and 1500 psi pressure in a free fall tubular reactor. The yield of liquid product was reported to be about 18-25 percent but the catalyst did not affect the conversion. Franklin et al¹⁴ studied the effect of mineral matter on rapid pyrolysis and hydrolysis of a bituminous coal and found no significant effect by iron-sulfur minerals at a hydrogen pressure of about 1000 psi. In this paper, the results of catalytic hydrolysis of coal in a hanging basket reactor and a fluid bed reactor are described. Refined distillate oils are obtained from coal at medium temperatures and pressures in the presence of a hydrocracking catalyst.

EXPERIMENTAL

The experimental work was done in a Hanging Basket Reactor (HBR) system shown in Figure 1 and a Fluidized Bed Reactor system shown in Figure 2. The Hanging Basket Reactor consists of a high pressure vessel of 2" i.d. and 4' long provided with a heater at the bottom and a basket at the top. The basket hangs from a shaft connected to a valve and carries a crucible. The HBR was designed for a pressure of 7000 psi at a temperature of 500°C. Physical mixtures containing one gram of coal and three grams of catalyst were taken in the crucible and the system was pressurized and heated to the desired conditions. After the system conditions were stabilized, the crucible was lowered to the hot zone and kept there for different periods of time and then raised to the original position. The lowering and raising operations take 2-3 seconds. After this operation, the system was cooled, depressurized and the crucible was taken out of the system. The weight lost by coal during the reaction was taken as the conversion. Some experiments were also done with 50 and 100 grams of coal in a 1-litre Magne-drive Autoclave under simulated conditions of the HBR work to prepare bulk quantity of liquid product for analysis.

The Fluid Bed Reactor System was designed for a working pressure of 4000 psi at a maximum temperature of 700°C. It consists of a fluid bed reactor of 1.5" i.d. and 4' height, two hydrogen heaters, three coolers, two liquid collection bottles, a steam injection system, a flow control valve, a dry gas meter and a pump to circulate chilled water through the coolers. The fluid bed reactor has a liner of 1.25" i.d. and 3.5' height which is provided with a perforated disc at the bottom to support the coal-catalyst mixture. The system is fully instrumented with controllers, indicators and recorders for temperature, pressure, Δp and gas flow. The reactor system was housed in a high pressure cell and operated from outside at the control panel.

The fluid bed reactor was operated in a batch mode with hydrogen flowing through it continuously. A physical mixture of coal and catalyst was placed in the liner which was then introduced into the reactor. The size of coal and catalyst and fluidization velocity were predetermined using a glass fluid bed reactor at ambient temperature. Fluidization studies with coal-catalyst mixtures showed that coal and catalyst particles of 35-150 mesh fluidize well with good mixing at velocities of 0.25 to 0.5 ft./sec. which give gas phase residence times of 6-12 seconds for a coal-catalyst fluid bed height of 3'. After the introduction of the liner into the reactor, the system was flushed with nitrogen, pressurized and closed to the atmosphere. The hydrogen heaters were heated to the desired temperature and the nitrogen in the system was replaced by hydrogen through a bypass line. Flow of hydrogen through the bypass was continued until the desired gas flow and temperature were attained. At that stage, the hot hydrogen flow was diverted through the reactor where it came into contact with the coal and catalyst and fluidized the mixture. The reaction was carried out for 10 to 30 minutes. At the end of the reaction period, the hydrogen flow was diverted back through the bypass and was replaced by nitrogen. During the operation, chilled water was circulated through the coolers. The liquid product was condensed in the coolers and was collected in the collection bottles. The gas was let out into the atmosphere through the gas meter where its volume was recorded. The solid char remained in the liner with the catalyst.

A bituminous coal from Utah was used in the HBR work. The analysis of the coal is given in Table 1. A Wyoming subbituminous and a Kentucky bituminous coal

were used in the FBR work. The analysis of the coals is given in Table 2.

Prereduced tungsten disulfide (WS_2) of -200 mesh size was used in the HBR experiments. A commercial catalyst containing sulfides of cobalt and molybdenum supported on silica-alumina was used in the FBR experiments. The catalyst was ground to 60-140 mesh size before use. The analyses of coals, coal liquids and gases were done by standard methods.

RESULTS AND DISCUSSION

The Hanging Basket Reactor experiments were done with and without the catalyst at 450-550°C under a pressure of 2000-4000 psi. The effect of reaction time and temperature on coal conversion is shown in Figure 3. The conversion increased with temperature and time. In the case of non-catalytic experiments, a maximum conversion of 43 percent was obtained at 550°C and 4000 psi pressure. The addition of catalyst increased the conversion significantly. Coal conversion of over 90 percent was obtained at 550°C and 4000 psi pressure. The data show that adequate catalytic effect can be obtained in coal conversion when coal and catalyst are present in a physical mixture at high temperatures, high pressures and high catalyst-coal ratios. The data also show that high coal conversions can be obtained in catalytic hydrolysis at short reaction times of less than 10 minutes.

The effect of hydrogen pressure and reaction time on coal conversion at 550°C is shown in Figure 4. Hydrogen pressure did not affect the non-catalytic conversion but increased the catalytic conversion significantly. It was reported in the earlier publications¹⁵ that hydrogen pressure increased conversion in the non-catalytic hydrolysis of coal. But most of the published work was carried out at lower pressures and thus can not be compared with the data obtained in the present work. It is therefore concluded from the data of Figure 4 that hydrogen pressure increases coal conversion in non-catalytic hydrolysis only at pressures lower than 2000 psi but it does not affect the conversion at pressures of 2000 psi or higher unless a catalyst is present. The pressure effect in catalytic hydrolysis appears to be similar to the effect observed in catalytic hydrogenation of coal.^{16,17}

Significant differences were observed in the nature of liquid and gaseous products obtained in the HBR work. Table 3 contains the analysis of liquid and gaseous products. The product obtained in the non-catalytic work was a very high boiling liquid and contained large quantities of preasphaltene, asphaltene, sulfur and nitrogen. On the other hand, the catalytic product was lighter and contained substantial amounts of light and middle oils. The preasphaltene, asphaltene, sulfur and nitrogen content of the product was very low. The properties of the catalytic liquid product indicate that the primary liquid formed from coal underwent hydrorefining and hydrocracking in the presence of the catalyst yielding a refined distillable oil. The data suggest that in catalytic hydrolysis the conversion of coal to liquid product takes place by a two step reaction mechanism shown in Figure 5. In pyrolysis, the organic matter of coal undergoes thermal breakdown forming an intermediate product consisting of reactive fragments. Some of the fragmented coal molecules undergo stabilization forming tar and some of the fragments undergo polymerization and condensation reactions forming coke or char. In hydrolysis, hydrogen reacts with the fragmented coal molecules and stabilize them before they undergo polymerization and condensation reactions which lead to coke or char formation. Tar yield

therefore increases in hydropyrolysis when compared to just pyrolysis of coal. In catalytic hydropyrolysis, the primary coal liquid appears to be forming due to pyrolysis and catalytic hydrogenation of coal. The primary coal liquid in turn undergoes catalytic hydrocracking forming a lighter liquid product.

It is concluded from the foregoing discussion on catalytic hydropyrolysis that physical contact between coal and a solid catalyst provides adequate catalytic effect to get high coal conversion of up to 90 percent. The coal undergoes liquefaction and the liquefied coal undergoes refinement in a single step, thus producing good quality light and middle oils. Though not discussed in this paper, catalyst to coal ratios of 3 to 1 were found to provide adequate catalytic effect and to reduce agglomeration of caking coals when the size of coal was >200 mesh. It is therefore feasible to produce refined distillate oils in high yields from caking bituminous coals in a single step by catalytic hydropyrolysis under the conditions used in the HBR work. The HBR system does not have any potential for use as a practical system to liquefy coal on a large scale in a continuous manner. An evaluation of several practical reactor systems led to the conclusion that a fluidized bed reactor is the most suitable for this application.

The results of the Fluidized Bed Reactor System are given in Tables 4-6. Table 4 contains the test conditions used in the FBR work. The size of coal and catalyst and fluidization velocity were determined from fluidization studies made in a glass fluid bed reactor at ambient temperature and atmospheric pressure with nitrogen as the fluidizing gas. The temperature and pressure were selected from the HBR work. Table 5 contains the material balance of FBR work. The yield of liquid product from the subbituminous coal was about 33 percent as compared to about 43 percent from the bituminous coal. The hydrogen consumption was 2.5 and 3.8 percent respectively. It is conceivable that the liquid product yield can be improved under optimal processing conditions. Table 6 contains the properties of liquid products. The coal liquids contain small amounts of sulfur and benzene insolubles and large quantities of light and middle oils. The liquid from the subbituminous coal contains 75 percent distillate and the liquid from the bituminous coal contains 86 percent distillate boiling up to a temperature of 450°C. The data indicate that coal liquefaction and refining of liquefied coal took place in a single step in the FBR which is in conformity with the HBR data. The data also support the two step reaction mechanism shown in Figure 5.

ACKNOWLEDGMENT

This work was supported by the Energy Systems Division of the National Aeronautics and Space Administration and the JPL Director's Discretionary Fund.

REFERENCES

1. Jones, J.F., Schmid, M.R., and Eddinger, R.T., "Fluid Bed Pyrolysis of Coal", *Chem. Eng. Prog.*, 60, No.6, 69 (1964).
2. Squires, A.M., Graff, R.A., and Dobner, S., "Flash Hydrogenation of a Bituminous Coal", *Science*, 189, 793 (1975).
3. Pelofsky, A.H., Greene, M.I., and LaDelfa, C.J., "Short Residence Time (SRT) Coal Hydropyrolysis", *American Chemical Society National Meeting, Fuel Chemistry Division Preprints*, 21, No.5, 154 (1976).
4. Coles, E.T., "CoalCon's Hydrocarbonization Technology", paper presented at the 82nd National Meeting of the American Institute of Chemical Engineers, Atlantic City, New Jersey, August 29 - September 1, (1976).
5. Beeson, J.L., Duncan, D.A., and Oberle, R.D., "Flash Hydrogenation of Lignite and Bituminous Coal in an Entrained Flow Reactor", *American Chemical Society National Meeting, Fuel Chemistry Division Preprints*, 24, No.3, 72 (1979).
6. Finn, M.J., Fynes, G., Ladner, W.R., and Newman, J.O.H., "The Formation of BTX by the Hydropyrolysis of Coal", *American Chemical Society National Meeting, Fuel Chemistry Division Preprints*, 24, No.3, 99 (1979).
7. Ranieri, F.D., Combs, L.P., and Falk, A.Y., "Experimental Investigation of Peat Hydrogasification", *American Chemical Society National Meeting, Fuel Chemistry Division Preprints*, 24, No.3, 64 (1979).
8. Cypres, R., "Hydrogenopyrolysis of Coal and Coal Derivatives", *American Chemical Society National Meeting, Fuel Chemistry Division Preprints*, 26, No.3, 44 (1981).
9. Anthony, D.B., and Howard, J.B., "Coal Devolatilization and Hydrogasification", *AIChE Journal*, 22, 625 (1976).
10. Belt, R.J., and Bissett, L.A., "Assessment of Flash Pyrolysis and Hydro-pyrolysis", METC/R1-79/2, U.S. Department of Energy, Morgantown Energy Technology Center, Morgantown, West Virginia, (1978).
11. Schroeder, W.C., U.S. Patent 3, 030, 298 (1962).
12. Friedman, S., Hiteshue, R.W., and Schlesinger, M.D., "Hydrogenation of New Mexico Coal at Short Residence Time and High Temperature", *Bureau of Mines Report of Investigations 6470*, United States Department of the Interior, (1964).
13. Steinberg, M., and Fallon, P., "Coal Liquefaction by Rapid Gas Phase Hydrogenation", *American Chemical Society National Meeting, Petroleum Chemistry Division Preprints*, 20, No.2, 321 (1975).
14. Franklin, H.W., Peters, W.A., and Howard, J.B., "Mineral Matter Effects on the Rapid Pyrolysis and Hydropyrolysis of a Bituminous Coal", *American Chemical Society National Meeting, Fuel Chemistry Division Preprints*, 26, No.3, 35 (1981).
15. Fallon, P.T., Bhatt, B., and Steinberg, M., "The Flash Hydropyrolysis of Lignite and Subbituminous Coals to both Liquid and Gaseous Hydrocarbon products", *American Chemical Society National Meeting, Fuel Chemistry Division Preprints*, 24, No.3, 52 (1979).
16. Qader, S.A., Haddadin, R.A., Anderson, L.L., and Hill, G.R., "Coal Can Also Yield Liquid Fuels", *Hydrocarbon Processing*, 48, No.9, 800 (1969).
17. Qader, S.A., "Catalytic Hydrosolvation Process Converts Coal to Low Sulfur Liquid Fuel", *Energy Sources*, 3, No.3/4, 323 (1978).

Table 1. Analysis of Utah Coal

| <u>Proximate Analysis, Wt. %</u> (Dry basis) | | |
|---|---|-------|
| Volatiles | : | 46.8 |
| Fixed Carbon | : | 46.5 |
| Ash | : | 6.7 |
| <u>Ultimate Analysis, Wt. %</u> (Dry basis) | | |
| Carbon | : | 81.22 |
| Hydrogen | : | 5.99 |
| Nitrogen | : | 1.61 |
| Sulfur | : | 2.41 |
| Oxygen (By difference) | : | 9.18 |

Table 2. Analysis of Coals

| <u>Proximate Analysis, Wt. %</u> (Dry basis) | Subbituminous Coal (Wyoming) | Bituminous Coal (Kentucky #6 and #11) |
|---|---------------------------------|--|
| Volatiles | : 43.22 | 46.43 |
| Fixed Carbon | : 50.55 | 44.17 |
| Ash | : 6.23 | 9.40 |
| <u>Ultimate Analysis, Wt. %</u> (Dry basis) | | |
| Carbon | : 70.21 | 73.44 |
| Hydrogen | : 4.94 | 5.30 |
| Nitrogen | : 1.05 | 1.21 |
| Sulfur | : 0.71 | 3.35 |
| Oxygen (By difference) | : 16.86 | 7.30 |

Table 3. Analysis of HBR Products

| <u>Reaction Conditions</u> | | | |
|---|------------------|----------------------|------------|
| | Temperature | : | 550°C |
| | Pressure | : | 400 psi |
| | Reaction time | : | 10 minutes |
| <u>Liquid product</u> | <u>Catalytic</u> | <u>Non-Catalytic</u> | |
| Sp. gr. at 25°C | : 0.9915 | - | |
| Sulfur, Wt. % | : 0.42 | 1.24 | |
| Nitrogen, Wt. % | : 0.68 | 1.34 | |
| Light oil, Wt. % (-200°C) | : 18.0 | 3.0 | |
| Middle distillate, Wt. % (200-450°C) | : 72.0 | 28.0 | |
| Heavy liquid, Wt. % (+450°C) | : 10.0 | 69.0 | |
| <u>Gaseous product</u> | | | |
| Methane, Vol. % | : 11.0 | 28.0 | |
| Ethane, Vol. % | : 24.0 | 40.0 | |
| Propane, Vol. % | : 36.0 | 17.0 | |
| Butanes, Vol. % | : 29.0 | 15.0 | |

Table 4. FBR Test Conditions

| | | |
|---------------------------------|---|--------|
| Wt. of coal in each test, g | : | 130 |
| Wt. of catalyst in each test, g | : | 145 |
| Size of coal, Tyler mesh | : | 35-60 |
| Size of catalyst, Tyler mesh | : | 60-140 |
| Fluidization velocity, ft./sec. | : | 0.45 |
| Temperature, °C | : | 550 |
| Pressure, PSI | : | 2000 |
| Reaction time, min. | : | 20 |

Table 5. FBR Material Balance
(daf Coal)

| | | Subbituminous Coal | Bituminous Coal |
|---|---|-----------------------|--------------------|
| <u>Input, g.</u> | | | |
| Coal | : | 100.0 | 100.0 |
| Hydrogen | : | <u>2.5</u> | <u>3.8</u> |
| TOTAL | | 102.5 | 103.8 |
| <u>Output, g.</u> | | | |
| Liquid | : | 32.6 | 42.7 |
| Gas (Includes H ₂ S and NH ₃) | : | 12.3 | 17.0 |
| Water | : | 3.5 | 5.3 |
| Solid | : | 54.1 | 38.8 |

Table 6. Analysis of FBR Liquid Product

| | | Subbituminous Coal | Bituminous Coal |
|--|---|-----------------------|--------------------|
| Sp. gr., 25°C | : | 1.02 | 1.04 |
| Sulfur, wt.% | : | 0.38 | 0.41 |
| Nitrogen, wt.% | : | 1.04 | 1.11 |
| Light oil, wt.% (-200°C) | : | 15.0 | 17.0 |
| Middle distillate, wt.% (200-450°C) | : | 60.0 | 69.0 |
| Benzene insolubles, wt.% | : | 9.1 | 6.1 |

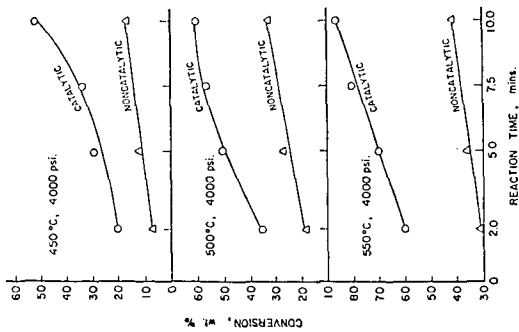


FIGURE 3. EFFECT OF TEMPERATURE AND REACTION TIME ON CONVERSION

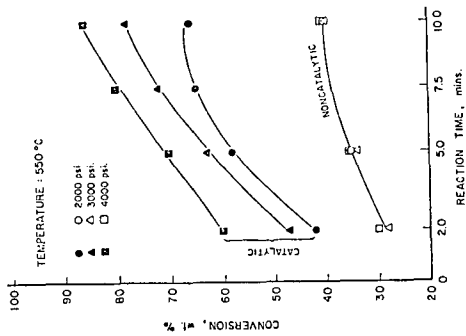


FIGURE 4. EFFECT OF PRESSURE AND REACTION TIME ON CONVERSION

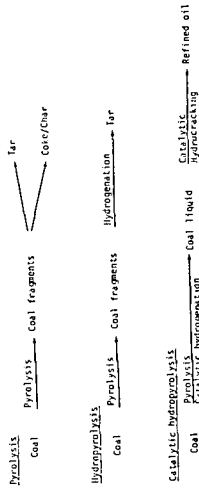


FIGURE 5. MECHANISM OF CATALYTIC HYDROLYSIS

THE APPLICATION OF FT-IR AND SOLID STATE ¹³C NMR
TO THE CHARACTERIZATION OF A SET OF VITRINITE CONCENTRATES

D.W. Kuehn, A.Davis, R.W. Snyder, M. Starsinic and P.C. Painter

The Pennsylvania State University, University Park, PA 16802

J. Havens and J.L. Koenig

Case Western Reserve University, Cleveland, Ohio 44106

INTRODUCTION

In a recent review of coal structure Neavel (1) remarked that coal is analogous to fruitcake in that it is an aggregate of different and distinguishable components. Consequently, the characterization of coal structure (or for that matter, fruitcake) demands a recognition and investigation of the separate components, macerals. For most U.S. coals the major maceral type present is vitrinite, so that an understanding of many structure/property relations will ultimately depend on a knowledge of the structure of this maceral. As part of a systematic study of the variability of coal properties within a single seam, a set of vitrinite concentrates has been obtained from samples taken from the Lower Kittanning seam (2). This seam is particularly interesting because of its broad extent and the range of environments by which it is thought to have been affected. However, even though the far from trivial task of obtaining and storing these maceral concentrates under optimum conditions has been accomplished (2), there remains the formidable task of structural characterization.

Because of the heterogeneous, non-crystalline, largely insoluble nature of coal, it is practically impossible to apply the traditional methods of organic and physical chemistry to structural characterization work. Such methods essentially rely on the separation and identification of the constituent simple molecules of a complex system. In fact, for coal it is a notoriously difficult task to obtain reliable data on even the most fundamental property, the average molecular weight and the molecular weight distribution of the macromolecular constituents. Consequently, the most useful information concerning coal structure that we can reasonably expect to obtain is a quantitative identification of the molecular types of hydrocarbons present (eg aromatic and aliphatic carbon) and the type and distribution of specific functional groups (aliphatic CH, CH₂ and CH₃; phenolic OH, alkyl OH, carbonyl etc). It is precisely this information that spectroscopic methods are uniquely capable of elucidating.

Spectroscopic techniques have been widely applied to the study of coal, but have met with only limited success (3-6). Advances in spectroscopic instrumentation however, should allow us to obtain new insights into coal structure. Of particular significance is the recent application of Fourier transform infrared (FT-IR) spectroscopy (7-17) and solid state ¹³C NMR spectroscopy, using magic-angle spinning in conjunction with cross-polarization and high power decoupling (18-21). In this communication we will consider the initial results of applying these two techniques to the set of vitrinite concentrates mentioned above.

SAMPLE CHARACTERISTICS

A set of 24 vitrinite concentrates were selected for initial study. These samples have been characterized by a number of methods and an extensive body of basic data has been reported (reference 2 and subsequent reports) Space does not permit reproduction of all of this data here. However, Neavel (1) has pointed out the critical importance of reporting reflectance values and the petrographic analysis of coals on which structural studies are performed. Accordingly, a plot

of reflectance as a function of carbon content of the concentrates used in this study is shown in Figure 1. Petrographic analysis of the concentrates demonstrated that most were 95-96% vitrinite with one or two higher (up to 98%) and one odd sample that was significantly lower (88% vitrinite).

TYPE OF INFORMATION THAT CAN BE OBTAINED FROM FT-IR AND ^{13}C NMR

Both FT-IR and ^{13}C NMR have already been used to obtain valuable information concerning coal structure. However, in many ways these techniques are still being developed and it should be possible to obtain new information as instruments and methodology are improved. In this section we will briefly describe the type of complementary information that can be obtained from each method and anticipate areas where we believe advances can be made.

Typically, infrared spectroscopy is sensitive to specific functional groups. The spectra of three of the vitrinite concentrates, chosen so as to represent samples of different rank, are presented in Figure 2. Four regions of the spectrum have been used to obtain quantitative information; the O-H stretching region near 3400 cm^{-1} , the aromatic C-H stretching modes between 3100 and 3000 cm^{-1} , the aliphatic C-H stretching modes between 3000 and 2800 cm^{-1} , and the aromatic C-H out-of-plane bending modes between 900 and 700 cm^{-1} .

The central problem with infrared spectroscopic studies of coal is the absence of reliable extinction coefficients (relating band intensities to the concentration of the corresponding functional group). Usually, the integrated intensity in an entire region of the spectrum (for example the aliphatic C-H stretching modes) is used and the extinction coefficients of individual bands are thus averaged. Calibration has in the past most often been based on model compound work or on proton magnetic resonance studies of coal extracts. More recently, Solomon (16,17) has equated the concentration of hydrogen containing functional groups to the total hydrogen determined by elemental analysis in order to obtain extinction coefficients. We have previously discussed the problems associated with infrared analysis (22,23), the most critical of which would appear to be the use of entire regions of the spectrum rather than individual bands. It may be that there is no viable alternative to this approach, but one possibility is to use well-defined curve resolving methods. We have previously reported (22,23) the use of such procedures in distinguishing the products of acetylation. This has allowed us to separately determine phenolic OH, alkyl OH and NH groups. We have recently applied these methods to the aromatic C-H out-of-plane bending modes between 900 and 700 cm^{-1} . These results will be considered below in the context of the analysis of vitrinite concentrates.

In most of the solid state ^{13}C NMR results reported to date, including those utilizing magic angle spinning and cross-polarization (18-21), only two broad bands are usually discerned, one for aromatic carbon and one for aliphatic. A careful examination of these spectra reveals the presence of shoulders, but the signal to noise ratio is such that they are not well defined. Nevertheless, the spectra allow useful estimates of the degree of aromaticity, f_a , to be obtained. We have recently applied to coal studies a spectrometer with a static field of 3.5T , approximately 2.5 times the field strength for which most ^{13}C spectra of solid coals have been reported. The resulting increase in sensitivity and potential resolution are considerable, as demonstrated by the spectrum of a vitrinite concentrate shown in Figure 3. Shoulders are clearly visible on both the aromatic and aliphatic peaks and can be readily assigned using appropriate polymer model compounds. We have previously reported the surprising but satisfying similarities between the infrared spectra of certain phenolic resins and coal (22). These materials should also be an important aid in assigning shoulders in the aromatic and aliphatic resonances of coals. The spectrum of a simple phenol-formaldehyde resin and a phenol/dihydroxynaphthalene-formaldehyde copolymer are also presented in Figure 3. Based on the known structure of these polymers a

number of assignments can be made. For example, in the model compounds aromatic carbons directly attached to hydroxyl groups resonate near 153 ppm and this agrees well with a low field shoulder on the aromatic resonance of vitrinite concentrates. This assignment can also be confirmed by acetylation studies. The ^{13}C NMR spectrum of a coal before and after acetylation is presented in Figure 4, together with a difference spectrum. A negative peak centered near 155 ppm indicates the loss of carbon attached to phenolic OH groups. Furthermore, the carbonyl resonance near 170 ppm and the methyl resonance near 22.2 ppm characteristic of the acetyl groups introduced into the coal can be clearly distinguished and used in conjunction with FT-IR studies of the same samples to obtain quantitative data.

The potential of suitable polymeric materials as models for coal is clearly outstanding. However, before proceeding to a discussion of some of the results of the analysis of vitrinite concentrates we wish to draw attention to another procedure that should be extremely useful in resolving shoulders on the broad aromatic and aliphatic resonances of coal macerals. We are presently only just starting to apply this method to coal studies, but preliminary results are sufficiently interesting to report here. It is possible to use pulse sequences to differentiate among carbons contributing to the broad aromatic and aliphatic resonances (21). Figure 5 shows the application of a sequence which incorporates a delay before the beginning of acquisition during which the proton pulse is switched off (24). The protonated carbons dephase preferentially during this period, leaving only the nonprotonated carbons to contribute to the accumulated free induction decay. It can be seen from the difference spectrum shown in Figure 5 that both the aliphatic and the high field side of the aromatic resonance consist of protonated carbons. This type of information should prove extremely valuable in conjunction with FTIR studies, where bands due to various aliphatic groups (CH , CH_2 and CH_3) and aromatic hydrogen arrangements (lone C-H, two adjacent C-H etc.) can be observed. It should be noted that weak spinning sidebands are observed in this spectrum. These arise when the magic-angle rotation rate is less than the chemical shift anisotropy, as is almost always the case for the aromatic resonances of coal. The contribution of these sidebands can be accounted for by various methods, but recently a pulse sequence has been introduced which allows elimination of first order sidebands (25). Both this pulse method and a correction based on the observed intensity of the high field aromatic sideband have been applied to coal studies. The aromatic carbon fraction f_a was determined to be the same.

ANALYSIS OF VITRINITE CONCENTRATES

Our initial aim in these studies is to correlate the concentration of various functional groups to rank parameters. In preliminary work we plotted the area of bands assigned to specific functional groups against %C (dmmf). A typical result is shown in Figure 6, where the area of the 1770 cm^{-1} band in the acetylated vitrinite concentrates has been used. This band area is a measure of the concentration of phenolic OH groups (22, 23). We found much less scatter when our spectroscopic data was plotted against reflectance, as illustrated in Figure 7. It can be seen that the concentration of phenolic hydroxyl groups drops off in an almost linear fashion with increasing rank of the coal. A band at 1740 cm^{-1} representing alkyl OH concentration (22, 23) displays precisely the same behavior, but its intensity is almost exactly half of the 1770 cm^{-1} band. (In fact, a plot of the 1770 cm^{-1} band against the 1740 cm^{-1} band is linear). Conversion factors relating the intensities of these bands have been determined (26) and total OH concentration, (measured as % O as OH) for the lowest rank coal shown in Figure 7 is about 6%.

In order to determine the concentration of aliphatic and aromatic CH groups as a function of rank equivalent extinction coefficients need to be determined. Values are available in the literature and we have applied similar calibration procedures. We have little faith in the results, however. There are a number of reasons for

this, the most important of which is that entire areas of the spectrum are used for measuring aliphatic and aromatic areas, as we noted in the introduction to this work. As the bands in these regions may each be independently related to rank parameters considerable scatter in the results can be anticipated. This is precisely what we observe, as shown in Figure 8. The aliphatic C-H stretching and aromatic out-of-plane bending modes ($900-700\text{ cm}^{-1}$) form almost a "scatter-shot" pattern. Of course this behavior could represent incompetent sample preparation and errors in methodology on our part, but the evidence indicates otherwise. The aromatic C-H stretching mode shows a nice consistent trend to increasing values with increasing rank. (Unfortunately, because this band is weak it is not the most useful for quantitative work). Furthermore, if we consider individual bands, carefully curve resolved using precisely defined criteria (22,23), then a relationship to rank of aliphatic and aromatic C-H groups to rank emerges. For example, Figure 9 shows the intensity of the 2853 cm^{-1} mode, representing aliphatic CH_2 groups, as a function of reflectance. The concentration of these groups clearly decreases with increasing rank. Similarly, certain bands in the aromatic C-H out-of-plane bending region increase in intensity as a function of the rank of vitrinite rank, as shown in Figure 10 using the 753 cm^{-1} band (4 adjacent aromatic C-H groups) as an example. Consequently, we can conclude that the scatter in the results observed using integrated intensities of entire spectral regions makes a major contribution to poorly defined behavior as a function of rank. However, if we consider individual bands assigned to specific functional groups, a pattern of behavior emerges.

One other reason for the scatter in the results obtained by plotting the integrated intensity of the aromatic C-H out-of-plane bending modes became apparent from our curve-resolving work. Also shown in Figure 10 is a plot of the intensity of a band near 830 cm^{-1} as a function of reflectance. Clearly, this band behaves differently to the 753 cm^{-1} band. The curve resolved $900-700\text{ cm}^{-1}$ region of the spectrum of a typical vitrinite concentrate is shown in Figure 11. (The initial positions and half widths of the bands were initially well defined using derivative techniques, as discussed previously (22,23), so that we can be reasonably confident that the bands shown in Figure 11 actually exist and are not artifacts of the curve resolving procedure). Bands at 801, 815 and 864 (assigned to 3 adjacent, 2 adjacent and lone aromatic C-H groups, respectively) display the same trend with rank as the 753 cm^{-1} band shown in Figure 10. However, the 785 cm^{-1} band displayed behavior similar to the 830 cm^{-1} band. We suggest that these bands have at least a partial contribution from CH_2 rocking modes that are expected to appear in this region of the spectrum. We are presently synthesizing phenolic resins that will allow us to assign these modes with more certainty. However, if we plot the total intensity of the aromatic out-of-plane bending modes, less the contribution of the 830, 785 cm^{-1} bands, against reflectance, a good correlation to rank emerges, as shown in Figure 12.

One result of these studies is that there is clearly an increase in aromatic C-H and loss of phenolic OH as a function of increase in rank. In fact, these two trends are related, as shown in Figure 13, where the area of the acetylated phenolic OH band (1770 cm^{-1}) is plotted against the total area of the $900-700\text{ cm}^{-1}$ out-of-plane modes (less the contribution of the 830, 785 cm^{-1} bands). Of course, there is not simply a straight replacement of phenolic OH by aromatic C-H with increasing rank, as the ^{13}C NMR results show an increasing degree of aromaticity with reflectance, as shown in Figure 14. (At the time of writing not all of the samples had been characterized by NMR).

Although these results demonstrate the trends in the concentration of specific functional groups in vitrinite concentrates as a function of rank, there is obviously additional work required to convert infrared band intensities to a quantitative measure of specific functional groups. In this respect we are pursuing the use of polymer model compounds and ^{13}C NMR pulse methods, which should provide the necessary data. It was shown above that the contribution of protonated carbons to

the NMR spectrum can be determined by such methods, allowing a quantitative determination of aromatic C-H. This can then be used to calibrate the intensities of the aromatic C-H out-of-plane bending modes.

ACKNOWLEDGEMENTS

The authors gratefully acknowledge the financial support of the Department of Energy under contract No. DE-AC22-OP30013 and the Penn State Cooperative Program in Coal Research.

REFERENCES

1. Neavel, R.C. Coal Structure and Coal Science: Overview and Recommendations, Chapter 1 in Coal Structure, Advances in Chemistry Series No. 192. (M.L. Gorbaty and K. Ouchi, editors).
2. Davis, A. "A data base for the analysis of compositional characteristics of coal seams and macerals", Quarterly Technical Progress Report, May-July 1980, D.O.E. contract DOE - 30013-2.
3. Friedel, R.A. in Applied Infrared Spectroscopy, p. 312, Edited by Kendall, D. N., Reinhold, New York (1966).
4. Dryden, I.G.C. in 'The chemistry of coal utilization' (H.H. Lowry, Ed.) Suppl. Vol. John Wiley and Sons, New York, p. 232 (1963).
5. Speight, J.P. Applied Spectroscopy Reviews (ed. E.G. Brame, Jr.) 5, 211 (1971).
6. Speight, J.G. in 'Analytical Methods for Coal and Coal Products', (C. Karr, Jr. ed.), volume II, 75 (1978) Academic Press.
7. Painter, P.C., Coleman, M.M., Jenkins, R.G., Whang, P.W. and Walker, P.L., Jr., Fuel, 57, 337 (1978).
8. Painter, P.C., Coleman, M.M., Jenkins, R.G., and Walker, P.L., Jr. Fuel, 57, 125 (1978).
9. Painter, P.C., Snyder, R.W., Youtcheff, J., Given, P.H., Gong, H. and Suhr, N., Fuel 59, (1980).
10. Painter, P.C., Stepusin, S., Snyder, R.W. and Davis, A. Applied Spectroscopy (In Press).
11. Painter, P.C., Youtcheff, J. and Given, P.H., Fuel, 59, 523 (1980).
12. Painter, P.C. and Coleman, M.M., Fuel, Vol. 58, 301 (1979).
13. Painter, P.C., Yamada, Y., Jenkins, R.G., Coleman, M.M. and Walker, P.L., Jr., Fuel, Vol. 58, 293 (1979).
14. Painter, P.C., Snyder, R.W., Pearson, D.E. and Kwong, J., Fuel 59, 282 (1980).
15. Painter, P.C., Coleman, M.M., Snyder, R.W., Mahajan, O., Kamatsu, M. and Walker, P.L., Jr., Applied Spectroscopy (In Press).
16. Solomon, P.R. ACS Division of Fuel Chemistry Preprints 24 #3, 184 (1979) and Advances in Chemistry series #192, 95 (1981).
17. Solomon, P.R. Paper presented at meeting, Chemistry and Physics of Coal Utilization, Morgantown, WV, June 2-4 (1980), to be published.
18. G.E. Maciel, V.J. Bartuska, and F.P. Miknis, Fuel 58, 391 (1979).
19. H.A. Resing, A.N. Garroway, and R.N. Hazlett, Fuel 57, 450 (1978).
20. E.P. Miknis, G.E. Maciel, and V.J. Bartuska, Org. Geochem. 1, 169 (1979).
21. F.P. Miknis, M. Sullivan, and G.E. Maciel, Org. Geochem., in press.
22. Painter, P.C., Snyder, R.W., Starsinic, M., Coleman, M.M., Kuehn, D. and Davis, A., Applied Spectroscopy, 35, 475 (1981).
23. Painter, P.C., Snyder, R.W., Starsinic, M., Coleman, M.M., Kuehn, D. and Davis, A., Adv. Chem. Ser. (to be published).
24. Frey, M.H. and Opella, S.J., J.C.S. Chem. Comm. 474 (1980).
25. Dixon, W.T. at the 22nd Experimental NMR Conference, Asilomar, CA (1981).
26. Snyder, R.W. and Painter, P.C. (to be published).

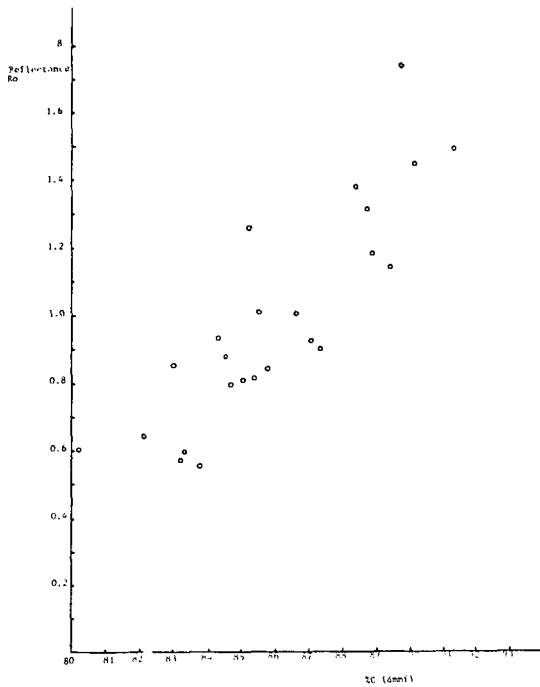


Figure 1. Plot of reflectance (Ro) values vs % C (dmmf) for a set of vitrinite concentrates.

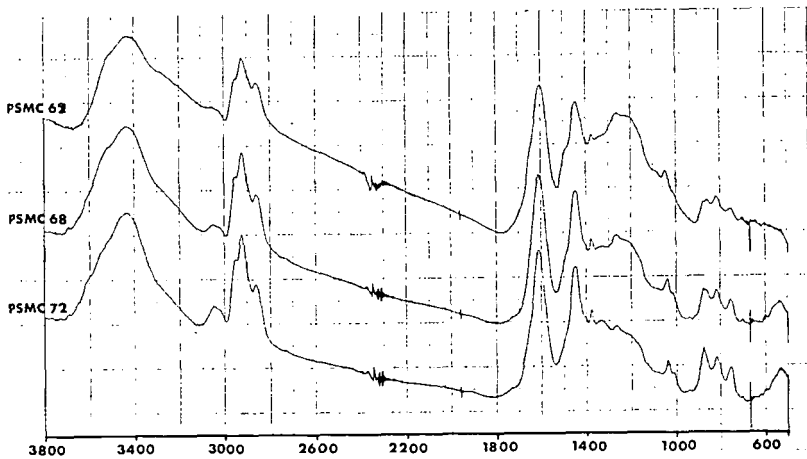


Figure 2. FT-IR spectra of three vitrinite concentrates obtained on a Digilab FTS 15B instrument (400 scans at 2 cm^{-1} resolution). Top to bottom, PSMC 67 (83.22% C dmmf), PSMC 68 (87.04% C dmmf), PSMC 72 (88.74% C dmmf).

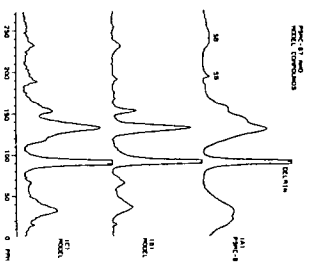


Figure 3. ^{13}C spectra of PSIG 67 (A) and model compounds. B: phenol-formaldehyde resin; C: phenol/dihydroxybiphenylene-formaldehyde copolymer (Spectra recorded on a Nicolet ND 150 instrument).

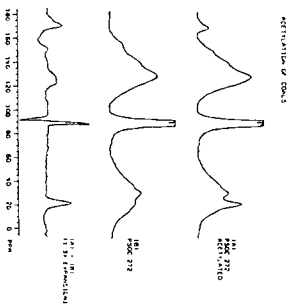


Figure 4. Spectra illustrating changes occurring in ^{13}C NMR spectra of acetylated coals.

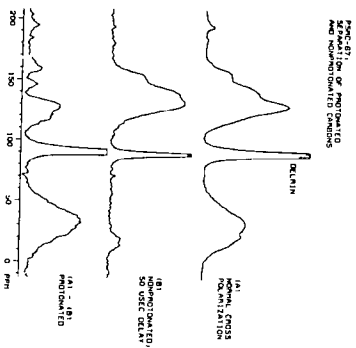


Figure 5. Spectra showing the isolation of protonated and nonprotonated carbons for a maceral, PSIG-67. Spectrum (B) is obtained by allowing the carbon spins to dephase for 50 msec by coupling to nearby protons before the beginning of acquisition. Digital subtraction is then performed to isolate the protonated carbons.

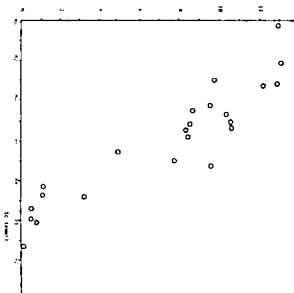


Figure 6. Plot of area of 1770 cm^{-1} band in acetylated vitrinites (proportional to phenolic OH content) vs % C (dmm).

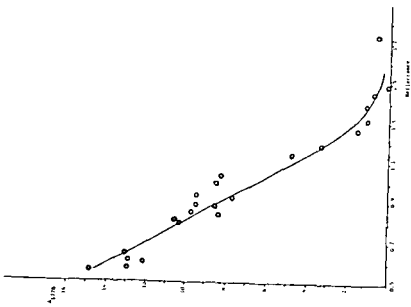


Figure 7. Plot of area of 1770 cm^{-1} band in acetylated vitrinites vs. reflectance (R_0).

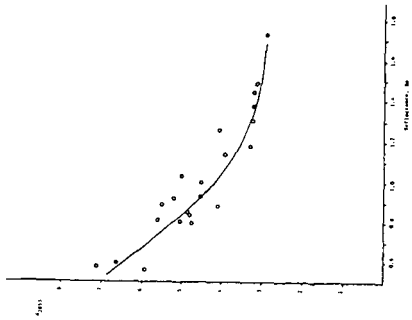


Figure 9. Plot of area of 2853 cm^{-1} band (aliphatic CH_2 mode) vs reflectance (R_0).

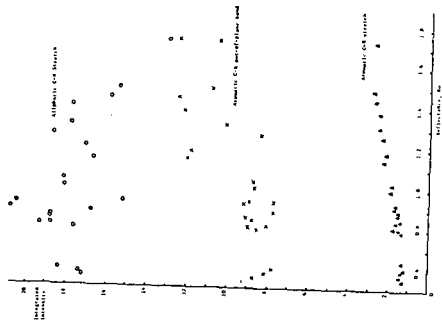


Figure 8. Plots of (top to bottom) integrated area of aliphatic C-H stretching modes; integrated area of aromatic C-H out-of-plane bending modes; integrated area aromatic C-H stretching modes vs reflectance (R_0).

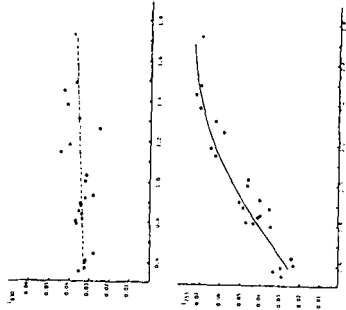


Figure 10. Top: Plot of peak height of 830 cm^{-1} band vs reflectance, (R_0) Bottom: Plot of peak height of 753 cm^{-1} band vs reflectance, (R_0)

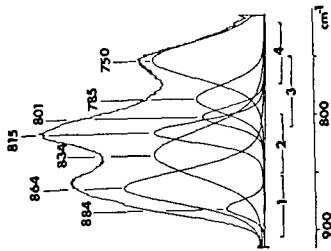


Figure 11. Curve resolved bands in the 900 to 700 cm^{-1} region of the FT-IR spectrum of a vitritinite concentrate.

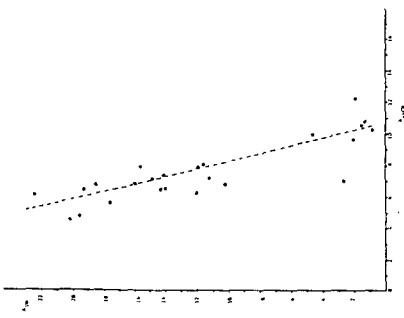


Figure 13. Plot of area 1770 cm^{-1} band in acetylated vitritinites (a measure of phenolic OH content) vs area of aromatic C-H out-of-plane bending modes (excluding 830, 785 cm^{-1} bands)

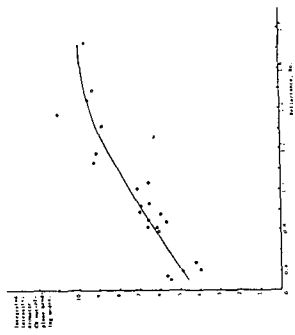


Figure 12. Plot of integrated intensity of aromatic C-H out-of-plane bending modes (excluding the 830, 785 cm^{-1} bands) vs reflectance (80).

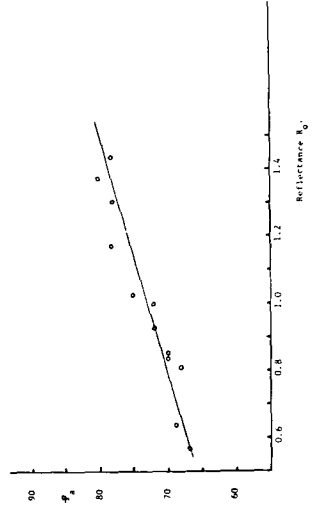


Figure 14. Plot of aromaticity f_a vs reflectance for vitritinite concentrates.

CHARACTERIZATION OF FRACTIONATED COAL
LIQUIDS BY ^{13}C NMR AND FTIR SPECTROSCOPY

K. S. Seshadri and D. C. Cronauer

Gulf Research & Development Company
P. O. Box 2038
Pittsburgh, Pennsylvania 15230

INTRODUCTION

Coal liquids derived from solvent refined processes are complex mixtures of widely differing compounds with a high proportion of nonpolar aromatic compounds. The remainder is made up of polar compounds. A knowledge of these compounds is of importance for upgrading coal liquids and producing useful chemicals.

Computer-assisted Nuclear Magnetic Resonance and Infrared Spectroscopy have opened up new possibilities for a fairly detailed characterization of coal liquids. The present trend has been to depend more on ^{13}C NMR spectrum which is often congested with multiple signals. Direct observation of ^{14}N and ^{15}N nuclei and derivitization of coal liquids to silicon and fluorine derivatives followed by the observation on ^{29}Si and ^{19}F nuclei are on the horizon. The results of spectroscopic techniques, despite their sophistication, is of little value unless assisted by chromatographic methods capable of separating coal liquids into fractions that differ according to their chemical functionality.

Several chromatographic separation schemes are described in literature including SARA⁽¹⁾ and SESC.⁽²⁾ In the latter technique the coal liquid is eluted from silica gel as the stationary phase with a sequence of solvents. We have expanded upon the analysis of combining SESC and spectroscopic techniques. Painter and Coleman⁽³⁾ have examined the IR spectra of fractions of whole coal liquid obtained by SESC. However, more detailed structural information can be obtained when the whole coal liquid is first separated into light, middle and heavy distillate and bottoms followed by SESC separation and spectroscopic analysis. We have taken this approach, and the results on middle and heavy distillate cuts are reported here.

EXPERIMENTAL

The coal liquid used in this work was from the Ft. Lewis SRC-II facility (Tacoma, WA). The nominal run conditions with Powhatan No. 5 coal were 455°C, a space time of 60 min, and a hydrogen pressure of 1250 psi. The distillate yield (C_5 -900°F) was about 40%, and the conversion of organic matter to pyridine solubles about 95%. The liquid was distilled into light distillate (C_5 -380°F), middle distillate (380-550°F), heavy distillate (550-900°F), and residue (>900°F). Further separation of these fractions was by SESC⁽²⁾ using Fisher S-662 silica gel of 60-200 mesh.

The ^{13}C NMR spectra of the fractions were recorded on a Varian FT-80A spectrometer. The solvent, CDCl_3 , was used as a field-frequency lock, and chemical shifts are in ppm downfield from internal TMS. Spectra of some of the fractions were obtained with Cr(III) acetylacetonate and by suppressing nuclear Overhauser enhancement. Infrared spectra were recorded on a Nicolet Model 7199 Fourier transform spectrometer. Each spectrum was obtained by the co-addition of 100 interferograms at 2 cm^{-1} resolution and as thin films between KBr windows.

RESULTS AND DISCUSSION

The relative quantities of the middle and heavy distillate (MD, HD) fractions are given in Table I along with the elemental analysis of the first four HD fractions. The ^{13}C NMR and FTIR spectra of individual fractions are examined in the

following sections to demonstrate the effectiveness of combining these two spectroscopic techniques with chromatographic separation.

Fraction 1MD (50.5% of Middle Distillate)

The ^{13}C NMR and FTIR spectra of this fraction are shown in Figures 1 and 2, respectively. Aromatic ring C-C vibrations result in IR absorptions near 1600 cm^{-1} and 1500 cm^{-1} . The relative intensity of the former depends on the nature of substitution on the ring. Here, the 1600 cm^{-1} band is of low intensity (vide infra) and the 3300 cm^{-1} region is flat, indicating that this fraction is composed of nonpolar aromatic compounds.

Certain features of the carbon spectrum, in particular multiple signals between 124.0 - 127.0 ppm, among which the signal at 125.7 ppm being most intense, suggest that naphthalene and alkyl naphthalenes are the dominant nonpolar compounds. The signals due to quaternary carbons are in the 132.0 - 137.0 region with a prominent signal at 135.1 ppm. The shielding of bridgehead or methyl-bearing carbon atoms in 1,8-dimethyl, 2,3-dimethyl, and 2-methyl naphthalenes is 135.2 or 135.4 ppm.⁽⁴⁾ Therefore, a substitution pattern is established by the signal at 135.1 ppm and the IR spectrum is in agreement with this pattern. Out-of-plane hydrogen vibrational frequencies in alkylbenzenes in the 900 - 670 cm^{-1} region correlates well with the number of adjacent hydrogen atoms in the ring, and this correlation is also applicable to naphthalene.⁽⁵⁾ Bands at 735 cm^{-1} , 780 cm^{-1} , and 805 cm^{-1} can be assigned to 4, 3, and 2-adjacent hydrogen wagging vibrations. The signals at 25.6 ppm, 21.5 ppm, and 19.2 ppm in the carbon spectrum are due to methyl carbons in 1,8-DIMeN, 2-MeN, and 1-MeN, respectively.⁽⁴⁾

The signals at 14.0 , 22.0 , 29.0 , and 32.0 ppm are due to short-chain alkanes. The signal at 14.2 ppm is definitely a doublet, and the less intense of the doublet along with the signal at 20.9 ppm could be assigned to methyl carbons in 1,2-dimethylnaphthalene. Tetralin and homologs of tetralin are also possible, accounting for signals near 29.0 ppm and 23.0 ppm.⁽⁶⁾

Fraction 2MD (3.0% of Middle Distillate)

The carbon and the IR spectra of this fraction are shown in Figures 3 and 4, respectively. This fraction, has a very low population of sp^3 carbons. In addition, the carbon spectrum has a signal at 118.9 ppm, suggesting a structure with carbon atoms in the vicinity of an oxygen nuclei. Since the IR spectrum has no evidence for phenolic compounds, aromatic ether is a possibility. The signals at 118.9 , 123.1 , 129.7 , and 157.3 ppm and their relative intensities favor diphenyl ether. The other signals at 141.2 , 128.7 , 127.2 , and 127.1 ppm have been assigned to biphenyl. About 62% of this fraction is diphenyl ether and the balance is biphenyl.

The signals in the IR spectrum also support the presence of diphenyl ether and a high aromaticity of the fraction. The intense signal at 1238 cm^{-1} is due to asymmetric C-O-C stretch. In aromatic ethers, the C-O bond has double bond character due to resonance and, therefore, higher force constant than aliphatic C-O bond.⁽⁵⁾ The signal due to the ether linkage, therefore, appears about 200 cm^{-1} higher than in aliphatic ethers. Other features of the IR spectrum are in agreement with the low population of sp^3 carbons.

Fraction 3MD (8.7% of Middle Distillate)

The carbon and the IR spectra of this fraction are shown in Figures 5 and 6, respectively. The IR spectrum has a broad absorption due to hydroxyl stretching near 3300 cm^{-1} with a narrower band at 3409 cm^{-1} . They are due to free and hydrogen-bonded NH groups and hydrogen-bonded phenolic hydroxyl groups. Therefore this fraction has phenolic and pyrrole-type compounds.

To understand the spectra of this and the subsequent fraction, reference is made to a library of carbon and IR spectra of alkyl phenols and indoles available in literature. (7,8,9)

The shielding of carbon nuclei in phenols bearing the -OH group extends from 155.0-152.0 ppm, and the exact location depends on the position of the methyl substitution. The carbon spectrum of this fraction has signals in the 153.5-151.0 ppm range, suggesting the presence of 2-, 2,5-, and 4-methylphenols. Signals around 15.5 and 15.2 ppm support this conclusion. A strong band at 752 cm^{-1} in the IR spectrum can be correlated with the vibrations of four adjacent unsubstituted aromatic H atoms. The band at 805 cm^{-1} correlates with two adjacent hydrogen wag or 4-methylphenol.

Other types of compounds that can be expected in this fraction are indoles and benzofurans. (2) The shielding of quaternary carbons in benzofuran and methylbenzofurans are in the 155.0-154.0 ppm range. Here this region has no absorptions. Moreover, furans and arylethers in our experiments are eluted along with nonpolar aromatics. Several features of the carbon spectrum agree well with indole and methylindoles. Part of the aromatic region of the carbon spectrum can be divided into five regions: (1) 130.0-126.9 ppm, (2) 124.2-119.6 ppm, (3) 116.6-113.5 ppm, (4) 111.1-108.7 ppm, and (5) 103.0-100.3 ppm. Many of the signals in these five regions are due to indoles. The signals in the fourth and the fifth regions are particularly diagnostic of indoles. They are due to carbons with an intervening carbon to nitrogen. The signals in the second region are due to carbons in the six-membered ring of the indoles and, since the shielding of three of them can be expected in this region, this region is congested. Indoles, at least those for which shielding data are available, (8) do not contribute to the third region, and signals in this region are due to phenolic compounds. The shielding of one of the quaternary carbons in indoles falls in the first region and that of the other quaternary carbon is near 136.0 ppm. The spectrum shown in Figure 5 was obtained with a short pulse delay. Therefore, the contribution to the intensity in the first region as well as the region around 136.0 ppm is marginal. Nevertheless, the first region has numerous signals, and they are indeed from protonated carbon atoms of phenolic compounds. Judging from the intensity distribution in the carbon spectrum, phenolic and the pyrrolic compounds are approximately in equal amounts.

In the saturated region of the spectrum, a strong signal is observed at 14.0 ppm. This signal is due to CH_3 carbons, and part of its intensity could be due to the CH_3 carbon in 2-methylindole. This is a reasonable structure since in the corresponding fraction of HD, carbazole has been recognized, and opening up of an aromatic ring could result in alkylindoles and possibly 2-methylindole.

Fraction 4MD (23.7% of Middle Distillate)

The carbon and the IR spectra of this fraction are shown in Figures 7 and 8, respectively. The broad absorption in the 3300 cm^{-1} region of the IR spectrum is due to hydroxyl stretching vibration. The band maximum is at 3320 cm^{-1} and it drops to the base line at almost 3600 cm^{-1} . The broad absorption is primarily due to hydrogen-bonded phenolic-hydroxyl groups. Bands due to N-H stretching vibrations also appear in this region of the spectrum. However, the carbon spectrum of this fraction has no absorption around 110.0 or 102.0 ppm, ruling out appreciable amounts pyrrolic nitrogen. Therefore, phenolic compounds are the major constituents of this fraction.

The aromatic region is again divided into appropriate regions to understand the types of phenolic compounds, namely: (1) 156.0-151.0 ppm; (2) 140.0-139.0 ppm; (3) 130.0-127.0 ppm; (4) 123.0-120.0 ppm; (5) 117.2-115.9 ppm; and (6) 114.0-111.0 ppm. The shielding of C-2 (C-6) in phenol is 115.4 ppm. However, in m-cresol relative to phenol, the shielding of C-2 is shifted downfield by about 0.8 ppm; whereas, due to the para shielding effect of the CH_3 group, C-6 is shifted upfield to

112.5 ppm. m-Cresol, 3,5-dimethylphenol (3,5-DMP), and similar structures are responsible for the sixth region. The signal at 116.4 ppm can also be associated with these structures. In the two model compounds mentioned above, the shielding of carbon bearing the CH_3 group is at 139.3 and 139.0 ppm, respectively, and indeed two signals at 139.8 and 139.5 ppm are observed in the second region. The shielding of CH_3 carbons in m-cresol, 3,5-DMP, and p-cresol are not perturbed by the -OH group relative to the corresponding CH_3 carbons in methylbenzenes. The signals at 21.2 and 20.4 ppm suggest phenols with - CH_3 groups, one or two carbons away from the carbon bearing the -OH group. The first region can be subdivided into a singlet at 155.3 and a group of signals from 154-153 ppm. The shielding of C-OH carbon in phenol, m-cresol, 3,5-DMP is 155.0, 155.0 and 155.4 ppm, respectively. In ortho- and para-cresols, in 2,6-DMP, in 2-isopropylphenol, and in 2-tert-butylphenol, the shielding is shifted upfield by about -2.8 ppm. Therefore, part of the signals in the first group suggest the presence of these compounds. The shielding of other quaternary carbon atoms in o-cresol and 2,6-DMP is at 124.0 and 123.8 ppm, and signals with reduced intensity are observed near 124.0 ppm. Most of the intensities in the fifth region are due to two signals at 115.4 and 115.5 ppm. These signals are due to C-2 and C-6 protonated carbons and are arising from ortho- and para-cresols. Other diagnostic signals in the carbon spectrum are those near 15.5 ppm. The shielding of CH_3 carbon in the immediate vicinity of the OH group is shifted upfield relative to that of CH_3 carbons in toluene or m-xylene. Therefore, these signals are in agreement with the presence of 2,6-DMP and o-cresol. Shielding of other carbons in the structures mentioned above are around 120.0 and 129.0 ppm, and resonances have been observed in these regions.

Most of the prominent signals have been assigned to specific carbons in phenolic compounds. However, the unassigned signals around 146.3, 136.4, and 28.7 ppm are conspicuous. The signal at 28.7 ppm is intense and could be due to CH_3 carbons in 2-t-butylphenol. The signal at 136.4 ppm could also be associated with this structure. The signals around 146.3 ppm are assigned to quaternary carbons in diphenols. These assignments are tentative.

The carbon spectrum has assisted in deciding the location of methyl groups relative to the OH group. Additional proof and other pertinent information can be derived from the IR spectrum. The C-C vibration of an aromatic ring can be divided into 1600 cm^{-1} and 1500 cm^{-1} vibrations. The 1500 cm^{-1} region has several components, depending on the number of alkyl substitutions. More importantly, the 1600 cm^{-1} vibration is less intense than the 1500 cm^{-1} vibrations. However, with electron donor or acceptor groups, the intensity of the former vibration is enhanced due to the dipole moment change provided by different groups. The 1600 cm^{-1} band of this fraction is more intense compared to the same band in the spectrum of fraction 1, due to the OH group on the aromatic ring.

The OH deformation and C-O stretch frequencies in the case of phenols are close to each other and, therefore, they are strongly coupled.⁽⁵⁾ They fall above 1100 cm^{-1} and extend up to 1330 cm^{-1} . A broad absorption is observed in this region due to the presence of numerous phenols. However, a well resolved signal is observed at 1156 cm^{-1} which is probably due to C-O stretch in a 3-substituted phenol.

The signals in the $650\text{--}850\text{ cm}^{-1}$ region are due to out-of-plane H vibrations and ring bending vibrations. The band at 696 cm^{-1} has been assigned to ring puckering mode and the other three bands to out-of-plane C-H vibrations. The signal at 776 cm^{-1} can be assigned to a phenol with three adjacent H atoms. In the structures that have already been considered, two adjacent H atoms and an isolated H atom are possible. The wagging vibrations of these hydrogen atoms are responsible for the bands at 856, 836, and 816 cm^{-1} .

In this fraction we have identified cresols and xylenols as major components. A small percentage of phenol cannot be ruled out. This fraction has 14% of phenolic oxygen estimated from the carbon spectrum. Among phenols, cresols and

xyleneols are in equal amounts--40% and 48%, respectively--and about 10% of phenol itself.

Fraction SMD (2.4% of Middle Distillate)

The carbon spectrum of this fraction is shown in Figure 9. An unusual feature of the carbon spectrum, is the signals at 156.0-159.0 ppm. These signals along with signals in the 152.0-146.0 ppm, an isolated signal at 136.7 ppm with satellites is a strong indication that pyridine and methylpyridines are present in this fraction. The carbon spectrum also suggests the presence of carbon nuclei in the vicinity of the OH group. The signals at 115.8 and 112.3 ppm are diagnostic of phenolic compounds. Further upfield there are prominent signals at 107.2, 107.0, 103.1, 102.7 ppm. These are probably due to carbon nuclei in the complexes of phenolic and basic nitrogen compounds.

Fraction 1HD (50.7% of Heavy Distillate)

This fraction, which is yellow in color, turns cloudy on refrigeration, suggesting the presence of waxy materials. The carbon spectrum has appropriate signals to substantiate the presence of alkanes. No attempt was made to assign the other signals to specific carbon nuclei. However, the spectrum has two signals around 111.5 ppm and a group around 156.0 ppm which are diagnostic of dibenzofuran (DBF).⁽¹⁰⁾ Since more than one signal has been observed in these regions, DBF and alkyl derivatives of DBF are possible. Subject to this assignment, the weight percent of oxygen in this fraction was obtained from the carbon spectrum (0.32%) agreeing fairly well with the results of elemental analysis (0.54%). This fraction has an equal amount of sulfur, that could be present as dibenzothiophene.

Fraction 2HD (24.5% of Heavy Distillate)

The carbon spectrum of this fraction is shown in Figure 10. Unlike the carbon spectrum of the previous fraction, only a limited number of signals are observed, partly due to the high aromaticity (92.5%) of the fraction. Signals at 131.9, 130.1, and 130.9 ppm are due to quaternary carbons. The former two have been assigned to phenanthrene and the latter to pyrene. The other signals in the spectrum support these structures. Weak signals in the spectrum are due to hydroaromatic hydrocarbons derived from phenanthrene and pyrene.

The signal at 131.9 and 130.9 ppm are of equal intensity. However, four carbons of pyrene contribute to the intensity of the latter signal; whereas, two carbons of phenanthrene are at 131.9 ppm. Therefore, phenanthrene is twice as abundant as pyrene in this fraction.

The low frequency region (900-700 cm^{-1}) of the IR spectrum is in agreement with the carbon spectrum. Bands in this region arise from C-H wagging vibration. The vibrational frequencies of C-H bonds approximately parallel to the long axis of the molecule are near 740 cm^{-1} , and those of C-H bonds approximately perpendicular to the long axis are near 850 cm^{-1} .⁽¹¹⁾ Also due to angular condensation, a characteristic band is observed between these two regions. The bands at 744 cm^{-1} and 736 cm^{-1} are assigned to C-H bonds parallel to the long axis in phenanthrene and pyrene, and those at 860 cm^{-1} and 840 cm^{-1} are assigned to CH bonds perpendicular to the long axis. The band at 810 cm^{-1} which is characteristic of C-H bending vibration in angular polynuclear aromatic hydrocarbons supports the two structures that we have selected to assign signals in the carbon spectrum.

Fraction 3HD (13.2% of Heavy Distillate)

The carbon and the IR spectra of this fraction are shown in Figures 11 and 12, respectively. The IR spectrum has a broad absorption at 3300 cm^{-1} and a narrower band at 3410 cm^{-1} , suggesting that this is analogous in composition to

fraction 2MD; that is, it has a structure with N-H linkage and phenolic compounds. The carbon spectrum has signals at 110.6, 119.20, 120.22, 123.2, 125.7, and 139.6 ppm. These match exactly with the resonances observed for carbazole.⁽¹⁰⁾ This fraction is very aromatic (93.1%) and, therefore, it is not surprising that one of the major components of this fraction is carbazole. The signals at 139.6 and 123.2 ppm appear with reduced intensity because they arise from quaternary carbons.

From the intensity of the signal at 110.6 ppm, the percentage of nitrogen is 2.3% compared to 3.27% from the elemental analysis. Therefore, most of the nitrogen in this fraction is accounted for by carbazole. Signals near 115.8 ppm and weak shoulders to signals at 110.6 ppm and 120.2 ppm suggest the presence of hydroxy aromatic compounds. However, in the absence of shielding data for hydroxy aromatic compounds with three or more rings, assignment of these signals to specific carbon nuclei has not been possible.

Fraction 4HD (7.8% of Heavy Distillate)

The carbon and the IR spectra of this fraction are shown in Figures 13 and 14, respectively. The aromaticity of this fraction is much less (61.5%) than that of the previous fractions.

The aromatic region of the spectrum is divided into four regions: (1) 157.0-150.0 ppm; (2) 147.0-132.0 ppm; (3) 132.0-125.0 ppm; and (4) 120.0-109.0 ppm. The first region has three well defined signals at 156.9, 156.2, and 154.7 ppm. The broad absorption near 3300 cm^{-1} and the enhanced intensity of 1600 cm^{-1} relative to the 1450 cm^{-1} band in the IR spectrum indicate the presence of hydroxy aromatic compounds. The shielding of carbon-bearing OH groups in phenols are in the 155-152 ppm region, whereas in naphthols and 9-hydroxyphenanthrol, the shielding of the corresponding carbon is shifted upfield to 153.0-151.0 ppm in CDCl_3 . If this trend should continue, the carbon spectrum, for example, of hydroxy-benzanthracene, should have a signal near 151.0 ppm. Therefore, signals around 156.0 ppm are somewhat surprising. This fraction has 1.3% nitrogen, and if this nitrogen is present as basic nitrogen, hydroxy basic nitrogen heterocyclics, like hydroxypyridines, have carbons with shieldings near 156.0 ppm. This possibility is unlikely since hydroxypyridines and 8-hydroxyquinoline do not have carbons with chemical shifts near 114.3 ppm. Therefore, the nitrogen is present as pyrrolic nitrogen, although there are no pronounced evidences both in the carbon and the IR spectrum for the N-H linkage.

The IR spectrum has two well defined signals at 730 cm^{-1} and 905 cm^{-1} which are characteristic of C-H wagging vibration in polynuclear aromatic hydrocarbons with four or more condensed rings. The 730 cm^{-1} is a singlet, except for a weak shoulder suggesting that PNAs are sparsely substituted. Therefore, the major portion of the sp^3 carbons are in the hydroaromatic rings, and the hydroaromatic structures account for the group of signals in the second region. The signals in the third and the fourth region arise from carbons well removed from the OH group and those in the immediate vicinity of the OH group, respectively.

These observations suggest that the hydroxyaromatic compounds in this fraction have partially hydrogenated three or more condensed rings. It is likely that in such structures the shielding of aromatic carbon bearing the OH group is near 156.0 ppm and not at 151.0 ppm as in 9-phenanthrol.

SUMMARY

The results presented here amply demonstrate that the combined results of ^{13}C NMR and FTIR spectroscopy can provide a wealth of information not only about the functional groups in coal liquids, but also details regarding the structure of molecules carrying these groups.

The first two fractions of SESC are homogeneous; they contain nonpolar aromatic compounds. Included in this category are the diaryl ethers, benzofurans, and benzothiophenes. The rest of the fractions are heterogeneous. All of them to a greater or lesser extent contain hydroxyaromatic compounds. However, fraction 3 is highly homogeneous, containing mainly phenolic compounds. The presence of phenolic compounds does not interfere with the identification of other functional groups in fractions 3 and 5 due to: (1) their low concentration and (2) high resolution of absorptions in the ^{13}C NMR spectrum. The type of functional groups in each fraction, according to the carbon and IR spectroscopic results are summarized in Table 2.

REFERENCES

1. Ruberto, R. G., Jewell, D. M., Jensen, R. K., and Cronauer, D. C., Advances in Chemistry Series, No. 151, Chapter 3, American Chemical Society, Washington, DC, 1976.
2. Farcasiu, M., Fuel 1977, 56, 9.
3. Painter, P. C., and Coleman, M. M., Fuel 1979, 58, 301.
4. Wilson, N. K., and Stothers, J. B., J. Mag. Resonance 1974, 15, 31.
5. Colthup, N. B., Daly, L. H., and Weberley, S. E., Introduction to Infrared and Raman Spectroscopy, Academic Press, New York and London, 1964.
6. Seshadri, K. S., Ruberto, R. G., Jewell, D. M., and Malone, H. P., Fuel, 1978, 57, 111.
7. Johnson, L. F., and Jankowski, W. C., Carbon-13 NMR Spectra, Wiley-Interscience, New York, 1972.
8. Breitmaier, E., Haas, G., and Voelter, W., Atlas of Carbon-13 NMR Data, Heyden, Long-Philadelphia-Rheine, 1979.
9. Shrewsbury, D. D., Spectrochimica Acta 1960, 16, 1294.
10. Seshadri, K. S., Unpublished results.
11. Jones, R. N., and Sandorfy, C., The Application of Infrared and Raman Spectroscopy to the Elucidation of Molecular Structure, Chapter IV, Volume IX, in A. Weissburger, Technique of Organic Chemistry, Interscience, New York, 1956.

Table 1

FRACTIONS OF MIDDLE AND HEAVY DISTILLATE OF
COAL LIQUID AND ELEMENTAL ANALYSIS OF HD

| <u>Fraction</u> | <u>Eluent</u> | <u>Wt% of MD</u> | | | | | | |
|--------------------|------------------------|------------------|------------------|----------|----------|----------|----------|----------|
| 1 | Hexane | 50.5 | | | | | | |
| 2 | Hexane + Benzene(15%) | 3.0 | | | | | | |
| 3 | Chloroform | 8.7 | | | | | | |
| 4 | Chloroform + Ether(4%) | 23.7 | | | | | | |
| 5 | Ether + EtOH(3%) | 2.4 | | | | | | |
| Losses (Volatiles) | | 11.7 | | | | | | |
| | | 100.0 | | | | | | |
| | | | <u>Wt% of HD</u> | <u>C</u> | <u>H</u> | <u>O</u> | <u>N</u> | <u>S</u> |
| 1 | | 50.7 | 90.60 | 8.11 | 0.54 | 0.00 | 0.54 | |
| 2 | | 24.5 | 92.18 | 5.91 | 0.31 | 0.10 | 0.47 | |
| 3 | | 13.2 | 81.92 | 7.16 | 3.69 | 3.27 | 0.23 | |
| 4 | | 7.8 | 82.25 | 7.40 | 5.54 | 2.03 | 0.12 | |
| 5 | | 2.9 | | | | | | |
| Losses | | 0.9 | | | | | | |
| | | 100.0 | | | | | | |

Table 2

TYPES OF COMPOUNDS IN THE FRACTIONS OF MD AND HD

| <u>Fraction</u> | <u>Type of Compounds</u> |
|-----------------|--|
| 1 and 2 | Nonpolar aromatics, diaryl ethers, benzofurans, and benzothiophenes. |
| 3 | Mainly nonbasic N compounds; hydroxy aromatic compounds. |
| 4 | Hydroxy aromatic compounds. |
| 5 | Basic N compounds; hydroxy aromatic compounds. |

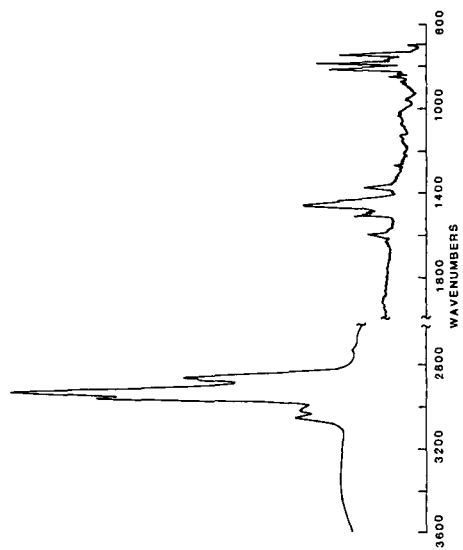


Figure 2 FTIR Spectrum of Fraction 1MD

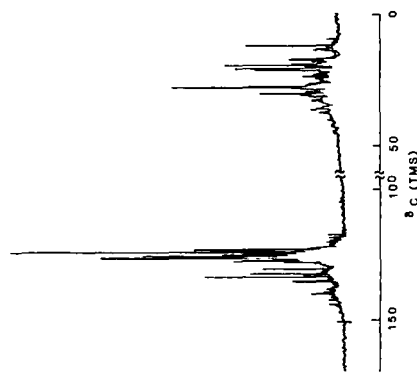


Figure 1 ¹³C NMR Spectrum of Fraction 1MD

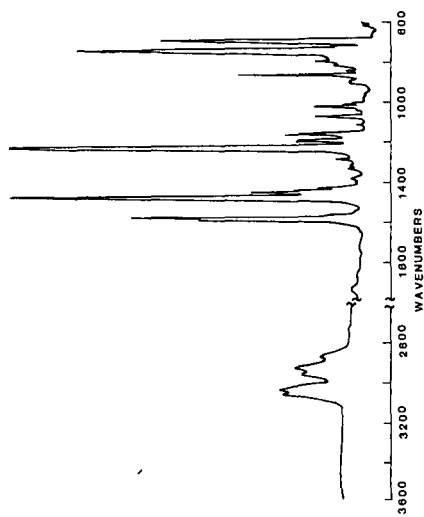


Figure 4 FTIR Spectrum of Fraction 2MD

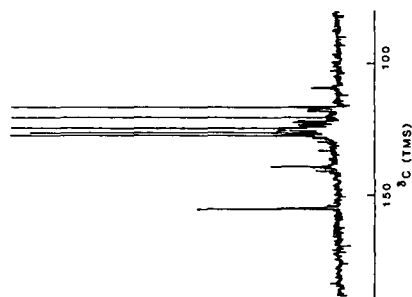


Figure 3 ¹³C NMR Spectrum of Fraction 2MD

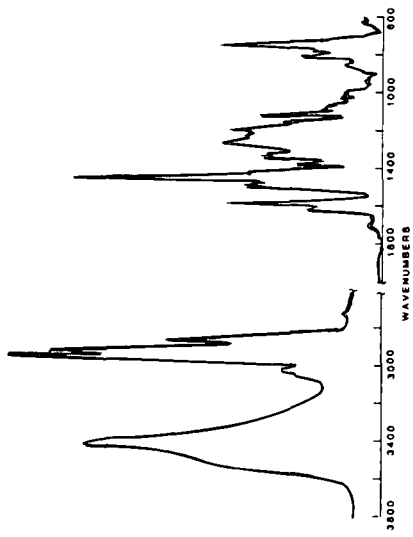


Figure 6 FTIR Spectrum of Fraction 3MD

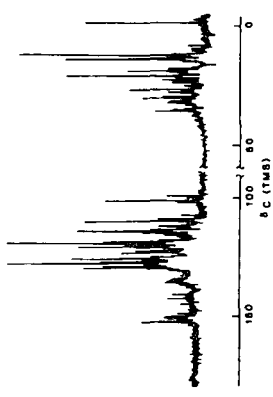


Figure 5 ¹³C NMR Spectrum of Fraction 3MD

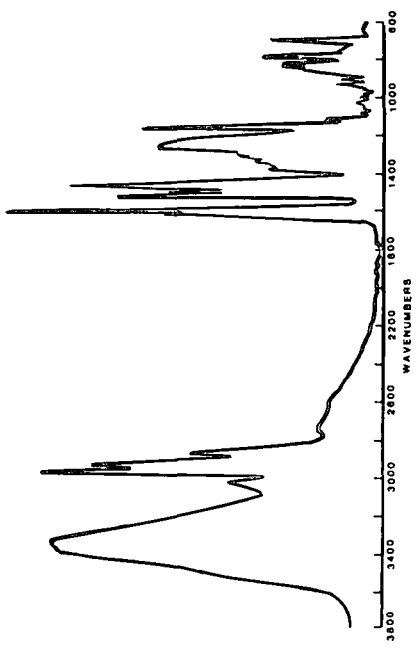


Figure 8 FTIR Spectrum of Fraction 4MD

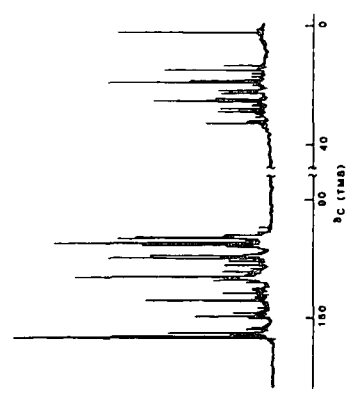


Figure 7 ¹³C NMR Spectrum of Fraction 4MD

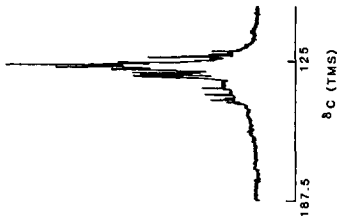


Figure 10 ¹³C NMR Spectrum of Fraction 2HD

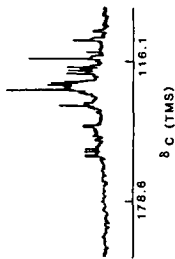


Figure 9 ¹³C NMR Spectrum of Fraction 5MD

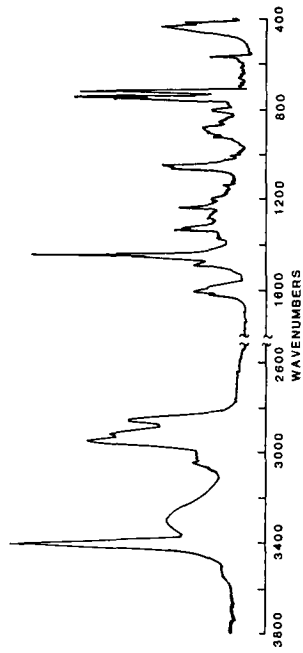


Figure 12 FTIR Spectrum of Fraction 3HD

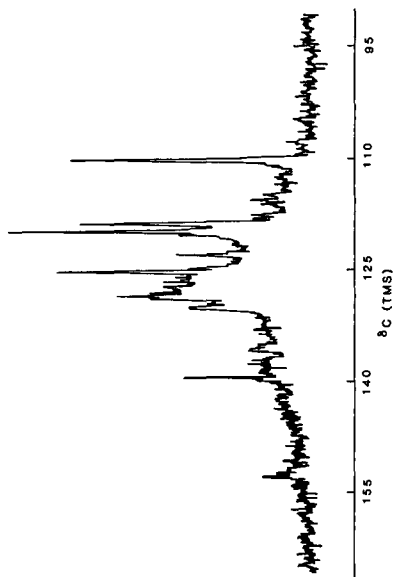


Figure 11 ¹³C NMR Spectrum of Fraction 3HD

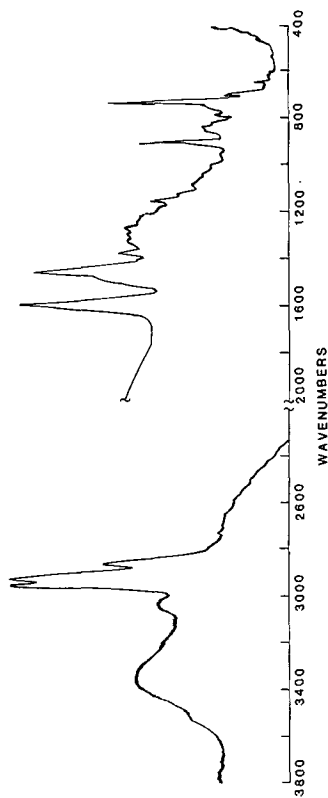


Figure 14 FTIR Spectrum of Fraction 4HD

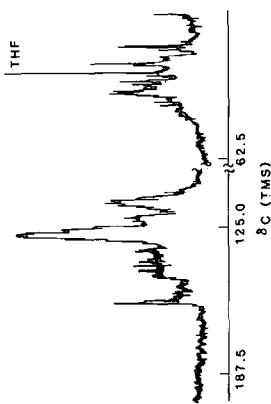


Figure 13 ¹³C NMR Spectrum of Fraction 4HD

OXIDATION AND FORMATION OF DEPOSIT PRECURSORS IN HYDROCARBON FUELS

Frank R. Mayo, S.E. Buttrill, Jr., Bosco Lan, G.A. St. John, and David Dulin

SRI International, Menlo Park, California 94025

The object of this research is to determine the mechanism of deposit formation in hydrocarbon fuels, and thus to predict and to prevent deposit formation (1). The deposits cause clogging of filters and hot fuel lines. Our premise is that such deposits, insoluble in hydrocarbons, arise from further condensation of soluble deposit precursors (2). The precursors are the oxidation products of the fuels and condensation products of these, formed in stepwise reactions. When their molecular weights and oxygen contents become high enough, they precipitate from solution (3) either on long storage or quick heating. The problems are: what oxidation products are most likely to condense; is the condensation a radical or nonradical reaction, or both; what fuels or fuel components are most likely to form precursors; and how can the reactions be prevented?

This paper describes our progress in applying field ionization mass spectrometry (FIMS) to these problems. We started with a No. 2 home heating oil (Fuel C) to represent an unstable jet turbine fuel, then used n-dodecane as a simple and common fuel component.

EXPERIMENTAL

As received, Fuel C was brown and contained so much material of high molecular weight and low solubility that it could not be used to follow the development of additional fuel precursors. It was therefore distilled at 2.3 kPa (17 torr) in a Claisen flask with a Vigreux neck. Aliquots of the distillate (10 mL) were oxidized by shaking them with air in 100-mL flasks in a bath at 130°C. Gas samples of 70 μ L were withdrawn through a septum and analyzed for O₂/N₂ by gas chromatography on a 183 x 0.32-cm stainless steel column at 0°C and 30 mL/min He flow rate. The column was packed with 13X molecular sieve.

Pure 99% n-dodecane was obtained from Phillips Chemical Company and distilled at 2.3 kPa. The first and last tenths were rejected.

Two mass spectrometers were used. In one, the whole 5- μ L fuel sample was injected through a septum into an evacuated 0.5-L glass expansion bulb of the batch inlet system. The sample vaporizes immediately and enters the field ionization source through a glass leak. Field ionization of this mixture produces molecular ions from each fuel component and gives a molecular profile of the fuel sample. A second FIMS system was used to analyze deposit precursors. A 0.5-mL sample of Fuel C was spiked with an internal standard, 10 μ g of decacyclene (molecular weight 450), then vacuum-evaporated to <100 μ L. A 5- μ L sample of the concentrate was placed in a standard mass spectrometer sample holder in the solids probe of the mass spectrometer. The probe was cooled to -50°C, introduced into the mass spectrometer vacuum system, and then warmed to 30° with continuous pumping to remove most of the remaining volatile components. The probe was then mated to the ion source. The field ionization spectrum of the residue, including deposit precursors and decacyclene internal standard, was collected with the PDP 11/10 computer system. The resulting FIMS spectra represent the composition of the least volatile components of the fuel sample including impurities. The concentrations of individual deposit precursors are calculated by comparing their intensities in the FI spectrum with that of the decacyclene standard.

Samples of oxidized dodecane were analyzed similarly, except that the internal standard was perylene (molecular weight 252). In general, the oxidation products con-

tained unoxidized fuel, which could not be entirely removed without loss of some oxidation products.

RESULTS

Fuel C. The molecular weight profile of Fuel C shows that the major components are alkanes with 10 to 14 C atoms, with a preponderance of alkylbenzenes with 3 to 5 side-chain C atoms at the low molecular weight end, alicyclics up to C₁₆ at the high end, and small proportions of a wide variety of hydrocarbons over the whole range.

Table 1 summarizes the results of one oxidation of distilled Fuel C; they show steady increases in rate of oxygen absorption (autocatalysis) and in concentration of less volatile materials.

TABLE 1. OXIDATION OF VACUUM-DISTILLED FUEL C AT 130°C

| Time at 130°C (min.) | 0 | 255 | 430 | 701 |
|---|-----|------|------|------|
| O ₂ consumed (mmol/liter) | 0 | 6.55 | 13.1 | 32.2 |
| Per minute ^a x 10 ² | | 2.6 | 3.7 | 7.0 |
| Deposit Precursor Properties | | | | |
| Concentration (ppm) ^b | 74 | 132 | 2450 | 2600 |
| Number Av. Mol. Wt., \bar{M}_n | 435 | 388 | 355 | 318 |
| Weight Av. Mol. Wt., \bar{M}_n | 496 | 440 | 419 | 381 |

^aDuring preceding interval.

^bBased on total materials found by FIMS.

Figures 1 and 2 summarize FIMS data after the first two oxidation periods in Table 1. The ordinate and the numbers in the upper left corners of the figures are the percentage of the summed ion intensities. Most of the material of molecular weight ~ 250 corresponds to incorporation of one to four atoms of oxygen into fuel molecules (precursor monomers), retained because they are much less volatile than the fuel. Most of the material with molecular weights between 300 and 450 represents combinations of monomer precursors (dimers). Material of intermediate molecular weight presumably represents condensation of monomer precursors and their fragments formed by cleavage of alkoxy radicals. The figures show that the development of monomer precursors and dimer precursors, like the rate of oxygen absorption, is autocatalytic. Development of trimers can also be seen.

During the last oxidation period, the solution became lighter and a dark brown precipitate formed on the reactor walls. During this period, the concentration of precursor monomers increased sharply (these may be the oxidation products that don't condense easily), and the concentrations of dimers and trimers appear to decrease perceptibly (compared with the decacyclene standard), perhaps because they have grown and separated from the fuel mixture.

The precipitate that formed, after washing with hexane and drying, weighed about 3 mg/g of initial fuel. Acetone extraction of this residue gave 0.137 mg of extract/g initial fuel; its \bar{M}_n in N-dimethylformamide was ~ 600. It therefore appears that the deposits precipitated more because of their oxygen and heteroatom contents than because of their high molecular weights.

Although the research described above provides excellent evidence for the deposit formation by stepwise condensation of deposit precursors, the data give us little

indication of the chemical structures or mechanisms involved. However, there is an indication in Figure 2 of a problem that becomes much more obvious with n-dodecane. All the principal components should have even mass numbers, as will all compounds of C, H, and O (but not N). However, 1.1% of natural C is ^{13}C , and so for any C_{12} compound, about 13% of the molecules will contain one ^{13}C . Therefore, all the major peaks will have an obvious satellite with mass number one unit greater. Figure 2 shows that the oxidized products have more than the expected 12 to 20% of materials with odd mass numbers (in the spaces between the peaks with even mass numbers). Odd mass numbers in C, H, and O compounds, except that due to ^{13}C , mean that fragmentation of parent molecules has occurred in the FIMS.

n-Dodecane. To eliminate the multicomponent problem with Fuel C, we investigated the oxidation of n-dodecane. Because the extents of evaporation varied before taking FIMS data, the absolute concentrations of products vary considerably in the three spectra. Dodecane (mass number 170 and its satellite at 171) predominated in the FIMS concentrates but are irrelevant and neglected in this discussion. Table 2 therefore lists the 12 strongest other peaks for each spectrum in order of their relative intensities.

Table 2-A shows that with the untreated oxidation product, the three strongest peaks, and 7 of the 12 strongest, have odd mass numbers. These must represent molecule fragments, uncommon from hydrocarbons, and so we examined the FIMS of known 3-dodecanol and 2-dodecanone. The dodecanol shows little of the parent ion (186), but it decomposes in the FIMS to give six principal significant products: 50 mol % is dodecyl (169 by loss of OH); 20% is decyloxy (157 by loss of ethyl); 18% is dodecene (168 by loss of water); 13% is dodecanone (184 by loss of H_2); 5% is dodecyloxy (185 by loss of H); and 4% is undecyloxy (171 by loss of methyl). The second and last products are probably specific for 3-dodecanol, leaving dodecyl as the principal product from mixed dodecanols. 2-Dodecanone is relatively stable. The parent peak (184) and its ^{13}C satellite (185) comprise >90% of the observed ions. An effort was made to avoid fragmentation by acetylating, methylating, or benzoylating pure higher alcohols but only 6-tridecyl benzoate gave mostly the parent peak.

In the first oxidation of dodecane in Table 2, 120.6 mmol of dodecane absorbed 1.35 mmole oxygen, 1.12 mol %, in 22.3 h at 130° . Part of the product was subjected to FIMS directly, part was heated for one hour at 180°C in the absence of oxygen to destroy peroxides. A major portion was treated with aqueous KI and acetic acid to decompose peroxides; the liberated iodine corresponded to 34% yield of hydroperoxide on the oxygen absorbed. Part of the KI-treated products was then heated for one hour at 180° in the absence of air, and another was benzoylated with 20% excess benzoyl chloride in pyridine. Even after purification, benzoic acid, benzoic anhydride and benzoyl ions gave major FIMS peaks, which are neglected.

In the oxidation products, the 182 and 183 peaks are probably fragments from dodecyl hydroperoxides because their proportions decrease upon heating and are succeeded by alcohol-derived peaks at 169 and 185. The 184 parent peak for dodecanone is little changed on heating. The 169 peak is associated with both alcohol and hydroperoxide but must come only from alcohol in the heated product. The new 203 peak in the heated sample arises from peroxides with >2 oxygen atoms. Mass numbers 194 to 203 and 213 to 217 are closely related products corresponding to gain or loss of H atoms by alcohols and ketones; the borderline between the parent compounds is fuzzy. Volatility considerations must favor the higher oxygen compounds in the data observed for C_{12} products.

Table 2-A shows other effects of heating; the appearance of butyl, pentyl and hexyl radicals (57, 71, 85) in the FIMS of the heated sample and the displacement of the 196, 197, and 217 peaks from the 12 most prominent products after heating. The small radicals can come from cleavage in the FIMS of alcohols or hydroperoxides in the unheated oxidation products,

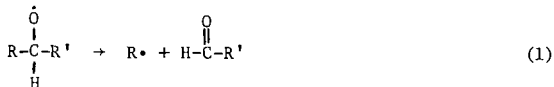


TABLE 2

PRINCIPAL IONS FROM 3-DCDECANOL, 2-DODECANONE, AND OXIDATION PRODUCTS OF n-DODECANE

| Ranking | No oxidation | | First oxidation | | | | benzoylated | Second oxidn. ^e Ph ₃ P |
|---|------------------|---------------|-----------------|------------------|------------------|------------------|------------------|---|
| | 3-Do-decanol | 2-Do-decanone | Un-treated | Heated to 180°C | KI + AcOH | KI + heating | | |
| A. Ranking for all mass numbers | | | | | | | | |
| 1 | 169 | 184 | 183 | 169 | 182 | 182 _c | 290 ^d | 169 |
| 2 | 157 ^a | 185 | 169 | 183 | 183 | 264 _c | 98 ^d | 184 |
| 3 | 168 | 182 | 199 | 184 | 169 _b | 296 _c | 184 | 168 |
| 4 | 131 | 122 | 184 | 185 | 311 _b | 183 _c | 182 | 182 |
| 5 | 184 | 183 | 182 | 203 | 370 _b | 328 _c | 198 ^d | 185 |
| 6 | 185 | 150 | 185 | 198 | 256 _b | 256 _b | 194 ^d | 157 |
| 7 | 171 ^a | 155 | 197 | 57 | 184 | 184 | 370 _d | 143 |
| 8 | 373 | 170 | 198 | 182 | 185 | 169 _c | 189 ^d | 129 |
| 9 | 186 | 186 | 217 | 199 | 198 _b | 256 _c | 203 ^d | |
| 10 | 183 | 136 | 370 | 85 | 297 _b | 266 _c | 302 ^d | |
| 11 | 182 | 156 | 196 | 71 | 283 _b | 213 _c | 185 | |
| 12 | 198 | 108 | 99 | 58 | 371 _b | 196 | 183 | |
| B. Ranking for mass numbers ≥ 337 only. | | | | | | | | |
| 1 | | | 370 | 337 ^f | 370 | 450 ^g | | |
| 2 | | | 385 | 385 | 371 | 466 | | |
| 3 | | | 399 | 399 | 385 | 436 | | |
| 4 | | | 371 | 353 | 399 | 366 | | |
| 5 | | | 337 | 367 | 337 | 385 | | |
| 6 | | | 367 | 371 | 469 | 337 | | |
| 7 | | | 369 | 355 | 355 | 340 | | |
| 8 | | | 353 | 366 | 353 | 338 | | |
| 9 | | | 355 | 370 | 339 | 365 | | |
| 10 | | | 450 | 338 | 367 | 399 | | |
| 11 | | | 436 | 351 | 338 | 451 | | |
| 12 | | | 366 | 369 | 366 | 367 | | |

Suggested identifications of ions above:

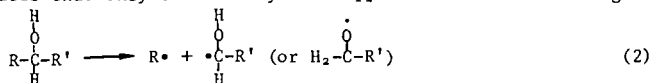
| | | |
|--|---|---|
| 171 and below, C ₁₁ H ₂₃ O and smaller fragments | 185 Dodecyl-O 186 Dodecanol | 338 Dimer, C ₂₄ H ₅₀ |
| 168 Dodecene | 194 to 232, mostly C ₁₂ compounds containing | 350 to 466, dimer + 0 + fragments |
| 169 Dodecyl | 2 to 4 O atoms | |
| 182 Dodecenone | | |
| 184 Dodecanone | | 506 Trimer, C ₃₆ H ₇₄ |

^a Specific products from 3-dodecanol. ^b Specific for KI.^c Appear or persist after heating KI product. ^d Peculiar to benzoilation product.

^e In 20 hours at 130°C, 7.25 g, 42.6 mmol, of n-dodecane absorbed 0.903 mmol O₂, 2.12 mol %. Hydroperoxide corresponding to 24.8% of the O₂ absorbed was found. The remainder of the product was then treated with 20% excess Ph₃P for 6 hours at 25° and then distilled at 1.7 kPa (13 torr) to remove Ph₃P and its oxide. Therefore, this sample should not contain high-boiling products.

^f Would rank 13 in Part A. ^g Peak height was 2/3 of that of the 196 peak.

but Table 2-A indicates that they come mostly from C₁₂ alcohols formed during heating:



Thus, 3-dodecanol apparently gave methyl and ethyl radicals. The short radicals probably do not come from short alcohols, which would be lost during concentration.

The KI treatment of the oxidation products was expected to decompose hydroperoxides to alcohols without forming free radicals or byproducts. However, the results indicate many byproducts, perhaps traces exaggerated by FIMS.

In comparison with the KI reduction, the triphenylphosphine reduction of the second oxidation products gives more products that are more typical of dodecanols (168, 169, 185) and thus may be a cleaner reduction. However, the absence of peaks above 190 in the triphenylphosphine products is probably due to distillation before FIMS.

The 370-371 peaks appear in several mixtures in Table 2-A and are prominent in all the mixtures in Table 2-B, except in the KI + heat group. They do not survive heating after KI treatment, but they survive benzylation and so are not associated with hydroxyl groups, even though mass number 370 corresponds to a dimer glycol.

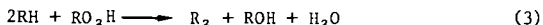
The heated products are similar to the KI products, containing considerable material of mass numbers 169, 182-185, and 198-199. However, the heated products contain more low mass number fragments and the KI products give more ions with mass number >256. Heating the KI products results in appearance or disappearance in Table 2-A of all products of mass number >256. Thus, substantial changes occur upon heating the KI product, even though there are no peroxides left, and hence nonradical reactions as well as radical reactions may lead to polymeric precursors.

Interposing the KI treatment before heating makes the dodecanone peak (182) most important, weakens or eliminates several peaks (57, 58, 71, 85, 185, 199, and 203) and forms several new ones, mostly >250.

The benzyolated KI-treated product contains more dodecyl benzoate (290) than anything else, and establishes hydroperoxide and alcohol as the major primary products. The absence of the 168 and 169 peaks shows that benzyolation of alcohol was essentially complete. The 182, 184, and 185 peaks that persist probably come from dodecanones, but in the KI-treated product, they and the 183 peak may also come from dodecanols.

Table 2-B show the relative ions concentrations from dimeric products. The most prominent also appear in Table 2-A. These products appear in groups corresponding to the dimer (338) and products containing 1, 2, and 3 additional oxygen atoms (near 354, 370, 386, and maybe 402) minus a few hydrogen atoms for formation of ketones or alkoxy radicals instead of alcohols. Starting at about mass number 399, most of the higher mass numbers must represent two dodecane residues plus oxygen plus additional carbon-containing fragments. No trimeric fragments (506 or above) have been observed, probably because of precipitation or volatility limitations. However, their absence may also be caused by low yields with dodecane, because trimers were observed with Fuel C.

We now consider the mechanism by which monomers are converted into dimeric products. The simplest condensation of dodecane by heating with a hydroperoxide would be:



The molecular weight of the C₂₄ dimer is 338, but none of this was found in an oxidation containing sufficient air. Instead, the C₂₄ products found had 2 to 4 oxygen atoms and mass numbers close to 370, 385, and 399. Thus, the dodecane oxidation products have

condensed during oxidation (whatever the mechanism) even though the parent dodecane concentration is 50 times greater than that of the oxidation products. However, the 337 ion, formed by loss of a hydrogen atom from the dimer, becomes a minor product when this oxidation product is heated and a major product in the heated portion of the oxidation in Table 2-B.

In the untreated oxidation products, the four most prominent peaks in Table 2-B correspond to a dimer plus two or three oxygen atoms and either a fourth oxygen atom or an additional carbon atom. The oxidation in Table 2, which absorbed less oxygen in more time, may have been depleted in oxygen, and tends to contain dimer units with fewer oxygen atoms and more fragments containing additional carbon atoms (436, 450).

Comparing the last two columns of Table 2-B shows that heating peroxide-free mixtures to 180° formed more compounds of molecular weight >400. Thus, there is a condensation or coupling reaction that does not depend on hydroperoxides, but probably involves other functional groups.

SUMMARY AND CONCLUSIONS

Our experimental results will now be used to formulate a general picture of deposit formation. Oxygen is required to produce deposits from hydrocarbon fuels, except at pyrolysis temperatures. For a given hydrocarbon, the process goes mainly through monomer oxidation, and coupling of these oxidation products to dimeric products. All of these are at first soluble in fuel, but as oxidation and condensation continue, the products become insoluble at molecular weights around 600. The insoluble products formed in storage probably remain soluble in good solvents (e.g., acetone), but when fuel containing soluble deposit precursors is heated, especially with a little oxygen, oxidation and condensation become rapid and precipitates form on the walls. These precipitates may at first be soluble in acetone but eventually become intractable. The oxidations are almost certainly conventional free radical chain reactions; the coupling of monomer units probably involves both a free radical coupling mechanism like Reaction 3, and a nonradical condensation (e.g., aldol (4)), in unknown proportions. Nitrogen and sulfur compounds concentrate in the precursors and deposits because they are more reactive in oxidation and condensation, and probably less soluble in fuel (5). Whether the effects of some very reactive fuel components are stoichiometric or catalytic remains to be determined.

Products and fragments between 190 and 338 (dimer) mass number must contain at least two oxygen atoms. Because peroxide links are not expected to survive FIMS, most products in this range contain two or more oxygen-functional groups. Their proportion is difficult to estimate with FIMS because of volatility differences, but the work of Jensen et al. (6) on the liquid-phase oxidation of hexadecane at 120 to 180°C shows that at least a quarter of the hydrocarbon molecules attacked contains two or more oxygen functions. Such products are more reactive than monofunctional compounds in radical-coupling and condensation reactions.

At 130°C in air, dodecane oxidizes much faster than Fuel C; it absorbs about 13.2 mmol of oxygen/mol fuel in 10 hours, compared with about 3.82 mmol for Fuel C in 20 hours. Fuel C oxidizes at a constant rate while the rate for dodecane is autocatalytic. However, by FIMS and observed deposit formation, dodecane produces fewer precursors and no visible deposits. Experiments with several Diesel fuels (to be described elsewhere) show little correlation between oxidation rate and gum formation, as measured by ASTM-D2274 before distillation. Paraffins usually predominate in fuels, but the gum formation apparently depends on the nature and amounts of other hydrocarbons, N and S compounds, and fuel history.

FIMS has been very useful for comparing fuel compositions, and for seeing the development of Fuel C deposit precursors at 130°C. Results with dodecane have been discouraging. The principal C₁₂ oxidation products, alcohols and hydroperoxides, fragment in the mass spectrometer and give similar peaks that overlap ketone peaks, probably in

different proportions, so that the primary products and their subsequent changes have been hard to identify. Yields of dimeric and trimeric precursors have been surprisingly low. Further, the relative concentrations of different compounds in the same mixture and of the same compound in different mixtures depend somewhat on the evaporation before the FIMS is taken.

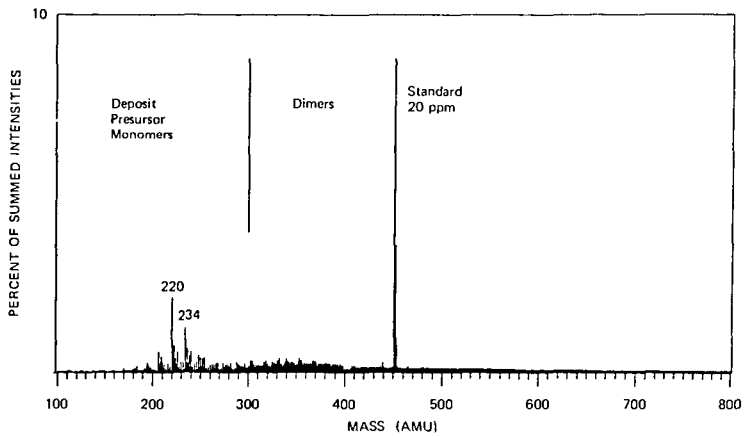
With enough oxygen, the C-C coupling reaction would be inhibited and the product would be unstable R_2O_2 . Hence gum and deposit formation may proceed best near the minimum oxygen concentration that permits oxidation. Some such measurements deserve a high priority.

ACKNOWLEDGMENT

This research was supported by Contracts NAS3-22510 with NASA-Lewis Research Center and DAAG29-80-C-0122 with the Army Research Office.

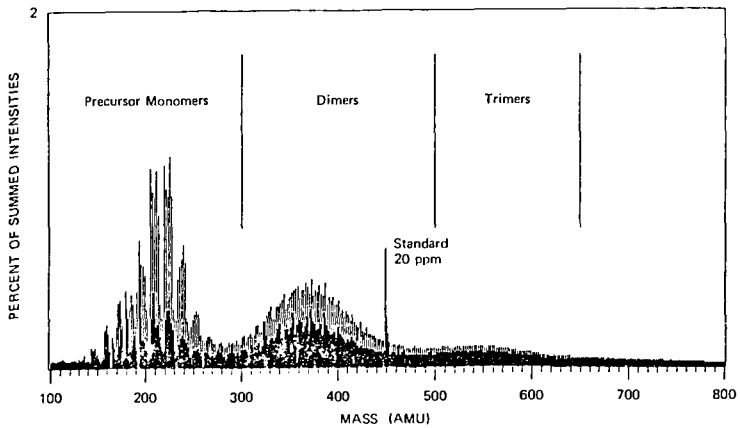
REFERENCES

1. A. C. Nixon, Chapter 17 in Autooxidation and Antioxidants, edited by W. O. Lundberg, Interscience Publishers, New York, London, 1962. An old but thorough review.
2. F. R. Mayo, H. Richardson, and G. D. Mayorga, Preprints, Division of Petroleum Chemistry, 20(1), 33 (1975). This paper is based on a final report, "The Chemistry of Fuel Deposits and their Precursors," prepared under Contract N00019-73-C-0318 for the Naval Air Systems Command (December 1973). This report briefly reviews the gas turbine fuel deposit problem.
3. R. M. Schirmer, "Morphology of Deposits in Aircraft and Engine Fuel Systems," Report No. 1, Naval Air Systems Command, Contract N00019-68-C-0252 (1968); SAE Preprint 700258 (April 1970).
4. G. E. Zaikov, E. A. Blyumberg, and N. M. Emanuel, Neftekhimiya, 5, 53 (1965); Chem. Abstr., 62, 1447 (1965), state that resins obtained by the liquid-phase oxidations of butane, methyl ethyl ketone, and ethanol are condensation products of acetaldehyde.
5. M. V. Shukkina, Ya. B. Chertkov, and T. I. Kirsanova, Neftekhimiya, 17 (2), 297 (1977); Chem. Abstr., 87, 87511 (1977).
6. R. K. Jensen, S. Korcek, L. R. Mahoney, and N. Zimbo, J. Amer. Chem. Soc., 101, 7574 (1979); 103, 1742 (1981).



JA-2115-2A

FIGURE 1 FI MASS SPECTRUM OF THE DEPOSIT PRECURSORS FORMED IN FUEL C AFTER OXIDATION FOR 255 MINUTES AT 130°C



JA-2115-4A

FIGURE 2 FI MASS SPECTRUM OF THE DEPOSIT PRECURSORS FORMED IN FUEL C AFTER OXIDATION FOR 430 MINUTES AT 130°C

SUPERCRITICAL CARBON DIOXIDE EXTRACTION OF RETAINED PYRIDINE FROM
PYRIDINE EXTRACTS

Barbara F. Smith, Clifford G. Venier, Thomas G. Squires,
Juliana C. Shei, and Jacqueline D. Hunt

Ames Laboratory*, Iowa State University, Ames, Iowa 50011

INTRODUCTION

Solvent extraction of coal is quite attractive to the organic chemist as a means of obtaining a coal model which (a) is directly related to coal, (b) is devoid of complicating mineral matter, and (c) is soluble in at least one solvent. Pyridine is one of the best common solvents for coals with a carbon content of less than 90% (1,2). It has been used extensively for bituminous coals, typically affording extraction yields of 15-30%.

Unfortunately, the use of pyridine as an extractant suffers the major disadvantage that significant amounts of pyridine are retained in coal extracts. Collins, et. al.(3) show that while only 0.24% of the extract weight is irreversibly bound pyridine, fully 11.8% by weight of pyridine cannot be removed under high vacuum (0.133 Pa) in 48 hours, and repeated benzene washing only lowers the pyridine content to 8.85% in an Illinois No. 6 coal extract.

Having qualitatively observed that at least some of the retained pyridine was removed from coal extracts by supercritical carbon dioxide (SC-CO₂), we proceeded to test the feasibility of SC-CO₂ extraction as a means of preparing pyridine free coal extracts.

EXPERIMENTAL

Supercritical CO₂ extraction: Pyridine extract (vlg) was placed in a 15x0.4 cm. stainless steel column containing 5 μ m frits on either end and 300 μ l. of water was added to the extract. The column was maintained at 40°C (the critical temperature of CO₂ is 31.3°C); the precolumn CO₂ pressure was 112 atm (11.4 MPa); a pressure drop of 12 atm (1.2 MPa) was measured across the column; and an exit flow rate of approximately one ml/sec. (atmospheric pressure) was maintained for 4 hours. A spiral glass tube connected to the exit valve collected any non-volatile material that was removed by CO₂ from the coal extract.

*Operated for the U.S. Department of Energy by Iowa State University under Contract No. W-7405-Eng-82. This research was supported by the Assistant Secretary for Fossil Energy, Office of Coal Mining.

Extraction of coal with pyridine: Extracts were obtained by ultrasonically mixing coal with five times its weight of pyridine for 30 minutes at room temperature with a Branson Sonifier 350 (20 kHz with an output power of 350 electrical watts to the converter) (4); filtering the mixture through a 0.5 μ m Teflon millipore pad; concentrating the filtrate on a rotary evaporator and freeze drying the concentrate with three times its volume of benzene overnight at a pressure of 1.33 Pa (5). Oxygen was excluded at all times.

RESULTS AND DISCUSSION

Figure 1 shows the difference spectrum generated by subtracting the infrared spectrum of the CO₂-washed extract from that of the unwashed pyridine extract of Western Kentucky #9 coal from the Ames Coal Library. The sharp spectrum standing out above the background is unambiguously that of pyridine (see Table 1), confirming that the major difference before and after the CO₂ washing is the amount of pyridine in the sample. A small amount of an oil which is primarily aliphatic in nature was also recovered in the eluent from the washing (see Table 3 for weights).

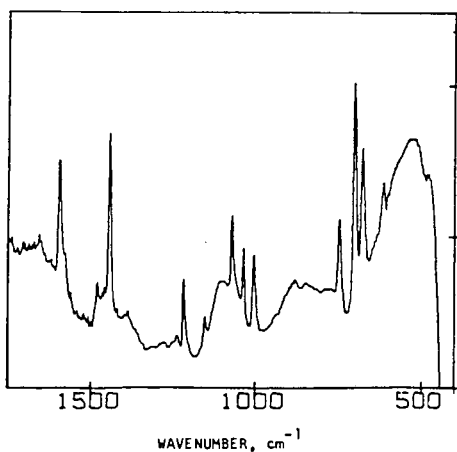


Figure 1. Difference Infrared Spectrum of the Pyridine Extract of a Western Kentucky No. 9 Coal Before and After Washing with Supercritical Carbon Dioxide.

Table 1. Infrared Absorption Maxima (cm⁻¹)

| Difference Spectrum (Fig. 1) | Pyridine ^a |
|------------------------------|-----------------------|
| 1593 | 1583, 1572 |
| 1479 | 1482 |
| 1442 | 1439 |
| 1213 | 1218 |
| 1148 | 1148 |
| 1067 | 1068 |
| 1034 | 1030 |
| 1003 | 992 |
| 748 | 749 |
| 703 | 700 |
| 679 | --- |
| 616 | 605 |

^aA. R. Katritzky and P. J. Taylor, "Infrared Spectroscopy of Heterocycles," in Physical Methods in Heterocyclic Chemistry, vol. 4, Academic Press, New York, NY, 1971, pp. 266-434.

The chemical analyses of coals, extracts and CO₂-washed extracts are in Table 2. Note that the amount of nitrogen in the sample is an important indication of excess pyridine. Assuming that pyridine is the only nitrogen containing compound which would be lost in the carbon dioxide washing, the retained pyridine can be expressed as equation 1.

$$\% \text{pyridine} = \frac{\%N_{\text{obs}} - \%N_{\text{ext}}}{\%N_{\text{pyr}} - \%N_{\text{ext}}} \times 100 \quad 1)$$

where %N_{obs} is the nitrogen found, %N_{pyr} is the nitrogen content of pyridine (17.72%) and %N_{ext} is the nitrogen content of the pyridine free extract

However, the value of the numerator in equation 1 is very sensitive to the exact choice of %N_{ext} and this means that the % pyridine cannot be accurately calculated or used as a reliable basis for comparing samples. By expressing the difference in pyridine levels between the extract before and after CO₂ washing as Δ% pyridine, we obtain equation 2, which is relatively independent of the %N_{ext}.

$$\Delta\% \text{ pyridine} = \frac{\begin{matrix} \text{before} & \text{after} \\ \%N_{\text{obs}} & - \%N_{\text{obs}} \end{matrix}}{\%N_{\text{pyr}} - \%N_{\text{ext}}} \times 100 \quad 2)$$

Table 3 shows the values for Δ% pyridine, the weight percent of a small amount of a highly aliphatic oil which was co-extracted, and the gravimetrically measured weight losses due to the extraction with CO₂. The amount of pyridine removed by the carbon dioxide extraction (8.5 to 10.2%) is in good agreement with Collins' finding that 8.8 to 11.6% pyridine is retained by the extract but not irreversibly bound to it.

The removal of pyridine from the solid extract is analogous to the selective extraction of alkaloids from plant materials with supercritical CO₂(6). In many cases water is as essential for the extraction of nitrogenous bases (e.g. caffeine from coffee beans(7), nicotine from tobacco leaves(8)), as it is for the extraction of pyridine from coal extracts. When dry coal extracts are washed with supercritical CO₂, even for extended periods of time, infrared spectra show that pyridine has been only partially removed.

One intriguing possibility is the pyridine removed under dry conditions is that pyridine which can be removed by benzene washing and that wet carbon dioxide removes the more tightly bound non-extractable pyridine.

TABLE 2. Chemical Analyses of Samples^a

| | ILLINOIS #6 | | | | WESTERN KENTUCKY #9 | | | |
|------------------|-------------------|---------|----------------------------------|--------|---------------------|---------|----------------------------------|--------|
| | Coal ^b | Extract | CO ₂ -Washed Extracts | | Coal ^b | Extract | CO ₂ -Washed Extracts | |
| | | | Exp. 1 | Exp. 2 | | | Exp. 1 | Exp. 2 |
| C | 78.82 | 80.93 | 79.02 | 79.30 | 82.39 | 81.86 | 80.97 | 80.99 |
| H | 5.50 | 6.45 | 6.19 | 6.08 | 5.83 | 6.48 | 6.33 | 6.27 |
| N | 1.59 | 2.91 | 1.52 | 1.53 | 1.91 | 3.67 | 2.22 | 2.09 |
| S _{org} | 2.29 | 2.08 | 2.07 | 1.98 | 2.37 | 1.58 | 1.89 | 1.80 |

^aAnalyses by Galbraith Laboratory, Knoxville, TN.

^bDmmf^c; % mineral matter = 1.13 (%Ash) + 0.47 (%S_{pyr}) + 0.5(%Cl), and

%C_{org} = %C_{dry} - 0.014(%Ash) - 0.0055(%S_{pyr}), and

%H_{org} = %H_{dry} - 0.013(%Ash) + 0.02(%S_{pyr}).

^cGiven, P. H. and Yarzab, R. F., in Karr, C., Jr., ed., Analytical Methods for Coal and Coal Products, Volume II, Academic Press, New York, NY, 1978, Chapter 20.

TABLE 3. Results of Carbon Dioxide Extraction of Pyridine Extract

| Source Coal | Δ% Pyridine ^a | % Oil Extracted | % Weight Loss ^b |
|--------------------|--------------------------|-----------------|----------------------------|
| Ill. No. 6 (1) | 8.6 | 2.3 | 11.2 |
| Ill. No. 6 (2) | 8.5 | 2.3 | 12.2 |
| W. Kent. No. 9 (1) | 9.3 | 0.2 | 13.3 |
| W. Kent. No. 9 (2) | 10.2 | 0.6 | 13.9 |

^aCalculated according to equation 2, assuming %N_{ext} = 1.5 for Ill. No. 6 and 2.0 for W. Kent. No. 9.

^bBased on weight of sample before and after CO₂ extraction.

The effectiveness of supercritical carbon dioxide for removing pyridine may be due to one or all of the following explanations:

- (1) Supercritical carbon dioxide can penetrate the interior of the solid extract more effectively than liquid benzene;
- (2) Carbon dioxide has the ability to displace pyridine whereas benzene cannot;
- (3) The extracting agent is actually carbonic acid, not carbon dioxide, and the process is an acid-base extraction.

Our results suggest that the carbonic acid extraction of the basic pyridine is the most satisfying explanation.

REFERENCES

1. Van Krevelen, D. W., Coal, Elsevier Publishing Co., N.Y. 1961, Ch. X, p. 177-200.
2. Wender, I.; Heredy, J. A.; Neuworth, M. B.; Dryden, I.G.C., "Chemical Reactions and the Constitution of Coal" in Chemistry of Coal Utilization, Second Supplementary Volume, M. A. Elliot, ed., Wiley, New York, N. Y., 1981, Ch. 8, p. 425-521.
3. Collins, C. J.; Hagaman, E. W.; Jones, R. M.; Raaen, V. F., Fuel 1981, 60, 359.
4. For discussion of the effects of ultrasonic irradiation on the dissolution of coal, see Kessler, T.; Friedel, R. A.; Sharkey, A. G. Jr., J. Appl. Chem. 1970, 20, 245.
5. Schweighardt, F. K.; Retcofsky, H. L., private communication to F. K. Schweighardt, as quoted on page 199 of Sharkey, A. G., Jr.; McCartney, J. T., "Physical Properties of Coal and its Products," in Chemistry of Coal Utilization, Second Supplementary Volume, Elliott, M. A., ed., Wiley, New York, 1981.
6. Stahl, E.; Schilz, W.; Shutz, E.; Willing, E., Angew. Chem. Int. Ed. Engl. 1978, 17, 731.
7. Zosel, K., Angew. Chem. Int. Ed. Engl. 1978, 17, 702.
8. Hubert, P.; Vitzthum, O.G., Angew. Chem. Int. Ed. Engl. 1978, 17, 710.

REACTION-INDUCED TEMPERATURE DEVIATIONS DURING
COAL DEVOLATILIZATION IN A HEATED GRID

J. D. Freihaut, M. F. Zabielski and D. J. Seery

United Technologies Research Center
East Hartford, CT 06118

INTRODUCTION

Previous investigations in this laboratory using a heated grid apparatus have indicated:

1. Tar yields and the thermal sensitivity of tar yields obtained in primary (pressure $\leq 10^{-2}$ torr, disperse phase of particles $\leq 100 \mu\text{m}$) devolatilization conditions are distinguishing characteristics of the devolatilization behavior of coal (1).
2. The evolution of coal nitrogen reflects the evolution of coal mass as char, tar or light gas during primary devolatilization. Via coupling to the tar yield, the evolution of coal nitrogen becomes a distinguishing feature of primary devolatilization (2).
3. Increasing the thermal drive (simultaneously varying apparent heating rate and final temperature) did little to alter the total volatile yield but did alter the distribution of volatiles. The most significant changes observed with variations in apparent heating rates from 10^2 C/sec to 10^3 /sec and final temperatures of 600 C and above related to the tar fraction of the volatiles yield (1,2).

A major limitation of the experimental design of these previous experiments was the coupling between the heating rate and final temperature. In addition, no effort was made to determine if the devolatilization process itself significantly influences the temperature history of the sample. To gain further insight into the primary devolatilization process, particularly with respect to the tar yields, a new control circuit was designed to permit any heating rate from 800 C/sec to 4×10^3 C/sec to any final temperature in the 300 to 1100 C range. With this circuit, the effects of sample characteristics on local heating of the grid were examined to assess the influence of devolatilization on programmed heating rates.

In addition to gaining further insight into the tar evolution process it is desirable to address such questions as:

1. Can the primary devolatilization process significantly alter the temperature history of the devolatilizing coal mass?
2. Do coals of varying rank characteristics show the same thermal requirement characteristics when subjected to the same rapid heating conditions?

EXPERIMENTAL DESIGN

Reactor-Analysis System

Figures 1 and 2 display the reactor-analysis system. Provisions are made to monitor one to three thermocouples, a pressure transducer, and the IR active light gases evolved during a devolatilization experiment. The temperature, total pressure and light gas data generated are real time data.

Power to the grid is provided by a programmable power supply (Harrison Model 6269A) operated in one of two modes. In the voltage programmed mode, the voltage delivered to the grid in any instant is determined by a voltage and time selection system (VATS), which will be described in detail elsewhere. Up to five step function increments, both plus and minus, in the grid voltage can be made. The duration of the increments are independently selectable. The response time of the power supply is 20 msec or less.

In the current program mode the screen is forced to conduct a constant current. The voltage across the screen floats to maintain the constant current condition. In the current and time select (CATS) mode, the heating rate and final temperature of the screen are coupled as previously noted (1,2). Figures 3 and 4 display typical temperature vs time plots obtained with each control system.

For synchronization, the FTIR is the master and all other electronic circuits (VATS, CATS, high speed camera, solenoid valve, etc.) are slaves.

Attempts to monitor the real time temperature of the grid by placing small (~75-100 μm dia) thermocouple beads between the folds of the grid produced inconsistent results particularly for heating rates of $\geq 10^3$ C/sec and final temperatures ≥ 800 C. Voltages were frequently induced across the thermocouple bead/leads as were indicated by discontinuities in the temperature-time curves. In the worst case, measured potentials (thermal plus induced) exceeded the maximum allowable for chromel-alumel thermocouples.

Consequently, the temperature of the grid system was monitored by spot welding the beads to the underside of the bottom fold of the grid. Even in this case, care had to be taken to insure a single-spot weld, as it was observed that welds with two or more contact points again produced spurious voltages across the bead. One to three thermocouples attached at different points to the grid could be monitored. Although sampling rates of 2 kHz are possible with the data acquisition system, thermocouple sampling rates of 500 Hz were commonly used. Figures 3 and 4 show typical temperature versus time plots for blank screen runs with the VATS and CATS system respectively.

The pressure was monitored in the devolatilization system with a capacitance manometer. The real time sampling rate of this device is limited to 125 Hz. This was found adequate to track the overall light gas evolution in real time.

The light gas evolution was monitored in real time by a Nicolet FTIR in the rapid scan mode. The rapid scan feature of this device allow collection of data over the complete wavenumber range of the detector as fast as every 120 msec at

8 cm^{-1} resolution. The amounts of identified gaseous species are determined by high resolution (0.5 cm^{-1}) scanning of the cell immediately following the devolatilization process.

Transfer rates between the devolatilization cell and IR cell were determined by slightly pressurizing the devolatilization cell with gas standards and activating the solenoid valve (Fig. 2). The rate of gas transfer from the devolatilization chamber to the IR cell was determined to be fast compared to the rate of evolution at the heating rates used in this study.

High speed films (2 msec/frame) were made of the devolatilization process for some runs. In these cases the camera was focused either upon the glass walls of the grid chamber or upon a KBr disk suspended about 0.4 cm above part of the coal sample within the grid. The purpose of the film was to monitor the real time evolution of the tar species released by following the visible condensation and buildup of the tars on a transparent surface. Under low ambient pressure conditions ($\ll 1$ torr) the tar molecular species are propelled in a line of sight path away from the devolatilizing coal and immediately condense upon striking a cool surface.

Procedure

325 mesh stainless steel screen (~ 7.5 cm long) is folded such that a screen sandwich (~ 1.00 cm wide) is formed. A fine chromel-alumel thermocouple (75-100 μm) bead is spot-welded to the underside of the bottom fold at the center of the screen. For some runs second or third beads are welded approximately 1.5 cm off of screen center, again to the underside of the bottom fold of the grid. The screens are prefired for the following reasons: (1) to obtain a constant tare weight; (2) to obtain nearly constant resistivity and emissivity; (3) to determine the exact control settings needed to produce a given blank screen heating rate, final temperature, and time at a final temperature.

After the prefiring, the screen is loaded with 10-25 mg of -100+325 mesh coal. The coal is vacuum dried at 105 C overnight. The sample is placed in approximately 2 cm length of the strip using the center thermocouple as the marker for the sample center. In the case of the two thermocouple runs the outer thermocouple resides about 0.5 cm from the bulk of the sample area. The "loaded" screen is repositioned in the reactor. The reactor is evacuated and the devolatilization experiment is performed.

The manner of applying power to the grid as well as the temperature monitoring differ significantly from other recent studies using heated grid techniques for rapid heating (3,4,5). For example, although other studies report spot welding a thermocouple to the grid, the weld is such that the bead is apparently positioned between the folds of the grid (5). Upon power application, the thermocouple is forced to follow programmed temperature trajectory by a monitoring-feedback system. In addition, little work has been reported for vacuum conditions despite the fact that it is well established that devolatilization under ambient pressure results in numerous secondary reactions for tar species formed in the primary, thermal devolatilization of the coal (1,6,7).

RESULTS AND OBSERVATIONS

Sample-Induced Temperature Deviations

Figure 5 displays a series of center thermocouple temperature profiles obtained with samples of an Appalachian province, high volatile bituminous coal using the VATS control circuit. In comparing the profiles to corresponding blank screen reference runs (Fig. 3) the deviations in the temperature-time path of the thermocouple are obvious.

Figure 6 displays a series of center thermocouple temperature profiles obtained with samples of a Rocky Mt. province, high volatile bituminous coal using the CATS control circuit. Again the sample-induced temperature deviations become obvious when comparing the profiles to the corresponding blank screen references (Fig. 4).

The Local Nature of the Temperature Deviations

Figure 7 displays temperature profiles for center and edge thermocouples in blank and sample loaded screens, respectively. The curves indicate that the "thermal loading" of the screen by the sample is a local effect. Runs performed with no sample over the center thermocouple but with 5-10 mg of sample placed around the edge thermocouple positions gave similar results but for opposite thermocouples, i.e., the center thermocouple with no sample load reproduced the blank screen temperature-time plot while the edge thermocouple produced a plot similar to the previous, loaded center thermocouple plot. The results indicate that the sample introduces a significant thermal load in the immediate area of the screen such that the local, sample-loaded screen cannot follow the programmed screen temperature.

Physical Loading of the Local Screen

Several types of experiments were performed to ascertain the influence of the physical characteristics of the sample on the programmed temperature profile. In these tests, samples with low volatile matter contents were employed. Figure 8 displays several blank and sample loaded temperature profiles for an anthracite coal. Figure 9 shows blank, coal loaded and resultant char loaded temperature profiles for a high volatile, Appalachian province bituminous coal. The curves obtained with samples of low volatile matter content indicate that the physical properties of the sample such as heat capacity and emissivity do indeed contribute to the local thermal loading of the screen. This perturbation of the physical state of the screen is manifested by a gradual deviation from the programmed heating rate and lower final temperatures achieved. In no case did tests with low volatile matter content produce temperature profiles such as those shown in Fig. 5 and 6. The temperature-time paths observed with coals of appreciable volatile matter are different in character than these observed with nonvolatile samples. The drop in edge thermocouple temperature (Fig. 7) indicates the screen is attempting to reach thermal equilibrium by thermal conduction under pseudo-steady state conditions.

Devolatilization-Induced Temperature Deviations

While Fig. 5 shows variations with programmed final temperature for a particular coal, Fig. 10 shows center thermocouple temperature plots for coals of varying rank using the VATS system. The high volatile bituminous coals appear to have a greater loading effect than coals of lower or higher rank. As noted above, the dip in the thermocouple temperature occurs as the VATS system switches the power output of the supply from the high output (temperature ramping state) to the lower output, temperature hold state. The temperature at the time of the switching is lower and the resultant dip is greater for the high volatile bituminous coals. Similar behavior occurs for lower final temperature runs with the VATS system (see Fig. 5). In these cases however the "warp" in the temperature path is not as severe. As noted above, such thermocouple behavior is not observed for non-volatile samples.

Figure 11 shows center thermocouple plots for 900 C final temperatures runs for coals of varying rank using the CATS system. Due to constant current programming in the CATS system, the instantaneous thermal power generation is different from the VATS system during the main phase of devolatilization process. Consequently, the characters of the temperature plots are different than the corresponding VATS plots for the same final temperatures (See Figs. 10 and 11). The high volatile bituminous coals again display a greater loading effect on the screen than lower or higher rank coals. However, the warp in the temperature plots are not as severe as those observed in the VATS system.

Figure 6 displays temperature curves obtained with a Rocky Mt. province, high volatile bituminous coal for different final temperature runs using the CATS system. The variation in the character of the temperature profile with programmed heating characteristics is apparent. It is to be noted that the product distribution varied significantly with heating conditions although total yield does not, as previously reported (1,2,6,7).

It is apparent from the character of the curves presented that the devolatilization process has a significant effect on the temperature history of the local screen complex. The actual temperature-time path followed is highly dependent on the devolatilization characteristics of the coal sample as well as the programmed, resistive heating of the screen. That is the observed thermocouple temperature path is the resultant of the coupled resistive heating and devolatilization process.

Tar and Light Gas Release Relative to the Thermocouple Temperature History

Figures 6 and 12 indicate the tar and light hydrocarbon (aliphatics) release relative to the thermocouple temperature history. In Fig. 12 the tar yields obtained for various power-on times were obtained by six independent runs for the times shown. The data indicate that the temperature and species evolution profiles are reproducible and that the temperature deviations are induced by the devolatilization process.

The data for the high volatile bituminous coals shown in Figs. 6 and 12 indicate that the tar and light hydrocarbon gases do not evolve simultaneously as has been previously assumed (8). The onset of the tar release precedes the

hydrocarbon light gas evolution for high volatile bituminous coals. For example, the data of Fig. 12 show that at 1.5 sec into a run nearly 50% of the potential tar yield has evolved while only 14% of the total CH₄ yield has evolved. Since the tar yield represents ~ 39% (dry basis) of the parent coal, the devolatilization process is nearly 40% complete before significant CH₄ evolution occurs.

To verify in real time the relative release times, high speed films of the tar release process were made in the manner described above. Several Appalachian and Rocky Mt. province high volatile bituminous coals were examined. Frame-by-frame inspection of these films were compared to the rapid scan infrared data and real time pressure and temperature data. For the coals tested:

1. The tar release was more closely associated with the initial temperature deviations.
2. The onset of the tar release precedes the onset of the light hydrocarbon release.
3. The light hydrocarbon gas evolution occurs mainly in the secondary temperature rise.
4. Rocky Mt. province high volatile bituminous coals displayed more overlap in the tar and light gas evolution than the Appalachian province high volatile bituminous coals.

Discussion and Summary

The results clearly demonstrate that the devolatilization process has a considerable influence on the time-temperature history of the local screen in immediate contact with the sample. Physical properties of the sample load (e.g. heat capacity, emissivity) cannot account for the character or magnitude of the non-steady state temperature deviations that are observed with volatile samples. With respect to the coal particles, the direct implication is that the temperature path is the resultant of several components: the resistive heating of the grid, the physical properties of the samples, the devolatilization properties of the sample. Once the range of devolatilization temperatures of a particular coal is achieved, the primary devolatilization process appears to dominate the temperature-time trajectory. Because the heat requirement of the primary devolatilization affects the temperature trajectory of the coal particle, a real time model of primary coal devolatilization must necessarily include a consideration of this requirement. In addition, the data appears to indicate that the heat requirement varies with the rank characteristics of the coal.

For a transient process such as rapid coal devolatilization the absolute magnitude of the heat required to vaporize the volatile components need not be large to result in a significant deviation from a programmed heating rate or a calculated heating rate of a nonvolatile particle. A modest heat requirement coupled to a sufficiently fast primary devolatilization process can cause appreciable changes in the temperature trajectory of a particle (9,10).

The results indicate that the tar release is closely coupled in time to the devolatilization-induced temperature deviations during primary devolatilization.

The onset of the tar release significantly precedes the slower light hydrocarbon gas evolution. Thus the rapid devolatilization heat requirement appears to be associated with the energy required to overcome intermolecular attractive forces (van der Waal, hydrogen bonds, dipole-dipole interactions) that exist among the mix of molecular species present in the coal. Once the devolatilization heat requirement is met, rapidly supplying additional thermal energy can result in thermal cracking of the primary tars, decreasing the tar yield while increasing light gas yields (See Fig. 6 and Ref. 1,2).

A quantitative real time model of coal devolatilization requires a quantitative estimate of the primary devolatilization heat requirement as well as real time data on the primary tar release rates and their susceptibility to thermal cracking. Provisions are being made to monitor the real time power delivered to the grid as well as the real time evolution of primary tars.

ACKNOWLEDGMENTS

The authors gratefully acknowledge the able technical assistance of Dave Santos and Gerald Wagner.

REFERENCES

1. Freihaut, J. D. and Seery, D. J., An Investigation of Yields and Characteristics of Tars Released During the Thermal Decomposition of Coal, ACS Fuel Chem. Preprints, 26, No. 1, 133 (1981).
2. Freihaut, J. D. and Seery, D. J., Evolution of Fuel Nitrogen During the Vacuum Thermal Devolatilization of Coal, ACS Fuel Chem. Preprints, 26, No. 3, 18 (1981).
3. Franklin, H. D., Mineral Matter Effects in Coal Pyrolysis and Hydropyrolysis. Thesis, MIT (1980).
4. Stangely, P. C. and Sears, P.L., Rapid Pyrolysis and Hydropyrolysis of Canadian Coals. Fuel, 60, 131 (1980).
5. Hamilton, L. H., Ayling, A. Bruce, and Shibaska, M., A New Experimental Device for Pyrolysing Coal Under Controlled Conditions Over a Wide Range of Heating Rates. Fuel, 58, 873 (1979).
6. Anthony, D. B., Howard, J. B., Hottel, H. C. and Meisner, H. P., Rapid Devolatilization of Pulverized Coal. 15th Symp. (Int) Combustion, Combustion Institute, Pittsburgh, p. 1303 (1975).
7. Suuberg, E. M., Rapid Pyrolysis and Hydropyrolysis of Coal. Sc. D. Thesis, MIT, 1977.
8. Solomon, P. R. and Colket, M. B., Coal Devolatilization. 17th Symp. (Int.) Combustion, Combustion Institute Pittsburgh, p. 131 (1979).
9. Freihaut, J. D. and Vastola, F. J., A Computational Examination of the Effect of Coupled Heat Transport and Chemical Kinetics Upon Single Particle Coal Pyrolysis. Presented at Eastern States Combustion Institute Mtg., Miami, Fla. (1978).
10. Freihaut, J. D., A Numerical and Experimental Investigation of Rapid Coal Pyrolysis. Thesis, Penn State Univ. (1980).

EXPERIMENTAL NETWORK

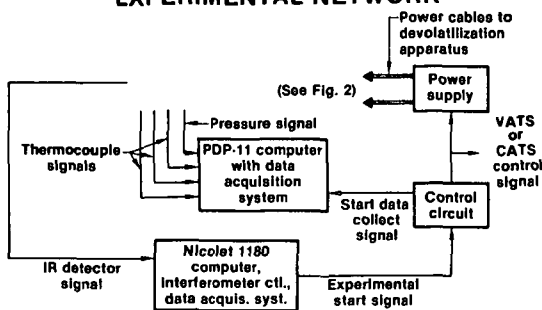


Fig. 1

HEATED-GRID DEVOLATILIZATION APPARATUS

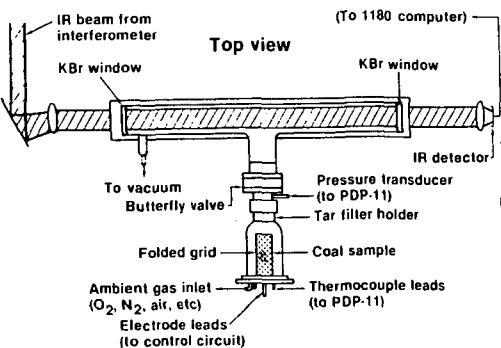


Fig. 2

BLANK SCREEN TEMPERATURE — TIME

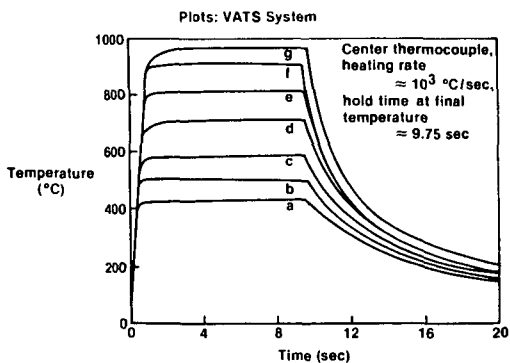


Fig. 3

TEMPERATURE — TIME PLOTS

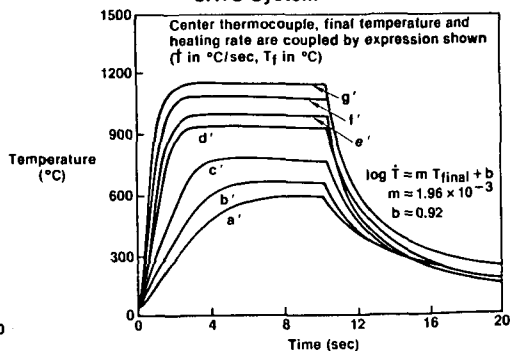


Fig. 4

CENTER THERMOCOUPLE TEMPERATURE — TIME

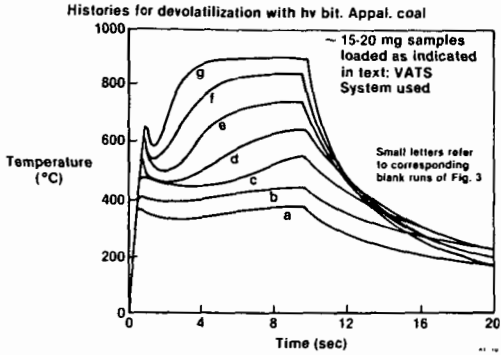


Fig. 5

CENTER THERMOCOUPLE TEMPERATURE — TIME

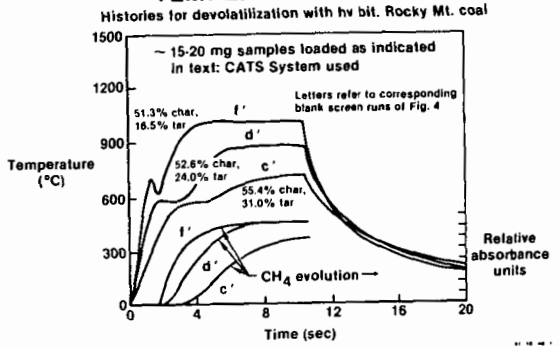


Fig. 6

CENTER AND EDGE THERMOCOUPLE TEMPERATURE HISTORIES

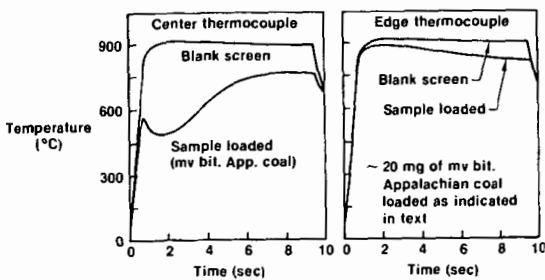


Fig. 7

BLANK AND SAMPLE-LOADED THERMOCOUPLE PLOTS: ANTHRACITE

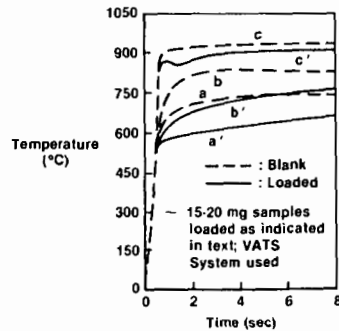


Fig. 8

COAL VS CHAR LOADING OF SCREEN

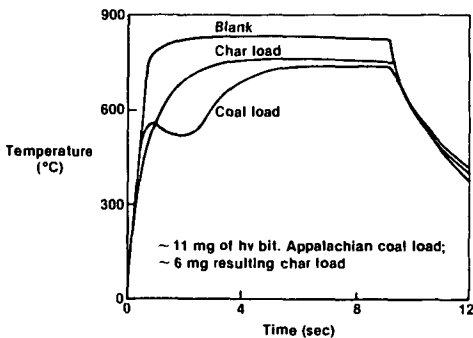


Fig. 9

VARIATION OF THERMAL LOADING WITH RANK-VATS SYSTEM

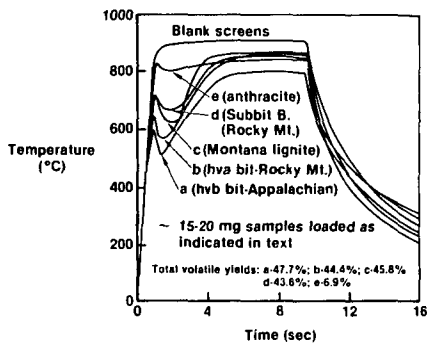


Fig. 10

VARIATION OF THERMAL LOADING WITH RANK - CATS SYSTEM

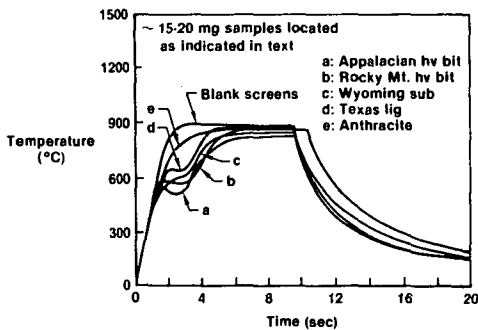


Fig. 11

TAR AND LIGHT HYDROCARBON YIELDS

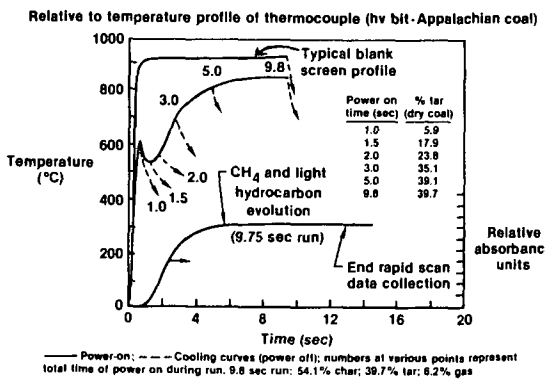


Fig. 12

TRACE ELEMENT DISTRIBUTION IN THE THREE TON PER DAY H-COAL PROCESS DEVELOPMENT UNIT

H. B. Booher, J. W. Adkins, A. W. Wells, and H. Schultz

U. S. Department of Energy
Pittsburgh Energy Technology Center
P. O. Box 10940
Pittsburgh, PA 15236

Introduction

Current research in coal conversion has identified a number of processes that potentially could produce clean burning fuel from coal. The shifting of combustion sources from oil to coal has accentuated the need for a clean burning fuel oil derived from coal. Scientists have studied possible degradation of the environment by tracking trace elements in coal burning power plants, in coal liquefaction pilot plants of various sizes, and in bench scale units (1,2,3,4,5). A study made of the Savannah River coal-fired power plant has given insight into trace element buildup in the environment surrounding the plant (1). The Synthane (coal gasification) process was studied, utilizing isotope dilution Spark Source Mass Spectrometry (SSMS) (2). Determination of trace metals in Solvent Refined Coal by means of INAA (Instrumental Neutron Activation Analysis) revealed much lower elemental concentrations in the SRC product than in the feed coal (3,4). The trace element studies of the Synthoil 1/2 ton per day coal liquefaction Process Development Unit also showed that trace element concentrations are lower in the product oil (CLP) than in the feed coal (5,6). In order to further our knowledge of the fate of the trace metals in coal hydro-liquefaction processes, a study was conducted of the H-Coal Process Development Unit (PDU) located in Trenton, N.J.

Experimental

In the H-Coal process, dried pulverized coal, clean oil tank material, and hydroclone overflow are reacted with hydrogen at pressures up to 3500 psig and temperatures up to 850°F (7). The PDU is unique in that a substantial amount of the liquid products are recycled to the slurry mix tank so equilibrium conditions can be maintained. The products of the process are the atmospheric overhead, which is a light distillate material, and the vacuum still bottoms. The vacuum still bottoms is a viscous material that becomes a semiliquid upon cooling. The severity of the reactor conditions determines the relative amounts of the individual products made (7). The reactor design uses the fluidized bed concept (8). Since the catalyst is in constant motion, spent catalyst may be extracted and fresh catalyst injected into the reactor while the PDU is in operation. Figure 1 shows the flow diagram of the HRI PDU #130 unit.

A sampling exercise was conducted at the H-Coal PDU in Trenton, N.J., the goal of which was to obtain representative, uncontaminated samples for trace element characterization. Factors considered in planning the sampling of the plant included transportation of the trace clean containers to the sampling site, transportation of the samples back to PETC, environmental conditions at the plant, and the PDU design. The flow rates and process streams sampled are listed in Table 1. The feed coal for the run sampled was Burning Star Illinois No. 6.

All liquid samples were collected in soft glass containers with teflon lid spacers where required. Coal samples were taken in polyethylene bags whose tops were sealed with rubber bands. The coal filled bags were placed in tared one-gallon paint cans that were then sealed. Cleaning the soft glass containers was accomplished by detergent washing, rinsing with distilled water, soaking in dilute hydrochloric acid, rinsing with deionized distilled water, and air drying. All liquid samples were drawn directly into the heated clean soft glass containers. Sample temperatures of up to 500oF were encountered when taking some of the liquid samples; so the containers had to be heated to prevent cracking. The head spaces of the precleaned sample containers were purged with nitrogen to prevent exposure of the bulk samples to air after the samples were taken.

Elemental analyses performed on a wide variety of coals has shown the presence of over half the elements in the periodic table (10). Sample inhomogeneity (5) and complex coal matrices (2) play an important role in the precision of analysis. Atomic absorption spectroscopy, both flame and flameless, has been employed successfully for the analyses of coal and coal by-products (11,12) and was therefore selected for this study. To obviate possible matrix effects, the method of standard additions was used, along with deuterium arc background correction. Small amounts of standard solutions of the elements of interest were added to separate aliquots of the sample for each element. The total concentration of each element after the addition was in no case more than three times the concentration in the original solution. Absorbance readings obtained for the sample and the three additions were entered into a desk top calculator programmed to calculate a correlation coefficient, an intercept, and a slope by the method of linear least squares. Concentration levels in the original sample were calculated using these values plus the sample weights, volumes, etc. This method was used with all samples. Method blanks were carried through all steps of the sample preparation with each set of samples.

Analysis of 19 coals in one study (10) and 11 coals in another (13) showed trace element concentrations varied widely between coals from the western and the eastern United States. Details of sample preparation in the determination of trace elements in coal and coal-derived materials have been previously described (9). Briefly the sample is ashed and extracted with dilute hydrochloric acid or dilute nitric acid. Remaining residues are dissolved using a fusion procedure. The dissolved ash is then combined with the acid extract. Four aliquots of the combined solution are taken, standard solution is added to three of the aliquots, and the solutions are analyzed as described above.

Experience has shown that the concentration of chromium, copper, manganese, and nickel in coal is usually greater than one part per million. The exact concentration of each of these elements in a specific coal depends largely on the geographic origin and the type of coal.

Cadmium is usually present in coal at concentration levels below one part per million (9). Lead concentrations are normally much higher. Although flame AA is quite sensitive to cadmium (0.025 $\mu\text{g/ml}$ for 1% absorption), the sensitivity for lead is only 0.5 $\mu\text{g/ml}$ for 1% absorption. Solvent extraction was used to increase the sensitivity of the Pb determination by increasing its concentration. Iodide complexes of Pb and Cd were formed in ascorbic acid media,

followed by extraction into MIBK (Methyl Isobutyl Ketone). Acidified MIBK was used to establish the instrumental base line. Blank solutions were carried through all steps of the analytical procedure.

Discussion

The recoveries of the determined trace elements, as indicated by the material balances around the slurry mix tank and the product separation unit, demonstrate the success of the sampling procedures and analytical methods employed in this study. The trace elements entering the PDU are accounted for within the precision of the data presented. Material balances (i.e., total input versus total output) ranged from 69% to 137% and are shown in Table II. Incomplete recoveries of Cu, Cr, Mn, and Pb may be indicative of an elemental buildup in the process streams analyzed. Statistical analysis of the available data do not indicate such a buildup, although further work may need to be done in this area.

Table I. HRI PDU #130 PROCESS STREAMS AND FLOW RATES

| PERIOD 14A | | | |
|--|---------------|--------------|--|
| <u>Process Streams</u> | <u>Lb/Hr*</u> | <u>Kg/Hr</u> | <u>Nature of Samples</u> |
| Feed Coal | 335.2 | 152.0 | Plant grind (98% through -50 mesh) |
| Hydroclone Overflow | 359.3 | 163.0 | Viscous oil held at 500°F (ash = 9.3%) |
| Clean Oil Tank Material | 321.7 | 145.9 | Comb. of vacuum still overhead & atmospheric still bottoms |
| Slurry Mix | 1,016 | 460.9 | Mixture of feed coal, atmospheric still bottoms, vacuum still overhead, & hydroclone overhead (ash = 7.2%) |
| Hydroclone Underflow | 278.3 | 126.2 | Viscous oil held at 500°F (ash = 13.7%) |
| Atmospheric Still Overhead | 49.9 | 22.6 | Light oil |
| Atmospheric Still Bottoms (COT) | 250.7 | 113.7 | Liquid feed to the clean oil tank |
| Injected Feed Water | 2.3 | 1.0 | Tap water |
| Sour Water | 33.1 | 15.0 | Comb. of feed water and water generated in the PDU |
| Vacuum Still Overhead (COT) | 44.8 | 20.3 | Liquid feed to the clean oil tank |
| Atmospheric Still Bottoms (product) | 8.5 | 3.9 | Sample stream outlet used for continuous sampling |
| Vacuum Still Overhead (product) | 1.0 | 0.5 | Sample stream outlet used for continuous sampling |
| Vacuum Still Bottoms | 234.1 | 106.2 | Product of run 130-88 period 14A |
| Atmospheric Still Bottoms (hydroclone) | 60.0 | 27.2 | Liquid feed to the hydroclone |
| Overhead Flash Material | 89.8 | 40.8 | Very light oil |
| Makeup Oil | 34.8 | 15.8 | Oil used when the PDU is not at equilibrium |

*Feed Rates as supplied by plant personnel.

Table II. RECOVERIES OF TRACE ELEMENTS IN THE H-COAL PDU.

#130 RUN 130-88 PERIOD 14A

| | (Weight in mg) | | | | | |
|-------------------------|----------------|-----------|-----------|-----------|-----------|-----------|
| | <u>Cu</u> | <u>Cr</u> | <u>Mn</u> | <u>Ni</u> | <u>Pb</u> | <u>Cd</u> |
| Slurry Mix Tank | | | | | | |
| Inputs | 2,900 | 6,100 | 17,200 | 3,500 | 3,300 | 40 |
| Outputs | 2,900 | 6,600 | 21,000 | 3,500 | 3,200 | 46 |
| % Recovery | 102 | 109 | 120 | 100 | 98 | 113 |
| Product Separation Unit | | | | | | |
| Inputs | 2,900 | 6,600 | 21,000 | 3,500 | 3,200 | 46 |
| Outputs | 2,900 | 5,900 | 19,700 | 3,500 | 2,900 | 56 |
| % Recovery | 97 | 89 | 94 | 101 | 90 | 122 |
| Complete Plant | | | | | | |
| Inputs | 1,400 | 2,900 | 9,300 | 1,600 | 1,700 | 27 |
| Outputs | 1,000 | 2,300 | 9,800 | 1,400 | 1,200 | 36 |
| % Recovery | 76 | 81 | 105 | 85 | 69 | 137 |

Appendix

TRACE ELEMENT ANALYSIS OF PROCESS STREAMS

From HRI PDU #130 PERIOD 14A

| <u>PROCESS STREAMS:</u> | ug/gm | | | | | |
|-------------------------------|-----------|-----------|-----------|---------------------|-----------|---------------------|
| | <u>Cu</u> | <u>Cr</u> | <u>Mn</u> | <u>Ni</u> | <u>Pb</u> | <u>Cd</u> |
| Feed Coal | 8.9 | 19 | 61 | 11 | 11 | 0.18 |
| Hydroclone Overflow | 8.4 | 20 | 48 | 12 | 9.6 | 0.08 |
| Clean Oil Tank Material | 0.6 | 0.2 | 0.9 | 0.1 | 0.1 | 0.002 |
| Slurry Mix | 6.2 | 14 | 45 | 7.7 | 7.0 | 0.10 |
| Hydroclone Underflow | 9.9 | 22 | 92 | 13 | 11 | 0.34 |
| Atmospheric Still Overhead | 0.036 | 0.022 | 0.015 | 0.017 | 0.003 | 0.04 ⁻² |
| Atmospheric Still Bottoms | 1.1 | 0.2 | 0.8 | 0.1 | 0.068 | ≤0.01 ⁻⁴ |
| Vacuum Still Overhead | 0.4 | 0.003 | 0.01 | ≤0.01 ⁻² | 0.019 | ≤0.01 ⁻⁴ |
| Injected Feed Water | 0.028 | ≤0.006 | 0.007 | 0.001 | ≤0.001 | 0.01 ⁻² |
| Sour Water | 1.2 | 0.029 | 0.021 | 0.032 | ≤0.001 | 0.004 |

REFERENCES

1. Horton, J. H., Dorsett, R. S., Cooper, R. E. Trace Elements in the Terrestrial Environment of a Coal-Fired Powerhouse. ERDA/EPA Interagency Agreement, DP-1475, Sept. 1977.
2. Koppelaar, D. W., Lett, R. G., Brown, F. R. Determination of Nickel, Copper, Selenium, Cadmium, Thallium, and Lead in Coal Gasification Products by Isotope Dilution Spark Source Mass Spectrometry. *Anal. Chem.* No. 52 (1980), pp. 44-49.
3. Filby, R. H., Shah, K. R., Sautter, C. A. A Study of Trace Element Distribution in the Solvent Refined Coal (SRC) Process Using Neutron Activation Analysis. *Journal of Radioanalytical Chemistry*, Vol. 37 (1977), pp. 693-704.
4. Filby, R. H., Shah, K. R., Sautter, C. A. Trace Elements in the Solvent Refined Coal Process. *Symposium Proceedings: Environmental Aspects of Fuel Conversion Technology III*, Hollywood, Florida, Sept. 1977.
5. Lett, R. G., Adkins, J. W., DeSantis, R. R., Brown, F. R. Trace and Minor Elemental Analysis of Coal Liquefaction Products. *PETC/TR-79/3*, August 1979.
6. Lett, R. G., Schmidt, C. E., DeSantis, R. R., Sharkey, A. G. Jr., Screening for Hazardous Elements and Compounds in Process Streams of the 1/2 Ton Per Day Synthoil Process Development Unit. *PERC/RI-77/12*, October 1977.
7. Hoertz, C. D., Swan, J. C. The H-Coal Process. *Coal Conversion Technology*, ACS Symposium Series, 110, pp. 91-101, 1979.
8. Kang, C. C., Johanson, E. S. Deactivation of Co-MO Catalyst During H-Coal Operations. *Preprints, Division Fuel Chemistry, ACS*, Vol. 21, No. 5, p. 32, 1976.
9. Schultz, H., Gibbon, G. A., Hattman, E. A., Booher, H. B., and Adkins, J. W. The Distribution of Some Trace Elements in the 1/2 Ton Per Day Synthoil Process Development Unit. *PERC/RI-77/2*, February 1977.
10. Ruch, R. R., Gluskoter, H. J., and Shimp, N. F. Occurrence and Distribution of Potentially Volatile Trace Elements in Coal. *Environmental Geology Notes*. Illinois State Geological Survey, No. 72, August 1974.
11. Schultz, H., Hattman, E. A., Booher, H. B. The Fate of Some Trace Elements During Coal Pretreatment and Combustion. In *Trace Elements in Fuel*, Babu, S. P., ed. *Advances in Chemistry Series 141*, ACS, Washington, D.C., 1975.
12. Coleman, W. M., Perfetti, P., Dorn, H. D., Taylor, L. T. Trace-element Distribution in Various Solvent Refined-Coal Fractions as a Function of the Feed Coal. *Fuel*, Vol. 57, pp. 612-616, October 1978.
13. Cavallaro, J. A., Deurbrouck, A. W., Schultz, H., Gibbon, G. A., Hattman, E. A. A Washability and Analytical Evaluation of Potential Pollution from Trace Elements in Coal. *Environmental Protection Agency, EPA-600/7-78-038*, March 1978.

AN ANALYSIS OF KEROGEN DISTRIBUTION IN GREEN RIVER OIL SHALE

John F. Patzer, II

Chemicals and Minerals Division
Gulf Research & Development Company
Pittsburgh, Pennsylvania 15230

ABSTRACT

The classification of Green River oil shales through density separation techniques reveals some new insights into the naturally occurring distribution of kerogen in shale. Twelve Colorado shales and one Utah shale, covering a range of sources and grades, were classified into fractions of varying kerogen content through heavy-media density separation. Analysis of the separation data reveals that the shales all have a linear relationship between the enriched grade kerogen content and the weight fraction of total kerogen recovered in the enriched grade. The slope of the linear relationship correlates with the original shale kerogen content. The correlation provides a powerful tool for a priori prediction of the results for any classification process which operates on density separation. The existence of such a linear relationship implies that the naturally occurring differential mass distribution function for kerogen in shale is an inverse relation between weight fraction of shale and kerogen content of the fraction, i.e., kerogen-lean fractions are present in much greater quantity than kerogen-rich fractions. Another aspect of the distribution function is the existence of clearly defined, sharp cut-points which contain the entire distribution within a range of kerogen content dependent upon the original shale grade.

The Green River oil shale formation comprises one of the largest fossil fuel energy reserves in the world. Commercial development of this source is very likely to become a reality within the next five to ten years. Initial development will almost certainly use current retorting technology. However, full scale development will probably occur only after second generation technology, now in development in many research labs, reaches commercial viability. Knowledge and understanding about how kerogen is distributed within the shale formation will aid in developing more selective, viable processes for recovery of the energy contained in the kerogen.

Gulf has been interested for several years in the potential possibility of selectively discarding very lean shales prior to retorting. If the economic cost of such selective rejection were low enough, the reduction in shale volume retorted for equivalent oil production could yield potential benefits through lowered capital and operating costs for a retort and, possibly, through lessened environmental impact because less shale would be processed.

The correlation between shale density and Fischer Assay yield has been known for many years.^{1,2} Figure 1, due to Smith,¹ shows the expected Fischer Assay as a function of density. The existence of such a correlation results from the wide separation between kerogen and mineral matter density in shale, about 1070 kg/m³ and 2720 kg/m³, respectively, and the narrowness of the mineral matter density range. Smith² developed the relations

$$(GPT) = (31.563 \cdot 10^{-6}) (D_T)^2 - 0.205998 (D_T) + 326.624 \quad (1)$$

$$x_w^o = \frac{D_o}{D_m - D_o} \left(\frac{D_s}{D_T} - 1 \right), \quad (2)$$

$$x_w^m = 1 - x_w^o = \frac{D_m}{D_m - D_o} \left(1 - \frac{D_o}{D_T} \right), \quad (3)$$

$$x_V^O = \frac{1}{D_m - D_o} (D_m - D_T), \quad (4)$$

$$x_V^m = 1 - x_V^O = \frac{1}{D_m - D_o} (D_T - D_o), \quad (5)$$

to describe the interrelationships between the shale density and shale organic content. Equation (1) is the least-squares representation of the correlation shown in Figure 1. Equations (2) to (5) are derived from simple material balance considerations. A best fit to numerous data requires the mineral matter density, $D_m = 2720 \text{ kg/m}^3$, and the organic density, $D_o = 1050$ to 1070 kg/m^3 .

Heavy-Media Separation

The relation between density and organic content provides the basis for a separations scheme based upon density differences.^{3,4} Twelve Colorado shales and one Utah shale, as shown in Table 1, were separated by heavy-media techniques at the Institute of Mineral Research, Michigan Technological University. The shales represent a variety of grades, ranging from 16.5 to 44.2 GPT, and a variety of particle sizes.

The separations were performed in both batch and continuous circuit operations as schematically depicted in Figure 2. The shale sample was immersed in a bath of given density and separated into sink-and-float fractions. The sink fraction was collected. The float fraction was immersed in a bath of lower density and split into sink-and-float fractions. The procedure was performed at least twice, and as many as five times, on the various shales. An air pycnometer was used to determine the density of each separate fraction produced by the sink/float operation. The original sample density was then back-calculated from the individual fraction densities. The heavy-media separations experiments provide cumulative weight fraction distribution curves as a function of specific gravity, as depicted in Figure 3 for shales D

and I. The relatively lean shale D and relatively rich shale I have distinctly different cumulative distribution curves. As is expected from the relation between Fischer Assay and density, the richer shale contains considerably more lower density material than the leaner shale.

The heavy-media separations were analyzed on the basis of splitting the original sample into two fractions, a rich shale fraction and a lean shale fraction, as depicted in Figure 4. The weight fraction organic, (X_w^O) , for each split was determined by calculating the density of each split and using Equation (2).

A measure of the efficiency of the separation process, i.e., the ability to selectively separate rich from lean shales, is obtained by plotting $(X_w^O)_1$, versus the organic recovery in the rich fraction,

$$R = (X_w^O)_1 (w_1) / (\bar{X}_w^O), \quad (6)$$

as shown in Figure 5. An enrichment plot, such as Figure 5, is a concise statement about the ability to perform a separation and the economic benefit of doing so. When the separations operating parameter, in this case, density, is a continuous variable, it is possible to draw a continuous performance curve which describes the separations potential for the mineral. The shape and properties of the performance curve will be determined solely by the distribution of the variable under consideration. Clearly, a very steep slope in the $R > 0.90$ range is desirable for a truly efficient separation process.

The results of the heavy-media separation experiments are shown in Figure 6. Four separate panels are shown only for clarity. The experimental data points are indicated by open symbols. The lines are the result of linear least-squares regression of the data. The most remarkable feature of Figure 6 is that all of the data can be adequately represented by the linear representation

$$(X_w^O)_1 = mR + b \quad (7)$$

Table II provides the calculated values for the slopes and the correlation coefficient for the regression. The goodness of the linear fit is indicated by the range of correlation coefficients, 0.95 to 0.99.

The ability to make an a priori prediction of the slope based only upon knowledge of the feed shale organic concentration, or equivalently, density, would allow prediction of heavy-media separation results. It would also provide a method for heavy-media process control. Figure 7 shows a relation between the slope and feed shale weight fraction organic, given by

$$m = 0.671 - 10.21 (\bar{x}_w^0) + 28.423 (\bar{x}_w^0)^2 \quad (8)$$

The equation, obtained from a quadratic least-squares regression, is only a marginal fit to the data. However, it provides a reasonable estimate for engineering purposes.

With a priori knowledge of the slope, it is possible to predict density separations results. The intercept, b , is obtained from

$$b = (\bar{x}_w^0 - m) \quad \text{at } R = 1 \quad (9)$$

Figure 8 depicts a comparison between the actual and predicted separations results for shales D and I. The linear fit correlation using the coefficients predicted by (8) and (9) reproduce the experimental least-squares relations within an average error of 9% and a maximum deviation of 19%. Thus, it is possible to make reasonable a priori predictions of heavy-media results.

Kerogen Distribution in Shale

The linear relation between weight fraction organic in the enriched shale and kerogen recovery can be used to obtain some basic information about the distribution of kerogen in oil shale. Assuming that the weight fraction

organic can be represented as a continuous variable, a differential weight fraction distribution function can be defined by

$$\int_{\tilde{X}_w^0}^{\tilde{X}_w^0} f(\tilde{X}_w^0) d\tilde{X}_w^0 = 1 \quad (\text{normalization}) \quad (10)$$

$$\int_{\tilde{X}_w^0}^{\tilde{X}_w^0} \tilde{X}_w^0 f(\tilde{X}_w^0) d\tilde{X}_w^0 = \tilde{X}_w^0 \quad (\text{expected value}) \quad (11)$$

where $f(\tilde{X}_w^0) d\tilde{X}_w^0$ represents the differential shale mass between organic content \tilde{X}_w^0 and $\tilde{X}_w^0 + d\tilde{X}_w^0$. The upper limit on \tilde{X}_w^0 is readily obtainable from the linear relation (7) as $(\tilde{X}_w^0)_{\max} = b$ at $R = 0$.

The functional form of the differential shale mass distribution function can be obtained by back-calculating f_j as a function of $(\tilde{X}_w^0)_i$ from (7) by incrementing R in even steps, as

$$(\tilde{X}_w^0)_{1,i} = mR_i + b = \frac{\sum_{j=1}^i f_j (\tilde{X}_w^0)_j}{\sum_{j=1}^i f_j} \quad (12)$$

$$w_{1,i} = \frac{R_i (\tilde{X}_w^0)_i}{(\tilde{X}_w^0)_{1,i}} = \frac{i}{\sum_{j=1}^i f_j} \quad (13)$$

to obtain

$$f_j = w_{1,i} - \sum_{j=1}^{i-1} f_j \quad (14)$$

$$(\bar{X}_w^0)_i = \frac{(\bar{X}_w^0)_{1,i} w_{1,i} - \sum_{j=1}^{i-1} f_j (\bar{X}_w^0)_j}{f_i} \quad (15)$$

The average kerogen concentration of the sample, (\bar{X}_w^0) , is a known and the values of m and b are prescribed through the linear correlation. In the limit as $i \rightarrow \infty$, one obtains the continuous differential shale mass distribution function

$$f(\bar{X}_w^0) = A/(\bar{X}_w^0) \quad (16)$$

by this procedure.

The final two unknowns for the differential distribution function, A and $(\bar{X}_w^0)_{\min}$, are obtained through application of the normalization and expected value properties of the distribution function,

$$\int_{(\bar{X}_w^0)_{\min}}^{(\bar{X}_w^0)_{\max}} f(\bar{X}_w^0) d\bar{X}_w^0 = A \ln [(\bar{X}_w^0)_{\max} / (\bar{X}_w^0)_{\min}] = 1 \quad (17)$$

$$\int_{(\bar{X}_w^0)_{\min}}^{(\bar{X}_w^0)_{\max}} (\bar{X}_w^0) f(\bar{X}_w^0) d\bar{X}_w^0 = A [(\bar{X}_w^0)_{\max} - (\bar{X}_w^0)_{\min}] = \bar{X}_w^0. \quad (18)$$

Note that the normalization property implies that there also exists a practicable minimum naturally occurring grade of shale present in any given deposit. Figure 9 shows the differential weight fraction distribution function for 20 GPT and 35 GPT shales based upon the predictive correlation of

equations (8) and (9). Although Figure 9 shows very sharp cut-off points in the distribution, naturally occurring distributions are likely to have some tailing effects.

Although a straight-line relation between weight fraction kerogen content and weight fraction kerogen recovery has the unique representation in differential shale mass distribution function space given by Equation (16), the actual distribution of kerogen in shale might differ somewhat from the inverse proportional relationship. This results because the straight-line relation is an inference from least-squares regression of the data and because the least-squares regressions are not perfect, i.e., correlation coefficient equal to one. In order to validate the differential distribution function, it is important to examine the cumulative weight fraction data of the heavy-media separations experiments in differential manner. Because of the small number of data points available per sample, such differential distributions are only crude representations of the actual distribution.

Figure 10 presents the histogram of weight fraction kerogen for shale D normalized so that the area under the bars equals one. Such a histogram is an approximation to the differential distribution function. The plotted histogram is similar to the derived inverse proportional distribution function. However, some tailing which is evident at the leaner grades of shale indicates that a rival distribution function, the log normal distribution function given by

$$f(\tilde{x}_w^0) = \frac{1}{\sqrt{2\pi} \sigma} \cdot \frac{1}{(\tilde{x}_w^0)} \exp \left[-\frac{(\ln \tilde{x}_w^0 - \xi)^2}{2\sigma^2} \right] \quad (19)$$

could also approximate the distribution.

The inverse proportional distribution function is described by the parameters A, $(\tilde{x}_w^0)_{\max}$ and $(\tilde{x}_w^0)_{\min}$ which are directly determinable and related in a fundamental, physical manner to the shale. The log normal distribution has two parameters, ξ and σ which have no readily determinable

physical relation to shale. They can be determined in a reasonable manner, however, by assuming that 95% of the shale has kerogen content less than the $(\bar{X}_w^0)_{\max}$ predicted by the a priori method, Equations (7), (8) and (9). Figure 11 contrasts the predicted inverse proportional and log normal differential distribution functions for a 20.6 GPT shale. The two distributions are similar, with rapid rise to a maximum in kerogen content and tailing off toward richer shales. The log normal distribution is more diffuse, with greater tailing at both the rich and lean ends of the distribution.

Figure 12 shows the predicted enrichment plot for a 20.6 GPT shale with the inverse proportional and log normal differential distribution functions as parameters. A heavy vertical bar is drawn at $R=0.20$ to emphasize that this was the smallest value on the abscissa which was obtained in the experimental study. The salient feature of Figure 12 is that for values of $R < 0.20$, both distributions could easily give least-squares representations as straight lines; significant curvature in the log normal distribution occurs at values of $R < 0.20$. Thus, it is doubtful that the experimental data can readily distinguish between the two distributions.

The inverse proportional distribution is, however, the recommended distribution function for describing a shale resource for three reasons. First, the parameters which define the distribution have real, physical meaning which readily define what is present in a shale deposit. Second, the functional form of the inverse proportional distribution is more easily worked with in analytical equations than is the functional form of the log normal distribution. Finally as demonstrated in Figure 13, the inverse proportional distribution function provides excellent agreement with experimental observations.

ACKNOWLEDGMENT

The author is indebted to O. A. Larson of GR&DC who conceived of and directed the experimental program which provided the data necessary for this analysis and to C. W. Schultz and E. L. Michaels who performed the experiments at the Institute of Mineral Research, Michigan Technological University.

NOMENCLATURE

| | |
|-----------------|--|
| b | intercept in linear relation |
| D_o | kerogen (organic) density, kg/m^3 |
| D_m | mineral density, kg/m^3 |
| D_T | oil shale density, kg/m^3 |
| GPT | oil shale Fischer Assay, gal/ton |
| m | slope in linear relation |
| R | weight fraction organic recovery |
| x_v^o | volume fraction kerogen (organic) in shale |
| x_v^m | volume fraction mineral in shale |
| x_w^o | weight fraction kerogen (organic) in shale |
| x_w^m | weight fraction mineral in shale |
| \bar{x}_w^o | average weight fraction kerogen (organic) |
| \tilde{x}_w^o | point weight fraction kerogen (organic) |
| w | weight fraction of shale |

subscripts

| | |
|---|---|
| 1 | riched fraction from heavy-media separation |
| 2 | lean fraction from heavy-media separation |
| i | increment index |
| j | increment index |

REFERENCES

1. Smith, John Ward, "Specific Gravity-Oil Yield Relationship of Two Colorado Oil Shale Cores," *Ind. Eng. Chem.*, 48 (3), 441 (1956).
2. Smith, John Ward, "Theoretical Relationship Between Density and Oil Yield for Oil Shales," USBM ROI 7248, 1976.
3. O. A. Larson, to appear in ACS Symposium Series.
4. J. F. Patzer, manuscript submitted to *Fuel*.

TABLE I
OIL SHALES USED FOR HEAVY MEDIA SEPARATION

| <u>SHALE</u> | <u>GPT</u> | <u>SIZE, CM</u> | <u>SOURCE</u> |
|--------------|------------|-----------------|--|
| A | 16.5 | 0.20-0.64 | C-8 TRACT, MAHOGANY ZONE |
| B | 19.2 | 0.64-5.08 | ANVIL POINTS MINE, 0 TO +20 FT, MAHOGANY MARKER |
| C | 19.3 | 0.64-5.08 | C-8 TRACT, MAHOGANY ZONE |
| D | 22.0 | 0.64-7.62 | RIFLE MINE, COMPOSITE BEDS A, B, C, E, F, G, H, I, J |
| E | 22.2 | 0.64-1.91 | RIFLE MINE, COMPOSITE BEDS A, B, C, E, F, G, H, I, J |
| F | 22.6 | 0.64-7.62 | RIFLE MINE, BEDS A, B, C |
| G | 26.7 | 0.64-5.08 | ANVIL POINTS MINE, -20 TO -40 FT, MAHOGANY MARKER |
| H | 29.8 | 0.64-7.62 | RIFLE MINE, BEDS E, F |
| I | 30.9 | 0.64-5.08 | ANVIL POINTS MINE, 0 TO -20 FT, MAHOGANY MARKER |
| J | 32.1 | 0.64-7.62 | RIFLE MINE, BEDS G, H, I, J |
| K | 36.1 | 0.64-5.08 | HELL'S COLE CANYON, UTAH, MAHOGANY ZONE |
| L | 38.7 | 0.64-15.2 | HORSE DRAW CREEK, R-3 ZONE, USBM 96" SHAFT |
| M | 44.2 | 0.64-15.2 | HORSE DRAW CREEK, R-4 ZONE, USBM 96" SHAFT |

TABLE II

LINEAR REGRESSION OF HEAVY MEDIA SEPARATION RESULTS

$$(X_w^0)_1 = mR + b$$

| <u>SHALE</u> | <u>SLOPE, m</u> | <u>CORRELATION COEFFICIENT</u> |
|--------------|-----------------|------------------------------------|
| A | -0.116 | -1.000 |
| B | -0.157 | -0.977 |
| C | -0.083 | -0.995 |
| D | -0.174 | -0.995 |
| E | -0.151 | -0.997 |
| F | -0.105 | -0.997 |
| G | -0.250 | -0.996 |
| H | -0.274 | -0.987 |
| I | -0.301 | -0.969 |
| J | -0.268 | -0.982 |
| K | -0.262 | -0.993 |
| L | -0.083 | -0.949 |
| M | -0.132 | -0.986 |

Figure 1

SHALE GRADE AS A FUNCTION OF DENSITY

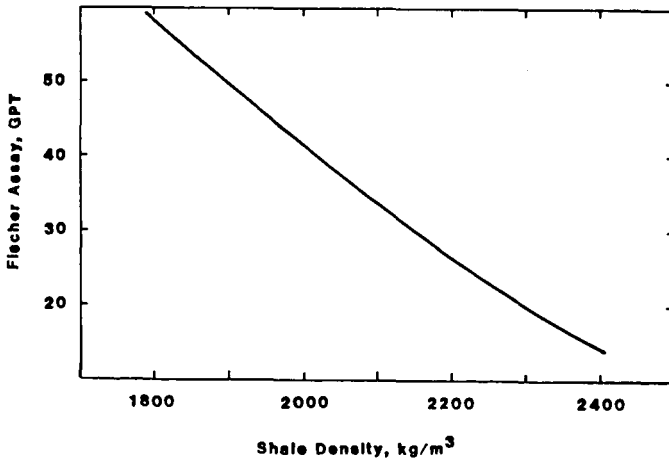


Figure 2
HEAVY MEDIA OIL SHALE SEPARATIONS

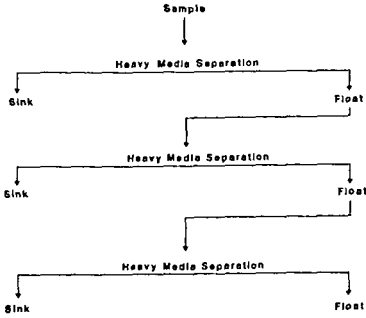


Figure 4
OIL SHALE BENEFICIATION ANALYSIS

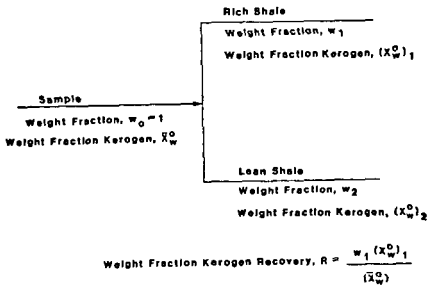


Figure 3
CUMULATIVE WEIGHT FRACTION DISTRIBUTION CURVE FOR HEAVY-MEDIA SEPARATION OF OIL SHALE AS A FUNCTION OF SPECIFIC GRAVITY

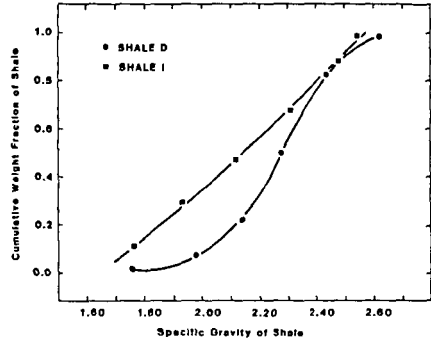


Figure 5
TYPICAL ENRICHMENT PLOT FOR OIL SHALE BENEFICIATION

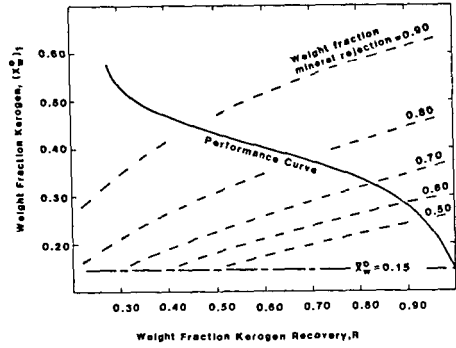


Figure 6
HEAVY MEDIA SEPARATIONS RESULTS

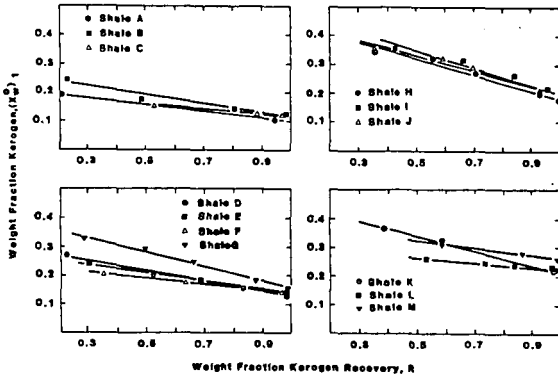


Figure 7
SLOPE OF LINEAR BENEFICIATION EQUATION
AS A FUNCTION OF FEED SHALE KERODEN CONTENT

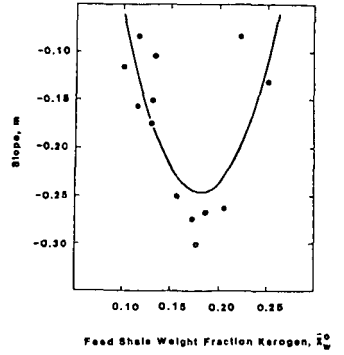


Figure 8
COMPARISON BETWEEN ACTUAL AND PREDICTED RESULTS
FOR HEAVY MEDIA SEPARATION OF SHALE

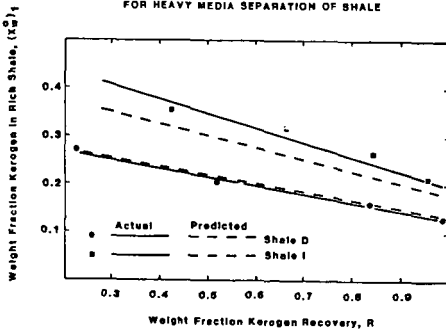


Figure 9
DIFFERENTIAL DISTRIBUTION FUNCTION

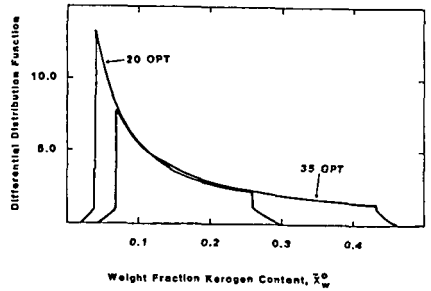


Figure 10
AREA NORMALIZED HISTOGRAM OF
WEIGHT FRACTION KEROGEN FOR SHALE D

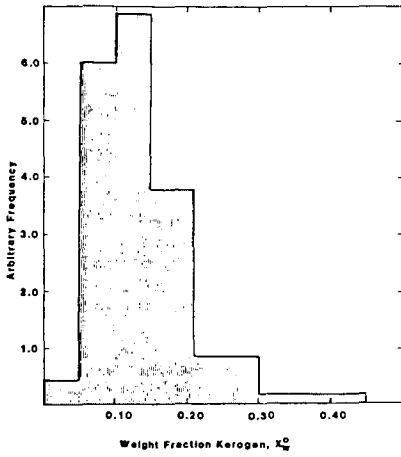


Figure 11
PREDICTED DIFFERENTIAL DISTRIBUTION
FOR 20.6 GPT ($\bar{x}_w^0 = 0.12$) SHALE

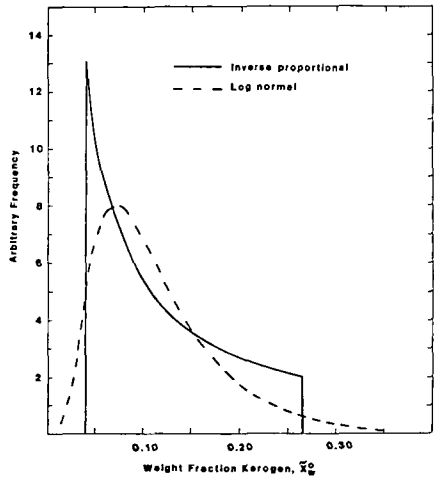


Figure 12
PREDICTED ENRICHMENT PLOT FOR 20.6 GPT ($\bar{x}_w^0 = 0.12$) SHALE

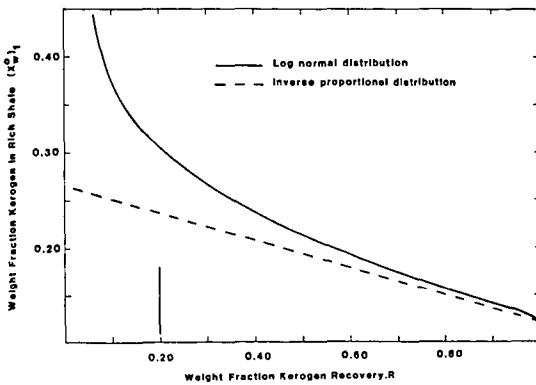
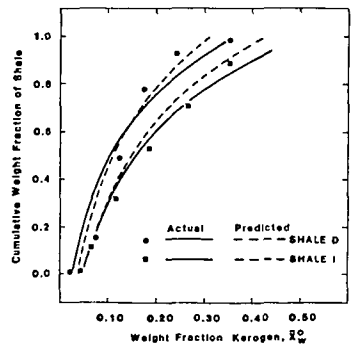


Figure 13
CUMULATIVE WEIGHT FRACTION DISTRIBUTION
CURVE FOR SHALE AS A FUNCTION OF WEIGHT
FRACTION KEROGEN



CHARACTERIZATION OF OIL SHALE
BY FTIR SPECTROSCOPY

D. C. Cronauer

Gulf Research and Development Company
P.O. Drawer 2038, Pittsburgh, PA 15230

R. W. Snyder and P. C. Painter

Polymer Science Section
The Pennsylvania State University
University Park, PA 16802

INTRODUCTION

The optical advantages and data handling capabilities of Fourier transform infrared (FT-IR) instruments have led to a resurgence of the use of infrared spectroscopy for the characterization of energy related materials. Most of the work that has so far been reported has involved the characterization of coal. Methods for the quantitative determination of mineral matter (1-5) and various studies of the organic components of coal (6-13) have been published. The only paper (to our knowledge) concerning the application of FT-IR to the study of shale was reported by Solomon and Miknis (14). These authors considered the analysis of both the mineral and organic components. However, they reported a number of problems with the mineralogical analysis of certain shales, particularly the determination of the carbonates present in samples from Colorado. The analysis of the organic component was confined to the aliphatic C-H stretching region of the spectrum near 2900 cm^{-1} . Unfortunately, these bands are often all that is detectable of the organic component in the infrared spectra of shales.

If FT-IR is to provide further insight into shale structure and composition, some of the problems associated with mineralogical analysis will have to be solved. In terms of the characterization of the organic component, studies of kerogen should provide more information concerning chemical structure than allowed by an analysis of whole shale. In this communication we will consider preliminary results of applying FT-IR to these particular problems.

FT-IR ANALYSIS OF MINERAL MATTER IN SHALE

The qualitative identification of the major mineral components present in a number of shale samples using dispersive infrared techniques was reported by Estep et al (15). In most of the shales considered the major mineral species were carbonates and the clays illite and montmorillonite. Because of the overlap of the bands of these components, a quantitative analysis could not be performed. We have discussed in a number of publications the advantages and utility of FT-IR in the analysis of such complex multicomponent systems (1-5). Essentially, a library of the spectra of mineral standards, stored in digital form on disk or magnetic tape, is used to analyze the shale (or coal low temperature ash) under consideration. The spectrum of the standard is subtracted from that of the shale. The subtraction parameter that results in the complete elimination of the bands of the particular mineral being subtracted then provides a measure of the weight fraction of that mineral present in the shale. There are some subtleties to the method that can be applied, such as the use of least-squares spectral fitting programs (4), but the method is relatively straightforward and will be demonstrated below. However, before proceeding to this illustration it is necessary to emphasize the critical importance of sample preparation.

In initial work (1) we ground samples in a Wig-L-Bug in the presence of 300 mg of KBr, so that standard infrared pellets could be subsequently pressed. Optimum

grinding times were determined for our particular grinding equipment. It is important to note that absorbance values in the final spectra of minerals and shale should be less than 1.0, to ensure a linear relationship between the amount of material in the infrared beam and the intensity of the absorption bands (Beer-Lambert law). This in turn requires the use of an accurate micro-balance, since optimum results are usually obtained with between 0.1 and 0.2 mg of sample for clays and between 0.3 to 0.5 mg for most other minerals. The grinding time was naturally dependant on the type of equipment used and could be as long as 30 mins for old equipment or as little as 45 secs for new, more vicious, instruments.

Recently a problem with this method of sample preparation as applied to the hard minerals has been pointed out to us by Elliott and co-workers (16). The absorption values for minerals such as quartz and dolomite can be dramatically increased by pregrinding the mineral with just a small amount of KBr (25 mg) followed by further grinding with the rest of this alkali halide (275 mg). However, this procedure produced less satisfactory results for the clays, presumably due to agglomeration and subsequent poor mixing of these materials under severe grinding conditions. Consequently, our procedure has been modified to account for these results in the following manner.

- 1) Clays are prepared using the method outlined above. With the new model Wig-L-Bug only 45 seconds of grinding are required.
- 2) Quartz and carbonate samples are prepared by first grinding the mineral with 25 mg of KBr for 30 seconds. The rest of the KBr (275 mg in our procedure) is then added to the capsule and the material is ground for another 30 seconds.

Because of the preponderance of 'hard' minerals in most shale samples, the latter method was used in sample preparation. Our initial studies indicate that the problems encountered by Solomon and Miknis (14) in determining carbonates in shale could (at least in part) be due to sample preparation problems. Carbonate minerals have strong bands near 1400 cm^{-1} , but different species are more clearly differentiated by the characteristic bands near 880 and 720 cm^{-1} . The peak positions of four different carbonate samples are listed in Table 1. Figure 1 compares the infrared spectra of two different shales. The strong bands at 882 and 729 cm^{-1} indicate that the most prevalent carbonate present is dolomite. We originally considered that it would be a straightforward task to subtract the bands of this mineral thereby revealing the presence of other carbonates, which could then be analyzed. However, we found that if the 729 cm^{-1} band was subtracted out there still remained considerable absorption at 882 cm^{-1} . Other carbonates have bands in this region, but at different frequencies (see Table 1). One possible explanation is the presence of isomorphous cation substitution in the dolomite. It has been shown that Fe can replace Mg in the dolomite structure in continuously variable proportions to give ankerite. (17) The spectra of ankerite samples we had available, however, showed frequency shifts as well as intensity changes compared to the spectrum of dolomite. Finally, at the moment we were about to abandon this problem in despair, we found that the sample preparation procedure recommended for hard minerals by Elliott et al (16) provided a solution to the analysis of shale. We had already preground our shale samples in the Wig-L-Bug as we had obtained them in the form of large particles. Pregrinding in the presence of the rest of the KBr, resulted in a change of the relative intensities of the 882 and 729 cm^{-1} bands, as shown in Figure 2. The difference spectra obtained by subtracting each of the two dolomite samples from that of the shale are shown in Figure 3. It can be seen that the subtraction of the dolomite prepared according to Elliott et al (16) worked very well leaving carbonate bands that, in fact, corresponded to one of our ankerite standards. Consequently, we believe it is now possible to obtain a good quantitative analysis of mineral matter in shale, but the importance of careful and reproducible sample preparation procedures in such analysis cannot be overemphasized.

FT-IR determination of the mineralogical composition of a set of shale samples (Green River shale, Mahogany Zone) is now being performed. The initial results are presented in Table 2, but are at the time of writing incomplete in that the analysis of the clay component could not be performed. A spectrum of one of the shale samples is shown in Figure 4 and the clay component is characterized by a strong band near 1040 cm^{-1} and a second weak band near 470 cm^{-1} . Unfortunately, we could not find an illite or montmorillonite standard in our spectral library that provided a match in terms of band positions and relative intensities. We are presently attempting to separate this clay from the shale in order to obtain the correct "standard".

The necessity of using mineral standards for analysis may at first sight seem a major disadvantage of the FT-IR method. However, all other techniques (eg x-ray diffraction) for quantitative analysis also rely on standards for calibration. At least with infrared subtraction methods subtle differences in the character and composition of a particular mineral in a shale relative to a "standard" can become apparent. For example, the subtraction of the spectrum of a dolomite sample from that of a shale is illustrated in Figure 5. If the 882 cm^{-1} band is subtracted to the baseline, as shown in the difference spectrum in this figure, the 725 cm^{-1} band is slightly negative, indicating over subtraction of this band. However, subtraction based on the elimination of the 882 cm^{-1} band is probably correct, since the very strong 1450 cm^{-1} band is eliminated by this procedure. The complete difference spectrum is shown in Figure 4 and it can be seen that with the 1450 cm^{-1} band subtracted a weak absorbance centered near 1460 cm^{-1} remains and this band can be assigned to CH_2 bending modes of the organic component. The difference in intensity of the 728 cm^{-1} band between the spectrum of the dolomite present in the shale and that of the standard is probably due to the presence of a small amount of iron in the dolomite lattice. FT-IR can only be used to quantitatively determine major mineral components, but the sensitivity of the spectrum to such subtle effects indicates the relative ease of selecting the correct standard. Subtraction of the wrong mineral naturally leads to obviously distorted difference spectra. However, the analysis will only be as good as the standards available, and we are presently extending our mineral library to include a number of dolomite and ankerite samples so as to cover a range of compositions.

FT-IR ANALYSIS OF KEROGEN

Solomon and Miknis (14) demonstrated that the aliphatic C-H content, as measured by the intensity of the C-H stretching mode near 2920 cm^{-1} , correlated reasonably well with oil yield. We have determined similar results in initial studies. Figure 6 shows the aliphatic CH stretching region of three shale samples. The plots have been made on the same absorbance scale, although the baselines have been offset for clarity. The oil yield of the samples decreased in the samples going from the top spectrum A to the bottom C, the values being 33.6, 20.3 and 14.2 gallons per ton, respectively. Not surprisingly, the intensity of the CH stretching modes is proportionally higher in the samples yielding the largest quantity of oil. A plot of the peak height of the 2920 cm^{-1} bands against yield or, as shown in Figure 7, organic carbon content, shows a roughly linear relationship (more scatter is observed in the plot of absorbance against oil yield, and our results are similar in this respect to those obtained by Solomon and Miknis (14)). Since Kerogen is a multi-component system we would anticipate some variations in the width at half height of the bands from sample to sample. Consequently, we are also in the process of determining peak areas (from curve-resolved spectra). Determinations of this type should certainly prove a useful tool for assaying oil shales, but in terms of structural characterization it necessitates the use of careful, well-defined curve resolving techniques and we have discussed such methods in terms of the analysis of coal(18). Derivative methods are used to determine the number of curves in a spectral profile and also provide initial estimates of the values of various band parameters (peak position, width at half-height) used in the subsequent curve resolving process. If these procedures are followed we can have a high degree of confidence in the results. The resolution of the C-H stretching region into five bands is shown in Figure 8. All

of these bands can be readily identified from well-established group frequencies. The bands at 2924 and 2855 cm^{-1} are the asymmetric and symmetric stretching modes (respectively) of methylene units; the bands at 2956 and 2872 cm^{-1} are the asymmetric and symmetric stretching modes of methyl groups; the 2895 cm^{-1} band has a contribution from lone C-H groups, but overtone and combinations of bending modes near 1450 cm^{-1} also absorb at this frequency. Curve resolving of the C-H stretching region has proved very successful, with a standard deviation of $\pm .2$ for the initial set of oil shale samples.

If we obtained values of the extinction coefficients, relating individual band intensities to the concentration of the corresponding functional groups, then we would have at our disposal useful structural information. It has been shown that paraffin standards can be used to obtain extinction coefficients for the analysis of petroleum fractions (19,20). However, in order to be able to use extinction coefficients from long chain paraffins (which can be readily prepared as KBr pellets, unlike the shorter chain material), we must determine whether the kerogen is sufficiently saturated and contains sequences of CH_2 units, so that extinction coefficients can be transferred with minimal error.

This knowledge can be determined from the 700 to 900 cm^{-1} region of the spectrum, where characteristic bands can be assigned to aliphatic CH_2 rocking modes and aromatic C-H out-of-plane bending modes. This region of the spectrum of a kerogen obtained from one of our Green River shale samples is shown in Figure 9, where it is compared to the spectrum of a kerogen obtained from a Rio Blanco shale. These samples were prepared at Gulf R&D by consecutively washing the whole shale with HCl, HF and HCL acids to remove the mineral components. The spectrum of the kerogen from Green River shale is dominated by a band at 724 cm^{-1} , characteristic of the CH_2 rocking mode of sequences of four or more methylene units (21). Consequently, we can have a high degree of confidence in applying extinction coefficients determined from various paraffins to the analysis of this shale. However, the Rio Blanco shale also displays overlapping bands near 730, 745 and 820 cm^{-1} characteristic of 3,2 and lone CH_2 groups, respectively. This shale would not seem to be a candidate for analysis based on extinction coefficients determined from long chain paraffins. Incidentally, the bands at 820 cm^{-1} and 745 cm^{-1} could have a small contribution from aromatic bending modes, and more work is necessary to sort out such relative contributions. We are still in the process of applying the extinction coefficients determined from paraffins to the analysis of our Green River shale samples, but these results clearly demonstrate a number of important points. The most important of these is that an examination of the CH_2 rocking region of the spectrum of shale reveals important structural information. In addition, the differences in the spectra of various shales in this region of the spectrum suggests that a single set of extinction coefficients will probably not prove adequate for analysis of all shales. Instead a range of values will probably have to be determined according to the sequence distribution of CH_2 units and the presumably corresponding degree of branching of the aliphatic structure present.

Finally, it is important to briefly indicate that other types of structural information can be obtained from the infrared spectrum of kerogen. Figure 10 shows the spectrum of a kerogen from Green River shale and it can be seen that there is a complex of bands between 1800 and 1500 cm^{-1} . The band near 1700 cm^{-1} is almost certainly due to carboxylic acid groups, but high frequency shoulders due to other carbonyl structures are apparent (possibly esters) and a strong band near 1630 cm^{-1} is also intriguing. By analogy with the spectrum of coal (13) this band could be due to aromatic structures, a highly conjugated hydrogen bonded carbonyl or COO groups. FT-IR studies of acid and alkali washed material and methylated samples (to convert COOH groups to esters) should clarify these assignments and allow further structural information to be obtained.

REFERENCES

1. Painter, P.C., Coleman, M.M., Jenkins, R.G., Whang, P.W. and Walker, P.L., Jr., Fuel, 57, 337 (1978).
2. Painter, P.C., Coleman, M.M., Jenkins, R.G., and Walker, P.L., Jr. Fuel, 57, 125 (1978).
3. Painter, P.C., Snyder, R.W., Youtcheff, J., Given, P.H., Gong, H. and Suhr, N., Fuel 59, (1980).
4. Painter, P.C., Rimmer, S., Snyder, R.W. and Davis, A. Applied Spectroscopy 35, 102 (1981).
5. Painter, P.C., Youtcheff, J. and Given, P.H., Fuel, 59, 523 (1980).
6. Painter, P.C. and Coleman, M.M., Fuel, Vol. 58, 301 (1979).
7. Painter, P.C., Yamada, Y., Jenkins, R.G., Coleman, M.M. and Walker, P.L., Jr., Fuel, Vol. 58, 293 (1979).
8. Painter, P.C., Snyder, R.W., Pearson, D.E. and Kwong, J., Fuel 59, 282 (1980).
9. Painter, P.C., Coleman, M.M., Snyder, R.W., Mahajan, O., Kamatsu, M. and Walker, P.L., Jr., Applied Spectroscopy 35, 106 (1981).
10. Solomon, P.R. ACS Division of Fuel Chemistry Preprints 24 #3, 184 (1979) and Advances in Chemistry series #192, 95 (1981).
11. Solomon, P.R. Paper presented at meeting, Chemistry and Physics of Coal Utilization, Morgantown, WV, June 2-4 (1980), to be published.
12. Painter, P.C., Snyder, R.W., Starsinic, M., Coleman, M.M., Kuehn, D. and Davis, A. Applied Spectroscopy, 35, 474 (1981).
13. Painter, P.C., Snyder, R.W., Starsinic, M., Coleman, M.M., Kuehn, D. and Davis, A. Adv Chem Ser (to be published).
14. Solomon, P.R. and Miknis, F.P. Fuel, 59, 893 (1980).
15. Estep, P.A., Kovach, J.J. Hiser, L.L., and Karr, C., Jr., in Spectrometry of Fuels. Ed R. A. Friedal, Plenum Press, 1970 pp. 228-247.
16. Elliott, J.J., Brown, J.M. and Baltrous, J.P. Private Communication - to be published.
17. Smith, J.W. and Robb, W.A. J. Sediment. Petrol. 36, 486 (1966).
18. Painter, P.C., Snyder, R.W., Starsinic, M., Coleman, M.M., Kuehn, D.W. and Davis, A., Applied Spectroscopy, 35, 475 (1981).
19. Hastings, S.H., Watson, A.T., Williams, R.B., and Anderson J.A., Jr., Analytical Chemistry, 24, 612 (1952).
20. Francis, S.A. Analytical Chemistry, 25, 1466 (1953).
21. Drushel, H.V., Ellerbe, J.S., Cox, R.C. and Lane, L.H. Analytical Chemistry, 40, 370 (1968).

TABLE 1

CHARACTERISTIC BANDS IN THE FTIR SPECTRA OF CARBONATES.

| <u>Mineral</u> | <u>Origin</u> | <u>Bands cm⁻¹</u> |
|----------------|--------------------------|----------------------------------|
| Ankerite | Hancock County, Illinois | 876 727 713 |
| Dolomite | Eiginvin Twp., Ontario | 882 729 |
| Siderite | Nova Scotia | 873 741 |
| Calcite | Unknown Origin | 877 713 |

TABLE 2

MINERALOGIC ANALYSIS OF GREEN RIVER SHALE SAMPLES
WEIGHT % OF WHOLE SHALE

| <u>GRDC Sample</u> | <u>Microcline</u> | <u>Quartz</u> | <u>Dolomite</u> | <u>Calcite</u> | <u>Aragonite</u> |
|------------------------|-------------------|---------------|-----------------|----------------|------------------|
| 13 | 10 | 15 | 22 | 15 | 15 |
| 14 | 15 | 15 | 35 | - | - |
| 15 | 8 | 15 | 25 | 10 | 9 |
| 16 | 10 | 16 | 30 | 9 | 14 |
| 17 | 15 | 15 | 20 | 15 | 11 |
| 18 | 12 | 15 | 27 | 8 | 14 |
| 19 | 12 | 17 | 35 | 7 | 10 |
| 20 | 10 | 16 | 34 | 9 | 15 |
| 21 | 5 | 16 | 28 | 15 | 11 |
| 22 | 10 | 18 | 35 | 10 | - |

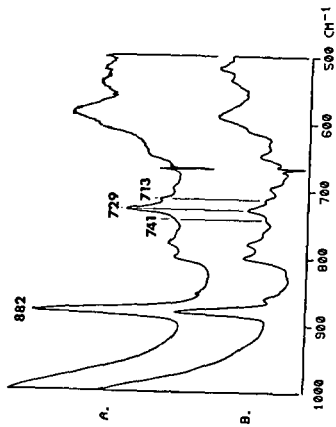


Figure 1: FT-IR spectra in the region 1000 to 500 cm^{-1} of two shale samples A. Piceance Basin Shale. B. Green River shale (Spectra recorded on Digilab FTS-15B, 400 scans, resolution 2 cm^{-1}).

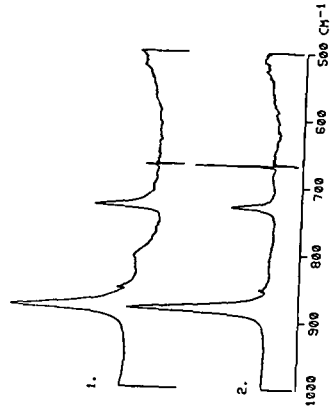


Figure 2: FTIR spectra of dolomite samples 1. Prepared using old grinding method. 2. Prepared according to Elliott et al (ref. 16).

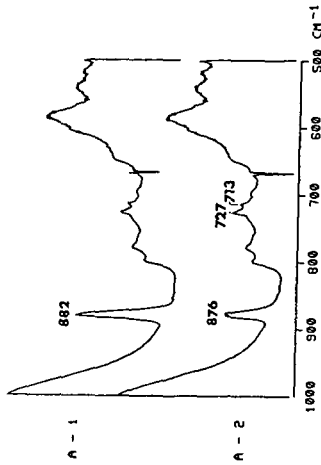


Figure 3: Difference spectra; A-1. Piceance basin shale - 'old' dolomite. A-2. Piceance basin shale - 'new' dolomite.

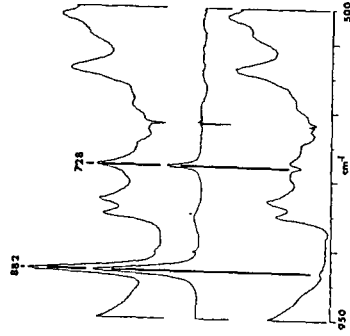


Figure 4: Top FT-IR spectrum of Green River shale, Mahogany zone sample. Middle. FT-IR spectrum dolomite. Bottom. Difference spectrum obtained by eliminating 882 cm^{-1} band.

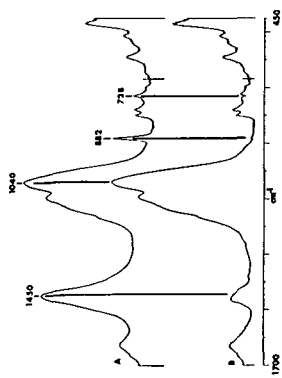


Figure 5: A. FT-IR spectrum Green River shale sample. B. Difference spectrum after subtraction of spectrum of dolomite.

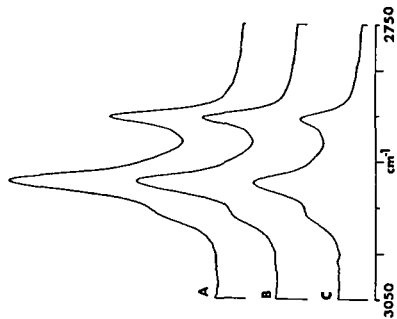


Figure 6: FTIR spectra of samples of Rio Blanco shale. A. 33.6 C.P.T. B. 20.3 C.P.T. C. 14.2 C.P.T.

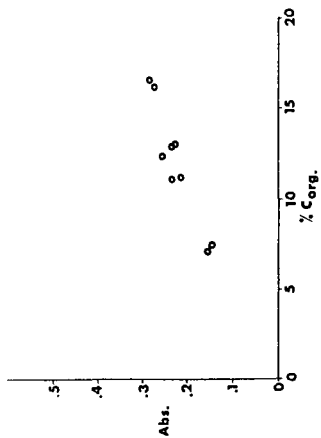


Figure 7: Plot of peak height 2924 cm^{-1} band against % organic carbon for Green River shale samples.

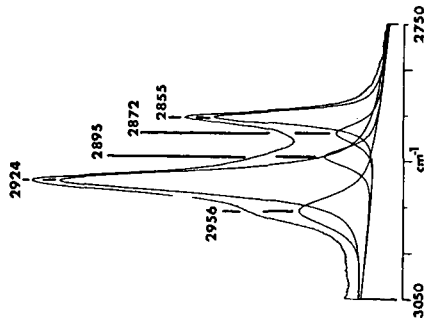


Figure 8: Curve resolved aliphatic C-H stretching region of FT-IR spectrum of shale sample.

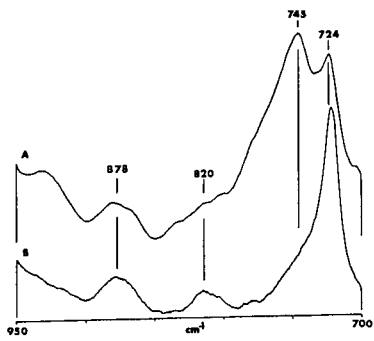


Figure 9: A. FT-IR spectrum (950-700 cm^{-1}) of kerogen from Rio Blanco shale. B. FT-IR spectrum of kerogen from Green River shale.

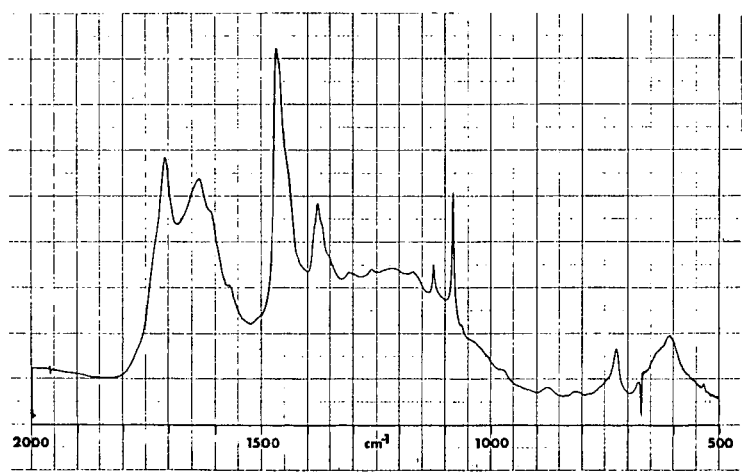


Figure 10: FT-IR spectrum of kerogen from Green River shale.

THE KINETICS OF THE THERMAL DECOMPOSITION OF MOROCCAN OIL
SHALE BY THERMOGRAVIMETRY

Deepak S. Thakur and H. Eric Nuttall
Department of Chemical and Nuclear Engineering,
The University of New Mexico, Albuquerque, New Mexico 87131
and
C. Y. Cha
Science Applications, Inc.,
Golden, Colorado 80401.

ABSTRACT

The kinetics of the thermal decomposition of Moroccan oil shale have been studied by isothermal and non-isothermal thermogravimetry. The effects of carrier gas flow rate and heating rate on kerogen decomposition have been examined. The weight-loss data obtained under non-isothermal conditions have been analyzed by the Coats-Redfern technique while the isothermal TG data have been correlated by using the integral method of kinetic analysis. A joint use of isothermal and non-isothermal TG measurements have shown that the oil shale decomposition involves two consecutive reactions with bitumen as an intermediate product. Kerogen decomposition into bitumen proceeds with an activation energy of 40 kJ/mole while the pyrolytic bitumen decomposes into products with an activation energy of 60 kJ/mole. A close agreement between the kinetic parameters, viz., activation energy and reaction order ($n = 1$) etc., obtained under both isothermal and non-isothermal conditions substantiates the validity of the first order rate equation. The fact that the kinetic parameters remain unchanged with variations in heating rate (K/min) indicates that these parameters are probably insensitive to the efficiency of heat transfer between the sample and surroundings. However, the low activation energy for bitumen decomposition indicates certain mass transfer limitations such as diffusion of organic matter through the mineral carbonate matrix.

INTRODUCTION

Morocco has moderate deposits of oil shale which can be exploited using American processing technology. To date, U. S. processes are based on the thermal treatment of the shale to decompose kerogen into the desired oil product. The key step in the thermal treatment is the pyrolysis stage and involves the kinetic rate of kerogen decomposition and the corresponding formation of oil. Because oil shales have differing origins and are found in differing geological environments, it is not surprising that they behave differently when subjected to pyrolysis conditions. This study was initiated to investigate the pyrolysis kinetics of Moroccan oil shale. Thermogravimetric analysis (both iso- and non-isothermal) was used to determine the kinetic parameters for kerogen decomposition. The present results will be compared with the literature data on Jordan and Colorado oil shale.

Insoluble organic matter in oil shale is called kerogen. The thermal decomposition of the kerogen is by far the simplest method for extracting oil from shale. Numerous attempts [Hubbard and Robinson 1950; Allred, 1966; Dericco and Barrick, 1956] dealing with the mechanistic and kinetic points of view have been made to understand the processes occurring during oil shale pyrolysis. Hubbard and Robinson [1950] have employed an isothermal technique to obtain the pyrolysis rate data on powdered samples. One of the sources of error in isothermal methods is the time required for the sample to reach the reaction temperature. Braun and Rothman [1975] have shown that the oil-production kinetics can be explained more exactly by including a thermal induction period in the analysis of data obtained by Hubbard and Robinson [1950]. Non-isothermal thermogravimetric analysis has come into wide use in the last decade for studying pyrolysis. There are certain advantages of this method over the classical isothermal method. First, this method eliminates the errors introduced by the thermal induction period. Second, it permits a rapid scan of the whole temperature range of interest. Herll and Arnold [1976] have studied the decomposition of Chattanooga Black shale by non-isothermal TG while Haddadin, et al [1974, 1980], have employed TGA and DTA to investigate the kinetics of Jordan oil shale pyrolysis. The thermal decomposition of Colorado oil shale has been a subject of many studies [Granoff and Nuttall, 1977; Campbell et al 1978; Rajeshwar, 1981].

Recently, Behnisch, et al [1980], have pointed out that a combined kinetic analysis of isothermal and non-isothermal TG measurements is an effective method for determining the most probable kinetic mechanism of a decomposition process of a polymer. The kinetics of Moroccan oil shale decomposition has, therefore, been studied by isothermal and non-isothermal thermogravimetry. The weight-loss data analyzed by Coats-Redfern technique [1964] shows that the kerogen decomposition proceeds in two consecutive steps via bitumen as an intermediate. The kinetics of Moroccan oil shale decomposition will be compared with that of Jordan and Colorado oil shale decomposition.

EXPERIMENTAL SECTION

The oil shale used in the present study originated from Timhadit Site, Morocco. Chemical analysis of the oil shale is given in Table 1. The samples were crushed and sieved to pass through a 200 mesh screen; the samples were used without further treatment.

A DuPont 951 thermogravimetric balance interfaced with a DuPont 990 thermal analyzer was used to obtain the weight-loss data as a function of time and temperature. Two kinds of experiments were performed. The first was to obtain non-isothermal kinetics of oil shale decomposition while the second one was performed under isothermal conditions.

In the first set, a known weight of sample (about 25 mg) was subjected to a linear heating rate in a dry stream of nitrogen. Decomposition was carried out by heating the sample from ambient temperature to 900°C. The heating rates of 1, 2, 5, 10, 20 and 50°C/min were employed. The weight-loss data and DTG curves were obtained in each case. In the second set of experiments, the sample was introduced into the furnace maintained isothermally at a desired temperature. End effects were considered negligible as the furnace was about ten times longer than the sample pan. The isothermal kerogen decomposition was carried out at 325, 375, 410, 425, 450, and 475°C.

The fraction of kerogen pyrolyzed, α was defined by the expression:

$$\alpha = \frac{W_0 - W_t}{W_0 - W_\infty} \quad (1)$$

where W_0 = initial weight of the sample (mg),

W_t = weight of the sample at "t" min (mg),

W_∞ = weight of the sample after complete pyrolysis of kerogen (mg).

Each run was duplicated in order to minimize the error.

Kinetic Expressions:

The general expression for the decomposition of a solid [Blazek, A. 1973] is given by

$$\frac{d\alpha}{dt} = kf(\alpha), \quad (2)$$

where α = fractional conversion at time t,

k = specific rate constant,

$f(\alpha) = (1 - \alpha)$ in first order reactions.

Equation (2) can be written as follows by substituting k in terms of activation energy and frequency factor.

$$\frac{d\alpha}{dt} = Z \cdot \exp(-E/RT) \cdot (1 - \alpha), \quad (3)$$

where Z = frequency factor (min^{-1}),

E = activation energy (J/g mole),

R = gas constant (J/g mole K),

T = temperature (K).

For non-isothermal decomposition of solids, Equation (3) can be modified by introducing heating rate as follows

$$\frac{d\alpha}{dT} \cdot \frac{dT}{dt} = Z \cdot \exp(-E/RT) \cdot (1 - \alpha) \quad (4)$$

or

$$\frac{d\alpha}{dT} = \frac{Z}{\beta} \cdot \exp(-E/RT) \cdot (1 - \alpha), \quad (5)$$

where $\beta = dT/dt$.

In the present study, two procedures were followed to evaluate the activation energy. The first was a graphical method while the second involved regression analysis.

The graphical method developed by Coats and Redfern [1964] was used here. The kerogen decomposition was considered to be first order in kerogen concentration [Rajeshwar, 1981; Campbell, et al 1978]. In this case, a plot of

$$\left[- \ln \left(- \frac{\ln(1 - \alpha)}{T^2} \right) \right]$$

against $1/T$ should result in a straight line of slope E/R .

In the second method, Equation (5) was rearranged and integrated to give

$$1 - \alpha = \exp - \frac{Z}{\beta} \int_0^T \exp(-E/RT) dT \quad (6)$$

or

$$= \exp - \left[\frac{Z}{\beta} \left(\frac{RT^2}{E + 2RT} \cdot \exp(-E/RT) \right) \right]. \quad (7)$$

Equation (7) can be written as follows

$$\ln \left(\frac{E + 2RT}{T^2} \cdot \ln \frac{1}{1 - \alpha} \right) = \ln \frac{ZR}{\beta} - \frac{E}{RT}. \quad (8)$$

Equation (8) is of the form

$$y = a + bx, \quad (9)$$

where

$$y = \ln \left(\frac{E + 2RT}{T^2} \cdot \ln \frac{1}{1 - \alpha} \right), \quad (10)$$

$$a = \ln \frac{ZR}{\beta}, \quad (11)$$

$$b = -E/R, \quad (12)$$

and

$$x = 1/T \quad (13)$$

With the aid of repeated regression analysis, the values of slope and intercept can be computed. In the first step, an initial guess of E was made to calculate y (Equation (10)). Next, y was corrected for calculated values of E from Equation (12), and a and b were redetermined from the regression. The iteration was continued until the accuracy of E and Z was satisfied.

For the isothermal decomposition of kerogen, Equation (2) was integrated to give

$$- \ln(1 - \alpha) = k \cdot t. \quad (14)$$

A plot of $[-\ln(1 - \alpha)]$ against t yields a straight line with slope equal to k . The values of t used here include the induction period t_0 as suggested by Braun and Rothman [1975].

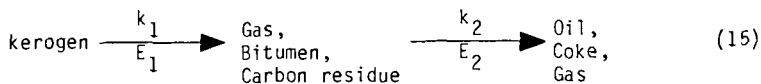
RESULTS AND DISCUSSION

Thermogravimetric Data

The weight loss data were obtained on powdered oil shale samples under non-isothermal and isothermal conditions. The oil shale decomposition was carried out using a small sample size and a thin platinum foil boat in order to obtain a steady state condition in a short time. In non-isothermal TGA, the sample was heated from ambient temperature to 900°C with heating rates ranging from 1 to 50°C/min. The isothermal TGA was carried out in the temperature range of 325 to 475°C. The results obtained under non-isothermal and isothermal conditions are comparable and they suggest that the kerogen decomposition proceeds via bitumen as an intermediate. First, the non-isothermal TG results are presented followed by the results obtained under isothermal conditions.

Figure 1 presents the weight-loss data for Moroccan oil shale as a function of temperature at various heating rates. The important features of this figure, which are worth mentioning here, are as follows: First, the total kerogen content in Moroccan oil shale was found to be about 9 percent (wt) of the total shale weight. Below 200°C, approximately 0.5 to 0.75 percent weight-loss was observed, which represented the moisture content of the shale. The carbonate decomposition commenced at temperatures above 525°C depending upon the heating rate and gave a weight-loss of about 25 to 26 percent. Second, and a more important observation, was regarding the effect of heating rate on total weight-loss. A complete decomposition of kerogen was effected at 500°C with a heating rate of 1 K/min while only 50 percent of the total kerogen was found to decompose at 500°C when a rate of 50°C/min was used. In the latter case, a temperature of 600°C was required to achieve the complete decomposition of kerogen into oil. This difference can be explained by the fact that the higher the heating rate the shorter is the exposure of sample to a particular temperature. However, as will be shown in the later part of this section, the variation in heating rate did not alter the kinetic parameters.

Figure 2 illustrates typical DTG curves corresponding to the data shown in Figure 1 for heating rates of 2, 5, 10 and 50 K/min. Three salient features of this figure are to be noted. First, there is a shift in rate maxima toward higher temperatures as the heating rate is increased from 5 to 50 K/min. These results are complementary to the above-mentioned findings on the effect of heating rates (Figure 1). These results are strikingly similar to those obtained by Herrell and Arnold [1976], and Chen and Nuttall [1979]. Second, the presence of two clearly defined rate maxima in the temperature range of 300 to 600°C indicate that the two reactions or processes occur consecutively in this temperature range. Actually, Allred [1966] had proposed the following mechanism for the pyrolysis of oil shale:



The present results are in accordance with his model, and they lead us to believe that the first peak at lower temperature corresponds to the decomposition of kerogen to bitumen while the second peak represents the decomposition of pyrolytic bitumen into oil and gas. Recently, Rajeshwar [1981] also reported similar results on Colorado oil shale. Third, the rate of weight-loss increased by a factor of three with an increase in heat rate from 2 to 5 K/min. However, a further increase in heating rate (5 to 50 K/min) did not accelerate kerogen decomposition rate appreciably.

Kinetic Analysis

The data presented in Figure 1 was used to determine the kinetic parameters of kerogen decomposition. A plot of

$$- \ln \left[1 - \frac{\ln(1 - \alpha)}{T^2} \right]$$

against $1/T$ shown in Figure 3 was used to evaluate the activation energy. The kerogen decomposition was assumed to be first order to kerogen concentration. Two sets of straight lines with different slopes (Figure 3) clearly demonstrate that the two consecutive reactions occur in the temperature range of 300 to 600°C. The first reaction occurring at lower temperature (kerogen + bitumen) proceeds with an activation energy of about 40.2 kJ/mole. The second reaction which occurs beyond 350°C has an average activation energy of 58.1 kJ/mole. The kinetic parameters are presented in Table II. The fact that the variation in heating rate does not alter the slope of the straight line plots presented in Figure 3 suggests that the kinetic parameters determined in the present study are probably not sensitive to the efficiency of heat transfer between the sample and surroundings. These results corroborate very well with those observed by Rajeshwar [1981].

The regression method was also used in this study to determine the kinetic parameters. The activation energies and frequency factors evaluated by this iteration method are listed in Table II. They compare fairly well with those obtained by the graphical method.

Results obtained under isothermal conditions will be discussed at this stage. Figure 4 shows the kerogen decomposition as a function of time at various temperatures. During the initial period of these isothermal runs less than 1 minute was required to attain steady state values of temperature. As explained earlier, the use of small sample size (~25 mg) small diameter furnace and thin platinum foil boat aided in obtaining steady-state conditions in short time. During the temperature-induced time lag period, very small weight losses were recorded; at temperatures higher than 450°C it amounted to about 12 to 14 percent of total weight-loss. Several workers [Campbell, et al 1978; Granoff and Nuttall, 1977; and Haddadin and Mizyet, 1974] have developed the kinetic expressions similar to Equation (14), assuming the shale particle temperature to be uniform and mass transfer rate to be high. In the present study, Equation (14) was used to evaluate the specific rate constant (Figure 5).

Table III compares the k values (computed from Figure 5) with the literature values for the decomposition of Jordan and Colorado oil shale. This comparison shows that at temperatures lower than 425°C, the decomposition rate of Moroccan shale is twice as fast as that of Jordan shale, and about three to four times as fast as that of Colorado shale. At 475°C the k values for

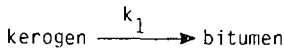
decomposition of Moroccan shale is about four times higher than that reported for the pyrolysis of Jordan shale, but it is almost identical to the k value for Colorado shale decomposition.

The Arrhenius plot shown in Figure 6 was used to determine activation energy and frequency factor. Figure 6 also shows two distinct reactions. Their kinetic parameters, $E_1 = 38.4 \text{ kJ mole}^{-1}$ and $E_2 = 62.3 \text{ kJ mole}^{-1}$, listed in Table II, are in good agreement with those obtained under non-isothermal conditions. Activation energy (E_a) for kerogen decomposition to bitumen compares fairly well with that reported by Braun and Rothman [1975]. The low activation energy (-40 kJ/mole) indicates that the decomposition of kerogen to bitumen involves the breaking of relatively weak chemical bonds [Braun and Rothman, 1975].

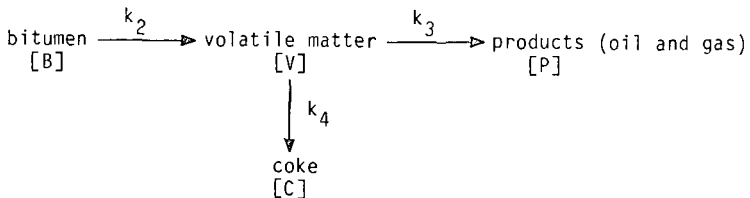
The low activation energy obtained in the present study under both the isothermal and non-isothermal experiments suggest certain physical processes controlling the reaction. The rate expressions used to determine the kinetic parameters in this investigation were developed assuming that there are no heat and mass transfer limitations and that the reaction kinetics controls the rate of weight-loss. The fact that the variation of heating rates (Figure 3) did not affect the activation energy value substantiates the validity of the assumption that there are no heat transfer limitations. Rejeshwar [1981] pointed out that the heating rate variations can be used as a diagnostic probe to obtain information on mechanistic aspects. Haddadin, et al [1974, 1980] also obtained low activation energy during the pyrolysis of Jordan oil shale. They postulated a mechanism in which the diffusion of organic matter through the carbonate matrix controls the rate process. Several diffusion-controlling models [Levenspiel, 1972; Blazek, 1973; Ginstling and Brounshtein, 1956] have been developed to analyze the fluid-solid reactions and solid decomposition. According to the method suggested by Levenspiel [1972], experimental curves obtained by plotting $(1 - \alpha)$ versus t/τ (τ is the time required for complete decomposition) are compared with the predicted curves for various mechanisms, e.g., chemical reaction, film diffusion and ash layer diffusion. The data obtained under isothermal conditions was used for this plot between $(1 - \alpha)$ and t/τ . It was deduced from this plot that the ash layer diffusion controls the reaction rate.

According to Haddadin and Mizyet [1974], Equation (15) can then be written as:

First Step:



Second Step:



where [B], [V], [P] and [C] denote the weight fractions of bitumen, volatile matter, products (oil and gas) and coke, respectively.

The first step involving the decomposition of kerogen to bitumen is relatively rapid [Haddadin and Mizyet, 1974] and can thus be omitted from consideration in the controlling kinetics. The second step which involves transport of oil vapor and gas to the atmosphere is the rate controlling step. The overall rate for this step is

$$\frac{d[P]}{dt} = k_3 [V] . \quad (16)$$

Assuming steady state concentration of volatiles during the process, we have

$$\frac{d[V]}{dt} = 0 = k_2[B] - k_3[V] - k_4[V] . \quad (17)$$

Solving for [V],

$$[V] = \frac{k_2}{k_3 + k_4} \cdot [B] \quad (18)$$

and substituting in Equation (18), we have

$$\frac{d[P]}{dt} = \frac{k_2 \cdot k_3}{k_3 + k_4} [B] . \quad (19)$$

If diffusion of volatile matter controls the reaction rate, we have

$$k_2 \gg k_3 ; \quad - \frac{d[B]}{dt} = \frac{k_2 k_3}{k_4} \cdot [B] = k[B] , \quad (20)$$

where k is the overall rate constant of the weight change. Equation (20) applies to a situation where the carbonate matrix acts as a porous diffusion barrier.

CONCLUSIONS

The combined use of non-isothermal and isothermal TG measurements has shown that the thermal decomposition of Moroccan oil shale involves two consecutive reactions, with bitumen as intermediate.



Both the reactions follow a first order kinetics.

Activation energy of 40 kJ/mole for the decomposition of kerogen to bitumen suggests that this step involves the breaking of a relatively weak chemical bond.

The rate of bitumen decomposition is controlled by the volatile matter transport through the inorganic matrix. Low value of activation energy obtained for this reaction are complementary to such a mechanism.

The decomposition rate of Moroccan oil shale is about 2-4 times higher than that of Jordan shale in the temperature range of 300 to 500°C.

A comparison of decomposition rates for Moroccan and Colorado Oil shales shows that at temperatures lower than 400°C, the Moroccan shale decomposes more rapidly than the Colorado shale; at 475°C the decomposition rates for both shales become almost identical.

LITERATURE CITED

- ALLRED, V. D., Chem. Eng. Prog. Symp. Ser., 1966, 62(8), 55.
- BEHNISCH, J., SCHAFF, E. and ZIMMERMANN, H., Thermochemica Acta 1980, 42, 65.
- BLAZEK, A., "Thermal Analysis," J. F. Tyson (Translation Ed.), Van Nostrand-Reinhold Co., London, U.K., 1973.
- BRAUN, R. L. and ROTHMAN, A. J., Fuel, 1975, 54, 129.
- CAMPBELL, J. H., KOSKINAS, G. and STOUT, N., Fuel, 1978, 57, 372.
- CHEN, W. J. and NUTTALL, H. E., paper presented at the 86th AIChE National Meeting, Houston, Texas, 1979.
- COATS, A. W. and REDFERN, J. P., Nature (London), 1964, 201, 68.
- DERICCO, L. and BARRICK, P. L., Ind. Eng. Chem. 1956, 48, 1316.
- GINSTLING, A. M. and BROUNSHTEIN, B. I., Zh. Prikl. Khim., 1956, 29, 1890.
- GRANOFF, B. and NUTTALL, H. E., JR., Fuel, 1977, 56, 234.
- HADDADIN, R. A. and MIZYET, F. A., Ind. Eng. Chem. Process Des. Develop. 1974, 13(4), 332.
- HADDADIN, R. A. and TAWARAH, K. M., Fuel, 1980, 59, 539
- HERRELL, A. Y. and ARNOLD, C., JR., Thermochemica Acta, 1976, 17, 165.
- HUBBARD, A. B. and ROBINSON, W. E., Rep. Invest. U.S. Bur. Mines, No. 4744, 1950.
- LEVENSPIEL, O., "Chemical Reaction Engineering," Second Ed., John Wiley and Sons, Inc., New York, New York, 1972, Ch. 12.
- RAJESHWAR, K., Thermochemica Acta, 1981, 45, 253.

TABLE I. CHEMICAL ANALYSIS OF MORROCCAN OIL SHALE

| | |
|---|------------|
| 1. Fischer Oil Assay | 71 k/tonne |
| 2. Density | 2.25 q/ml |
| 3. Chemical composition of raw shale compound | |
| A. Keragen | 9.5 wt% |
| C - 69.7% (wt) | |
| H - 6.7 | |
| S - 9.1 | |
| N - 2.3 | |
| O - 12.2 | |
| B. Dolomite | 14.4 |
| C. Calcite | 37.7 |
| D. Quartz | 17.2 |
| E. Argiles (Illite-Kaolinite) | 12.2 |
| F. Pyrites | 1.6 |
| G. $FeCO_3 + Fe_2O_3$ | 1.6 |
| H. $TiO_2 + Phosphate$ | 2.2 |
| I. Other constituents | 3.4 |

TABLE II. KINETIC PARAMETERS FOR THE NON-ISOTHERMAL AND ISOTHERMAL DECOMPOSITION OF MORROCCAN OIL SHALE

| Method | Activation Energy (kJ/mole) | | Frequency Factor (s/min) | |
|--------------------------------------|-----------------------------|-------|--------------------------|-------------------|
| | E_1 | E_2 | Z_1 | Z_2 |
| Non-Isenthal Mode, Graphical Method | 40.2 | 58.1 | 6.9×10^4 | 2.8×10^5 |
| Non-Isenthal Mode, Regression Method | 43.0 | 64.8 | 7.2×10^4 | 3.2×10^5 |
| Isothermal Mode | 38.4 | 62.3 | 4.6×10^4 | 4.8×10^5 |

TABLE III. A COMPARISON OF FIRST ORDER RATE CONSTANTS FOR OIL SHALE DECOMPOSITION

| Temp. (°C) | First Order Rate Constants (min ⁻¹) | | | |
|------------|---|------------------------------|---------------------------|-------------------------|
| | Moroccan Shale | Jordan Shale | Colorado Shale | |
| | Present Study | [Haddadin and Mizzyet, 1974] | [Braun and Rothman, 1975] | [Campbell et al., 1978] |
| 325 | 0.05 | - | - | - |
| 330 | - | 0.024 | - | - |
| 360 | - | 0.037 | - | - |
| 375 | 0.09 | - | - | - |
| 400 | - | - | 0.02 | 0.025 |
| 405 | - | 0.057 | - | - |
| 410 | 0.18 | - | - | - |
| 425 | 0.20 | - | - | 0.090 |
| 440 | - | 0.078 | - | - |
| 450 | 0.31 | - | 0.18 | - |
| 475 | 0.41 | 0.113 | 0.48 | - |

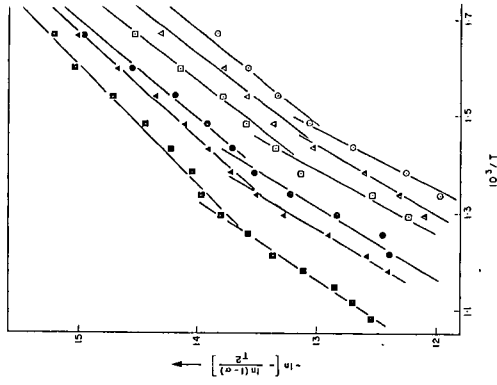


Figure 3. Analysis of the TG data for Moroccan oil shale by the Coats-Redfern method. Heating rates: (○) 1 K/min, (△) 2 K/min, (□) 5 K/min, (●) 10 K/min, (▲) 20 K/min, and (■) 30 K/min.

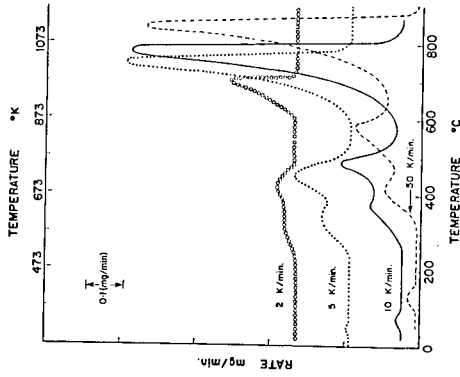


Figure 2. DTG curves for Moroccan oil shale at 2 K/min, 5 K/min, 10 K/min, 20 K/min, and 50 K/min.

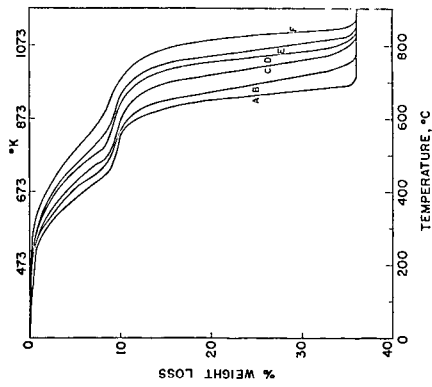


Figure 1. Non-isothermal TG curves for Moroccan oil shale at various heating rates: [A] 1 K/min, [B] 2 K/min, [C] 5 K/min, [D] 10 K/min, [E] 20 K/min, and [F] 50 K/min.

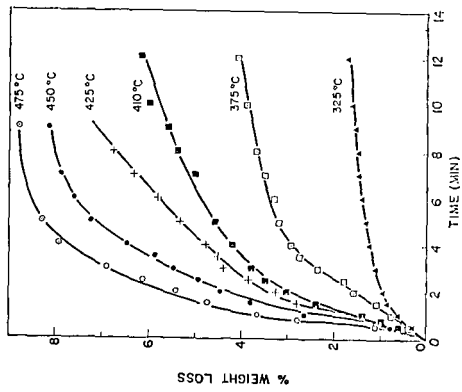


Figure 4. Percent weight loss for Mexican oil shale at various temperatures (isothermal TG curves).

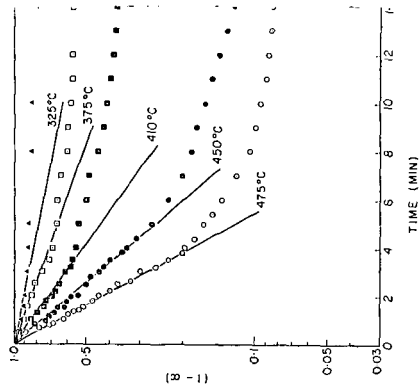


Figure 5. Analysis of isothermal TG data (from Figure 4).

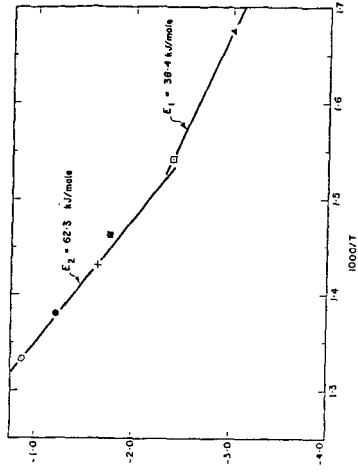


Figure 6. Arrhenius plot of $\ln k$ versus $1000/T$ using isothermal TG data.

METALLOORGANIC, ORGANIC AND MUTAGENIC
PROPERTIES OF OIL SHALE RETORT WATERS

A. P. Toste and R. B. Myers

Physical Sciences Department
Pacific Northwest Laboratory
Richland, Washington 99352

INTRODUCTION

Considerable technological research is currently underway to develop a shale oil industry in the United States. The feasibility of shale oil production is being tested using various technologies, most of which are presently at the bench-level to pilot-plant stages of development. Concern about the potential health and environmental impacts of such an industry has, in turn, prompted intensive biomedical and environmental research, much of it directed at chemically and biologically evaluating the genotoxicity/carcinogenicity potential of shale oils. It has already been demonstrated that certain crude and chemically fractionated shale oil samples are mutagenic using carcinogen-screening bioassay systems such as the Ames Salmonella assay.(1-6)

Retort waters are co-produced with shale oil during the retorting of oil shale. The quantity and chemical properties of the retort water vary depending upon the retorting technology used;(7) aboveground retorting processes generate much less retort water than shale oil, whereas in situ processes generate approximately equal amounts of retort water and shale oil. All of the retorting processes designed to date provide for complete recycling of all process waters, with no discharge into the environment. Nevertheless, considering the enormous amounts of retort waters that may be produced in a large-scale shale oil industry, there is considerable concern about the health and environmental impacts associated with the recycling of these waters and any accidental release into the environment.

Much is known about the inorganic properties of retort waters, notably the metal and trace metal content.(8) Less is known about their organic content. Information about specific classes of organic compounds (9,10) and organometallic species (11) is available; even a few comprehensive studies of numerous classes of organics have been reported.(12) Much remains to be elucidated, however, about the relationship of the retort waters' organic content to mutagenicity and chelation of the metals present, i.e. metallorganics.

The primary goal of this study was to evaluate the mutagenic, organic, and metallorganic properties of oil shale retort waters. Four retort water samples were analyzed in the mutagenesis/organics study: a storage water and a condensate water from the Paraho aboveground retort; a retort water from the Occidental vertical, modified in situ retort; and a retort water from the horizontal, true in situ retort at Vernal, Utah.

A second goal of this study was to develop and evaluate improved methods of chemically fractionating the complex organic content of retort waters to facilitate their chemical and mutagenic characterization. To begin the mutagenesis study, we tested several methods for extracting hydrophobic organics from the retort waters: 1) solvent extraction with pH adjustment; 2) XAD-4 partition chromatography; and 3) C_{18} -partition chromatography. We then tested the usefulness of high-performance liquid chromatography (HPLC) for fractionating the hydrophobic organic fraction. Each method was evaluated both chemically and biologically. For the metallorganics/organics study we decided to test steric-exclusion chromatography as a means of fractionating metal-organic chelates.

EXPERIMENTAL

Mutagenesis/Organics Studies

C₁₈-Partition Chromatography. Each retort water used in the mutagenesis studies was initially fractionated by partition chromatography on a C₁₈-cartridge based on a method described by Riggin and Howard.(13) In our procedure, the C₁₈-cartridge was pre-conditioned by eluting 2 ml of methanol through it, followed by 4 ml of milli-Q-purified water. Each retort water (24-150 ml) was then loaded onto the C₁₈-cartridge. The organic-loaded C₁₈-cartridge was then washed with 4 ml of milli-Q water. The hydrophobic organic fraction of the retort water was then eluted from the C₁₈-cartridge with 2 ml of methanol.

HPLC Analysis. The hydrophobic organic fraction of each retort water was further fractionated on the basis of polarity by normal phase HPLC using an NH₂-column and a three-solvent mobile phase system. Hexane flowed through the column isocratically at 5 ml/min. for the first 5 min., followed by a 10 min., linear gradient to 100% methylene chloride; 100% methylene chloride flowed isocratically for 5 min., followed by a 10 min., linear gradient to 100% isopropanol; finally, 100% isopropanol flowed isocratically for 5 min. The NH₂-column was reconditioned by cycling back to hexane using a 10 min., linear gradient, followed by 100% hexane isocratically for 10 min.

Fifty μ l of sample (50 to 100 mg/ml) were injected onto the NH₂-column per HPLC run; 10 to 20 runs of each sample were repetitively collected into 250 ml roundbottom flasks. The HPLC effluent was monitored by UV absorbance at 250 nm. Each HPLC fraction was concentrated by rotary evaporation, transferred to a pre-weighed vial, evaporated to dryness under N₂, weighed, and redissolved in 1 ml of methylene chloride. Half of the sample was set aside for combined gas chromatography-mass spectrometry (GC-MS) analysis; the other half was redried and dissolved in 0.5 ml DMSO for the Ames bioassay.

GC-MS Analysis. The organics in the HPLC fractions were analyzed on a Hewlett Packard 5982 GC-MS instrument in the electron impact (70 eV) mode. A 15 m x 0.30 mm I.D. glass capillary column coated with 0.25 μ m film thickness of SE-52 was programmed from 40°C to 100°C at 32°C/min., then programmed at 8°C/min. to 290°C, where it was maintained isothermally for 30 min. A Grob splitless injection system was used. The GC column was interfaced to a mass spectrometer via platinum-iridium tubing. The mass range of 50 to 300 a.m.u. was scanned by computer (HP5934A) every 1.8 sec.

Mutagenesis Assay. Agar-plate mutagenicity assays were carried out essentially as described by Ames et al.(14) The TA98 strain of Salmonella typhimurium was used with the S9 fraction from rat liver homogenate (induced with Aroclor 1254) as a metabolic activator. Dimethylsulfoxide (DMSO) was used as the solvent for all of the standards and HPLC fractions that were bioassayed. After 24 to 36 hr. incubation of the inoculated plate, revertant colonies of TA98 were counted on a New Brunswick Scientific Company Biotran II automated colony counter.

Metallorganics/Organics Studies

Sephadex G-15 Chromatography. Each retort water (2-10 ml) was loaded on a Sephadex G-15 column (2.5 cm x 31 cm) and chromatographed at a specific flow rate ranging from 23-31 ml/hr. with milli-Q-purified water. Replicate runs were made with each sample, with and without Blue Dextran as a void volume marker. The column effluent was monitored by UV absorbance at 254 nm and collected in 4 ml fractions on an Isco fraction collector. Each column fraction was divided in half: one aliquot was set aside for metals analysis by plasma emission spectroscopy (PES); the other half was methylated, prior to GC and GC-MS analysis.

Methylation. Each column subfraction was extracted with an equal volume of chloroform to remove hydrophobic organics. The chloroform extract was set aside for GC analysis. The aqueous fraction, believed to contain polar organic compounds which

might chelate metals, was evaporated to dryness under N_2 at $\sim 100^\circ C$. The dried residue of each fraction was then methylated by adding 1 ml of BF_3 /methanol (14% w/v) and incubating at $100^\circ C$ for 40 min. in a sealed vial. After cooling, chloroform (1 ml) was added and the mixture was transferred to a test tube containing buffer solution (3 ml of 1M KH_2PO_4 , pH 7). After vortexing for one min. and centrifugation, a specific amount of the chloroform layer (0.4-0.7 ml) was transferred to a glass vial and the chloroform was evaporated under N_2 at R.T. The residue was redissolved in chloroform (100-200 μl) and an aliquot (1-2 μl) was analyzed by GC and GC-MS.

GC Analysis. The organics in the methylated fractions were initially analyzed on a Hewlett Packard 5880 gas chromatograph equipped with a flame ionization detector. A fused silica capillary column (30 m x 0.25 mm I.D.) coated with 0.25 μm of SE-52 was programmed from $40^\circ C$ to $300^\circ C$ at $4^\circ C/min.$, where it was maintained isothermally for 10 min.

GC-MS Analysis. Following the GC analysis, the organics in the methylated fractions were analyzed on a Hewlett Packard 5985 GC-MS instrument in the electron impact (70 eV) mode. A 60 m x 0.25 mm I.D. fused silica capillary column coated with 0.25 μm of SE-54 was programmed from $40^\circ C$ to $300^\circ C$ at $5^\circ C/min.$, where it was maintained isothermally for 8 min. A splitless injection system was used to introduce the sample onto the GC-MS instrument. The GC column was interfaced directly to the mass spectrometer. The mass range of 50 to 400 a.m.u. was scanned every 1 sec. by computer (HP 2100MX equipped with the HP 7920 Large Disc Drive).

PES Analysis. Each Sephadex column fraction was analyzed for metals (Fe, Mo, Ni, Mn and Zn) on a Spectrometric Spectra Span III, three-jet, direct-current plasma emission spectrometer equipped with a multi-element cassette. The instrument was operated according to the manufacturer's recommendations. A standard solution consisting of 1 ppm each Fe, Mo, Ni, Mn and Zn (dissolved in a buffer of 2000 ppm Li, 1% HNO_3) was used to calibrate the instrument. A solution of Li-buffered (with 1% HNO_3), deionized water was used to blank the instrument. The instrument's detection limits were 2 ppb for Mn and 5-10 ppb for Fe, Ni, Mo and Zn.

Materials

Samples. The Paraho storage water was sampled on August 26, 1977, and the condensate water was sampled on October 13, 1980, at the Paraho aboveground retort (Anvil Points, Colorado). The Occidental retort water was sampled on March 7, 1979, at the Occidental vertical, modified in situ retort (Room 6) at Logan Wash, Colorado. The Vernal retort water was sampled on July 11, 1978, at Vernal, Utah, horizontal, true in situ retort.

Standards. Most of the standards used in the HPLC and GC studies were purchased from Aldrich Chemical Company (Milwaukee, Wisconsin) and RFR Corporation (Hope, Rhode Island).

Chromatographic Columns. The C_{18} -Sep Pak cartridges used for the C_{18} -partition chromatography and the μ Bondapak NH_2 -columns and precolumns used in the HPLC analyses were purchased from Waters Associates, Inc. (Milford, Massachusetts). The NH_2 -column was a semi-preparative column (7 mm x 30 cm). The glass columns (2.5 cm x 45 cm) and Sephadex G-15 used in the metallorganics/organics study were purchased from Pharmacia Fine Chemicals (Piscataway, New Jersey).

Solvents and Glassware. All of the solvents used in the chromatographic analyses were redistilled-in-glass solvents purchased from Burdick and Jackson Laboratories, Inc. Deionized water was passed through a milli-Q system (Millipore) containing two ion exchange resins and two charcoal filters. All glassware was acid cleaned.

RESULTS

Mutagenesis/Organics Study

All of the various methods tested for extracting organics from retort waters

TABLE 1. Organics in Oil Shale Retort Waters.

| RETORT WATER | ORGANIC ¹ FRACTION (mg/ml) | TOTAL ORGANIC CARBON (mg/ml) | pH |
|---------------------|---------------------------------------|------------------------------|-----|
| PARAHO | 29.85 ± 0.08 | 42.75 | 8.4 |
| PARAHO (CONDENSATE) | 1.28 ± 0.13 | 4.08 | 8.7 |
| OCCIDENTAL | 1.47 ± 0.01 | 4.23 | 8.9 |
| VERNAL | 1.02 ± 0.15 | 2.93 | 8.5 |

1 EXTRACTABLE BY C₁₈ PARTITION CHROMATOGRAPHY WITH MeOH ELUTION.

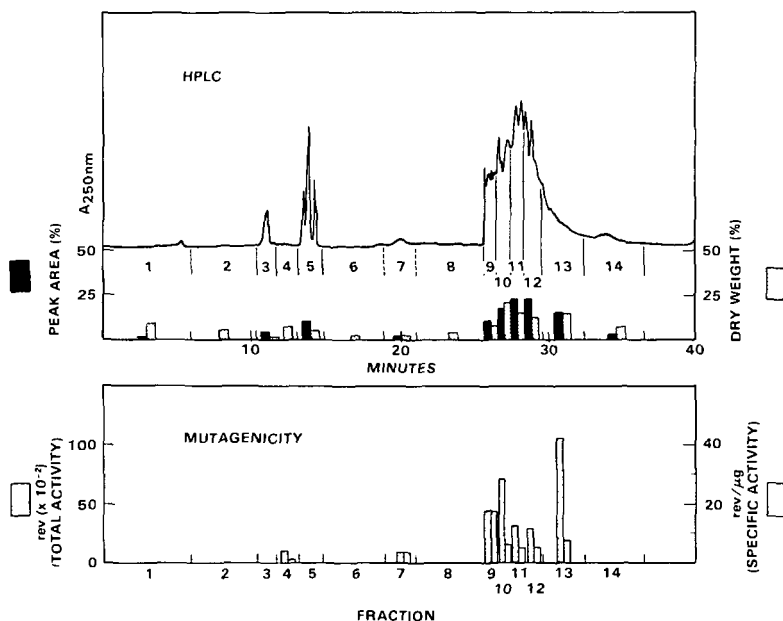


FIGURE 1. HPLC of Hydrophobic Organic Fraction from Paraho Storage Retort Water.

extracted some mutagenic activity. C_{18} -partition chromatography yielded the highest recovery of mutagenic activity (2-4 rev/ μ g); the amounts of organics extracted were also quite reproducible (Table 1). Solvent extraction with pH adjustment also yielded appreciable mutagenic activity (2.6 rev/ μ g) but the efficiency of extraction varied considerably. HPLC fractionation of the hydrophobic organic fraction or C_{18} -extractable organics, resulted in considerable fractionation of the organics and mutagenic activity for all of the retort waters studied (Figure 1).

On the basis of the HPLC fractionation, most of the species in the hydrophobic organic fraction of each retort water chromatographed in the polar HPLC region but some species chromatographed in the moderately polar HPLC region (Figure 1). The organic content of the various samples appeared to be quite heterogeneous. GC-MS analyses of the HPLC fractions of the oil shale retort waters revealed that the moderately polar HPLC region contained mainly nitrogenous compounds: pyridine, alkyl-pyridines, aniline, alkyl-anilines, quinolines and alkyl-quinolines. The polar HPLC region mainly contained oxygenated and mixed-function compounds: carboxylic acids, dicarboxylic acids, phenols, alkyl-phenols, and amides.

The mutagenic activity of each retort water was confined to its hydrophobic organic fraction. The Paraho storage water was the most mutagenic (1.29 rev/ μ g), followed by Occidental (0.06 rev/ μ g), Vernal (0.04 rev/ μ g) and Paraho condensate water (0.02 rev/ μ g). No mutagenic activity was detected in the complementary hydrophilic, or aqueous, fraction. After HPLC fractionation of the hydrophobic organic fraction, virtually all of the mutagenic activity was concentrated in the polar HPLC region (Figure 1). The mutagens of the Paraho storage water chromatographed throughout the polar HPLC region, indicating a high degree of heterogeneity. The mutagens of the Paraho condensate water appeared to be less heterogeneous. The mutagens of the Occidental and Vernal retort waters were even less heterogeneous, confined exclusively to one region of the polar HPLC region.

Metallorganics/Organics Study

Sephadex G-15 chromatography fractionated the organics in retort waters into several discrete peaks (Figure 2). Each of the waters studied yielded a distinct chromatographic pattern. Detailed GC and GC-MS analyses revealed considerable fractionation of the organics (Figure 3). On the basis of the GC analysis, the first peak fraction (Number 27) contained quite a variety of polar organics. The second peak fraction (Number 36) was easily the most complex, containing a broad spectrum of organics ranging from N-heterocycles to carboxylic acids. Interestingly, Fraction 39, a non-UV-absorbing region, contained a homologous series of organics. Finally, the third peak fraction (Number 41) contained a moderate variety of polar organics. The metals analysis performed by PES indicated that metals were fractionated as well (Figure 3). Fe and Zn chromatographed over a wide region, most of which was also associated with organic species. In contrast, most of the Mn chromatographed in very narrow regions associated with organics (Fractions 27 and 29).

DISCUSSION

The chromatographic procedures developed for the mutagenesis and metallorganics studies yielded considerable fractionation of the retort waters' organics. On the basis of the mutagenesis study, C_{18} -partition chromatography appears to be well-suited for extracting mutagens from retort waters and probably other aqueous samples as well. It is noteworthy that all of the retort waters' mutagenicity was confined to the C_{18} -extractable, or hydrophobic organic, fraction. As Table 1 indicates, this fraction generally constituted a small percentage of the retort waters' total organics. Normal phase HPLC with the NH_2 -column proved useful for further fractionation of the hydrophobic organic fraction. As a result of the HPLC analyses, it is clear that the retort waters' mutagens are polar and, in some cases, quite heterogeneous. The exact identity of the mutagens remains a mystery, however. None of the numerous organic species identified to date by GC-MS are known mutagens. On the basis of the HPLC studies, polar, mixed-function compounds, perhaps N- and O-containing species, are likely candidates.

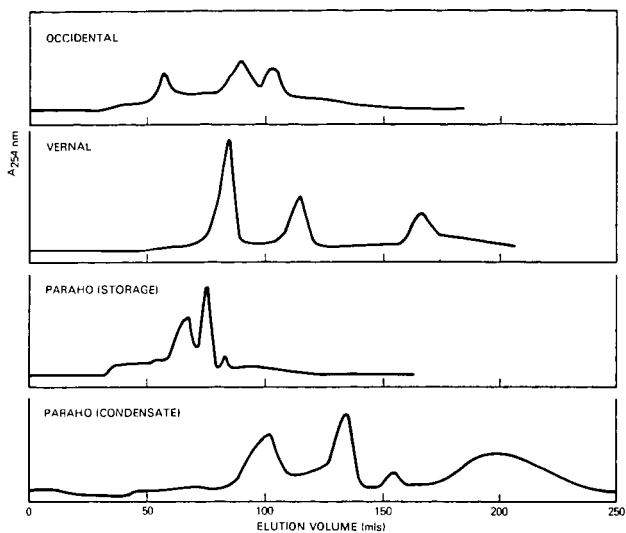


FIGURE 2. Steric Exclusion Chromatography of Oil Shale Retort Waters with Sephadex G-15.

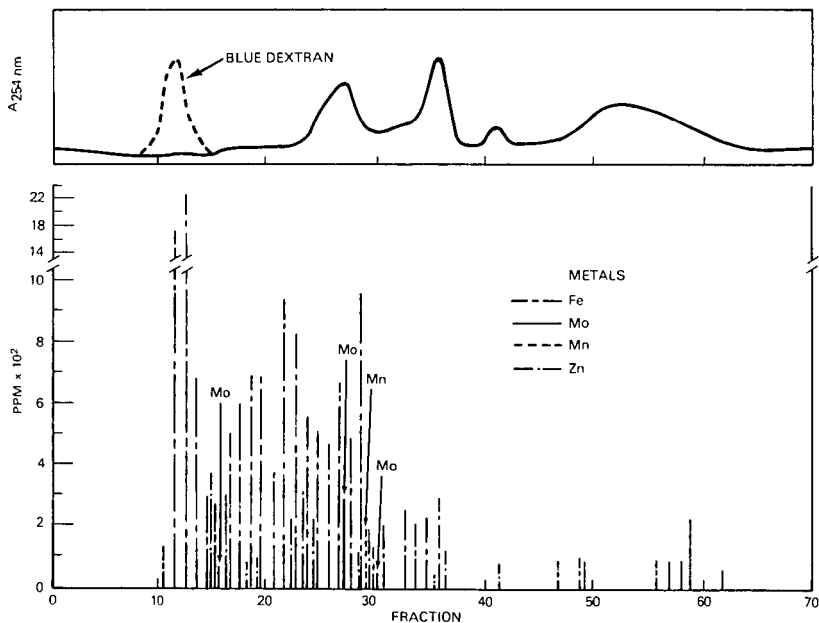


FIGURE 3. Fractionation of Organics and Metals in Paraho Condensate Retort Water with Sephadex G-15.

Steric-exclusion chromatography with Sephadex G-15 also provided considerable fractionation of the retort waters' organics. This type of chromatography appears to be amenable to the studies such as the metallorganics study (15) in that it constitutes a rather mild form of chromatography, unlike ion-exchange chromatography, for example. One might reasonably expect organic-metal chelates to survive the chromatography. Indeed, in our studies to date with the retort waters, certain metals, and organic species appear to co-elute, presumably as distinct complexes or aggregates. Interestingly, each retort water appears to contain several distinct aggregates with nominal MW's ≤ 1500 , based on Sephadex G-15's nominal fractionation range as calibrated against Dextran standards.

Acknowledgments

The authors are indebted to Dr. R. A. Pelroy for the mutagenesis assays, T. R. Pahl for some of the GC-MS analyses, and K. B. Olsen for the PES analysis. This study was supported by the U. S. Department of Energy under Contract DE-AC06-76RLO-1830.

References

- (1) Epler, J., Larimer, F., Rao, T., Nix, C., and Ho, T., Environ. Health Perspect., 27:11-20 (1978).
- (2) Epler, J., Rao, T., and Guerin, M., Environ. Health Perspect., 30:179-184 (1979).
- (3) Pelroy, R. A., and Petersen, M. R., Application of Short-Term Bioassays in the Fractionation and Analysis of Complex Environmental Mixtures, Waters, Nesnow, Huisingsh, Sandhu and Claxton (eds.), pp.465-475, Plenum Press, New York, (1979).
- (4) Pelroy, R. A., and Petersen, M. R., Environ. Health Perspect., 30:191-203 (1979).
- (5) Wilson, B. W., Pelroy, R. A., and Cresto, J. T., Mutation Res., 79:193-202 (1980).
- (6) Toste, A. P., Sklarew, D. S., and Pelroy, R. A., Proceedings of the 20th Hanford Life Sciences Symposium, in press.
- (7) Jackson, L. P., Poulson, R. E., Spedding, T. J., Phillips, T. E., and Jensen, H. B., Quarterly Colorado School of Mines, 70:105-134 (1975).
- (8) Fox, J. P., Farrier, D. S., Poulson, R. E., Laramie Energy Technology Center Report of Investigations No. 7817, 47p. (1978).
- (9) Ho, C.-h., Clark, B. R., and Guerin, M. R., J. Environ. Sci. Health, A-11, 101 (1976).
- (10) Riley, R. G., Skiosaki, K., Bean, R. M., and Schoengold, D. M., Anal. Chem., 51:1995-1997 (1978).
- (11) Fish, R. H., Brinckman, F. E., and Jewett, K. L., submitted to Environ. Sci. and Tech. (1981).
- (12) Pellizzari, E. D., Castillo, N. P., Willis, S., Smith, D., and Bursey, J. T., Measurement of Organic Pollutants in Water and Wastewater, C. E. Van Hall, Ed., American Society for Testing and Materials STP686, 256-274 (1979).
- (13) Riggan, R. M., and Howard, C. C., Anal. Chem., 51(2):210-214 (1979).
- (14) Ames, B., McCann, J., and Yamasaki, E., Mutation Res., 31:347-364 (1975).
- (15) Means, J. L., Crerar, D. A., and Duguid, J. O., Science, 200:1477-1481 (1978).

A PHYSICO-CHEMICAL INVESTIGATION OF EASTERN AND WESTERN SHALE OILS
PRODUCED BY THE IGT HYTORT AND FISCHER ASSAY PROCESSES

Daniel A. Netzel and Francis P. Miknis

U. S. Department of Energy
Laramie Energy Technology Center
P. O. Box 3395, University Station
Laramie, WY 82071

INTRODUCTION

The major interest in oil shale development within the United States, thus far, has focused on the oil shales in the Green River Formation in Colorado, Utah and Wyoming. However, a substantial portion (nearly 250,000 square miles) of the Eastern United States is underlain by the Devonian Black Shales, and in principle, represents a sizeable potential resource. These shales, however, yield only less than one-half as much liquids upon heating as do the Green River Formation oil shales, because of the lesser hydrogen contents of the Devonian shales. Therefore, processes to extract liquids or improve recovery ratios from the Devonian shales must necessarily deal with special retorting techniques for hydrogen deficient materials. One such candidate process is the Institute of Gas Technology's Hytort process, which retorts oil shale under hydrogen pressure with the result that oil yields of Devonian shales are increased 2.5 times over those obtained by the standard Fischer assay. Characterization of the Eastern and Western oils that are produced by the IGT and Fischer assay processes would be beneficial toward: a) assessing the quality of the product oils, b) understanding the retort process and c) providing information for optimizing the process.

Nuclear Magnetic Resonance (NMR) is a technique that has been used extensively to characterize petroleum fractions. An advantage of NMR is that it can be applied to whole oils to determine gross compositional and structural changes that might occur during the process. This information in turn, can be used by process engineers to determine what parameters to vary or control, and by chemists to determine the need for further fractionation and characterization.

This paper reports the results of NMR studies of shale oils produced by the IGT Hytort and Fischer assay processes and hydrotreated shale oils from the Hytort process. The Fischer assay is the standard method for evaluating an oil shale's potential for conversion to liquids and thus, oils produced from the Fischer assay represent baseline oils for comparison purposes. Few papers have appeared on the analysis of shale oils using NMR techniques(1,2). Those that have, have discussed shale oils produced primarily from Green River oil shales. Shale oils produced from Eastern oil shales, coupled with the ones produced from processes other than the Fischer assay, offer a set of shale oils different enough to assess the utility of NMR methods.

EXPERIMENTAL PROCEDURE

A. Shale Oil Source

The NMR studies were conducted on shale oils obtained from a Western Eocene shale (Colorado, Piceance Basin) and two Eastern Devonian shales (Kentucky Sunbury and Kentucky New Albany from Lewis and Bullitt Counties, Kentucky, respectively). The shale oils from the three shales were obtained using the IGT Hytort Process Development Unit at IGT(3) and the Fischer Assay retort method at LETC(4). The Eastern shale oils were further upgraded using the IGT catalytic hydrotreating unit at IGT(5).

B. Nuclear Magnetic Resonance

Samples were prepared in 5mm tubes for ^1H and 10mm tubes for ^{13}C experiments. Tetramethylsilane (TMS) was used as a reference for both nuclei and CDCl_3 as the solvent for all samples. Concentrations of approximately 50/50 and 65/35 by volume of sample to solvent were used for proton and carbon-13 spectra, respectively. Six percent TMS in CDCl_3 provided the lock signal for ^1H and the solvent CDCl_3 provided the lock signal for ^{13}C NMR spectra.

C. Average Molecular Structure Parameters

The average molecular structure parameters for the various shale oils were calculated from the normalized ^1H and ^{13}C spectral areas. The equations used to compute the parameters were assembled from the literature and partly derived by Netzel and Hunter(6). The equations were modified to include the presence of olefins(7).

RESULTS AND DISCUSSION

A. Shale Oil - Analytical Data

Table I lists the elemental composition and the H/C weight ratios of the Eastern and Western shale oils obtained from the Fischer assay and IGT Hytort retorting processes. Also included in the Table are the elemental compositions and H/C weight ratio of the hydrotreated shale oils.

As shown in Table I, the H/C weight ratio of the shale oil appears to be independent of the retorting process for a given shale. However, for the hydrotreated IGT Hytort shale oils, the H/C ratio increases as one would expect upon hydrogenation of aromatic and olefinic molecules to form saturate molecules. The H/C weight ratio of the Eastern shale oils are significantly lower than that of the Western shale oil indicating greater aromatic content for the Eastern shale oils.

The total sulfur content of the Western shale oils is lower than the Eastern shale oils and appears to be independent of the retorting process. The nitrogen content is slightly higher for the Colorado shale oil relative to the two Kentucky shale oils. The IGT Hytort process relative to the Fischer assay method tends to increase the nitrogen content of the shale oils independent of the source of the oil shale. This increase may be due to the more severe conditions used in the Hytort process. As expected the hydrotreated shale oils have markedly reduced nitrogen and sulfur contents.

B. Shale Oil - NMR Data

Figure 1 shows the ^1H NMR spectrum of the Colorado Fischer assay shale oil. Most of the quantitative information on the composition of shale oil is derived from the ^1H spectrum since the chemical shift ranges for the various hydrogen types found in hydrocarbons are fairly well defined⁶.

Figure 2 shows the ^{13}C NMR spectra of the Colorado shale oil produced from the Fischer assay method and the IGT Hytort process. The region from 100 to 150 ppm represents the aromatic/olefinic carbon resonances. The two sharp resonances at 114 and 138 ppm are due to 1-alkenes(1). The aliphatic carbon resonances are found in the region from 0 to 50 ppm. The five intense signals (14, 23, 29, 30 and 32 ppm) in this region correspond to the five signals associated with carbon chain greater than 9. The greater the intensity of the resonance at 30 ppm relative to the intensity of the resonance at 14 ppm, the longer the carbon chain length. The less intense signals in this region are due to branched and cyclic alkanes and alkyl groups of alkylaromatics(2). It is not possible to infer the individual molecular species from neither the ^1H nor ^{13}C NMR spectra but only the average molecular type.

Figure 3 shows the carbon-13 spectra of the Kentucky Sunbury shale oils produced by the Fischer assay and the IGT Hytort processes. The two Eastern shale oils produced by the IGT Hytort process were catalytically hydrotreated. The carbon-13 spectrum of the hydrotreated Kentucky New Albany shale oil is shown in Fig. 4. The spectrum of the hydrotreated Kentucky Sunbury is nearly identical and is not given.

C. Average Molecular Structure Parameters

Average molecular structure parameters and the composition of the hydrocarbon types can be determined from the integration of the area of the various carbon and hydrogen regions in the NMR spectra(6). When calculating the average molecular structure parameters for any hydrocarbon mixture including shale oil several assumptions must be made. These assumptions are: (1) The sample contains only mono- and diaromatics which in most cases is valid because the concentration level of triaromatics in shale oil is small, (2) the unsubstituted non-bridged aromatic ring carbon protons of mono- and diaromatics are sufficiently separated in the ^1H spectrum such that the ratio of mono- to diaromatics protons can be determined, (3) the number of substituents in the mono- and diaromatic components is the same, (4) the concentration of heteronuclear molecules is low (a weak assumption), (5) one hydrogen per olefinic carbon and (6) long carbon chain alkyl substituents on aromatic rings and long alkyl carbon chains of olefins are computed as saturate hydrocarbons.

Because the shale oils were collected over a large temperature range, the validity of average structural parameters in representing molecular type is almost meaningless. The structural parameter data are valuable in that they quantitatively represent observed changes in the ^1H and ^{13}C NMR spectra of the shale oils, and thus trends may be established.

Tables II, III, and IV give the average molecular structure parameters. Two important parameters are the hydrogen and carbon aromaticities. The hydrogen aromaticity, f^{H} , is defined as the area measurement of the aromatic hydrogens divided by the total^a area of all hydrogens in the ^1H spectrum. Values for f^{H} for the Eastern and Western shale oils produced by the Fischer assay, IGT Hytort and the hydrotreated Hytort methods are given in the tables.

The ratio of the integrated aromatic carbon region to the total integrated carbons in the ^{13}C spectrum gives the carbon aromaticity, f^{C} . Carbon aromaticities for the various shale oils are also given in Tables II, III, and IV. It should be noted that the carbon aromaticity value is not totally due to aromatic carbons but also olefinic carbons.

The measurement of f^{H} and f^{C} are obtained directly from their respective NMR spectrum. That is, no assumptions (aside from olefinic contribution to f^{C}) are made in computing these values. Thus these values are important in representing any changes which might occur in a system under retorting conditions or hydrotreating.

Tables II through IV also list the mole percent of hydrocarbon types in the various shale oils. To a very good first approximation, the data can be used to compare shale oil source and retorting methods. To convert the mole percentages to weight or volume percentages requires additional assumptions regarding average molecular weights and average densities for the hydrocarbon types and thus is not germane to the discussion. More so than the H/C weight ratios (Table I), the mole percent of aromatics (which includes nitrogen sulfur and oxygen heteroaromatics), olefins and alkanes in Tables II through IV show clearly the differences in Eastern and Western shale oils obtained from the two retorting and hydrotreating processes.

It is readily seen from the data in Tables II-IV that the Eastern shale oils produced by the Fischer assay method and the IGT Hytort processes contain about twice as much aromatics compared to the Colorado shale oil. For the Colorado shale

oil, the mole percent of aromatics are nearly same regardless of the retort method (probably due to less severe conditions used in the Hytort process). However, for the Eastern shale oils, the IGT Hytort process increases the mole percent of aromatics relative to the Fischer assay method. This increase in aromatics for the Eastern shale oils over the Colorado shale oil is the result of (1) higher aromatics in the raw oil shales which is supported by solid state NMR data and (2) retorting in a hydrogen atmosphere which may free more aromatics from the matrix.

The Fischer assay method produces more olefins for the Colorado shale oil relative to the two Kentucky shale oils (see Tables II-IV), while the IGT Hytort process produces less olefins overall. However, the Colorado Hytort shale oil still has more olefins than the Kentucky Hytort shale oils. This in part may be due to the fact the hydrogen pressure used in the IGT Hytort of the Colorado shale was lower than the hydrogen pressure used for the Eastern shales.

As expected, the hydrotreating of the Kentucky Hytort shale oils considerably reduces the mole percent of aromatics and olefins with a corresponding increase in the mole percent of alkanes.

CONCLUSIONS

It has been shown that computing the average molecular structure parameters from NMR data of shale oils can be useful in describing changes in the oils resulting from different retorting methods and source of the oil shale.

Eastern shale oils are more aromatic than the Western shale oil regardless of the retort method. It also has been observed that the IGT Hytort process increases the aromatic content and lowers the olefinic content of the Eastern shale oils, relative to the Fischer assay method.

REFERENCES CITED

1. Netzel, D. A., "High Resolution NMR Spectroscopy: Its Application to Shale Oil Component/Type Analysis," Proc. of IGT Synthetic Fuels from Oil Shale Symposium, Atlanta, GA., Paper, 1979 (Pub. 1980), p. 271. See also references cited therein.
2. Netzel, D. A., D. R. McKay, R. A. Heppner, F. D. Guffey, S. D. Cooke, D. L. Varie, and D. E. Linn, "Proton and Carbon-13 NMR Studies on Naphtha and Light Distillate Saturate Hydrocarbon Fractions Obtained from In Situ Shale Oil," Fuel 60, 307 (1981).
3. Feldkirchner, H. L., "The Hytort Process," Proc. of IGT Synthetic Fuels from Oil Shale Symposium, Atlanta, GA., paper, 1979 (Publ. 1980), p. 489.
4. Baughman, G. L., "Synthetic Fuels Data Handbook," 3rd Ed.; p. 55, Denver, CO., Cameron Engineers, Inc., 1978. Standard method of test for oil from oil shale (resource evaluation by USBM Fischer assay procedure) ASTM Method D 3904-80.
5. "Synthetic Fuels from U. S. Oil Shales a Technical and Economic Verification of The Hytort Process," DOE/ET/14102-2, Subject Category UC-91.
6. Netzel, D. A. and Hunter, P. M., "Hydrocarbon Type Analysis of Jet Fuels by ^1H and ^{13}C NMR," Report of Investigation DOE/LETC/RI-81-1.
7. Ozubko, R. S., Clugston, D. M. and Furimsky, E., "Comparison of Mass Spectrometry and Nuclear Magnetic Resonance Spectrometry for Determination of Hydrocarbon Type," Anal. Chem., 53, 183 (1981).

TABLE I ELEMENTAL ANALYSES OF SHALE OILS AND HYDROTREATED SHALE OILS

| | Elemental Analysis, Wt% | | | |
|--------------------------------------|-------------------------|-------|------------|----------------------------|
| | Fischer Assay | | IGT-Hytort | IGT-Hytort Hydrotreated |
| | A | B | | |
| <u>Colorado Shale Oil</u> | | | | |
| Carbon | 85.08 | 84.30 | 84.57 | |
| Hydrogen | 11.44 | 11.42 | 11.40 | |
| Sulfur | .73 | .63 | 0.62 | |
| Nitrogen | 1.80 | 1.90 | 2.13 | |
| Oxygen | 1.31 | 1.50 | 0.98 | |
| H/C Weight Ratio | 0.135 | 0.136 | 0.135 | |
| <u>Kentucky New Albany Shale Oil</u> | | | | |
| Carbon | 84.91 | 84.97 | 85.46 | 88.27 |
| Hydrogen | 9.83 | 10.08 | 9.42 | 11.70 |
| Sulfur | 1.02 | 1.61 | 1.52 | .05 |
| Nitrogen | 1.52 | 1.56 | 2.12 | .40 |
| Oxygen | 1.72 | 2.00 | 1.61 | .12 |
| H/C Weight Ratio | 0.116 | 0.119 | 0.110 | 0.133 |
| <u>Kentucky Sunbury</u> | | | | |
| Carbon | 84.36 | 84.59 | 85.45 | 87.30 |
| Hydrogen | 9.96 | 9.98 | 9.56 | 12.60 |
| Sulfur | 1.33 | 1.59 | 0.99 | .06 |
| Nitrogen | 1.33 | 1.48 | 2.12 | .17 |
| Oxygen | 2.12 | 2.36 | 1.22 | .28 |
| H/C Weight Ratio | 0.118 | 0.118 | 0.112 | 0.144 |

TABLE II AVERAGE MOLECULAR STRUCTURE PARAMETERS AND MOLE PERCENT AROMATICS, OLEFINS, AND ALKANES FOR COLORADO SHALE OILS OBTAINED FROM THE FISCHER ASSAY AND IGT HYDROT PROCESSES

| | Shale Oil Processes | | |
|--|---------------------|------|---------------|
| | Fischer Assay | | IGT Hytort |
| | A | B | |
| Hydrogen Aromaticity | .054 | .055 | .070 |
| Carbon Aromaticity* | .244 | .244 | .269 |
| Mole Percent Aromatics** | 26.5 | 26.1 | 28.1 |
| Percent Mono- | 24.9 | 24.3 | 25.3 |
| Percent Di- | 1.6 | 1.8 | 2.8 |
| Fraction of Substituted & Bridged Carbons | .158 | .154 | .156 |
| Fraction of Unsubstituted Carbons | .087 | .090 | .113 |
| Number of Alkyl Substituents/Ring | 3.3 | 3.2 | 2.8 |
| Mole Percent Olefins | 6.3 | 7.2 | 4.9 |
| Mole Percent Alkanes | 67.2 | 66.7 | 66.9 |
| Fraction of n-alkanes | .35 | .40 | .51 |
| Fraction of branched Alkanes*** | .65 | .60 | .49 |
| CH ₂ /CH ₃ Ratio | 2.1 | 2.3 | 2.2 |
| Carbon Chain-Length | 11.7 | 14.3 | 17.1 |
| Total Atomic H/C Ratio | 1.60 | 1.61 | 1.61 |
| Aromatic H/C Ratio | .36 | .37 | .42 |
| Alkane H/C Ratio | 2.01 | 2.02 | 2.04 |

* Includes olefinic carbons

** Includes heteroaromatics

*** Includes cyclic alkanes and alkyl substituent carbons on aromatic rings

TABLE III AVERAGE MOLECULAR STRUCTURE PARAMETERS AND MOLE PERCENT AROMATICS, OLEFINS AND ALKANES FOR KENTUCKY NEW ALBANY SHALE OILS OBTAINED FROM THE FISCHER ASSAY, IGT HYTORT AND HYDROTREATMENT PROCESSES

| | Shale Oil Processes | | | |
|---|---------------------|------|--------|--------------|
| | Fischer Assay | | IGT | IGT Hytort |
| | A | B | Hytort | Hydrotreated |
| Hydrogen Aromaticity | .102 | .114 | .171 | .078 |
| Carbon Aromaticity* | .362 | .373 | .468 | .177 |
| Mole Percent Aromatics** | 46.4 | 46.9 | 60.0 | 32.9 |
| Percent Mono- | 41.1 | 42.5 | 51.4 | 30.0 |
| Percent Di- | 5.3 | 4.4 | 5.6 | 2.9 |
| Fraction of Substituted & Bridged Carbons | .244 | .212 | .221 | .055 |
| Fraction of Unsubstituted Carbons | .225 | .161 | .141 | .123 |
| Number of Alkyl Substituents/Ring | 3.0 | 2.8 | 2.3 | 2.7 |
| Mole Percent Olefins | 4.4 | 5.1 | 4.0 | 0.0 |
| Mole Percent Alkanes | 49.2 | 48.0 | 39.1 | 67.1 |
| Fraction of n-alkanes | .29 | .29 | .27 | .23 |
| Fraction of branched alkanes*** | .71 | .71 | .73 | .77 |
| CH ₂ /CH ₃ Ratio | 1.04 | .9 | .8 | 1.1 |
| Carbon Chain-Length | 9.2 | 10.7 | 10.0 | 11.2 |
| Total Atomic H/C Ratio | 1.38 | 1.41 | 1.31 | 1.58 |
| Aromatic H/C Ratio | .39 | .43 | .48 | .69 |
| Alkane H/C Ratio | 1.94 | 2.00 | 2.05 | 1.77 |

* Includes olefinic carbons

** Includes heteroaromatics

*** Includes cyclic alkanes and alkyl substituent carbons on aromatic rings

TABLE IV AVERAGE MOLECULAR STRUCTURE PARAMETERS AND MOLE PERCENT AROMATICS, OLEFINS, AND ALKANES FOR KENTUCKY SUNBURY SHALE OILS OBTAINED FROM THE FISCHER ASSAY, IGT HYTORT AND HYDROTREATMENT PROCESSES

| | Shale Oil Processes | | | |
|---|---------------------|------|--------|--------------|
| | Fischer Assay | | IGT | IGT Hytort |
| | A | B | Hytort | Hydrotreated |
| Hydrogen Aromaticity | .125 | .119 | .171 | .048 |
| Carbon Aromaticity* | .383 | .382 | .453 | .184 |
| Mole Percent Aromatics** | 52.3 | 48.7 | 62.9 | 19.8 |
| Percent Mono- | 47.9 | 41.8 | 53.6 | 17.3 |
| Percent Di- | 4.5 | 6.9 | 9.4 | 2.5 |
| Fraction of Substituted & Bridged Carbons | .205 | .214 | .225 | .101 |
| Fraction of Unsubstituted Carbons | .178 | .168 | .229 | .084 |
| Number of Alkyl Substituents/Ring | 2.7 | 2.8 | 2.5 | 2.7 |
| Mole Percent Olefins | 6.6 | 6.0 | 3.1 | 0.0 |
| Mole Percent Alkanes | 41.1 | 45.3 | 33.9 | 80.2 |
| Fraction of n-alkanes | .31 | .31 | .28 | .22 |
| Fraction of branched alkanes*** | .69 | .69 | .72 | .78 |
| CH ₂ /CH ₃ Ratio | .6 | .7 | .3 | 1.3 |
| Carbon Chain-Length | 10.0 | 9.7 | 10.4 | 8.7 |
| Total Atomic H/C Ratio | 1.41 | 1.41 | 1.33 | 1.72 |
| Aromatic H/C Ratio | .46 | .44 | .50 | .45 |
| Alkane H/C Ratio | 1.99 | 2.00 | 2.02 | 2.00 |

* Includes olefinic carbons

** Includes heteroaromatics

*** Includes cyclic alkanes and alkyl substituent carbons on aromatic rings

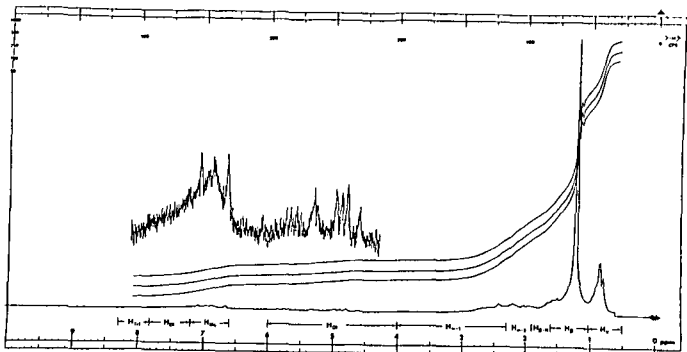


Figure 1 ^1H NMR SPECTRUM OF THE COLORADO SHALE OIL OBTAINED FROM THE FISCHER ASSAY METHOD

Carbon-13 NMR

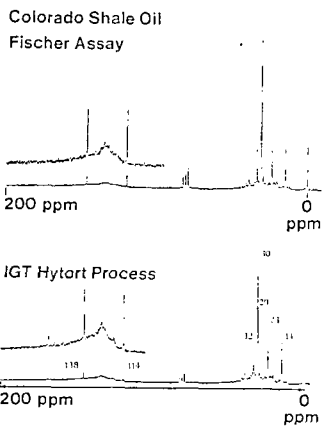
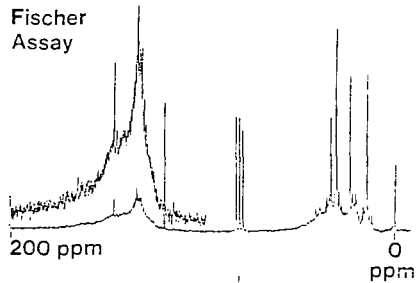


Figure 2 ^{13}C NMR SPECTRA OF THE COLORADO SHALE OILS OBTAINED FROM THE FISCHER ASSAY AND IGT HYTORT PROCESSES

Carbon-13 NMR

Kentucky New Albany Shale Oil
Fischer
Assay



IGT Hytort Process

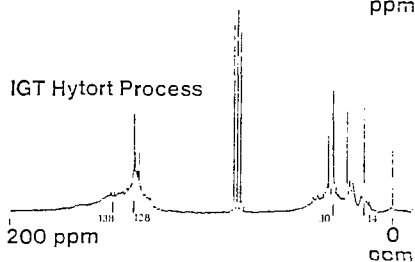


Figure 3 ^{13}C NMR SPECTRA OF THE KENTUCKY NEW ALBANY SHALE OILS OBTAINED FROM THE FISCHER ASSAY AND IGT HYTORT PROCESSES

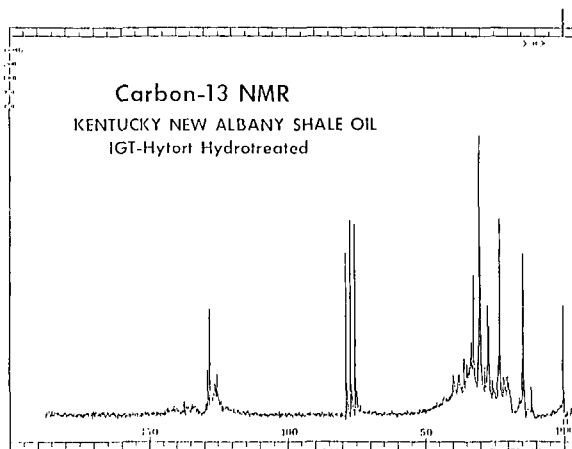


Figure 4 ^{13}C NMR SPECTRUM OF THE HYDROTREATED KENTUCKY NEW ALBANY SHALE OIL OBTAINED FROM THE IGT HYTORT PROCESS

THERMAL DEGRADATION OF SHALE OIL

D. S. Thakur, J. P. Vora, E.S. Wilkins, and H.E. Nuttall
Department of Chemical and Nuclear Engineering
The University of New Mexico
Albuquerque, New Mexico 87131.

ABSTRACT

A new procedure has been developed to study the mechanisms of shale oil degradation, which occurs during the VMIS retorting process. The very complex processes of oil degradation have been studied under carefully controlled conditions of temperature, residence time, carrier gas flow rate, etc. The experiments presented in this study have been designed to separate the three potential oil loss mechanisms, namely, (1) low temperature coking (liquid phase), (2) successive distillation (liquid phase), and (3) high temperature cracking (vapor phase). The shale oil from Occidental's retort No. 6 has been used as a starting material. The steady state nature of operation used here makes it possible to achieve an accurate material balance for degraded products. In the liquid phase oil degradation experiments, oil was heated to 450°C at a linear heating rate of 1°C/min in both an autogenous atmosphere and using various sweep gases such as steam, N₂, CO₂, CO and H₂. Low temperature coking showed only minor losses. A 35 percent oil loss occurred during successive distillation under autogenous conditions. It was reduced to 15 percent by injection of sweep gases, especially steam. A tubular continuous flow reactor was used to study the vapor phase degradation under steady state conditions of temperatures (425 to 625°C) and residence time (2 to 10 sec) with nitrogen and steam as carrier gases. A 3² factorial design was conducted to assess the influence of temperature and residence time on oil degradation. The kinetic data were analyzed by a first order rate equation giving an activation energy of 17.3 kcal/mole.

INTRODUCTION

Shale oil is a potentially important fossil fuel which could augment energy supplies in future years. Modified in-situ retorting of oil shale may offer a new and viable method for extracting oil from shale. A key consideration in this new and rapidly developing technology is the problem of maximizing oil recovery from each underground retort, since thousands of retorts will be required. In this process gas composition, temperature, heating rate, particle size distribution and retorting rates are major factors. Low oil yields have been observed from tests on large retorts. Since the oil losses that occur during the pyrolysis of oil shale are quite substantial, a considerable amount of work is directed towards the elucidation of oil loss mechanisms.¹⁻¹² Within a retort, one encounters a situation downstream of the retorting front where product oil condenses on the raw shale. Oil trapped in this zone can be exposed to modest temperatures for months. This leads to low temperature oil degradation by coking. At the leading edge of the thermal wave, a continuous vaporization and condensation of oil will occur which may also cause significant oil degradation. In the VMIS process, loss in oil yields also results from the

large particles and wide size distributions. The large blocks are heated at a slower rate than the surrounding matrix because of poor heat transfer. The exposure of oil vapor, liberated from large particles, to high temperatures leads to its thermal degradation. Several factors contribute to the degradation mechanisms among which residence time, temperature, and sweep gas atmosphere are prominent candidates. It is well known that oil shales (raw and spent) could catalytically initiate certain undesired reactions leading to oil loss. It is also conceivable that the mechanism responsible for liquid phase oil degradation is different from that for vapor phase one.

When hydrocarbons are brought to high temperature, they undergo thermal cracking via free radical mechanisms. The radicals thus formed can undergo scission to give large amounts of ethylene. Jacobson, et al¹ observed that during oil shale pyrolysis, ethylene/ethane ratio increased with temperature. Based on these findings, they developed the retorting index (R. I.) which is given by the following equation:

$$R.I. = T^{\circ} (F) = \frac{1000}{0.8868 - 0.4007 \log \frac{\text{ethylene}}{\text{ethane}}}$$

The ratio of ethylene to ethane was found to depend upon the heating rate and residence time. Campbell, et al², have studied the effect of heating rate and particle size on oil evolution and intraparticle oil degradation. They correlated the alkene/alkane ratio to the liquid phase oil degradation (coking).³ During the last few years, the alkene/alkane ratio has been used extensively as an index of thermal degradation.⁵⁻⁹ Burnham, et al^{10,15,16} have studied the oil degradation mechanism in vapor phase with raw oil shale as the starting material. It was found that the alkene to alkane ratio decreases with increased coking while it increases with increase in cracking of the shale oil. If both reactions occur simultaneously one cannot use this ratio as an index of oil degradation. Hence, a naphthalene/(C₁₁+ C₁₂) straight chain hydrocarbons ratio was recommended by Burnham, et al¹⁵ as an index of cracking or vapor phase oil loss.

The experiments presented in this study were designed in such a way as to separate the following processes:

1. Low temperature coking (liquid phase).
2. Successive distillation (liquid phase), and
3. High temperature cracking (vapor phase).

Such a design yielded information about the most important features of liquid and vapor phase oil degradation. In this study, shale oil was used to permit accurate characterization of the starting material in contrast to other studies which used the oil generated by heating oil shale in a small laboratory-scale retort. Advantages and disadvantages of the approach used in the present study are described below. Advantages are as follows:

1. The feed can be well characterized and compared to the degraded product.
2. Since the experiment is operated in a steady state manner, an accurate material balance for degraded products is achieved.

3. Because of the steady state and continuous nature of operation used here, residence time can be determined and controlled more precisely as compared to batch operation studies. In the latter studies the batch method of oil generation makes the determination and control of residence time rather difficult, and introduces time varying feed rate.
4. It is possible to investigate the effect of mineral matter present in the shale oil either as colloidal suspension or in solution. By using the total molecular weight distribution, effects such as auto-catalytic cracking, if it occurs, can be studied.
5. The shale oil used in this study was from Occidental's retort No. 6 and was thus characteristic of the oil product from a large-scale retort.

The shortcomings of this approach are few and may be overcome.

1. The feed oil has already been exposed to some undetermined amount of degradation which may affect its subsequent behavior. One way to overcome this problem is to test the oil from various sources.
2. Storage of the oil for a prolonged time may alter its properties and composition. Very little literature data are available on the effect of storage. This problem can be avoided by obtaining fresh samples of oil.
3. Oil may contain a colloidal suspension of minerals which might catalyze the oil degradation or cracking. This phenomenon needs further study involving filtration or demineralization of oil.

In this paper, results obtained by subjecting the oil to coking conditions (low temperature soaking and successive distillation) will be compared to those obtained by treating the shale oil under cracking conditions. In addition, effect of carrier gas such as steam, N_2 , CO_2 , CO and H_2 on low temperature liquid phase degradation will be discussed.

EXPERIMENTAL PROCEDURE

LIQUID PHASE DEGRADATION

Apparatus

A standard bench-scale glassware assembly was used. The apparatus consisted of a heating mantle, a 4-necked flask (3000 ml), stirrer, sparger, condensers and receivers for liquid, and gas samples. In low-temperature soaking experiments, a reflux condenser was used to return the oil vapor to the heating flask, while in the successive distillations a regular condenser was used and low boiling fractions were collected in the receivers. When experiments were performed in an autogenous environment, a stirrer was used to ensure uniform mixing and avoid spurting. When the experiments were carried out in sweep gas environment a sparger was used to bubble the gas through the shale oil.

Procedure

Low-Temperature Soaking

About 1 liter of shale oil was placed in the 4-necked flask. The flask was covered with glass wool in order to insulate it from the surroundings. The flask was then heated gradually at the rate of 1°C/min to the desired temperatures (170 to 400°C) with constant stirring. The temperature was controlled within $\pm 1^\circ\text{C}$ by means of a temperature controller and a variac. Time of thermal treatment was about 10 to 12 hours. The low-boiling, condensable oil fractions were collected in the receiver while the gas produced, if any, was collected in the gas samplers. The shale oil (before and after thermal treatment) and condensate were analyzed on a capillary column gas chromatograph as described earlier, while the hydrocarbon and permanent gases were analyzed by using 1/8 in. i.d. 6-ft long Poropak Q and Molecular Sieve 13X columns. ¹³

Successive Distillation

The procedure was similar to that described in the preceding paragraph except that after each distillation the condensate was mixed with the residue in the still and the mixture was redistilled until no appreciable loss due to coke formation or gas evolution was observed. The carrier gas was introduced through the side tube during the distillation.

The liquid products (condensate and residue in the flask) were analyzed on a SP-2100 fused silica column by using an HP 5840 A gas chromatograph; the gas analysis was performed on Poropak Q and carboxieue columns by using an HP 5840 gas chromatograph. Condensate and residue in the distillation flask were weighed. A known amount of methylene chloride was then added to the distillation flask so as to dissolve the tar-like organic matter. The flask was reweighed, the difference between the two readings was taken as the amount of coke formed during these experiments. By measuring the amount of gas, condensate and residue, a material balance of 98 percent was achieved.

VAPOR PHASE OIL DEGRADATION

Apparatus

A tubular continuous flow reactor, with on-line gas chromatograph, was used to study the vapor phase oil degradation under steady state conditions of temperature and residence time. Fisher and Porter flow meters (model 10A1379) were used to control the flow rates of nitrogen and water before they entered the preheaters. Shale oil was injected into the stream of carrier gas at a steady rate by means of a Sage syringe pump model 341. Glass-lined stainless-steel tubes (8 mm i.d., 200 mm long) were used to generate steam from water and to heat the fluid mixture to about 400°C before its entry into the reactor. The maximum residence time of the fluid in the preheaters was less than 1 sec (at the lowest flow rate). The thermal degradation of oil (at 400°C) at the exit of the preheaters was predetermined; it was less than 1 percent. An empty quartz tube (25 mm i.d. and 300 mm long) served as a reactor in the present study. The reactor was heated by means of a Lindberg heavy duty tubular furnace, the temperature of which was controlled within $\pm 1^\circ\text{C}$ by a Lindberg temperature controller. The product collection assembly consisted of condensers and receivers, and either a filter or an electrostatic precipitator to

prevent the oil vapor (aerosol) from escaping with the uncondensable gases. The gases passed through a flow meter and a gas sampling valve to the gas chromatograph (HP 5840) for periodic analysis.

Procedure

The reactor and preheaters were heated to the desired temperature in a flow of nitrogen. After the steady state conditions of temperature and nitrogen flow rate were attained (about 3 to 4 hours), shale oil was metered through the sage pump at a fixed rate (~0.75 ml/min.). During experiments in which steam was used, water was simultaneously injected into the carrier gas and heated in a separate preheater. The steam to nitrogen ratio (vol/vol) was 0.3. The residence time was varied by varying the flow rates of carrier gas. The effects of residence time and temperature were assessed by studying the reaction at temperatures between 425 and 626°C and residence time ranging from 2 to 10 sec. Duration of each run (with shale oil flow) was about 1-1/2 hours, which was considered to be sufficient for the system to attain equilibrium. The total liquid product mix was collected and weighed for mass balance. Liquid and gases were analyzed by gas chromatography as described earlier. The reactor was weighed before (W_i) and after the reaction. A known amount of methylene chloride was added to the reactor to dissolve the tar-like soluble material formed during the reaction. The reactor was dried in air and reweighed (W_f). The difference between the final weight (W_f) and initial weight (W_i) gave the amount of coke formed. The flow meter at the exit of the apparatus gave the amount of gases evolved during the reaction. The total oil loss was defined as follows

$$\% \text{ Total oil loss} = \frac{\text{amount of oil fed} - \text{amount of condensate}}{\text{amount of oil fed}} \times 100$$

A total material recovery calculated from amount of condensate, gas and coke was between 95 to 98 percent.

As indicated earlier, several researchers have been using ethylene/ethane, alkene/alkane and naphthalene/($C_{11} + C_{12}$) hydro-carbon ratios to determine the extent of degradation. In addition to these ratios, hydrocarbon gas/coke ratio was also monitored in the present study.

RESULTS AND DISCUSSION

Low Temperature Soaking

The results obtained by refluxing the shale oil at a constant temperature are presented in Table 1. No noticeable oil loss occurs until a temperature of 300°C is reached. Gas evolution occurred at temperatures higher than 300°C, which indicates the commencement of oil degradation at these elevated temperatures. The amount of gas collected was, however, quite small (~3 percent) at 400°C. Table 2 gives the analysis of gas samples collected at 400°C.

Successive Distillation

During successive distillation and condensation, a considerable amount of oil is converted into coke and hydrocarbon gases. Overall oil losses and those due to coking and gas formation during successive distillation of shale oil (with and without addition of carrier gases) are shown in Figures 1, 2 and 3, respectively.

Figure 1 shows that in the absence of carrier gas the total oil loss at the end of five distillation runs was as high as 35 percent. About 10 to 15 percent of the initial oil is converted to hydrocarbon gas while the rest undergoes slow polymerization leading to solidification (coke formation); gas to coke ratio remained constant around 0.5 to 0.55. No appreciable amount of thermal degradation was observed below 300°C. At temperatures above 400°C, a considerable amount of gas evolved and at 450°C, a solid residue (coke) was obtained. Hydrocarbon gases evolved are richer in ethane than in ethylene (Figure 4). This phenomenon is just the opposite of that observed in vapor phase oil degradation. These findings are in accordance with the reported literature, and suggest that the mechanism responsible for the oil loss in liquid phase is different from that occurring in vapor phase.

Addition of carrier gas has a beneficial effect on oil yield. When a mixture of steam and nitrogen was bubbled through the shale oil, a total oil loss of 13 percent was observed while the injection of nitrogen alone resulted in a total loss of 20 percent (Figure 1). The use of carbon dioxide resulted in 18 percent oil loss whereas carbon monoxide and hydrogen resulted in 17 and 15 percent oil loss, respectively. Total oil loss decreases by the addition of carrier gas because of the fact that a major portion of the oil is distilled over at much lower temperatures (<300°C) as compared to the run in which no carrier gas is used, thus has less exposure to the high temperature.

Figure 3 shows that about 24 percent coke was formed at the end of five distillation runs when no carrier gas was injected. The use of carrier gas reduced the amount of coke formed. A mixture of steam and nitrogen resulted in 2 to 3 percent coke as compared to 10 percent when nitrogen, carbon dioxide, and carbon monoxide was passed. When hydrogen was used as a carrier gas about 7 percent of the oil was converted to coke (Figure 3). Substantial decrease in the amount of coke formed when steam is added suggests that steam reacts with coke to give gaseous products, according to the coke steam ($C + H_2O \rightarrow CO + H_2$) and the water gas shift ($CO + H_2 \rightarrow CO_2 + H_2$) reaction. Indeed, the gas analysis shows increased CO_2 and H_2 concentrations thereby substantiating the occurrence of above-mentioned reactions.

Figure 3 shows that the total hydrocarbon gas evolved was 13 percent when no carrier gas was used. About 10 percent hydrocarbon gas evolved when a mixture of steam and nitrogen was used as compared to 6 percent with hydrogen, carbon dioxide and carbon monoxide as a carrier gas.

The use of steam resulted in lowest oil losses because steam reduces the boiling point of most of the compounds present in shale oil and thus the oil is not exposed to high temperatures. Gas analysis for successive distillation (without carrier gas) is presented in Table 2. The ethylene/ethane ratio is plotted as a function of the number of distillation in Figure 4. It decreases from 0.25 to 0.15 and remains practically unchanged beyond this point.

VAPOR PHASE OIL DEGRADATION

Vapor phase thermal degradation of shale oil was studied as a function of two variables, namely, temperature and residence time. A 3^2 factorial design of experiments was used to investigate the main effects and interactions of these two parameters with oil yield as the response. Effect of steam on oil degradation formed another important part of this investigation.

The dependence of oil degradation on temperature and residence time is presented in Figure 5, from which it can be seen that the oil loss increases from 18 percent at 425°C to about 55 to 60 percent at 625°C (residence time ~8 to 9 sec.). It should be noticed here that the oil loss curve at 625°C reaches a maximum level at about 6 sec (residence time), beyond which the rate slows down considerably. Thus, at higher temperatures, increase in residence time beyond 6 sec does not seem to have an appreciable effect. At relatively lower temperatures (below 500°C), about 20 to 25 percent oil loss is observed, which indicates that even at these temperatures, a significant amount of oil undergoes degradation.

The conditions under which the cracking was carried out represent those existing inside the large blocks in an in-situ retort. The present results demonstrate that the oil generated in the interior of these large blocks will suffer extensive degradation (~50 percent) as it migrates to the hot block surface.

The influence of the two factors, residence time (x_1) and temperature (x_2) was determined using a 3^2 factorial design of experiments. The three levels of each factor will be designated by -1, 0, and 1, while the units of the design will be denoted by

$$x_1 = \frac{\text{time} - 5}{3} \quad \text{and} \quad x_2 = \frac{\text{temp} - 525}{100}$$

The oil losses (y) were measured at temperatures of 425, 525 and 625°C, and residence times of 2, 5 and 8 sec. It was assumed that a second-degree equation of the type

$$y = a_0 + a_1x_1 + a_2x_2 + a_{11}x_1^2 + a_{22}x_2^2 + a_{12}x_1x_2 \quad (1)$$

would correlate the oil loss (y) to the temperature and time adequately. The coefficients, evaluated by the method outlined by Davies, were substituted in Equation (1) to give the following equation

$$y = 21.70 + 9.60x_1 + 18.0x_2 - 3.4x_1^2 + 8.26x_2^2 + 2.82x_1x_2 \quad (2)$$

Fig. 6 shows a good agreement between the experimental data and the results calculated from Equation (2) with coefficient of correlation close to 0.99. Thus, one can use Equation (2) to predict the percent oil degradation at 425 to 625°C and 2 to 10 sec residence time.

The data presented in Figure 5 are used to obtain the rate equation for total oil degradation. Kinetics of the oil degradation or cracking can be correlated by a first order rate expression:

$$- \ln (1 - x) = kt, \quad (3)$$

where x is the fraction of oil lost, t is the residence time (sec), and k is the first order rate constant (sec^{-1}). Table 3 compares the k values computed from Equation (3) with those reported by Burnham and Taylor¹⁰ and reveals very clearly the two regions of interest; the low temperature region, 400 to 500°C, and the high temperature region above 500°C. The k value obtained at 475°C in the present study is 2 to 2.5 times higher than the value reported by them at 506°C, which suggests that the oil yields show strong sensitivity to degradation even at lower temperatures. At higher temperatures, the present results are in fairly good agreement with their data.¹⁰

Activation energy of 17.3 kcal/mole was obtained from the Arrhenius plot. The activation of 37.1 kcal/mole reported by Burnham and Taylor¹⁰ for thermal cracking of shale oil over burnt shale at 500°C is much higher than that found in the present study. The low activation energy observed in this investigation suggests certain catalytic or auto-catalytic effects exhibited by certain compounds (mineral matter) present in shale or those evolved during the cracking reaction (for example, H_2S).

Figure 7 gives the production of methane as a function of time and temperature. Increase in temperature from 425 to 625°C increases the weight percent of methane by a factor of 6. This data was used to obtain the specific rate constants and activation energy for methane production. In this case also a low value of activation energy (13 kcal/mole) was obtained which supports our supposition that certain autocatalytic effects are taking part in shale oil cracking.

The effect of steam was investigated at various temperatures and residence time. It was not surprising to note that the addition of steam decreased the coke build-up in the reactor. However, it did not seem to have any beneficial effect in reducing the overall oil loss. Hydrocarbon gas/coke, ethylene/ethane and naphthalene/($\text{C}_{11} + \text{C}_{12}$) hydrocarbons ratios were monitored during the course of cracking reaction. The increase in these ratios clearly shows that the cracking reaction dominates at high temperatures and that the chemical reactions taking place in vapor phase degradation are different from those in liquid phase degradation.

The ratio of hydrocarbon gases to coke formed during the reaction is plotted as a function of temperature in Figure 8 at two residence times (3 and 8 sec). Both the curves exhibit maximum at 525°C beyond which a plateau is observed. Increase in this ratio with temperature suggests that the cracking is more prevalent than coking at higher temperatures.

The ethylene/ethane ratio is plotted as a function of temperature (residence time ~5 sec) and oil loss in Fig. 9. It increases with increase in temperature and oil loss. An interesting phenomenon is that at low temperatures (below 500°C) the ethylene/ethane ratio decreases slightly with an increase in residence time (at a fixed temperature) while at higher temperatures the ratio remains practically constant (independent of the residence time).

It is worth mentioning here that the ethylene/ethane ratio is also a function of whether the oil degradation has taken place in vapor phase or liquid phase. The ratio increases if the oil is subjected to vapor phase degradation, while it decreases when the oil suffers degradation in liquid phase. These results also suggest the mechanism operative in vapor phase is different from that in liquid phase.

The naphthalene/(C₁₁ + C₁₂) hydrocarbon ratio was monitored during the shale oil cracking. The following expression was developed to correlate the overall oil loss with this ratio:

$$\% \text{ oil loss} = -0.0185 + 0.129 R + 1.134 R^2,$$

where R is naphthalene/(C₁₁ + C₁₂) hydrocarbons ratio and (C₁₁ + C₁₂) is the sum of undecane, 1-undecene, dodecane and 1-dodecene.

Figure 10 gives the chromatograms of two shale oil samples, one of which was subjected to successive distillation while the other one underwent vapor phase thermal degradation at 625°C. A distinctive feature that needs further consideration is the alkene/alkane ratio. The chromatograms exhibit the characteristic homologous hydrocarbon series ranging from C₁₀ through C₂₀ with the first peak of each doublet corresponding to the 1-alkene. The sample treated in liquid phase seems to be richer in alkane than in alkene (the ratio alkene/alkane < 1) while that treated at 625°C in vapor phase has an alkene/alkane ratio for (C₁₁, C₁₂, ...) greater than unity. These results agree fairly well with the findings of Burnham, et al.^{8,9} Campbell, et al.^{2,3,4} and Uden, et al.

CONCLUSIONS

The present results lead us to the following conclusions:

1. The experimental design described in this paper permits a separate study of the principal mechanisms of shale oil degradation under steady state conditions equivalent to retorting conditions.
2. Low-temperature, long-term soaking below 300°C showed only minor oil losses while successive distillation and condensation under autogenous conditions showed considerable oil losses (~35 percent). During vapor phase thermal cracking about 55 percent oil loss occurs over 5 to 6 sec (residence time) at 625°C.
3. The steam suppressed coke formation and oil degradation during successive distillations (liquid phase) but it did not seem to reduce the overall oil loss during vapor phase thermal cracking.
4. The injection of carrier gas during distillation helped in reducing total oil loss.
5. The ethylene/ethane and alkene/alkane ratios decreased when oil suffered degradation in liquid phase (coking) while all the ratios used as indices of oil degradation increased with increase in oil loss due to cracking (vapor phase).
6. Minimizing the gas phase residence time in large retorts should improve oil yields.

REFERENCES

1. Jacobson, I. A., Decora, A. W. and Cook, G. L., Science and Technology of Oil Shale, Yen, T. F. (Ed.), Ann Arbor Science Publishers, Ann Arbor, Michigan (1976), p. 103.
2. Campbell, J. H., Koskinas, G. H., Stout, N. D. and Coburn, T. T., In Situ (1978), 2, 1.
3. Coburn, T. T., Bozak, R. E., Clarkson, J. E. and Campbell, J. H., Anal. Chem. (1978), 50 (7), 958.
4. Evans, R. A. and Campbell, J. H., In Situ (1979), 3, 33.
5. Raley, J. H. and Braun, R. L., Lawrence Livermore National Laboratories, Livermore, UCRL-78098 (1976).
6. Raley, J. H., Proceedings of 12th Oil Shale Symp., Gary, J. H. (Ed.), Colorado School of Mines Press, Golden, Colorado, August (1979), p. 342.
7. Raley, J. H., Fuel (1980), 59, 419.
8. Robillard, M. V., Siggia, S. and Uden, P. C., Anal. Chem. (1979), 51 (3), 435.
9. Crowley, R. J., Siggia, S. and Uden, P. C., Anal. Chem. (1980), 52 (8), 1224.
10. Burnham, A. K. and Taylor, J. R., Lawrence Livermore National Laboratories, Livermore, UC10-18284 (1979).
11. Stout, N. D., Koskinas, G. H., Raley, J. H., Santor, S. D., Opila, R. J. and Rothman, A. J., Lawrence Livermore National Laboratories, Livermore, UCRL-77831 (1976).
12. Stout, N. D., Koskinas, G. H. and Santor, S. D., Lawrence Livermore National Laboratories, Livermore UCRL-52158 (1976).
13. Wilkins, E. S., Nuttall, H. E., and Thakur, D. S., Proc. 2nd World Congr. Chem. Eng., Montreal, Canada (1981), p. 463.
14. Nelson, W. L., "Petroleum Refinery Engineering," 4th Edition, McGraw-Hill Kogakusha Ltd., Tokyo (1958), p. 651.
15. Burnham, A. K. and Clarkson, J. E., Proc. 13th Oil Shale Symp., Gary, J. H. (Ed.), Colorado School of Mines Press, Golden, Colorado (1980), p. 269.
16. Burnham, A. K., Lawrence Livermore National Laboratories, Livermore, UCRL-84913, November (1976).

Table 1

Low Temperature Soaking Results Under Refluxing Conditions

| Temperature (°C) | Coke (%Wt) | Liquid Condensate (%Wt) | Gases (%Wt) | Liquid in Still (%Wt) |
|---------------------|---------------|----------------------------|----------------|--------------------------|
| 150 | nil | -- | -- | 99.0 |
| 200 | nil | 1.0 | 0.1 | 98.5 |
| 250 | nil | 1.5 | 0.4 | 98.0 |
| 300 | nil | 17.0 | 0.5 | 81.0 |
| 350 | nil | 30.0 | 1.0 | 68.1 |
| 400 | nil | 47.1 | 3.0 | 47.6 |

Table 2

Analysis of Gases
(temperature of reaction = 400°C)

Gas Composition (%Wt)

| | I* | II** |
|-----------------------|------|------|
| Hydrogen | <1 | <1 |
| Methane | 44.3 | 41.4 |
| Ethylene | 2.2 | 2.8 |
| Ethane | 11.1 | 17.7 |
| Propylene | 3.2 | 3.7 |
| Propane | 15.0 | 18.3 |
| Butenes and Butanes | 16.9 | 15.5 |
| Pentenes and Pentanes | 6.1 | 5.1 |
| CO + CO ₂ | <1 | <1 |

*I - Low temperature coking.

**II - Successive distillation and condensation.

Table 3

Specific Reaction Rate Constants at Various Temperatures

| Temperature °C | Present Work sec ⁻¹ | Literature Values ¹⁰ sec ⁻¹ |
|-------------------|-----------------------------------|--|
| 475 | 0.026 | -- |
| 506 | -- | 0.01 |
| 525 | 0.046 | -- |
| 558 | -- | 0.04 |
| 575 | 0.086 | -- |
| 585 | -- | 0.10 |
| 610 | -- | -0.15 |
| 625 | 0.178 | -- |

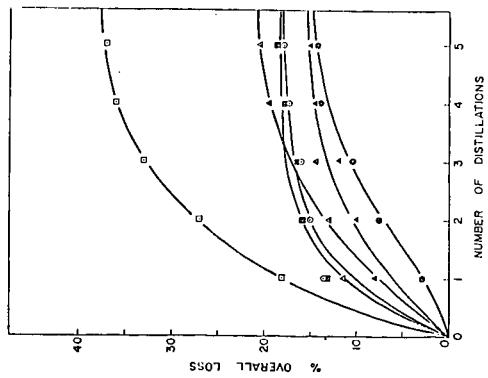


Figure 1. Percent total overall loss versus number of distillations. (□) no gas addition; (Δ) adding hydrogen; (○) adding carbon monoxide; (▲) adding hydrogen and nitrogen; (◻) adding carbon dioxide.

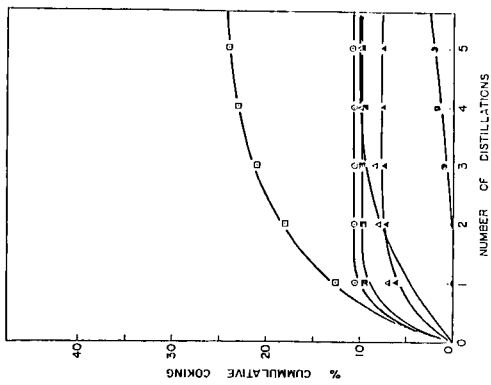


Figure 2. Percent cumulative oil loss versus number of distillations. (Same symbols as in Figure 1 are used.)

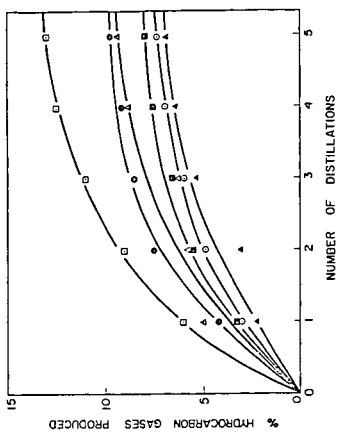


Figure 3. Percent hydrocarbon gases produced versus number of distillations. (Same symbols as in Figure 1 are used.)

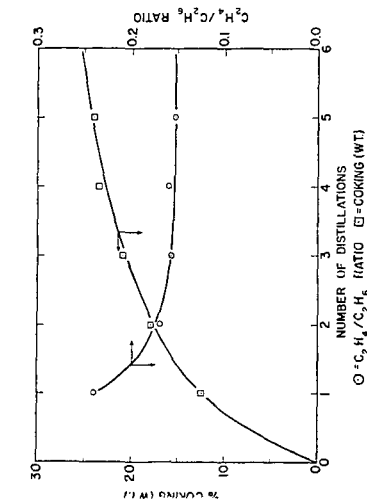


Figure 4. Ethylene/ethane ratio and percent coke as a function of number of distillations when no carrier gas was passed.

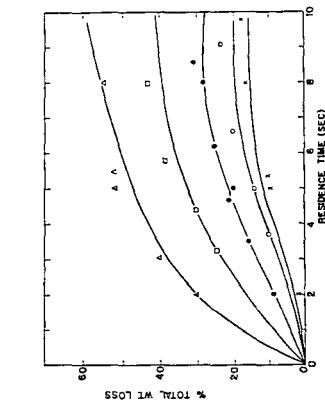


Figure 5. Dependence of shale oil degradation (wt) on residence time at various temperatures. (Δ) 475°C, (\circ) 475°C, (\square) 525°C, (\diamond) 575°C, (Δ) 625°C.

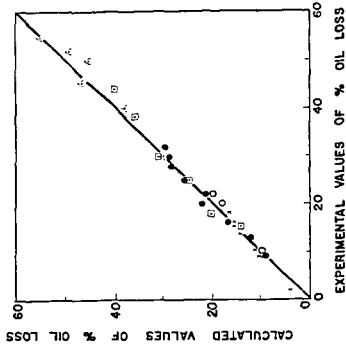


Figure 6. Experimental and predicted values (Eqn. 2) of % oil loss, at various temperatures. Solid lines represent predicted values. Symbols used in Figure 5.

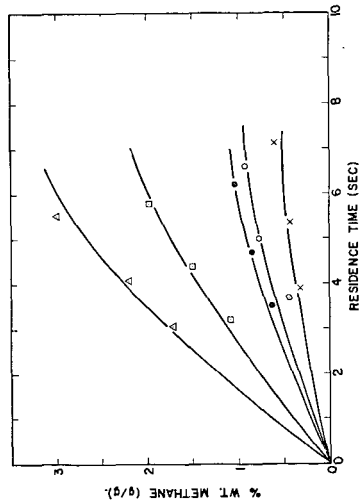


Figure 7. Percent methane (g/g oil) produced as a function of residence time and temperature. (Same symbols as in Figure 5).

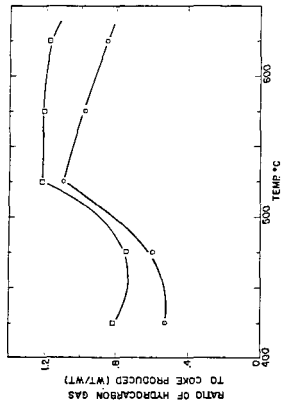


Figure 8. Hydrocarbon gas/coke ratio versus temperature at residence times, 3 sec (○) and 6 sec (□).

FLUIDIZED-BED PYROLYSIS OF OIL SHALE

J. H. Richardson and E. B. Huss
Chemistry and Materials Science Department
Lawrence Livermore National Laboratory
Livermore, CA 94550

Abstract

Several quartz isothermal fluidized-bed reactors have been constructed in order to measure kinetics and oil properties relevant to surface retorting by fluidized-bed processes. The rate of volatile total hydrocarbon evolution is measured with a flame ionization detector, although various techniques are currently being evaluated for doing species-selective (as opposed to total hydrocarbon) kinetics. Oil yield experiments are performed separately from the kinetic experiments due to the experimental conditions necessary to minimize mist formation and maximize oil collection. Oil composition is determined via subsequent analysis (gas chromatography). Gas evolution kinetics, oil yield and oil composition are determined both as a function of oil shale parameters (e.g., particle size, grade, Eastern vs. Western deposits) and fluidized-bed parameters (temperature, sweep gas composition, gas velocity, bed particle size, and bed geometry). An ultimate goal is the development of diagnostic methods relating oil composition to processing parameters.

*Work performed under the auspices of the U. S. Department of Energy by the Lawrence Livermore National Laboratory under contract number W-7405-ENG-48.

7912o/10/81

INTRODUCTION

There is considerable commercial interest in aboveground oil shale retorting using fluidized-bed processing techniques.¹ Such techniques are characterized by rapid heating of the oil shale followed by essentially isothermal retorting with the subsequent rapid removal of the pyrolysis products. Recently a kinetic study by Wallman, et al. using one type of oil shale has been reported which is applicable to these processing techniques.² Their study indicated a particle size dependence for both the oil yield and the pyrolysis kinetics, where the particle size was varied between 0.4 and 3 mm. These results were interpreted with the aid of a two-step model for kerogen decomposition with each step following first-order kinetics. The initial kerogen decomposition rate constant varied from 1 to 10 min⁻¹ over a temperature range of 480-540°C; the rate constant for the second step varied from 0.1 to 1 min⁻¹ over the same temperature range. This second rate constant was associated with the decomposition of a heavy oil intermediate, which, along with a predominantly lighter hydrocarbon fraction, was the result of the initial kerogen decomposition step.

The purpose of our work is twofold: 1) to extend the kinetic studies of Wallman, et al.² to a variety of oil shales, thereby testing their general applicability; 2) to characterize the oil produced in a fluidized-bed reactor with the goal of developing diagnostic techniques similar to those previously determined for MIS retorting.^{3,4} In this paper we present both our preliminary kinetic results and our preliminary oil characterization results. Generally there is good agreement between our results and those of Wallman, et al.² for the initial kerogen decomposition step; however, we have not determined such a definite particle size dependence for the second decomposition step. Although preliminary, initial gas chromatograms of collected oil show a relatively high amount of isoprenoid compounds; observed 1-alkene/n-alkane ratios are consistent with those expected from extrapolated trends of data obtained at lower heating rates.

EXPERIMENTAL

Figure 1 is a schematic of the experimental apparatus. The fluid bed and condenser are quartz, connected with stainless steel unions and graphite

ferrules. The distributor is a multiorifice plate (seven hole grid design).

The bed itself consists of 100-150 g of sand (Baker), ground, sieved, and washed (-0.250 + 0.125 mm). To date only helium has been used as a fluidizing medium. Typical flow rates are 60-80 cc/s (NTP), corresponding to a superficial velocity in the fluid bed of about 13 cm/s at 500°C. This is approximately a factor of ten above the calculated minimum fluidization velocity,^{6,7} and the bed appears nicely fluidized (smooth fluidization⁷).

The heat source is a Lindberg three zone furnace. Typically the temperature in the sand is isothermal to $\pm 1^\circ\text{C}$. For the oil collection experiments, the temperature profile inside the quartz reactor is isothermal to $\pm 2^\circ\text{C}$ throughout the region heated by the furnace; outside the furnace, the temperature is maintained between 300-350°C with heating tape. Consequently, from the standpoint of gas-phase oil cracking losses, the mean residence time in the hotter fluid bed is approximately two seconds. For the kinetic experiments, the temperature refers only to that of the sand; the rest of the quartz fluid bed is cooler (e.g., when the sand was 560°C the temperature profile inside monotonically decreased to 450°C at the furnace exit).

A quartz capillary samples the pyrolysis products at a distance approximately 8 inches above the sand bed and nearly on the vertical axis through the fluid bed. A Varian flame ionization detector with Wilkens gas chromatograph electrometer is used to monitor the rate of hydrocarbon generation. Preliminary experiments demonstrated the need for a back pressure regulator at the system exit to ensure that the detector response was attributable solely to changes in hydrocarbon concentration and not pressure fluctuations. The FID response is calibrated with primary standards of methane in helium. The maximum detector response at 560°C to a typical 50 mg oil shale sample is comparable to that obtained with a 1% methane/helium mixture. The temporal response of the detection system was less than three seconds (10%-90%). Larger samples are used for the oil collection experiments (up to 5 g); although the larger sample does result in an initial temperature drop, the sand temperature is still constant to $\pm 2^\circ\text{C}$ during the course of the oil generation.

The FID results are digitized and manipulated using an HP1000 computer system. Currently most of the kinetic data is treated with a five-point smoothing routine and then by linear regression analysis, although programs for further smoothing the raw data and expressing the data in integral form are being developed.

The oil is collected in a condenser similar in design to that used by Wallman, et al.² Fines are excluded from the condenser by quartz wool and a quartz frit. The ice bath is maintained at 0°C ($\pm 2^\circ\text{C}$); currently no effort has been made to collect the non-condensables. All chromatography of the oil was done with a HP5880 gas chromatograph with data acquisition and subsequent data reduction using an HP1000 computer system; the procedures have been previously described.⁵

Table I summarizes the assays of the five oil shales used in this study; three of the samples are Western shales from the Piceance Basin (RB 432, RB 560, and Anvil Points) and two samples are Eastern shales from Lewis County, Kentucky (Sunbury shales CLE-002 and SUN-002). The oil yields for the Western shales are estimated from previously published correlations with percent organic carbon;⁸⁻¹⁰ the average of the three correlations is listed.

RESULTS AND DISCUSSION

Kinetics

In general the FID kinetic data is currently analyzed by first taking the ln of the normalized response and then fitting by linear regression analysis to the form,

$$\ln(\text{rate}) = -k_1 t + A_1 \quad (1)$$

for short times ($0 \leq t \leq \tau$) and to the form

$$\ln(\text{rate}) = -k_2 t + A_2 \quad (2)$$

for long times ($t > \tau$), where τ is empirically determined by inspection. The directly determined value for k_1 is reported without correction for k_2 .

Figure 2 illustrated a typical kinetic result, plotting the \ln of the normalized FID response versus time for RB 432 and two different particle sizes. Figure 3 illustrates similar data for a leaner shale, RB 560. In the latter case there is little motivation to empirically fit more than one line to the data. However, with both RB 432 and Anvil Points shale two line segments were used to fit the data over an experimental time interval corresponding to a relative reduction in the rate of hydrocarbon generation by nearly two orders of magnitude. In all cases, the square of the correlation coefficient for the first line segment was greater than 0.93 and usually it was greater than 0.97; the second line segment had a somewhat lower correlation coefficient (r^2 ranging from .90 to .98) corresponding to more noise at the lower signal level. Further digital smoothing of the data and/or larger sample sizes may improve the linear correlation at low rates.

Figure 4 illustrates typical data used for an Arrhenius plot. In all cases, irrespective of particle size, the Western shales exhibited a similar dependence of k_1 on temperature; a similar dependence of k_2 on temperature was observed with RB 432 and Anvil Points. The Eastern shales had a significantly different rate of kerogen decomposition (Figure 5).

Figures 6-9 are Arrhenius plots comparing our results with those of Wallman, et al.² Figure 6 compares the value of k_1 determined for similarly sized particles from four different oil shales; Figure 7 does the same thing for the value of k_2 . Two conclusions are apparent: 1) the difference in retorting rate between Western and Eastern Oil shale is attributable to differences in k_1 ; 2) there is approximately a factor of five difference in the rate between Chevron's k_2 and ours (irrespective of oil shale source). Figures 8 and 9 compare the effect of particle size on k_1 and k_2 , respectively, for both Western and Eastern oil shale. There is none.

Table II summarizes the kinetic parameters determined in this work and compares them to the values previously reported. The calculated value of k_1 for Western shale at 500°C using our values is very similar to that calculated using the results of Wallman, et al.² (2.81 min^{-1} vs. 2.72 min^{-1} , respectively). It is seen that the preexponential A factor is the major difference between the two expressions for k_2 ; the activation energies are

reasonably similar. In the case of the Eastern shale, the lower preexponential A factor is consistent with the general description of Eastern shale being more "coal-like" than Western shale (i.e., a lower H/C ratio), although several other factors are also likely to influence the A factor.

Agreement between our values for k_1 with Western shales and those of Wallman, et al.² is encouraging; conversely, the disagreement between the values for k_2 suggests further experiments are necessary. In general, our rate data exhibits considerable fluctuations from sample to sample at relatively low rates (less than 5% of the maximum); probably we would have better data (and better linear correlations) with larger and therefore more homogeneous samples (with further digital smoothing and/or integration). At this stage, we do not feel that a two-step sequential mechanism is unequivocally indicated for all oil shales by the phenomenological fitting of most of our data with two rate constants. Furthermore, we would be reluctant at this point to interpret the variation in E and A for the various rate constants in terms of a mechanistic model. More detailed kinetic studies, including species selective monitoring by either mass spectroscopy or Raman techniques, is currently being evaluated.

Oil Characterization

Oil collection currently has not been optimized. We are now consistently collecting only $95 \pm 5\%$ of the expected Fischer assay yield (of oil and water). A higher rod temperature (350°C instead of 150°C) leading to a larger thermophoretic effect aids in oil collection as does increasing the surface area (glass wool instead of glass beads). Larger sample aliquots for a given mass, as opposed to more but smaller aliquots totaling the same mass, also leads to larger collection efficiencies. All three of these observations are consistent with maximizing mist collection and minimizing mist formation.¹¹ Gas chromatographic analysis suggests that the lighter ends are still not being collected efficiently. Current problems with the precision and reproducibility of oil collection preclude making any inferences as to the effect of particle size on oil yield from various shales. Previously published results did demonstrate oil yields from smaller particles which slightly exceeded Fischer assay results (e.g., up to 109% Fischer assay at 427°C for 0.4 mm particles).²

Two representative gas chromatograms of oil retorted in the fluidized-bed apparatus are shown in Figure 10. The identification of isoprenoid compounds, indicated by I₁ and listed in Table III, is taken from reference 5.

Three observations can be readily made from Figure 10. First, the relatively high 1-alkene/n-alkane ratio is qualitatively consistent with a high heating rate, and the higher pyrolysis temperature consistently gives a higher ratio (Figure 11). Extrapolation of 1-alkene/n-alkane ratio data obtained⁵ at much lower heating rates (10^{-2} to 10^1 °C/min) to the present ratio indicates a heating rate (10^3 to 10^4 °C/min) consistent with the present experiment. Experimentally, we observe an FID response approximately seven seconds after the shale is dropped into the fluid bed; this implies a heating period of approximately 4 to 5 sec, or 10^3 to 10^4 °C/min.

For comparison, Figure 11 also shows the 1-alkene/n-alkane ratio for two other oils generated from different oil shales, TOSS #3-3 and LETC R-14. TOSS #3-3 was generated from a leaner sample of RB 432 under pseudo-Fischer assay conditions with an external sweep gas, and LETC R-14 was a simulated MIS retort with an even lower heating rate.

In addition to the higher alkene/alkane ratios for oil retorted in the fluidized-bed, Figure 11 also illustrates the pronounced even-odd trend in the ratios. This trend has been previously observed.^{5,12,13} The explanation is not well understood but probably relates to both the structure of kerogen and undoubtedly to the pyrolysis conditions; consequently, such a pronounced even-odd trend may have potential as a process diagnostic.

Secondly, the ratio of the sum of certain isoprenoid alkenes plus alkanes to the sum of normal alkenes plus alkanes has been shown to be largely independent of heating rate for modest heating rates.⁵ That trend appears to hold for the higher heating rates present in the fluidized-bed. Obviously, ratios which are a function of heating rate are more useful as potential diagnostics of oil processing conditions.

Thirdly, the predominance of prist-1-ene in the gas chromatograms is particularly striking. For example, the ratio of prist-1-ene to the sum of the C₁₇ and C₁₈ normal alkanes plus alkenes is 0.45, 0.66, 0.16, and

0.09 for fluidized-bed 462°C, fluidized bed 524°C, TOSS #3-3 and LETC R-14, respectively. These results indicate the potential application of a ratio based on prist-1-ene as a diagnostic to oil processing conditions. Furthermore, several major species, currently unidentified, are present in the gas chromatogram of oil generated in the fluidized-bed which are not present to a significant extent in oils generated under different retorting conditions. Further work is needed to characterize these compounds.

ACKNOWLEDGEMENTS

We would like to thank M. O. Bishop and J. R. Taylor for the construction of the apparatus, J. E. Clarkson and V. L. Duval for the gas chromatographic analysis, and L. L. Ott for assistance with the kinetic data reduction.

DISCLAIMER

This document was prepared as an account of work sponsored by an agency of the United States Government. Neither the United States Government nor the University of California nor any of their employees, makes any warranty, express or implied, or assumes any legal liability or responsibility for the accuracy, completeness, or usefulness of any information, apparatus, product, or process disclosed, or represents that its use would not infringe privately owned rights. Reference herein to any specific commercial products, process, or service by trade name, trademark, manufacturer, or otherwise, does not necessarily constitute or imply its endorsement, recommendation, or favoring by the United States Government or the University of California. The views and opinions of authors expressed herein do not necessarily state or reflect those of the United States Government thereof, and shall not be used for advertising or product endorsement purposes.

REFERENCES

1. P. W. Tamm, C. A. Bertelsen, G. M. Handel, B. G. Spars, and P. H. Wallman, American Petroleum Institute 46th Midyear Refining Meeting, Chicago, IL (May, 1981).
2. P. H. Wallman, P. W. Tamm, and B. G. Spars, "Oil Shale, Tar Sands, and Related Materials," ACS Symposium Series 163, 93 (1981).
3. A. K. Burnham and J. E. Clarkson, 13th Oil Shale Symposium, Golden, CO (April, 1980), pp 269-278.
4. J. H. Raley, Fuel 59, 419 (1980).
5. A. K. Burnham, J. E. Clarkson, M. F. Singleton, C. M. Wong, and R. W. Crawford, Geochim. Cosmochim. Acta, submitted for publication (1981).
6. F. A. Zenz and D. F. Othmer, FLUIDIZATION AND FLUID-PARTICLE SYSTEMS, (Reinhold Publishing Corp., New York, NY, 1960) Chapter 7.
7. D. Kunii and O. Levenspiel, FLUIDIZATION ENGINEERING, (R. E. Krieger Publishing Co., Huntington, NY, 1977), Chapter 3.
8. E. W. Cook, Fuel 53, 16 (1974).
9. R. N. Heistand and H. B. Humphries, Anal. Chem. 48, 1192 (1976).
10. M. F. Singleton, G. J. Koskinas, A. K. Burnham, and J. H. Raley, manuscript in preparation (1981).
11. S. Goren, University of California (Berkeley), private communication.
12. A. K. Burnham and R. L. Ward, "Oil Shale, Tar Sands, and Related Materials," ACS Symposium Series 163, 79 (1981).
13. I. Klesment, J. Anal. Appl. Pyrol. 2, 63 (1980).

Table I. Assay parameters of oil shale used in this work.

| Oil Shale | % Total C | % Org. C | % H | Gal/Ton |
|--------------|-----------|----------|------|-------------------|
| RB 432 | 22.7 | 18.4 | 1.33 | 41.3 ^a |
| RB 560 | 14.1 | 8.8 | 1.45 | 19.4 ^a |
| Anvil Points | 15.2 | 10.4 | 2.49 | 23.0 ^a |
| CLE-002 | 14.1 | 14.1 | 1.69 | 14.0 |
| SUN-002 | 13.9 | 13.9 | 1.65 | 14.2 |

^aCalculated from correlations in refs. 8-10.

Table II. Comparison of kinetic parameters.

| | k_1 | | k_2 | |
|------------------------|--------------|-----------------------|-------------------|----------------------|
| | E, kcal/mole | A, s ⁻¹ | E, kcal/mole | A, s ⁻¹ |
| Western shale | | | | |
| This work ^a | 41.1 | 1.95×10^{10} | 26.5 ^c | 5.7×10^{5c} |
| Ref. 2 | 43.6 | 9.63×10^{10} | 22.6 | 3.0×10^3 |
| Eastern shale | | | | |
| This work ^b | 32.0 | 8.4×10^7 | 26.5 ^c | 5.7×10^{5c} |

^aIncludes data from RB 432 and Anvil Points.

^bData from CLE-002.

^cIncludes data from RB 432, Anvil Points, and CLE-002.

Table III. Identification of isoprenoid compounds labeled in Figure 10 (*tentative).

| | |
|-----|--|
| I2 | 2,6-dimethylundecane (C ₁₃) |
| I2' | 2,6-dimethylundecene |
| I3 | 2,6,10-trimethylundecane (C ₁₄) |
| I3" | 2,6,10-trimethylundec-2-ene* |
| I4 | farnesane (C ₁₅) |
| I4' | farnesene |
| I5 | 2,6,10-trimethyltridecane (C ₁₆) |
| I5' | 2,6,10-trimethyltridecene |
| I6 | norpristane (C ₁₈) |
| I6' | norpristenes* |
| I7 | pristane (C ₁₉) |
| I7' | prist-1-ene |
| I8 | phytane (C ₂₀) |

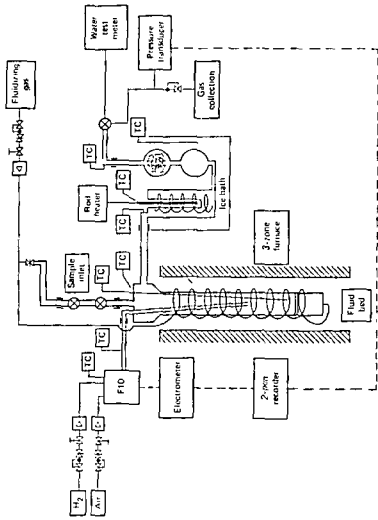


Figure 1. Schematic of the experimental apparatus for fluidized bed pyrolysis of oil shale.

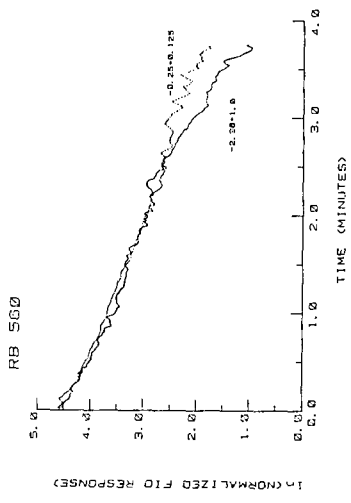


Figure 3. Typical kinetic results for RB 560 at 480°C. The ln of the normalized FID response is plotted vs. time for two particle sizes, -2.36 ± 1.0 mm and -0.25 ± 0.125 mm.

ANVIL POINTS -1.0+0.5

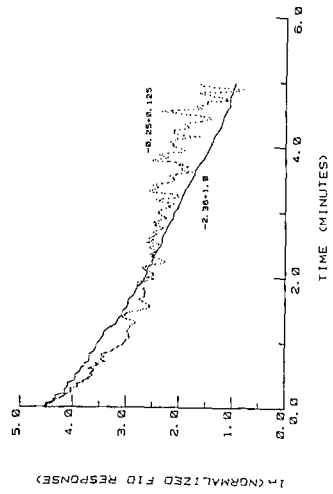


Figure 2. Typical kinetic results for RB 432 at 458°C. The ln of the normalized FID response is plotted vs. time for two particle sizes, -2.36 ± 1.0 mm and -0.25 ± 0.125 mm.

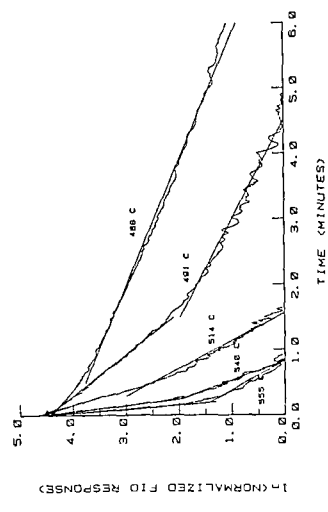


Figure 4. Typical kinetic results used to generate Arrhenius plot.

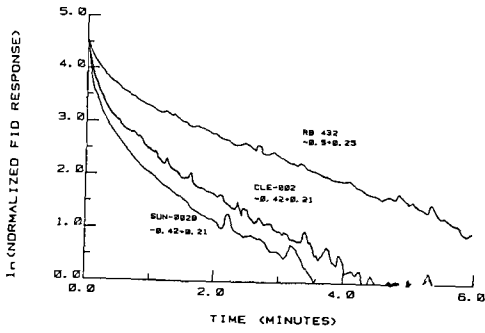


Figure 5. Comparison of kinetic results for Western vs. Eastern shales (466°C).

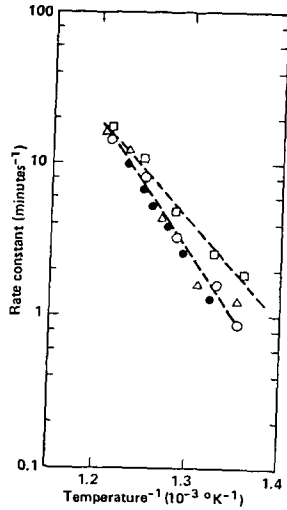


Figure 6. Arrhenius plot of k_1 , one particle size: (●) Chevron's results; (△) Anvil Points, -1.0 ± 0.5 mm; (○) RB 432, -1.0 ± 0.5 mm; (□) CLE-002, 1.0 ± 0.1 mm.

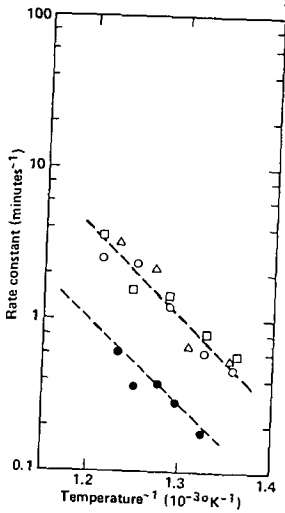


Figure 7. Arrhenius plot of k_2 , one particle size: (●) Chevron's results; (△) Anvil Points, -1.0 ± 0.5 mm; (○) RB 432, -1.0 ± 0.5 mm; (□) CLE-002, 1.0 ± 0.1 mm.

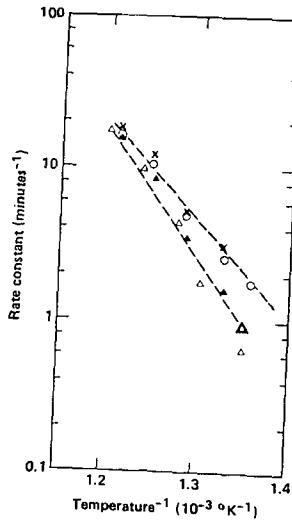


Figure 8. Arrhenius plot of k_3 , different particle sizes: (△) RB 432, -2.36 ± 1.0 mm; (○) RB 432, -1.0 ± 0.5 mm; (□) CLE-002, -1.0 ± 0.1 mm; (X) CLE-002, -0.42 ± 0.21 mm.

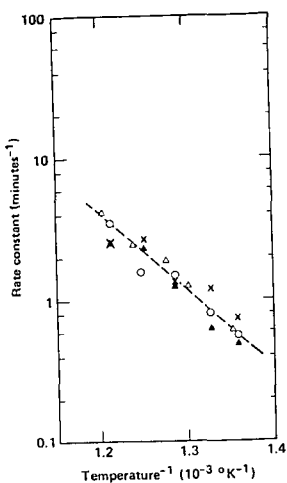


Figure 9. Arrhenius plot of k_p , different particle sizes: (Δ) RB 432, -2.36 ± 1.0 mm; (\bullet) RB 432, -1.0 ± 0.5 mm; (\circ) CLE-002, -1.0 ± 0.1 mm; (\times) CLE-002, -0.42 ± 0.21 mm.

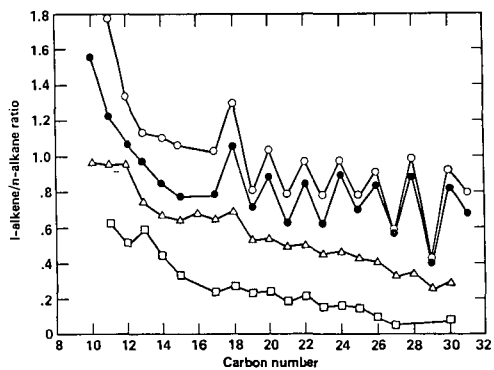


Figure 11. 1-alkene/n-alkane ratios for oils generated under different conditions: (\circ) RB 432 reformed in the fluidized bed, at 52°C; (\square) RB 432 reformed in the fluidized bed, at 462°C; (Δ) TOSS 13-3, modest heating rate ($\sim 10^\circ\text{C}/\text{min}$), inert sweep gas; (\diamond) LFTC R-14, simulated MFS.

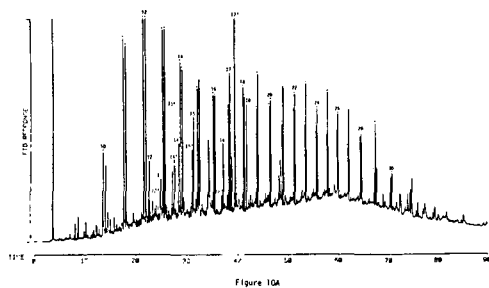


Figure 10A

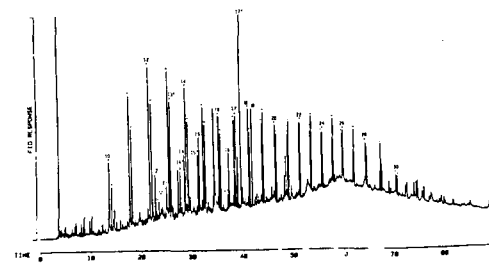


Figure 10. Gas chromatograms of oil reformed in the fluidized bed reactor. 1-alkanes and 1-alkenes are indicated by a dot, with the 1-alkene having the shorter retention time and even carbon numbers as indicated. Identified isoprenoid compounds are listed in Table II. A) 462°C; B) 52°C. Both oil shale samples were RB 432.

JET FUELS FROM SHALE OIL BY SINGLE-STAGE HYDROCRACKING

A. M. Tait and A. L. Hensley
Amoco Oil Company

ABSTRACT

Extensive screening of novel catalysts has led to the development of a single catalyst capable of the direct upgrading of a whole shale oil into high yields of jet fuels on a once-through basis. To maximize jet fuels a catalyst must have the ability to sequentially saturate, denitrogenate, and hydrocrack the feedstock in the presence of high levels of contaminants such as organic nitrogen compounds and ammonia while maintaining high selectivity toward jet fuel boiling-range material. Catalysts incorporating these functions, along with high temperature stability, were developed by optimization of both chemical and physical properties. The effectiveness of the final single catalyst for the direct upgrading of an Occidental shale oil has been demonstrated in a 100-day test. The feed, containing approximately 15 wt% JP-4 material and 13,000 ppm nitrogen, was upgraded to a water-white product containing approximately 75 wt% JP-4 material and 1 to 3 ppm nitrogen. The hydrogen consumption was 1800 to 1900 SCFB.

INTRODUCTION

Development of new processes and catalysts to enable U.S. refiners to produce conventional products from unconventional raw materials such as shale oil, tar sands, coal liquids, and heavy petroleum residues is especially important now because of national concerns for the price, quality, and stability of supply of petroleum products. Various sources have estimated that U.S. reserves of shale and tar sands oil are more than four times that of conventional oil and could provide a secure source of energy for about 100 years if economic means can be found to convert these reserves to usable products.

Given this impetus, the U.S. Air Force and Wright-Patterson Air Force Base entered into a 19-month contract with Amoco Oil late in 1979 to develop a catalyst for increased jet fuel production from shale oil. Although other companies have conducted more extensive process and design work, Amoco's investigation was limited to the development of improved catalysts. However, in order to test catalysts, a processing scheme was required, and we chose to develop a single catalyst capable of the direct conversion of the shale oil into jet fuel boiling-range material on a once-through basis.

The contract called for four major tasks:

- I. A process variable study on existing proprietary catalysts.
- II. A catalyst composition study, i.e., metals concentration and support.

III. A catalyst physical properties study.

IV. An activity maintenance test on the preferred catalyst.

Results have been presented previously for the first two tasks.

Table I shows analytical data for three shale oils. Although such oils are basically similar to petroleum crudes with respect to chemistry (i.e., the same types of compounds are present but in different relative amounts), they do exhibit some unique properties.

Shale oils typically have high pour points dictating on-site processing or the use of wax modifiers or heated transportation pipelines for off-site processing. The H/C atomic ratios are on the low end of the scale for petroleum crudes and hence upgrading will require additional hydrogen to produce equivalent product qualities. The high nitrogen content of up to two or more percent is an order of magnitude higher than for petroleum crudes and represents the major upgrading difficulty since organic nitrogen compounds act as severe poisons for downstream catalytic cracking and reforming processes and cause product instability.

Thus, to maximize jet fuels from shale oils, a catalyst must have the ability to sequentially saturate, denitrogenate, and hydrocrack the feedstock in the presence of high levels of contaminants such as organic nitrogen compounds and ammonia while maintaining high selectivity towards the jet fuel boiling-range material.

RESULTS AND DISCUSSION

The Occidental shale oil was used throughout the study. Although the oil contained 26 ppm arsenic and about 60 ppm iron plus nickel, it was not pretreated nor was a guard chamber used to remove these contaminants.

The initial process variable study on existing proprietary catalysts indicated that a catalyst containing cobalt, chromium, and molybdenum salts on an alumina support could effectively remove nitrogen and effect moderate conversion of the feed into JP-4 jet fuel boiling-range material. Initial product qualities at one set of processing conditions are shown in Table II. For this catalyst, nitrogen removal was found to be first order in nitrogen and hydrogen pressure.

The next study on catalyst composition included optimization of the metal oxide concentrations and the support composition. Catalysts were prepared with various combinations of metal oxides on alumina and screened at 780°F, 1800 psig and 0.5 LHSV. The optimized metal oxide loadings were determined to be 1.5% cobalt oxide, 10% chromium oxide and 15% molybdenum oxide. Although the presence of the chromium oxide actually lowered denitrogenation activity, the 10% level was required to impart high temperature stability to the catalyst.

For the support composition, catalysts with the optimized metal loadings were prepared on different supports. The most active catalysts were

prepared on supports of alumina, 20% silica on alumina, and 30% Ultrastable (US) sieve on alumina. Results are shown in Figure 1 in a plot of relative activity for denitrogenation versus days on oil. The activities given are based on first-order kinetics and are relative to the 1.5% CoO/10% Cr₂O₃/10% MoO₃ catalyst (Activity = 100) prepared on the same alumina as was used for the catalysts previously mentioned. These results indicate a 60% to 100% increase in nitrogen removal activity when acid functions are introduced into the support.

Table III shows how the increased activity affects product qualities for these three systems. Compared to the alumina system, the 20% silica/alumina and the 30% US sieve/alumina catalysts gave almost complete nitrogen removal. The presence of silica did not, however, affect other product qualities whereas incorporation of the US sieve resulted in a significant increase in cracking activity, resulting in a lower pour point and a high yield of JP-4 boiling-range material.

Based on these results, the US sieve-containing catalyst appeared promising for the direct hydrocracking of the shale oil. Consequently, additional catalysts with various US sieve contents and the optimized metal loadings were prepared and screened at 780°F, 1800 psig and 0.5 LHSV. Figures 2 and 3 summarize pertinent results.

The effect of increasing sieve content from 20 to 50 wt% was to almost double the JP-4 yields from approximately 40 to 77 wt% with a corresponding decrease in both the diesel and gas oil fractions. The C₁-C₄ gas make increased moderately from 3.7 to 5.6 wt%. It should be noted that the yield structures for the catalyst containing 20 wt% sieve were not much different from the pure alumina based catalyst. At the 50% sieve level, approximately 95% of the product boiled below 650°F. As expected, the increase in JP-4 yield was accompanied by a smooth increase in the hydrogen consumption from approximately 1400 SCFB to approximately 1900 SCFB, Figure 3.

For the three sieve catalysts, activity maintenance for jet fuel production is detailed in Figure 4. Both the 20% and 30% sieve-containing catalysts initially give high yields of JP-4 but rapidly lost activity to give lined out yields of approximately 50 and 35 wt% JP-4. For comparison, the nonsieve-containing catalyst yielded a constant 38 wt% JP-4 over the same time period. The 50% US sieve catalyst maintained the higher activity for JP-4 production and appeared to undergo a less severe loss in activity.

The estimated JP-4 yields used in Figure 4 were obtained from Figure 5, which represents a correlation between JP-4 yields from simulated distillation data and whole product API gravities. The solid data points represent all previously tested US sieve-containing catalysts whereas the open points represent all other catalysts previously tested, independent of support type or metals loading, and all 50% US sieve alumina catalysts tested subsequently. The correlation can be represented by:

$$\text{JP-4, Wt\%} = 3.46 \text{ API}^{\circ} - 98$$

Simulated distillation data agreed within one to two percentage points with actual distillation data for all samples so that Figures 4 and 5

represent actual yields of JP-4 to a high degree of accuracy. This correlation proved valuable for monitoring catalyst cracking activities on a daily basis.

Results from the previous task indicated that the 1.5/10/15 catalyst on a 50% US sieve/alumina support was the system of choice for further investigation. The catalyst resulted in low product nitrogens and gave highest yields of JP-4 material with the lowest cracking activity decline rate.

To this point, catalyst physical properties were kept within fairly narrow ranges for sets of catalyst within each task. With the metals optimized, and the support type and composition determined, the next task was designed to optimize the support physical properties.

Eight supports, consisting of 50% US sieve in alumina, were prepared to give a range for each of three physical properties as detailed in Table IV. These variations were achieved by modification of the alumina component, since modification of the sieves themselves could destroy their original nature and their inherent activity for cracking.

Data for the screening runs at 780°F and 1800 psig are given in Table V. Since the previous tasks had demonstrated that high sieve-containing catalysts could reduce the nitrogen content to less than 10 ppm at 0.5 LHSV, the possibility existed that all eight of the above-detailed catalysts could exhibit similar high nitrogen removal at that space velocity and hence negate the purpose of the task. To avoid that possibility, each catalyst was additionally tested at the higher space velocity. At constant sieve content, the relationship between JP-4 yield and hydrogen consumption for these eight catalysts is shown in Figure 6. Hydrogen consumption appears to increase linearly with JP-4 yields in the range of approximately 40 to 70 wt%. (See also Figure 3.) Below approximately 40 wt% JP-4, hydrogen consumption increased with little increase in product JP-4, probably as a result of saturation reactions required prior to cracking reactions. Above approximately 70 wt% JP-4, hydrogen usage appears to increase more rapidly than JP-4 content, probably as a result of additional long-chain paraffin cracking which, in addition, reduces product pour point.

A relationship between pour point and JP-4 yield for these eight US sieve-containing catalysts is given in Figure 7, which indicates a rapid drop in JP-4 yield for whole products with pour points greater than about 40°F. Data for the 20%, 30%, and 50% US sieve catalysts tested previously can also be represented by Figure 7.

The effect of product nitrogen on JP-4 yield is shown in Figure 8. The results indicate that JP-4 yield remained at approximately 30 wt% for product nitrogen above 600 ppm and increased with decreasing nitrogen content. To produce a product with approximately 50 wt% percent JP-4, product nitrogen must be reduced to approximately 10 ppm. Product nitrogen must be virtually eliminated to produce JP-4 yields of approximately 70 wt% or more.

Hydrogen usage to achieve these levels of product nitrogens is shown in Figure 9. About 1550 SCFB of hydrogen was required for 10 ppm product nitrogen (50% JP-4 yield). About 400 SCFB additional hydrogen was required to decrease product nitrogen to near zero and to increase JP-4 yields to 80%. These results are instructive in that correlations important to the overall hydrocracking scheme have been developed within this set of catalysts.

Nitrogen removal kinetic plots for these catalysts are shown in Figure 10. Of the eight catalysts tested, only one, 3838-023, performed well at both 0.5 and 0.75 LHSV with respect to nitrogen removal in particular, conversion, and activity maintenance at the lower throughput. Nitrogen removal for this catalyst appears to be first order as shown in Figure 10, whereas all other catalysts display less than first-order (or mixed-order) kinetics. This type of kinetic behavior is perhaps a reflection upon nitrogen removal efficiency and suggests an axial dependence on nitrogen content, or an accelerating nitrogen removal reaction promoted by the sieve itself.

In general, it is difficult to obtain correlations between the physical properties of catalysts containing molecular sieves and catalyst performance because of the complexity of the systems. Figure 11, however, does reflect a correlation between catalyst average pore diameters (calculated as $4V \times 10^4/A$) and product nitrogen. At 0.75 LHSV, the correlation is reasonable but is somewhat less so at 0.5 LHSV. Both sets of results indicate that greatest nitrogen removal occurs with the catalysts of smallest average pore diameters. The two best catalysts in the series, 3838-023 and 3838-039, have APD's close to 700A, but only the former is "efficient" at both space velocities and has the highest cracking activity and best activity maintenance. Comparison of the pore size distributions for these two catalysts indicates a sharper distribution of pores for catalyst 3838-023 when compared to catalyst 3838-039. All other catalysts in this series, with one exception, have broader pore size distributions. Other catalyst physical properties, namely surface area and pore volumes, did not show any correlation with product nitrogens.

Results from the catalyst physical properties study indicated that for high denitrogenation and cracking activity the preferred support of 50% US sieve in alumina should have pores of average pore diameters near 700A combined with a high surface area and a sharp pore size distribution.

Some data for an activity maintenance test using the preferred catalyst are detailed in Table VI. Start-of-run conditions were 0.4 LHSV, 2000 psig hydrogen, and 770°F and were chosen to maximize hydrogenation and hydrocracking reactions while allowing for an increase in reactor temperature in case catalyst deactivation occurred.

In contrast to all other previous tests, the activity maintenance test was subjected to numerous unit upsets during the first 50 days on stream. As a result of some of these upsets, catalyst activity was seriously reduced. To compensate, reactor temperature was raised 150°F over the first 48 days on stream to maintain high yields of JP-4 material.

As a result of these unit upsets, the test was extended to 103 days with processing conditions held constant at approximately 786°F, 0.4 LHSV, and 2000 psig for the periods 49 through 93. For the last ten days, reactor temperature was deliberately raised to 790°F and then lowered to 780°F in order to obtain the cracking temperature response.

Figure 12 shows product nitrogens as a function of days on oil. With the exception of those upsets which affected product nitrogens (shown as solid points), product nitrogens were maintained generally in the 1 to 3 ppm range throughout the test. As indicated previously (Figure 8), 10 ppm product nitrogen would reduce JP-4 yields to approximately 50 wt% or less whereas a JP-4 yield of >70 wt% would require <2 ppm nitrogen in the product. High cracking activity to produce JP-4 is critically dependent upon very low product nitrogen levels.

Daily JP-4 yields, estimated from product API gravities and Figure 5, are shown in Figure 13. The solid symbols represent upsets affecting JP-4 yields or cracking activity. The following points can be drawn from Figure 13.

- (i) For the first ten days on oil at 770°F, cracking activity declined as reflected in the drop in JP-4 yields from approximately 82 wt% to approximately 68 wt%.
- (ii) The unit upset of day 19 (unit depressurized, subjecting catalyst to high temperature without hydrogen) seriously affected catalyst cracking activity at 775°F as reflected in the drop in JP-4 yields from approximately 80 wt% to approximately 67 wt%. This loss in activity was also reflected in the JP-4 yields at 777°F being lower than initially achieved at 775°F.
- (iii) The unit upset on day 43 (very little hydrogen flow for 16 hours) also seriously affected cracking activity as evidenced by the poor temperature response upon raising temperatures from 777°F to 786°F.
- (iv) At 786°F, over approximately a 50-day period, cracking activity declined steadily as indicated by the drop in JP-4 yields from about 80 to 67 wt%. This decline may have been affected by the upset on day 65.

In order to calculate catalyst life at a specified JP-4 yield, temperature response factors need to be calculated. This was done by using the data at the end of the test at 785°F (period 93), 790°F (period 96), and 780°F (period 101) assuming zero-order kinetics, no nitrogen inhibition in the actual cracking zone, and constant activity. Hydrocracking reactions in the presence of nitrogen are generally zero order over the total catalyst system, and in this case all samples contained <10 ppm nitrogen.

Using a constant JP-4 yield of 50 wt%, temperature response factors of 62.5, 67.9, and 65.6 Kcal mole⁻¹ were calculated for the three temperature couples, the average being 65.4 Kcal mole⁻¹. This value is not unusual for full-range, high-boiling feedstocks containing large amounts of nitrogen.

Based upon the temperature response factor, a catalyst life of approximately four and one-half months can be calculated for a constant JP-4 yield of 75 wt% by increasing reactor temperatures from 775°F to 800°F at 2000 psig and 0.4 LHSV. However, due to the operational problems encountered in the test, this should be considered a minimum life and six months is probable. A deactivation rate of approximately 0.18°F/day was calculated from the data for periods 53 and 93 using zero-order kinetics.

Within the same constraints, catalyst life would be longer for lower JP-4 yields. As discussed previously, several unit upsets seriously affected catalyst activity and one of these upsets occurred during the period used to calculate the activity decline rate. Thus, the projected life for constant 75% JP-4 yields should be viewed as a rough estimate. Detailed process variable studies which were not part of this contract would be needed to more accurately define a deactivation rate.

The data for the distillations of the products from the activity test to produce JP-4 and JP-8 jet fuel fractions are given in Table VII. All samples for periods 1 through 73, with the exception of those samples containing more than 10 ppm nitrogen or having an API gravity less than 45°, were combined to yield approximately four gallons of product. The composite was washed with water and then dried. Two distillations to yield JP-4 and JP-8 fractions were completed. The JP-4 yield was 76 wt% on the composite product with a JP-8 yield of 61 wt%. The analytical data indicates that the samples would meet all specifications with perhaps one exception. The pour point of -40°F for the JP-8 fraction is high in view of the freeze point specification of -58°F. However, the simulated distillation data indicates an end point very close to the specified limit. A slightly lower temperature cut point, and perhaps a slightly lower initial point, would lower the pour point and hence bring the freeze point to the specified value.

Based on the qualities measured, with one exception, saleable jet fuels were produced in high yields by the single-catalyst process.

CONCLUSIONS

A single-catalyst system capable of direct hydrocracking of a whole shale oil containing large amounts of nitrogen has been developed. The novel catalyst, consisting of cobalt, chromium, and molybdenum salts on a base of 50% US sieve in alumina is multifaceted in that it combines both the saturation and denitrogenation activity of alumina with the cracking activity of the sieve. The combination is more effective than alumina alone for hydrocracking with the cracking zone confined to that part of the bed at the bottom where the nitrogen content has been reduced to <10 ppm. This cracking zone would vary with changes in process conditions.

The ability of the optimized catalyst to hydrocrack a whole shale oil into high yields of jet fuel boiling-range material was demonstrated in

a 103-day (approximately 2500 hours) test. Although several unit upsets marred the results and perhaps affected catalyst activity, a high yield of JP-4 boiling-range material was sustained. The whole product was water white in color and contained only a few ppm nitrogen. Even though unit operations were poor during the catalyst life test, a minimum life of 4.5-month was demonstrated and a catalyst life of six months is expected for the specified 75 wt% yield of JP-4 boiling-range material. It should be emphasized that a guard bed to remove arsenic and iron was not used for the life test. The presence of such a bed should extend the catalyst life considerably.

Table I
Selected Shale Oil Properties

| | <u>Tosco</u> | <u>Paraho</u> | <u>Occidental</u> |
|----------------|--------------|---------------|-------------------|
| API° | 21.0 | 20.2 | 23.8 |
| Pour Point, °F | 75 | 90 | 60 |
| H/C | 1.56 | 1.61 | 1.67 |
| N, Wt% | 1.88 | 2.18 | 1.32 |
| S, Wt% | 0.75 | 0.66 | 0.64 |
| O, Wt% | 1.39 | 1.16 | 1.33 |

Table II
Initial Product Qualities
Co/Cr/Mo on Alumina
(1800 psig, 0.55 LHSV, 790°F)

| | <u>Product</u> | <u>Feed</u> |
|----------------|----------------|-------------|
| API° | 39 | 23.8 |
| Pour Point, °F | 80 | 60 |
| Nitrogen, ppm | 116 | 13,200 |
| JP-4, Wt%* | 37 | 15.5 ** |
| 650°F-, Wt% | 74 | 44 |
| SCFB Hydrogen | 1400 | - |

* 20% distilled at 290°F, 90% distilled at 470°F

** Heavy JP-4 fraction, IBP of 290°F

Table III

Effect of Support Composition on Product Qualities

| | <u>Al₂O₃</u> | <u>20% SiO₂/ Al₂O₃</u> | <u>30% US Sieve/ Al₂O₃</u> |
|------------------|------------------------------------|---|--|
| API ^o | 39.2 | 39.7 | 44.6 |
| Nitrogen, ppm | 83 | <10 | < 5 |
| Pour Point, °F | 80 | 65 | 30 |
| JP-4, Wt% | 38 | 38 | 54 |
| 650°F-, Wt% | 76 | 77 | 87 |
| SCFB Hydrogen | 1400 | 1400 | 1660 |

Table IV

Catalyst Physical Properties

(50% US Sieve/alumina)

| <u>Catalyst ID 3838-</u> | <u>Surface Area m²/g</u> | <u>Pore Volume cc/g</u> | <u>Avg Pore Diameter (4 V/A), °A</u> |
|------------------------------|---|-----------------------------|--|
| 023 | 280.5 | 0.477 | 68.0 |
| 028 | 255.2 | 0.545 | 85.5 |
| 030 | 222.4 | 0.505 | 90.8 |
| 031 | 312.5 | 0.824 | 105.4 |
| 034 | 305.0 | 0.589 | 77.2 |
| 035 | 276.3 | 0.784 | 113.4 |
| 037 | 280.4 | 0.710 | 101.3 |
| 039 | 234.0 | 0.417 | 71.4 |

Table V

Product Qualities from Catalysts with Different Physical Properties

0.5 LHSV

| <u>Catalyst ID 3838-</u> | <u>Nitrogen, ppm</u> | <u>Pour Point °F</u> | <u>650°F-, Wt%</u> | <u>JP-4, Wt%</u> | <u>SCFBH</u> |
|------------------------------|--------------------------|--------------------------|------------------------|----------------------|--------------|
| 023 | 1 | -50 | 92.5 | 79.5 | 1930 |
| 028 | 4 | 35 | 86.5 | 62.7 | 1670 |
| 030 | 600 | 75 | 65.6 | 29.6 | 1190 |
| 031 | 76 | 70 | 72.5 | 36.8 | 1390 |
| 034 | 5 | 55 | 71.2 | 50.6 | 1520 |
| 035 | 46 | 65 | 75.8 | 43.9 | 1380 |
| 037 | 77 | 70 | 74.0 | 39.9 | 1360 |
| 039 | 1 | 40 | 79.5 | 57.1 | 1660 |

0.75 LHSV

| | | | | | |
|-----|------|----|------|------|------|
| 023 | 44 | 75 | 67.5 | 33.8 | 1310 |
| 028 | 1510 | 75 | 83.0 | 30.1 | 1300 |
| 030 | 1240 | 75 | 65.5 | 29.4 | 1190 |
| 031 | 985 | 75 | 62.6 | 30.1 | 1200 |
| 034 | -- | -- | -- | -- | -- |
| 035 | 1950 | 75 | 64.6 | 29.3 | 1120 |
| 037 | 1560 | -- | 66.4 | 28.3 | 1150 |
| 039 | 289 | 75 | 60.4 | 33.3 | 1260 |

Table VI
Product Qualities from the Activity
Maintenance Test

| Day | 3 | 9 | 17 | 19 | 27 | 32 | 39 | 46 | 53 |
|-----------------|-------|-------|-------|-------|-------|-------|-------|-------|-------|
| Temperature, °F | 770.1 | 770.3 | 775.8 | 774.5 | 777.2 | 777.1 | 777.5 | 777.0 | 786.0 |
| API° | 52.4 | 46.0 | 51.2 | 47.0 | 48.8 | 49.2 | 48.9 | 42.4 | 50.3 |
| Nitrogen, ppm | 2 | 1 | 1 | 2 | 1 | 2 | 6 | 11 | 3 |
| Sulfur, ppm | 18 | 133 | 728 | 36 | 64 | 92 | 234 | 22 | 60 |
| Pour Point, °F | -30 | 5 | -10 | 20 | -15 | -15 | 20 | 60 | -15 |
| 650°F., Wt% | 86.7 | 87.7 | 84.4 | - | 91.1 | 91.7 | 88.6 | 88.6 | 94.4 |
| JP-4, Wt% | 84 | 89 | 79 | - | 72 | 79 | 67 | 49 | 77 |
| SCFBH | 1960 | 1770 | 1740 | 1740 | 1850 | 1800 | 1800 | 1515 | 1920 |
| Day | 80 | 67 | 73 | 80 | 87 | 93 | 96 | 101 | |
| Temperature, °F | 785.5 | 785.4 | 788.0 | 788.0 | 785.8 | 785.5 | 789.7 | 779.9 | |
| API° | 49.6 | 47.4 | 48.4 | 49.9 | 48.1 | 47.4 | 50.3 | 43.8 | |
| Nitrogen, ppm | 2 | 15 | 1 | 1 | 30 | 1 | 1 | 10 | |
| Sulfur, ppm | 36 | 229 | 76 | 70 | 121 | 20 | 85 | 100 | |
| Pour Point, °F | 5 | 10 | 10 | -5 | -10 | 5 | -10 | 55 | |
| 650°F., Wt% | 89.4 | 89.3 | 90.9 | 91.7 | 90.2 | 89.4 | 93.2 | 84.5 | |
| JP-4, Wt% | 70 | 68 | 73 | 73 | 70 | 67 | 76 | 57 | |
| SCFBH | 1890 | 1740 | 1810 | 1850 | 1850 | 1720 | 1940 | 1400 | |

Table VII
Jet Fuel Qualities

| | Composite | JP-4 | JP-8 |
|-----------------------|-----------|--------------|--------------|
| API° | 48.7 | 49.4 (48-57) | 43.4 (37-51) |
| Weight % | 100 | 70 | 01 |
| Carbon, Wt% | 86.82 | 85.99 | 86.10 |
| Hydrogen, Wt% | 14.17 | 14.00 (13.6) | 13.88 (13.6) |
| Nitrogen, ppm | 1.1 | 0.7 | 1.1 |
| Pour Point, °F | -5 | -85 | -40 |
| Viscosity (40°C), cst | 1.33 | - | - |
| Aromatics, Vol% | - | 16.0 (25.0) | 16.0 (25.0) |
| Olefins, Vol% | - | 1.0 (5.0) | 2.5 (5.0) |
| Distillation, D-2637 | | | |
| IBP, °F | -47 | 22 | 250 |
| 10% | 203 | 190 | 322 (267) |
| 20% | 268 | 238 (206) | 353 |
| 30% | 321 | 278 | 390 |
| 40% | 372 | 312 | 413 |
| 50% | 410 | 346 (305) | 436 |
| 60% | 448 | 377 | 461 |
| 70% | 487 | 405 | 489 |
| 80% | 547 | 440 | 520 |
| 90% | 624 | 490 (482) | 564 |
| EP, °F | 789 | 663 (608) | 622 (626) |

Values in parenthesis are maximum (minimum for hydrogen content) specification limits.

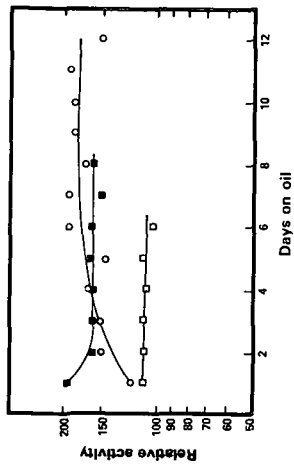


Figure 1 — Effect of Support Type on Relative Denitrogenation Activity for Various Catalysts. o, Alumina; □, 30% US Sieve Alumina; ■, 20% Silica Alumina

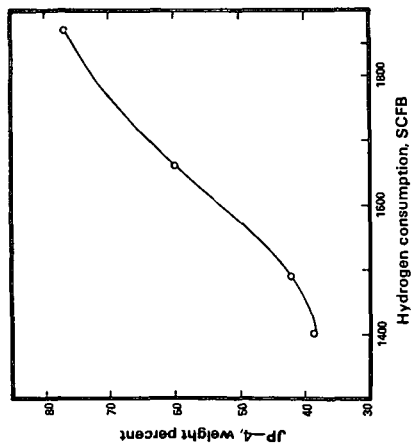


Figure 3 — Correlation Between JP-4 Yields and Hydrogen Consumption for Catalysts Containing 0, 20, 30, and 50% US Sieve

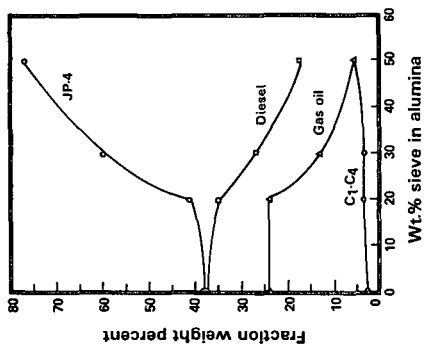


Figure 2 — Product Yield Structures as a Function of US Sieve Content in the Support

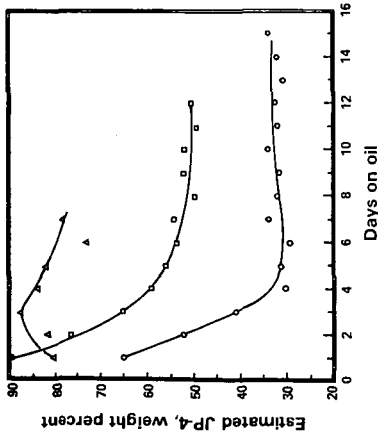


Figure 4 — Estimated Daily Yields of JP-4 for Catalyst of Different Sieve Content, o, 20%; □, 30%; and △, 50% US Sieve

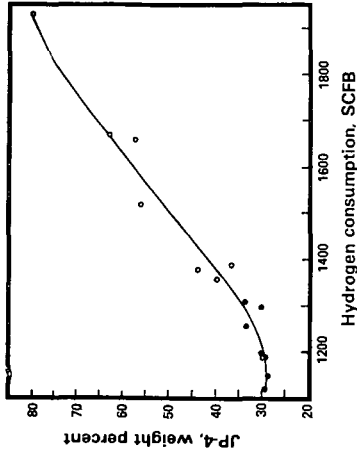


Figure 6 — Correlation Between JP-4 Yields and Hydrogen Consumption for Catalysts Containing 50% US Sieve, o, 0.75 LHSV; □, 0.5 LHSV

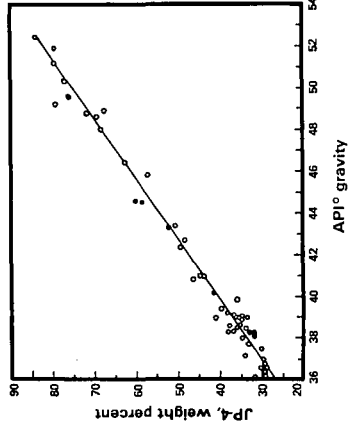


Figure 5 — Correlation Between Product API Gravity and JP-4 Yields

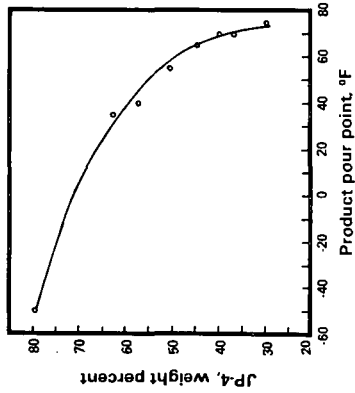


Figure 7 — Correlation Between Product Pour Point and JP-4 Yields for Catalysts Containing 50% US Sieve

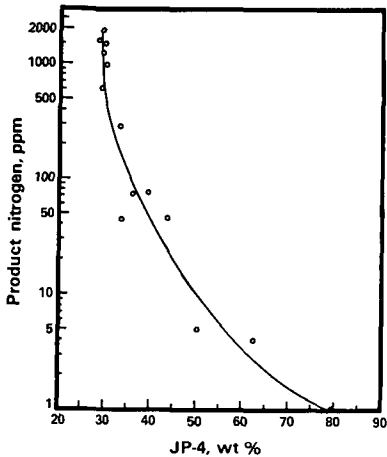


Figure 8 — JP-4 Yields as a Function of Product Nitrogen for Catalysts Containing 50% US Sieve

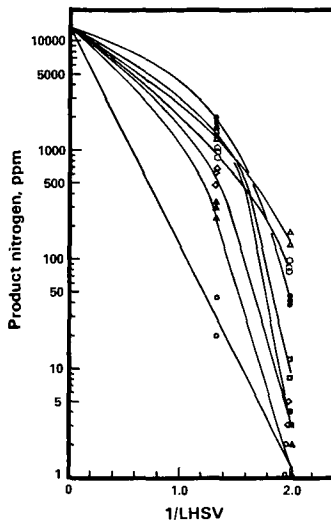


Figure 10 — Effect of Space Velocity on Product Nitrogens for Catalyst with Different Physical Properties. Catalysts 3838-023 (○); -028 (□); -030 (△); -031 (◊); -034 (◊); -035 (●); -037 (■); -039 (▲).

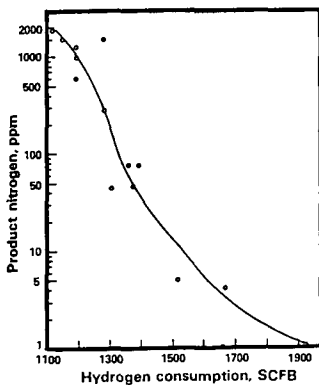


Figure 9 — Hydrogen Consumption as a Function of Product Nitrogen for Catalyst Containing 50% US Sieve

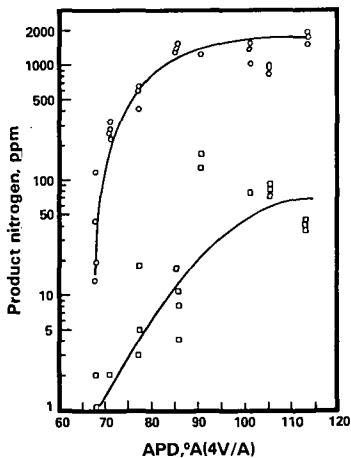


Figure 11 — Correlation Between Catalyst Average Pore Diameters and Product Nitrogen for 50% US Sieve Alumina Catalysts. ○, 0.75 LHSV; □, 0.5 LHSV.

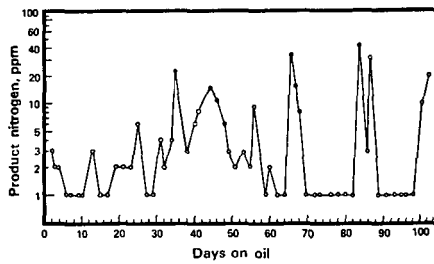


Figure 12 — Product Nitrogen as a Function of Days on Oil for the Activity Maintenance Test

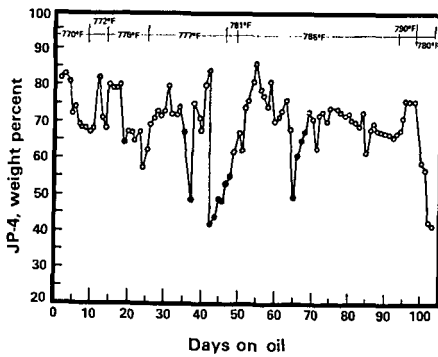


Figure 13 — Daily JP-4 Yields for the Activity Maintenance Test

CHARACTERIZATION OF ORGANIC BASES
IN HYDROCRACKED SHALE OIL FUELS

Dennis Hardy and Robert N. Hazlett
Naval Research Laboratory, Code 6180
Washington, D.C. 20375

and

Jeffrey Solash
Gulf Science and Technology Co.
Pittsburgh, PA 15230

As part of a continuing in-depth fuel characterization program for fuels produced in the U.S. Navy's shale programs (1,2,3,4), an extensive determination of acid extractable organic nitrogen compounds in Shale-II fuels has been completed. This report provides a description of an improved GC-MS system which simplifies the analysis. In addition, qualitative and some quantitative data on the organic bases in the fuels are presented. Since shale oil contains a significantly higher weight percent of Nitrogen than petroleum and Nitrogen containing compounds at low levels in finished fuels have long been implicated in fuel stability problems (5), we have been looking at samples from the fuel refining stream available from the Shale-II project. Ultimately this chemical composition information will be utilized in attempts to account for fuel stability problems both at high temperatures and at ambient temperatures.

EXPERIMENTAL

The hydrocracked shale oil refining process details used in the Shale-II exercise have been previously described (6). Following hydrocracking and fractionation, the fuels were acid and clay treated. Table I shows the nitrogen content of three fuels from the refinery before final acid/clay treatment. The nitrogen concentration for the fuels, the fuels after extraction and the acid extracts were determined by pyrolysis/combustion at 1000 degrees C and measurement of chemiluminescence from the reaction of NO with ozone (7). The crude shale oil contained 2.1 percent nitrogen (w/w). The relative deviation of the values was +5 percent. The basic nitrogen fraction of the three fuels was obtained by extracting with 1N HCl, neutralizing with aqueous NaOH, and back extracting into ether.

A Hewlett-Packard 5982A GC-MS was modified at the GC-MS interface in order to accommodate a 50m x 0.3mm I.D. flexible fused silica column with a stationary phase coating of SP2100 (relatively non-polar, similar to OV-101). The MS ion source flange was connected to the GC oven interior wall by a heated 1/8" O.D. copper tube. The capillary column was threaded into the heated 1/8" tube from the GC oven, through the tube, into the MS source so that the column outlet was positioned about 1.0 cm behind the electron beam of the ion source. The 1/8" tube was sealed to high vacuum at the MS source flange and in the GC oven at the point where the capillary column entered the tube. Flow rates through the capillary column were measured near atmospheric pressure and related linearly to column head pressure. Flows were measured between 0.5 ml/min and 1.5 ml/min of helium carrier gas. Under vacuum conditions the MS source region normally attains pressures of about 5×10^{-7} torr; at helium flow rates of 1 ml/min into the source region pressures of about 1×10^{-6} torr were attained.

The split ratio of the Hewlett-Packard 18740B capillary injector was set at 80:1 and 0.2 to 0.5 μ l injections of the fuel extracts were made. The carrier gas flow for most sample runs was 1.0 to 1.1 ml/min helium (nominal at atmospheric pressure). The column temperature was held for 2 min at 85 degrees C, programmed at 8 degrees C/min to 220 degrees C and held at the upper temperature for 8 mins. Mass spectra were taken between m/z 50 and m/z 300 at the rate of about 1 spectrum/1.5 sec.

RESULTS AND DISCUSSION

A reconstructed total ion chromatogram for the JP-5 extract is shown in Figure 1. The excellent resolution, column efficiency and minimal tailing of the polar Nitrogen containing components is typical of the chromatograms which can be produced by the all glass system and interface described above. At 14.1 min the column efficiency is 125,000 theoretical plates. The chromatographic advantages of eluting components directly into the high vacuum ionization region are obvious. The absolute sensitivity of the technique is enhanced by the wide bore (0.3 mm ID) of the column which permits up to 1.0 μ l injections of the fuel extracts without signs of column overload. Even at the relatively high source pressures encountered, the mass spectra observed are identical to normal electron impact (70ev) spectra generally taken at 10(exp-7) torr.

The results of the capillary GC-MS analysis of the acid extraction of Shale-II naphtha are shown in Table II. Over thirty nitrogen containing compounds were detected, most of which were $C_nH_{2n-5}N$ type compounds. These pyridines accounted for over 90 percent of the basic nitrogen compounds by weight. The average molecular weight for this naphtha fuel extract was 125. The most frequent isomers encountered contained three or four carbons in side chains.

The JP-5 acid extract results are given in Table III. Over seventy nitrogen containing compounds were identified. As in the naphtha extract, the bulk of the material was composed of $C_nH_{2n-5}N$ type compounds. These pyridines contributed 85 percent of the extracted Nitrogen compounds by weight. The average molecular weight was 172 and most of the compounds contained from five to eight carbons in side chains. A significant amount of $C_nH_{2n-11}N$ (quinolines) and $C_nH_{2n-7}N$ (tetrahydroquinolines) averaging 2 to 3 carbons in side chains were also detected. The hydrotreatment of the crude shale oil in the refinery is the most likely explanation for the presence of tetrahydroquinolines in the jet fuel.

Table IV outlines the findings for DFM (Diesel Fuel Marine). Over one hundred nitrogen containing compounds were detected in this extract. Over 60 percent of them were in the class $C_nH_{2n-9}N$. Seven, ten and twelve carbon side chain isomers predominated, and the average molecular weight was 195. As in the JP-5 sample, a significant amount of $C_nH_{2n-11}N$ and $C_nH_{2n-7}N$ compounds were identified. Also over 20 percent of the nitrogen compounds by weight were of the type $C_nH_{2n-9}N$ (indoles) which were primarily seven and eight carbon side chain isomers. Indole types were not detected in the JP-5 extract.

Although only 0.2% nitrogen remained in the neutral, acid fraction of DFM, GC/MS analysis of a silica gel column fraction eluted by chloroform revealed the presence of both $C_nH_{2n-9}N$ (indoles) and $C_nH_{2n-15}N$ (carbazoles).

CONCLUSIONS

The major compound class isomers found in the acid extract of Shale-II naphtha were 3 to 4 carbon side chain substituted pyridines. In the Shale-II JP-5 sample prior to final refinery acid/clay treatment, the major compound class isomers were 5 to 8 carbon

side chain pyridines, 1 to 3 carbon side chain tetrahydroquinolines and 2 to 3 carbon side chain quinolines. In the DFM extract the major compound class isomers found were 5 to 12 carbon side chain pyridines, 3 to 4 carbon side chain tetrahydroquinolines, 5 to 8 carbon side chain indoles and 3 to 5 carbon side chain quinolines.

The outlined analytical procedure could be improved by the addition of suitable internal standards to facilitate quantitation of particular compounds of interest.

REFERENCES

1. Solash, J., Hazlett, R.N., Hall, J.M. and Nowack, C.J., Fuel, 1978, 57, 521.
2. Solash, J., Hazlett, R.N., Burnett, J.C., Beal, E. and Hall, J.M.; ACS Symposium Series, No. 163, 1981, 237.
3. Affens, W.A., Hall, J.M., Beal, E., Hazlett, R.N. and Leonard, J.T.; ACS Symposium Series, No. 163, 1981, 254.
4. Nowack, C.J., Delfosse, R.J., Speck, G., Solash, J. and Hazlett, R.N.; ACS Symposium Series, No. 163, 1981, 267.
5. Hazlett, Robert N. and Hall, James M., Fouling of Heat Transfer Equipment, ed. E.F.C. Somerscales and J.G. Knudsen, Hemisphere Pub., Co., Washington, D.C., 1981, p. 501.
6. Robinson, E.T. and Wasilk, N.J., ACS Symposium Series, No 163, 1981, 223.
7. Drushel, H.F., Anal. Chem., 1977, 49, 932.

TABLE I

SHALE II PRE-ACID TREATED FUELS
NITROGEN ELEMENTAL ANALYSIS PPM (W/W)

| <u>Sample</u> | <u>Fuel</u> | <u>Ext. Fuel</u> | <u>% N Ext.</u> | <u>Acid Ext.</u> |
|---------------|-------------|------------------|-----------------|------------------|
| G-1 (Naphtha) | 900 | 3 | 99.7 | 103000 |
| J-7 (JP-5) | 2100 | 85 | 96.0 | 62000 |
| D-7 (DFM) | 3000 | 5 | 99.8 | 61000 |

Acid Extract = 1N HCl

TABLE II
SHALE II - NAPHTHA
COMPOUNDS IN ACID EXTRACT BY EI-MS

| <u>Compound Class</u> | <u>Number of Carbons in Side Chain</u> | <u>Number of Isomers Detected</u> | <u>Relative Amount of Class</u> |
|---------------------------------|--|-----------------------------------|---------------------------------|
| Piperdines ($C_n H_{2n+1} N$) | 2 | 2 | 7% |
| | 3 | 3 | |
| Pyridines ($C_n H_{2n-5} N$) | 1 | 1 | 93% |
| | 2 | 4 | |
| | 3 | 10 | |
| | 4 | 8 | |
| | 5 | 3 | |

TABLE III
SHALE II - JET
COMPOUNDS IN ACID EXTRACT BY EI-MS

| <u>Compound Class</u> | <u>Number Carbons in Side Chain</u> | <u>Number of Isomers Detected</u> | <u>Relative Amount Of Class</u> | | |
|-------------------------------------|--|-----------------------------------|---------------------------------|---|-----|
| Pyridines ($C_n H_{2n-5} N$) | 3 | 1 | 85% | | |
| | 4 | 4 | | | |
| | 5 | 9 | | | |
| | 6 | 10 | | | |
| | 7 | 8 | | | |
| | 8 | 11 | | | |
| | 9 | 3 | | | |
| | 10 | 3 | | | |
| | Tetrahydroquinolines ($C_n H_{2n-7} N$) | 1 | | 3 | 10% |
| | | 2 | | 5 | |
| 3 | | 4 | | | |
| 4 | | 1 | | | |
| 5 | | 2 | | | |
| Quinolines ($C_n H_{2n-11} N$) | 1 | 1 | 5% | | |
| | 2 | 4 | | | |
| | 3 | 3 | | | |
| | 4 | 2 | | | |
| | 5 | 1 | | | |

TABLE IV
 SHALE II - DFM
 COMPOUNDS IN ACID EXTRACT BY EI-MS

| <u>Compound Class</u> | <u>Number of Carbons in Side Chain</u> | <u>Number of Isomers Detected</u> | <u>Relative Amount Of Class</u> |
|---|--|-----------------------------------|---------------------------------|
| Pyridines (C _n H _{2n-5} N) | 3 | 1 | |
| | 4 | 3 | |
| | 5 | 7 | |
| | 6 | 6 | |
| | 7 | 14 | 64% |
| | 8 | 5 | |
| | 9 | 6 | |
| | 10 | 9 | |
| | 11 | 3 | |
| | 12 | 13 | |
| Tetrahydro-quinolines (C _n H _{2n-7} N) | 2 | 5 | |
| | 3 | 2 | |
| | 4 | 4 | 8% |
| | 5 | 0 | |
| | 6 | 2 | |
| Indoles (C _n H _{2n-9} N) | 4 | 2 | |
| | 5 | 2 | |
| | 6 | 3 | 21% |
| | 7 | 8 | |
| | 8 | 9 | |
| Quinolines (C _n H _{2n-11} N) | 2 | 1 | |
| | 3 | 2 | |
| | 4 | 2 | |
| | 5 | 2 | 7% |
| | 6 | 1 | |

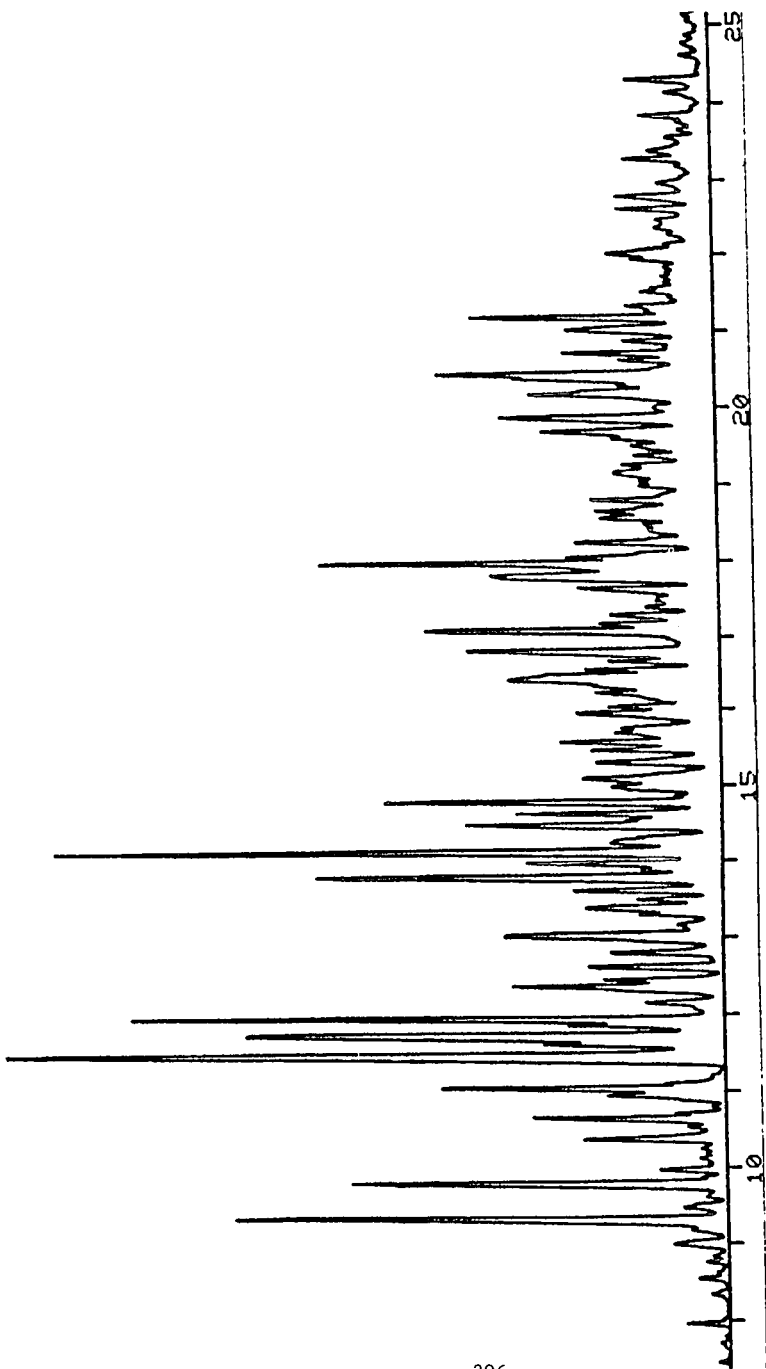


FIGURE 1. Reconstructed total ion chromatogram of J-7 (JP-5) acid extract. Retention times are in minutes.

TRANSPORTATION AND MARKETING
OF SHALE OIL

Gary L. Baughman, Ph. D.
Ronald L. Gist
Edwin H. Bentzen

Colorado School of Mines Research Institute
Box 112
Golden, Colorado 80402

Historically, oil shale developers have tacitly assumed that if and when they began producing shale oil and other products, somebody would be ready and willing to buy them. Considering all the technical, economic, environmental, political, and institutional problems facing the developers, this assumption was reasonable. In fact, during recent "severe" liquid fuels shortages, the assumption may have been perfectly valid. With the current energy situation, fuels pricing structure, political environment, and the nearing commercial reality of oil shale development, the assumption that a ready market exists for oil shale products requires further examination.

Not only must a developer determine whether someone will buy the products, but he must also determine what that prospective buyer will pay. The selling price of shale oil was historically assumed to be the price of conventional crude oil less some penalty for its high nitrogen content and pour point. Because the economics of oil shale production were not very precise, this was a reasonable approach. As the day of commercial production nears, however, construction cost estimates are becoming more refined, and costly design decisions are being made based on the marketing and transportation options anticipated. Estimates must be made, then, as accurately as possible regarding the ultimate disposition of the products to ensure that costly design errors are not made at this critical point in the planning program.

One interesting aspect of the transportation and marketing question is that the constraints and input parameters keep changing with new technology developments, revised product pricing structures, new environmental regulations, and changes in the availability of and demand for conventional and alternate fuels. A perfectly logical choice of transportation method and market made today may be totally unrealistic next year. For instance, several years ago a suggested market for raw shale oil was as a boiler fuel in California, with transport by a pipeline. Today, the EPA questions the acceptability of burning shale oil, California has more than an adequate supply of boiler fuel, and existing pipelines are now pumping Alaskan oil eastward out of California. Similar observations can also be made regarding coproducts such as ammonia, sulfur, and coke. Even the perceived demand for nahco₃ite and soda ash may fall victim to as yet unforeseen events.

Because the information that must be processed to arrive at a final decision is constantly changing, developing a system to manage this information is necessary. This system must permit the information to be processed quickly, yet be flexible enough to respond to changing conditions. A methodology

developed by Colorado School of Mines Research Institute satisfies these criteria, but to discuss the solution would be premature until the scope of the problem is first defined. Disposing of shale oil in the most economical fashion consists of two separate, but related, problems -- marketing and transportation. Addressing the marketing question, the first task is to define what is being marketed. That is, either raw shale oil, an upgraded product, or some intermediate-quality product can be marketed. Next, the quantity of the particular product to be marketed must be defined. In the initial stages of production, whether that be from a so-called demonstration plant or a single train of a larger operation, the output will likely be several thousand barrels per day. At full commercial production levels, perhaps as much as 50,000 to 100,000 barrels per day will be produced. Some markets will be more amenable to one production level than another and the costs per barrel for processing, in particular upgrading, will be significantly different for the two production rates.

Raw or upgraded shale oil may be marketed at a number of locations and may be used for several different purposes. In general, three basic uses exist for raw or upgraded shale oil -- as a boiler fuel, a refinery feedstock, and a petrochemical feedstock. Some market sites exhibit all three uses; others, only one or two.

Associated with each of these markets, by both location and use, is a selling price -- the price the shale oil product would bring at the buyer's plant gate. However, these figures are based on the assumption that the buyer wants the product, and this may not be a valid assumption. For instance, a particular shale oil product may be physically and chemically equivalent to a No. 6 fuel oil currently being fired in a utility boiler. The market value of the product could then be assumed to be equivalent to the price paid for the fuel oil, but if the utility company has a long-term contract with a dependable fuel oil supplier, the calculated market value is meaningless because a market really does not exist.

A similar example is the marketing of raw shale oil as a refinery feedstock. To calculate the market price of the product, it is possible to determine a value that could be subtracted from the price of a conventional feedstock to adjust the price of the shale-derived product downward to account for high pour point, nitrogen, and trace metals content. However, the refiner would only pay that price if the necessary equipment were available for processing the raw shale oil, and very few refineries currently possess that capability. Likely, he would rather pay the higher price for an oil he can handle.

Simplistic economic approaches are, therefore, inadequate for properly evaluating a potential marketing strategy, because associated with each marketing option is a market "quality" rating. This rating is a function of many factors, including availability of other crude supplies, long-range corporate plans, market size, and others. Figure 1 illustrates the market-related aspects that have been discussed so far.

Having now defined the market location and end use, the expected price, and the quality of the market, the next question to be addressed is how to get the product from the oil shale plant to the buyer's plant. Several transportation methods may be available, but it may not be advantageous to use the same method all the way to the buyer's plant. Rather, intermediate transfer points may be used to change from one mode to another, often to great advantage.

Essentially three transportation methods are available for shale oil transport -- railroads, pipelines, and trucks -- each with its own advantages and

disadvantages. Except for some situations in which truck transport may be ruled out, several options exist for transporting the shale oil product between any two adjacent points. Therefore, many possible transportation combinations for moving oil between the oil shale plant and the market should be considered.

Having defined the choices of where to go and how to get there, the cost and feasibility of moving the shale oil by each possible method must next be determined. Costs are the easiest information to acquire, in that this type of information is available from the respective pipeline companies and railroads, or can be calculated based on realistic capital and operating cost estimates. Any cost estimate, however, assumes that transport by that particular method is feasible -- which it may not be. For instance, published tariff rates by Amoco Pipeline for the line between Sinclair, Wyoming, and Sterling, Colorado, indicate the cost to be \$0.15 per barrel to transport oil over the route. However, closer investigation reveals that the capacity of that line is only about 40,000 barrels per day, and it is likely that the excess capacity in the 1990 time frame will be considerably less. In addition, the contaminants in raw shale oil may adversely affect the quality of the conventional oil subsequently shipped through the line, and the pipeline companies may have a legal right to refuse shipment of raw oil through their common carrier lines, even if the pour points and viscosities meet their standards. Thus, the quality of a particular transportation method must be considered as well as its cost. Figure 2 illustrates the complexity of the overall problem, including the transportation-related aspects.

The complexity of marketing and transporting shale oil; the time required to design, permit, and construct transportation systems; and the risks involved in any decision requires that more than just intuition be used in establishing a prospective marketing and transportation strategy.

With the problem thus defined, the next logical step is to solve it. CSMRI has developed a methodology to organize and evaluate all the various transportation and marketing options. The approach is geared to the specific needs of a particular project, the unique marketing constraints of the respective developers, and the particular stage of project development. It is a flexible methodology capable of providing quick evaluations and yet providing a basis for sophisticated operations research-oriented studies.

Knowledgeable input is required in four basic areas to make accurate evaluations:

- . Market prices
- . Transportation costs
- . Market quality
- . Transportation segment quality

It would seem that market prices would be the most easily acquired values, being based merely on the prices paid for equivalent fuels or feedstocks. Unfortunately, determining what fuels are "equivalent" to shale oil products requires an understanding of conventional petroleum refining and marketing, and some sage engineering judgment. In some cases, there is no equivalent fuel, so some economic extrapolation is required.

Transportation costs fall into three general categories: (1) estimates based on known tariffs, (2) estimates provided by transportation companies using data from similar systems, and (3) estimates based on capital and operating costs for new systems. In those rare instances where tariffs exist, rates are readily available. The costs estimated by the transportation companies may be overly optimistic or excessively conservative, depending on which poses the least risk for the company. Finally, costs based on capital and operating cost estimates are difficult to develop due to the multitude of assumptions inherent in such calculations.

Nevertheless, it is relatively easy to subtract from each market price the appropriate transportation costs (including transfer charges for changing modes at intermediate transfer points) to arrive at a consistent "plant-site" value. When appropriate, an upgrading cost can also be subtracted, leaving a value of raw shale oil at the retort site.

The development of economic cost estimates should reasonably be based on objective analyses, but a considerable degree of subjective input is required as well. Therefore, the individuals using the results of these studies must be directly involved in the development of the assumptions to ensure that the conclusions accurately reflect a particular oil shale developer's unique situation.

While the first two items, market prices and transportation costs, require some subjective input, market quality and transportation quality require even more. Market quality itself is determined by a number of factors, including the following:

1. Long-term potential
2. Short-term potential
3. Market flexibility
4. Independence from legislation
5. Independence from other oil shale developers

To use the method developed by CSMRI, subjective ratings are made for each market in each category, and each category is given a "weighting factor" to indicate its relative importance for a particular evaluation. Applying the weighting factors to the respective quality ratings then yields a single quality value for each market option. The value calculated for each market is then used to compare the relative "goodness" of the options. By changing the weighting factors, different aspects of the marketing problem can be emphasized and studied.

A similar rating system is also applied to the transportation options, except that each transportation option involves a set of individual transportation segments. A transportation quality for the entire option is calculated by combining the ratings for the component segments. For each transportation segment, the quality rating may be based on several factors including:

1. Ease of permitting
2. Short-term viability
3. Long-term viability

As with the market evaluations, each category is assigned a weighting factor which in turn is applied to the quality ratings for each segment to yield an overall segment quality. These values are then combined to yield a quality rating for each transportation option.

Having acquired all of the necessary objective and subjective inputs for the market and transportation options under investigation, and performing all of the necessary mathematical calculations, three values for each option are developed that may be used for comparison purposes to determine the most viable transportation and marketing option. These values are plant-site value of the raw shale oil, the quality of the market, and the quality of the transportation made.

A hypothetical example, shown in Table 1, can be used to illustrate the value of this approach. A purely economic evaluation would indicate that the best option is to sell raw shale oil as a boiler fuel in the Midwest and transport it there by pipeline. The economics do not take into account that the common carrier pipelines may not transport the raw oil or that government regulations may preclude the use of oil as a boiler fuel. The economic evaluation only implies that a good profit could be made if you could do it. On the other hand, there may exist a good market for hydrotreated shale oil as a refinery feedstock in the Midwest, and it is quite feasible to transport it there by pipeline, but the economic return is very low, principally because of the high cost of hydrotreating such a small quantity of product. Shipping raw shale oil by rail to refiners in the Midwest with capacities to handle the raw oil, however, provides a reasonable economic return, while at the same time maintaining high market and transportation qualities. As may be noted, however, should any of the fundamental assumptions concerning either transportation or market quality change, the relative ranking of the options will be changed as well.

Option selection must also be based on considerations about the preliminary tasks required to implement the options. That is, emphasis must be placed on selecting options that do not preclude implementation of alternative options, should the assumptions used in the evaluation change. For instance, the highest rated option may involve transport of raw shale oil whereas the next five highest rated options may involve on-site upgrading. Due to the time required to design an upgrading facility and incorporate it into the overall oil shale plant, dismissing the concept of upgrading would not be prudent, as conditions may change prior to commercial production, thus reducing the ranking of the raw oil transport concept. The lack of preliminary planning efforts regarding upgrading facilities might jeopardize the implementation of the now more desirable upgrading options.

This brief description is certainly not adequate to explain all of the complexities and problems involved in acquiring the data for this type of study, or with the finer points of data manipulation. Hopefully, it has conveyed the scope of the problem and introduced the methodology developed by CSMRI to evaluate the available options. The methodology can address the many problems, prejudices, and desires of each specific shale oil producer, thus making the approach very project-specific. Additionally, it is capable of being quickly and easily updated to evaluate the effects of new information as it becomes available. The time is fast approaching when major decisions are going to be made based on predicted shale oil transportation and marketing strategies and these predictions must be based on comprehensive evaluations that account for option qualities as well as hard economics.

TABLE 1

Typical Option Evaluation

Basis: 10,000 Barrels Per Day Production Level

| <u>Option</u> | <u>Plant Site Value (\$/bbl)</u> | <u>Market Quality (0-100)</u> | <u>Transportation Quality (0-100)</u> |
|--|--|---------------------------------------|---|
| 1. Raw shale oil/boiler fuel/Midwest/ pipeline | 30 | 45 | 50 |
| 2. Hydrotreated shale oil/refinery feedstock/Midwest/pipeline | 15 | 95 | 90 |
| 3. Raw shale oil/refinery feedstock/ Midwest/rail | 25 | 80 | 90 |

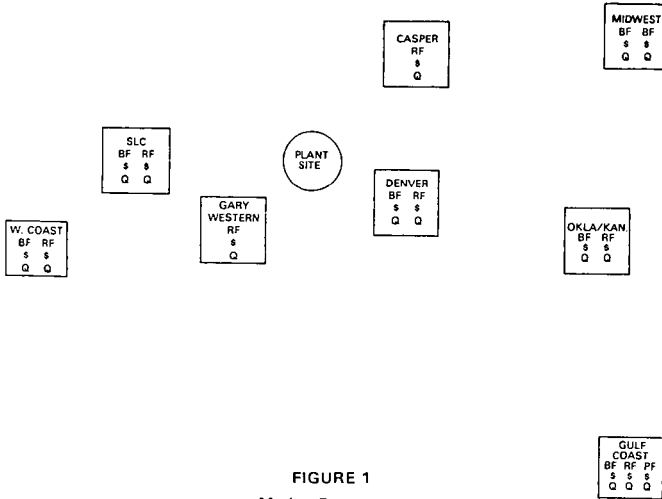


FIGURE 1
Market Parameters

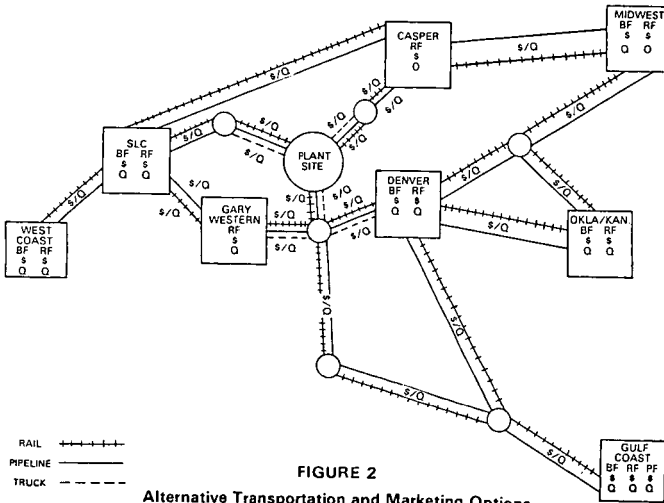


FIGURE 2
Alternative Transportation and Marketing Options

COKING KINETICS OF ARAB HEAVY VACUUM RESIDUUM
BY THERMOGRAVIMETRIC ANALYSIS

R. C. Schucker
Exxon Research and Development Laboratories
P. O. Box 2226
Baton Rouge, Louisiana 70821

INTRODUCTION

The increased demand for gasoline and heating oil in recent years coupled with the progressively heavier nature of available feedstocks has put a premium on efficient, low cost processes to convert residuum into lighter products. Traditionally, the process of choice has been coking wherein higher molecular weight species are converted to lighter ones by thermal decomposition at elevated temperatures. Coking may be done in either the delayed mode which is a semi-continuous process or in the fluid mode which is fully continuous. Fluid coking results in higher gas and gas oil yields, lower coke production and a higher octane number for the naphtha fraction than delayed coking and is therefore the preferred process to meet current fuel demands. Recent introduction of Exxon's FLEXICOKING process has made this option even more attractive. FLEXICOKING differs from conventional fluid coking in that some of the coke is gasified at $\sim 1800^{\circ}\text{F}$ to produce low BTU fuel gas and has been shown commercially to produce more naphtha and less heavy gas oil than conventional fluid cokers.

Despite these advances, there is still a need to increase the yield of desirable liquids from cokers. This, however, implies an alteration of the basic free radical pathways by which residuum molecules decompose -- pathways which presently are at best poorly understood. In addition, attempts to gain kinetic and mechanistic insight into the thermal reactions involved in residuum conversion are always hampered by the complexity of the feed. The objectives of this study were therefore to (1) determine the coking kinetics of a feed of commercial interest (Arab Heavy vacuum residuum) and (2) attempt to simplify the overall coking kinetics by first separating this feed into subfractions and studying each of these individually. The experimental technique used in this work was thermogravimetric analysis operated in the nonisothermal mode and was similar to that used by others [1-5] for analysis of polymers and oil shale. The emphasis of this study was on the coking kinetics of the whole residuum and its subfractions in contrast to recently published work [6] which focused on the mechanistic aspects of only the asphaltene fraction.

EXPERIMENTAL

The instrument of choice for this study was the Cahn 113 thermogravimetric analyzer (see Figure 1). At the heart of the system is the Cahn 2000 recording electrobalance which has a sensitivity 0.1 μg and a capacity of 1.0 gram. The sample to be analyzed is suspended from the balance in a platinum pan by a nichrome hangdown wire inside a quartz hangdown tube. The external split shell furnace operates from 100°C to 1100°C and is controlled by microprocessor temperature programmer capable of executing 40 individual programming steps. Programming of the temperature controller (a three mode digital device) provides for automatic variation in gain, reset and rate during operation and insures an extremely linear heating rate up to $\sim 100^{\circ}\text{C}/\text{min}$. The ability to measure the rate

of weight loss is enhanced by the addition of a time derivative computer built into the system which continuously monitors and plots the rate of weight change.

In a typical tga experiment approximately 20 mg of sample was placed into the platinum dish which was in turn suspended from the balance. The glassware was then assembled and the system was pumped down to ~ 0.1 torr, backfilled with dry nitrogen and a constant purge of 38 cc/min helium was passed through the system. The sample was then weighed to determine its initial weight to 0.01mg. The temperature program consisted of ramping from room temperature to 100°C in 5 minutes, holding at 100°C for 10 minutes, ramping from 100°C to 525°C at the desired heating rate and holding at 525°C for 30 minutes. At this point a blend of 80% He/20% O₂ was introduced into the system at ~ 75 cc/min. and the temperature was ramped to 700°C in 20 minutes to burn off the coke. Organic material balances obtained in this manner ranged from 99.5%-100%. The kinetic equations used to evaluate rate parameters are shown in Figure 2.

Arab Heavy vacuum residuum with a nominal cutpoint of 1050°F (565°C) was used as the feed in this study. A portion of this feed was deasphalted with n-heptane; and the maltene (or n-heptane soluble fraction) was then separated into resins and oils on Attapulugus clay [7]. The oils were further separated into aromatics and saturates by the method of Drushel [8] as shown in Figure 3. Analyses of the whole residuum and the resulting four subfractions are shown in Table 1.

RESULTS AND DISCUSSION

Nonisothermal kinetic experiments were carried out thermogravimetrically at heating rates of 1°C/min to 20°C/min. Typical thermograms for the whole feed and each of its fractions at a 10°C/min heating rate are shown in Figure 4. As can be seen, the asphaltenes produce the least volatiles (47.5%) followed by the polar aromatics (82.4%), aromatics (98.6%) and the saturates (99.8%). Weighting of each of these curves by the amount of that fraction separated from the initial feed and summing each of their contributions produced a curve which was very similar to that of the whole residuum.

The asphaltene thermograms were then analyzed to determine the rates of volatilization at various levels of volatile formation (V/V_0). These data were plotted according to equation 4 (Figure 2) and the resulting Arrhenius plot is shown in Figure 5. In agreement with theory, we find straight lines whose slopes can be used to determine activation energies for various stages of asphaltene reaction. In contrast to the oil shale work of Shih [5] who found all of his lines to be of essentially equal slope, we observe a gradual increase in slope (and therefore the activation energy) as a function of reaction, suggesting a change in mechanism, chemistry or both as a function of conversion. Similar plots for the polar aromatic, aromatic and saturate fractions as well as the whole residuum are shown in Figures 6-9 and a summary of the derived activation energies as a function of conversion for all of these fractions is given in Table 2.

It is interesting to note that while activation energies for each of the fractions tend to increase with conversion, only the asphaltenes exhibit such a wide range. It is also interesting that the saturates exhibit a generally higher level of activation energies even though they react more quickly than any other fraction. Finally, we note that the whole residuum seems

to mimic the sum of its parts in that it exhibits fairly low activation energies at low conversions, but has a broad range showing the asphaltene influence at higher conversions.

CONCLUSIONS

We have found that the kinetics of thermal decomposition reactions of a vacuum residuum can be effectively determined by nonisothermal thermogravimetric analysis. Furthermore, separation of the residuum into subfractions before such analysis provides kinetic insight into the behavior of molecules of varying size and chemical composition. Significantly, our results have shown that the activation energies for the coking reactions of all components of the residuum increase with conversion. This suggests that attempts to model residuum coking kinetics using a single activation energy would produce incorrect results; and that it would be more appropriate to use a distribution of activation energies such as that used by Anthony and Howard [9] in coal pyrolysis experiments.

REFERENCES

1. Flynn, J. H. and L. A. Wall, "General Treatment of the Thermogravimetry of Polymers." Journal of Research of National Bureau of Standards, A. Physics and Chemistry, 70A (6), 487-523 (1966).
2. Campbell, J. H.; G. H. Koskinas and N. D. Stout, "Kinetics of Oil Generation from Colorado Oil Shale," Fuel, 57, 372-376 (1978).
3. Campbell, J. H.; G. H. Koskinas; G. Gallegos and M. Gregg, "Gas Evolution During Oil Shale Pyrolysis. 1. Nonisothermal Rate Measurements," Fuel, 59, 718-726 (1980).
4. Campbell, J. H.; G. Gallegos and M. Gregg, "Gas Evolution During Oil Shale Pyrolysis. 2. Kinetic and Stoichiometric Analysis," Fuel, 59, 727-732 (1980).
5. Shih, S. M. and H. Y. Sohn, "Nonisothermal Determination of the Intrinsic Kinetics of Oil Generation from Oil Shale," Ind. Eng. Chem. Process Des. Dev., 19, 420-426 (1980).
6. Cotte, E. A. and J. L. Calderon, "Pyrolysis of Boscan Asphaltenes: Process Description and Nature of Products," Prepr. Div. Petr. Chem., ACS, 26(2), 538-547 (1981).
7. Schucker, R. C. and C. F. Keweshan, "The Reactivity of Cold Lake Asphaltenes," Prepr. Div. Fuel Chem., ACS, 25(3), 155-165 (1980).
8. Drushel, H. V., "Analytical Characterization of Residua and Hydrotreated Products," Prepr. Div. Petr. Chem., ACS, 17(4), F92-F101 (1972).
9. Anthony, D. B. and J. B. Howard, "Coal Devolatilization and Hydrogasification," AIChE J., 22(4), 625-656 (1976).

Table 1

Chemical Analyses of Fractions of Arab Heavy Vacuum Residuum

| <u>FRACTION</u> | <u>WHOLE RESID</u> | <u>n-C₇ ASPHALTENES</u> | <u>POLAR AROMATICS</u> | <u>AROMATICS</u> | <u>SATURATES</u> |
|--------------------------|--------------------|------------------------------------|------------------------|------------------|------------------|
| WT. % | 100.0 | 23.9 | 60.3 | 10.4 | 5.4 |
| C (WT. %) | 83.13 | 82.65 | 82.65 | 84.92 | 84.93 |
| H (WT. %) | 9.79 | 7.91 | 9.92 | 11.91 | 13.76 |
| O (WT. %) | 0.58 | 0.88 | - | - | - |
| N (WT. %) | 0.68 | 1.18 | 0.56 | <0.3 | <0.3 |
| S (WT. %) | 5.71 | 7.51 | 5.45 | 2.41 | 0.016 |
| (H/C) _{AT} | 1.41 | 1.15 | 1.44 | 1.68 | 1.94 |
| \bar{M}_n (TOL., 50°C) | ~2500 | ~7500 | ~1900 | ~900 | ~900 |
| C _A (MOLE %) | - | 48.4 | 39.7 | 35.4 | - |

Table 2

Calculated Activation Energies
for Arab Heavy Vacuum Residuum and Fractions

| <u>FRACTION OF TOTAL VOLATILES</u> | <u>ACTIVATION ENERGY (KCAL/MOLE)</u> | | | | |
|------------------------------------|--------------------------------------|---------------|------------------|------------------|--------------------|
| | <u>ASPH.</u> | <u>POLARS</u> | <u>AROMATICS</u> | <u>SATURATES</u> | <u>WHOLE RESID</u> |
| 0.2 | 42.1 | 37.6 | 36.3 | 40.4 | 36.8 |
| 0.4 | 43.2 | 37.9 | 41.3 | 38.7 | 42.9 |
| 0.6 | 51.0 | 40.0 | 44.3 | 44.6 | 45.9 |
| 0.8 | 67.2 | 43.5 | 43.6 | 51.7 | 49.9 |
| 0.9 | 80.5 | 45.6 | 46.8 | 52.9 | 60.5 |

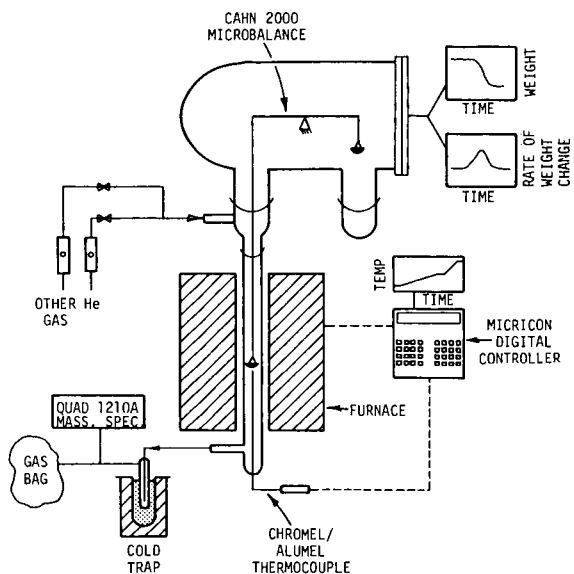


Figure 1. Schematic of Thermogravimetric Analysis System



$$\frac{dV}{dt} = (1-a)kA \quad (2)$$

$$\frac{1}{V_0} \frac{dV}{dt} = k_0 e^{-E/RT} (1-V/V_0) \quad (3)$$

$$\ln \left(\frac{1}{V_0} \frac{dV}{dt} \right) = \ln k_0 + \ln (1-V/V_0) - E/RT \quad (4)$$

Figure 2. Kinetic Model Used in Coking Study

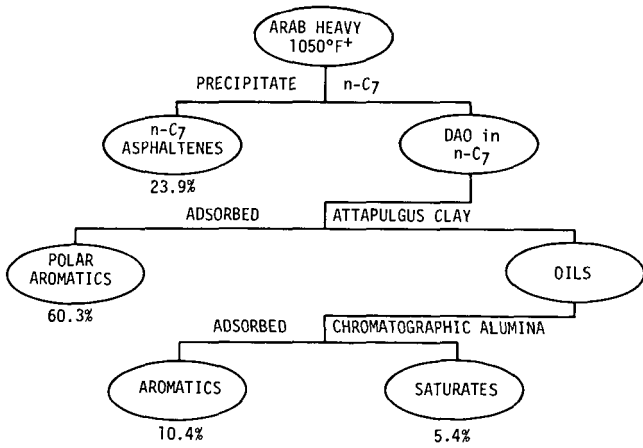


Figure 3. Residuum Separation Scheme

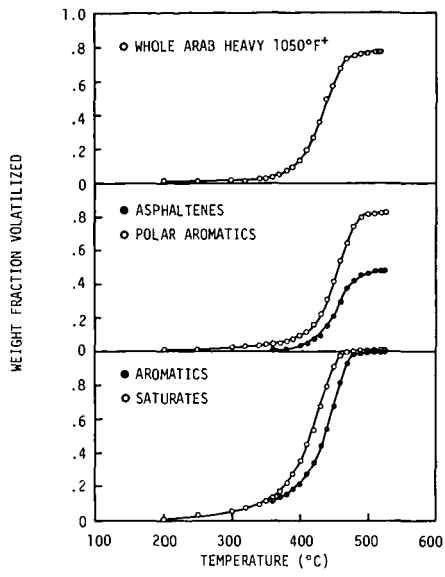


Figure 4. Volatile Evolution from Arab Heavy Vacuum Residuum and Fractions at Heating Rate of 10°C/min

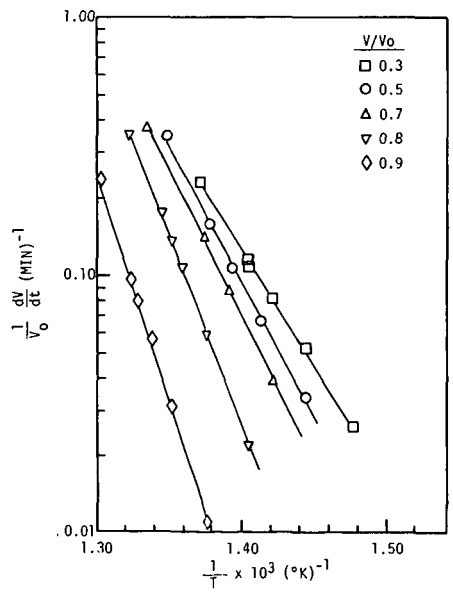


Figure 5. Arrhenius Plot for Asphaltene Fraction

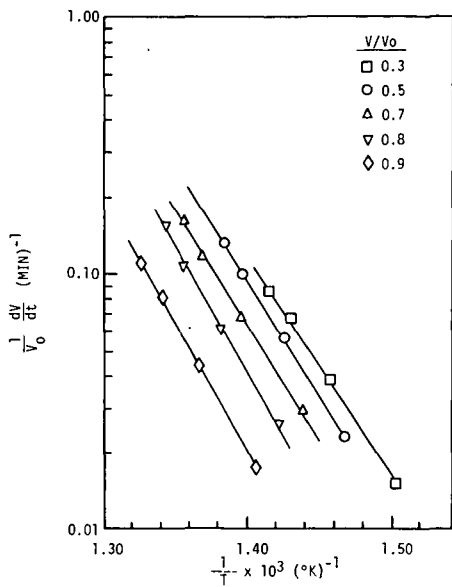


Figure 6. Arrhenius Plot for Polar Aromatic Fraction

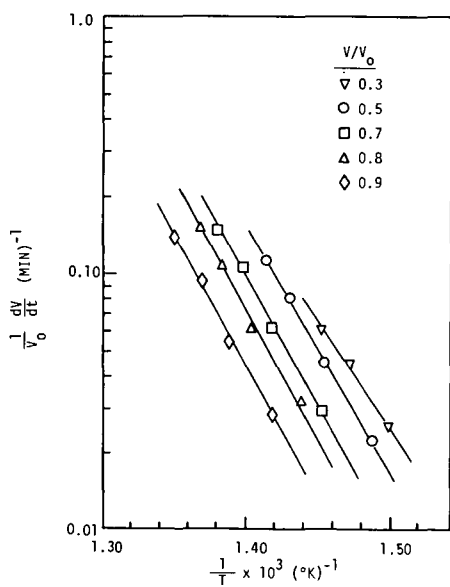


Figure 7. Arrhenius Plot for Aromatic Fraction

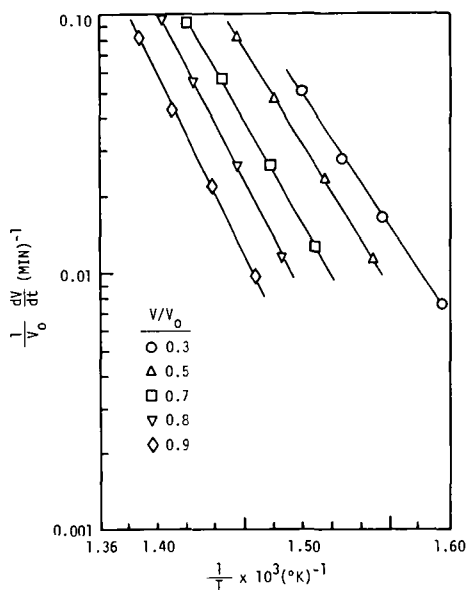


Figure 8. Arrhenius Plot for Saturate Fraction

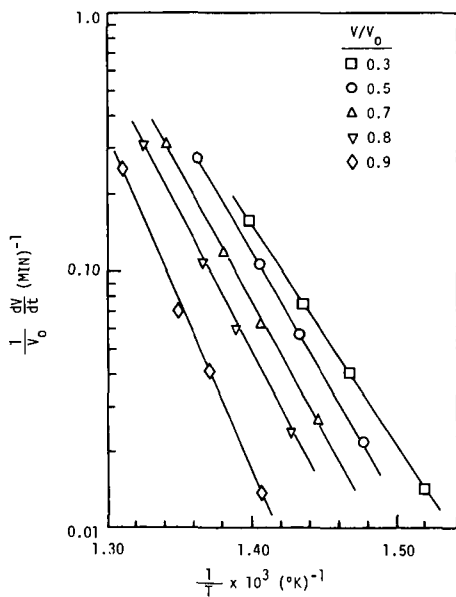


Figure 9. Arrhenius Plot for Whole Resid

THE OXIDATION OF FRACTIONS OF FUEL OIL #6 BY DIFFERENTIAL
SCANNING CALORIMETRY AND THERMOGRAVIMETRY.

J.A. Ayala, J. Ruiz and M.E. Rincón.

Instituto de Investigaciones Eléctricas
División Fuentes de Energía
Departamento de Combustibles Fósiles
Cuernavaca, Mor., México

INTRODUCTION.

Since a few years back, it has been realized throughout the world the need to find new and/or alternative energy sources to replace fossil fuels. Today, however, most of the countries in the world still depend on fossil fuels, and in particular on residual oil to meet their energy requirements. This situation, will continue to be as such for at least the next twenty years, and may be longer. The residual oil, as it is used today for the production of electricity by the utilities, contains sulfur, and trace metals, besides its usual elemental composition. As it is well known, when the residual oil is burned in a big industrial boiler the above mentioned elements, will produce substances which are dangerous for the environment. These substances, also have a high influence in the loss of availability, and efficiency of the boilers due to the formation of deposits within the furnace, and the corrosiveness of some of the products. Moreover, with the utilization of better technologies in crude oil refining processes the residual oil will increasingly have higher amounts of sulfur and metals, and will become heavier. Also, the use of a heavier oil usually leads to an increase in unburned particles, and in polyaromatic hydrocarbons in the flue gas. In order to attain the appropriate protection for the environment, and for the industrial boilers it is necessary to understand how the harmful products are formed, during the combustion of the residual oil. To reach such an understanding, we believe it is necessary to have a better knowledge about the oxidation chemistry of the oil.

In a previous paper(1), we have reported the utilization of differential scanning calorimetry (DSC) to study the thermo-oxidation of fuel oil #6. It was shown, that it is possible to utilize, the techniques in thermal analysis to obtain kinetic information about the oxidation behavior of the fuel. We have also shown(2), that the results from the thermogravimetric analysis (TGA) of the fuel are highly complimentary with the results from the DSC. These two techniques, combined for the study of the oxidation of fuel oil #6, in the temperature range between 200-600°C, have provided us with an insight into the different mechanisms of oxidation of the fuel. In the present work, we have separated the asphaltenes from a sample of mexican residual oil. The oxidation profile of both, the asphaltene, and asphaltene-free fractions was obtained by means of DSC and TGA, between 200°C and 600°C. We also have attempted to obtain kinetic information from the data, and have compared the results with those previously obtained for the fuel.

EXPERIMENTAL.

A sample of a previously studied(1,2) mexican residual fuel oil was chosen for the present work. The asphaltene, or heavy fraction was

separated from the oil by means of extractions with n-pentane. Elemental analysis, and analysis of sulfur and vanadium content were performed on both, the asphaltene and asphaltene-free fractions. Distribution maps of sulfur and vanadium were obtained for the asphaltenes, with an X-ray fluorescence microprobe attachment to a scanning electron microscope (SEM).

The oxidation profile of both fractions was obtained by means of a Perkin-Elmer DSC-2 differential scanning calorimeter, and a TGS-2 thermogravimetric system. The TGS-2 was provided with the signal derivative attachment. Two types of experiments were performed: a) dynamic, and b) isothermic. In the dynamic runs, the sample was charged at room temperature, and the temperature varied at a rate of 10°C/min. In the isothermic experiments, the sample was charged at a given temperature, which was held constant over a period of time, or until the sample weight was depleted. For the asphaltene-free or light fraction the isothermic experiments were run at various temperatures between 230 and 290°C, and between 380 and 460°C. For the heavy fraction, the isothermic runs were made at temperatures between 390 and 480°C. The sample pans in the DSC experiments were made of aluminum, and the sample covers had to be perforated in order to obtain meaningful results. The sample pans in the TGA experiments were made of platinum. All the experiments were performed with a flow of oxygen of ~25 ml/min, and the sample weight was ~1 mg, and ~2 mg for the asphaltene and asphaltene-free fractions, respectively.

RESULTS AND DISCUSSION.

The fuel oil studied here has an asphaltene content of 14%. Table 1, shows the results of the elemental analysis, the sulfur and vanadium content, and the hydrogen: carbon ratio for the fuel, and the fractions. As expected, all the vanadium remains in the asphaltenes. Approximately 75% of the sulfur from the oil remains in the light fraction. The H/C ratio decreases from a value of 1.5 for the fuel, and the asphaltene-free fraction, to a value of 1 for the heavy fraction. The H/C ratio of the asphaltenes is very typical(3) for this kind of hydrocarbons. This ratio, is close to that found for some coals(4). Thus, this result may speak by itself about the difficulties to obtain adequate conditions for the complete combustion of the asphaltenes. Figures 1, 2, and 3 reveal another interesting feature of the heavy fraction. Figures 2, and 3 are the distribution maps of V, and S respectively of the SEM image for the asphaltenes in figure 1. In these maps, at least some of the sulfur of the heavy fraction seems to be closely associated with the vanadium. Most of the structures proposed for the asphaltenes(3,5), do not include heteroatoms eventhough there usually is a high sulfur content in this fraction. Some of the vanadium in the asphaltenes, is often associated with porphyrin-like structures(6,8) in which sulfur is not included, but very little is known about non-porphyrinic vanadium. Dickson and Petrakis(8), have proposed some possible sulfur environments around a VO system, to account for non-porphyrinic vanadium. The types of system proposed by Dickson and Petrakis are consistent with the results shown in figures 2, and 3. The association of sulfur, and vanadium in the asphaltenes needs to be the object of further investigation since the chemistry of such complexes may be quite different from that of porphyrinic vanadium(7).

Figure 4, shows the DSC results in the region between 200-600°C, for the fuel and its fractions. This plot shows two exothermic

regions, one at $\sim 300^{\circ}\text{C}$ (zone I), and a second region (zone II) which starts at $\sim 400^{\circ}\text{C}$. At the beginning of the zone II, there are several sharp peaks. These peaks, indicate a highly unstable region with respect to the oxidation of the hydrocarbons involved.

The asphaltene fraction, does not show any peaks in the first zone of the thermogram, whereas the light fraction shows the biggest peak within this region. In the second zone we observe that the asphaltenes show the least amount of instability, and they peak earlier in temperature than both, the fuel and the light fraction. The weight of asphaltenes utilized to obtain the thermograms in figure 4, was approximately half of the weight utilized for the fuel and the light fraction. Thus, the asphaltenes also show the biggest area under the peak within the zone II in figure 4. On the other hand, the light fraction gives the smaller peak, and higher temperatures in the second zone. These results, are confirmed by the experimental results with the TGA, which will be discussed later. The differences, in the zone II, among the heavy, and light fractions are not easy to explain. It is possible, that the metals in the asphaltenes are acting as catalysts in the oxidation of this fractions. Therefore, we may have the peak shifted to lower temperatures, with respect to the fuel. In the case of the light fraction, it is possible that the sulfur contained within this fraction is acting as an inhibitor(9) for the oxidation of these hydrocarbons. Thus, an inhibiting mechanism may shift the peak of the light fraction towards the higher temperatures.

Figure 5, shows the typical results for the dynamic TGA experiments, along with the derivative curves (DTGA) of the TGA signals. It is observed in figure 5, the resemblance between the DTGA curves, and the curves in figure 4. Thus, the DTGA thermograms confirm the results obtained for the fuel and its fractions, by DSC. That is, the asphaltene fraction does not show a peak at $\sim 300^{\circ}\text{C}$. Also, for the region between $400\text{--}600^{\circ}\text{C}$ the heavy fraction shows the largest peak at lower temperatures, and the light fraction gives the smallest peak at higher temperatures, with respect to the peak of the fuel. According to the TGA results, there is a mass loss of $\sim 20\%$ for both, the fuel, and the asphaltene-free fraction up to a temperature of $\sim 250^{\circ}\text{C}$. This loss of weight in the samples, has not released or absorbed heat such that it could be accounted for in the DSC experiments. The mass loss before 250°C , could be due to either the evaporation of volatile compounds, or to a very mild oxidation or pyrolysis of the fuel, with the production of volatile species. The TGA, DTGA, and DSC results at 300°C confirm the existence of an exothermic reaction at this temperature in the fuel, and the light fraction. The TGA for the light fraction, in this temperature region shows that the percentage of the mass lost during the reaction is higher than it is for the fuel. This result, explains why the area under the peak in zone I for the asphaltene-free fraction is bigger than the area under the peak of the fuel. These results, indicate that the same type of oxidation reaction is taking place for the fuel and the light fraction in the zone I. However, more material is reacting at these temperatures in the asphaltene-free fraction than it is in the fuel. The end of the first region of oxidation for the fuel and the light fraction is signaled in the TGA plot by a drastic change in the slope of the curve. The new slope indicates a much slower rate in the mass loss. Finally, the TGA curve of the fuel and the asphaltene fraction, shows another change in the slope towards higher rates of mass loss indicating the beginning of the zone II. The new change in slope is more gradual in the light fraction than in the fuel. The TGA curve of the asphaltens, shows almost no change in the weight

of the sample until $\sim 400^\circ\text{C}$. At $\sim 400^\circ\text{C}$, there is a rapid fall-off of the signal, which indicates a rate of mass loss higher than even that for the fuel, in the same temperature region. The slow rate in the mass loss of the asphaltene-free fraction, and a high rate of mass loss for the asphaltenes within the same temperature region go along with the results in the DSC for both fractions. Therefore, we may argue again that there is an inhibiting mechanism for the oxidation of the light fraction taking place in the zone II. We may also argue that, a catalytic effect is at least partially responsible for the results obtained with the asphaltene fraction.

The isothermic TGA curves have been kinetically analyzed. It was assumed, as it was the case for the fuel(1,2), a pseudo-first order kinetics, which means a first order with respect to the fractions. Figures 6 and 7 present the Arrhenius plots for the zones I and II of the light fraction, respectively. Figure 8 shows the Arrhenius plot for the asphaltenes. In Table 2, we have compared the activation energies(E_a) for the fuel, and its fractions. The E_a 's for the fuel, and the light fraction are similar to each other. On the other hand, the E_a of the asphaltene fraction is considerably higher than the E_a 's for the fuel, and the light fraction. These are results, which are somewhat expected since the light fraction represents 86% of the fuel. The high activation energy for the asphaltenes, should also be considered as normal due to the oxidation resistance of this fraction. It is probable that the first oxidation zone in the fuel, and the light fraction, is due to the paraffinic content plus some of the lighter aromatic hydrocarbons in the fraction. This observation is based on the low activation energy for the reaction in zone I. However, the results from DSC and TGA show that the heat of oxidation, and the loss of mass are small in this zone. Thus, since the paraffinic content of the fuel is not so small, it is also probable that the degree of oxidation of the reactive species of the fuel, and the fraction in zone I is low.

Another interesting feature of the asphaltene fraction is shown in Figure 9. The curves in figure 9, are the isothermic TGA runs at 470 and 480 $^\circ\text{C}$. These two curves show a smooth curve for approximately 2.5 and 2 minutes, respectively. After this time, there is a sudden loss of mass until the sample mass is almost depleted. The minute amount of mass remaining after the sudden change continues its oxidation, but at a much slower rate. The sudden change, is an ignition of the asphaltene fraction. The important fact is that at lower temperatures there is no ignition of the sample, but a gradual oxidation of the asphaltenes. Starting at $\sim 470^\circ\text{C}$ there is an ignition of the sample, but it is preceded by an induction period. This behavior, is not found in the asphaltene-free fraction. In the light fraction, at $\sim 470^\circ\text{C}$, there is an spontaneous ignition of the sample without a measurable induction period.

CONCLUSIONS

- At least some of the sulfur in the asphaltenes, seems to be closely associated with some of the vanadium of this fraction.
- The light fraction shows two regions of oxidation in the temperature range between 200-600 $^\circ\text{C}$. These regions are similar to those of the fuel, but shifted toward slightly higher temperatures.
- The heavy fraction shows only one region of oxidation in between 400-600 $^\circ\text{C}$. This oxidation region peaks at slightly lower temperatures than the similar regions in the fuel, and in the light fraction.
- The activation energies of the light fraction are similar to those of

the fuel.

- The E_a for the asphaltene fraction is considerably higher than the activation energies of the fuel, and the asphaltene-free fraction.
- At 470°C the asphaltenes ignite spontaneously after an induction period of ~2.5 min.
- The light fraction at ~470°C ignites spontaneously without a measurable induction period.

Finally, the overall results of this work, agree well with the idea that the overall behavior of the fuel is an average of the behavior of the two separate fractions. However, some of the differences shown by the DSC, and TGA curves need to be further investigated. Especially, - those features that can be related to catalytic or inhibiting properties of some chemical species within the fuel.

ACKNOWLEDGEMENT

This work was performed under the project FE/F14 of the Instituto de Investigaciones Eléctricas.

REFERENCES

- 1) J.A. Ayala and M.E. Rincón, ACS Division of Fuel Chemistry Preprints 26 (3), 120 (1981).
- 2) J. Ruiz, M.E. Rincón and J.A. Ayala, "The Oxidation of Fuel Oil #6 by Thermogravimetry". Presented before the XVI Congreso Mexicano de Química Pura y Aplicada, Morelia, Mich., México, November 1981.
- 3) J.G. Speight, "The Structure of Petroleum Asphaltenes-Current Concepts", Information Series 81, Alberta Research Council, 1978.
- 4) "STEAM/its generation and use", Babcock & Wilcox, New York 1975, p. 5-15.
- 5) A. Bukowski and E. Gurdzinska, ACS Division of Petroleum Chemistry Preprints 25 (2), 293 (1980).
- 6) A.J.G. Barvise and E.V. Whitehead, ACS Division of Petroleum Chemistry Preprints 25 (2), 268 (1980).
- 7) K.A. Gould, ACS Division of Petroleum Chemistry Preprints 25 (2), 288 (1980).
- 8) F.E. Dickson and L. Petrakis, Analytical Chemistry 46, 1129 (1974).
- 9) G.E. Cranton, Thermochemica Acta, 14, 201 (1976).

T A B L E 1

ELEMENTAL COMPOSITION OF THE FUEL AND ITS FRACTIONS

| | C WT % | H WT % | N WT % | S WT % | V PPM | CENIZAS WT % | H / C ATOMIC RATIO |
|-----------------------|-----------|-----------|-----------|-----------|----------|-----------------|-----------------------|
| FUEL OIL | 84.7 | 10.4 | 0.4 | 3.8 | 158 | 0.05 | 1.5 |
| ASPHALTENE-FREE FRAC. | 84.8 | 10.9 | 0.2 | 3.6 | -- | -- | 1.5 |
| ASPHALTENES | 83.3 | 7.2 | 1.3 | 6.7 | 1040 | 0.42 | 1.0 |

T A B L E 2

ACTIVACION ENERGIES FROM THE ISOTHERMIC TGA FOR
THE FUEL AND ITS FRACTIONS.

| FUEL OIL | | ASPHALTENE-FREE FRACTION | | ASPHALTENES |
|----------------------|----------------------|--------------------------|----------------------|----------------------|
| ZONE I | ZONE II | ZONE I | ZONE II | -- |
| E_a Kcal MoI | E_a Kcal MoI | E_a Kcal MoI | E_a Kcal MoI | E_a Kcal MoI |
| 19.5 ± 0.3 | 31.6 ± 2.9 | 23.5 ± 0.5 | 29.4 ± 0.5 | 42.6 ± 0.4 |

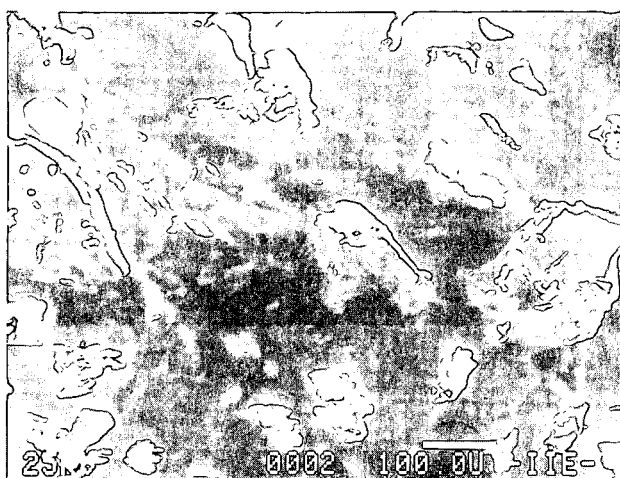


FIGURE 1. SEM IMAGE OF THE ASPHALTENES

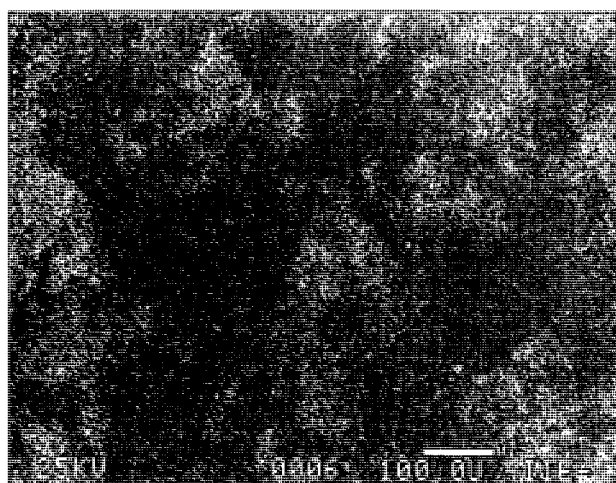


FIGURE 2. VANADIUM DISTRIBUTION IN FIGURE 1

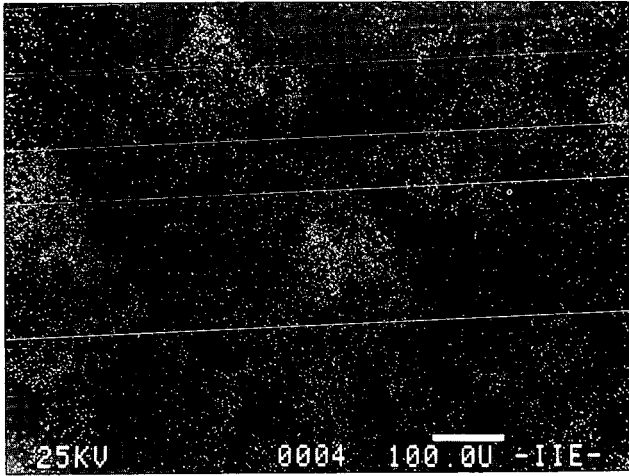


FIGURE 3. SULFUR DISTRIBUTION IN FIGURE 1

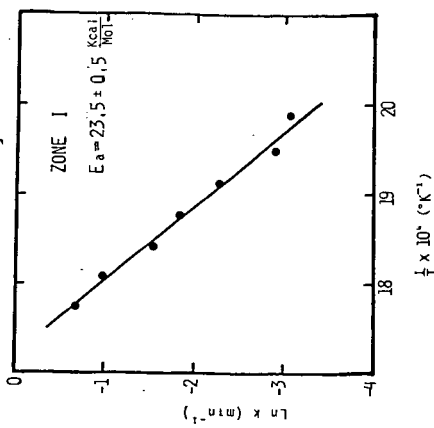


FIGURE 6. ARRHENIUS PLOT FOR THE OXIDATION OF THE ASPHALTENE-FREE FRACTION, ZONE I.

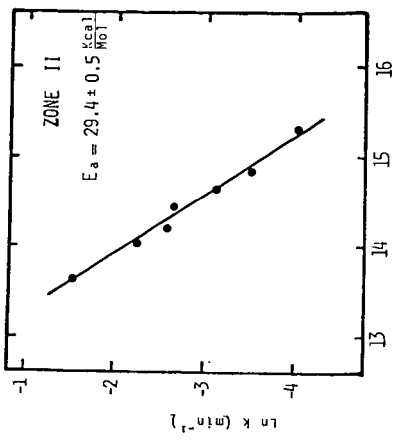


FIGURE 7. ARRHENIUS PLOT FOR THE OXIDATION OF THE ASPHALTENE-FREE FRACTION, ZONE II.

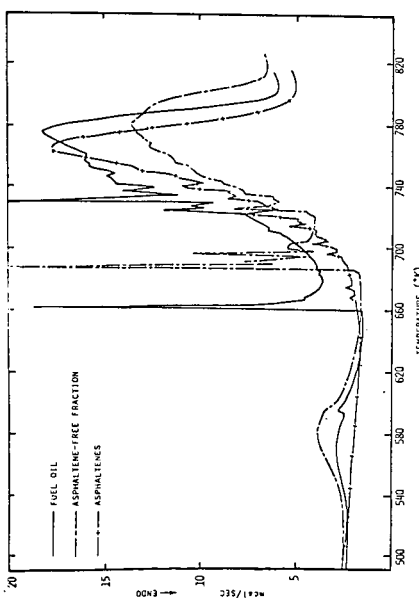


FIGURE 4.- DSC CURVES FOR THE FUEL OIL AND ITS FRACTIONS

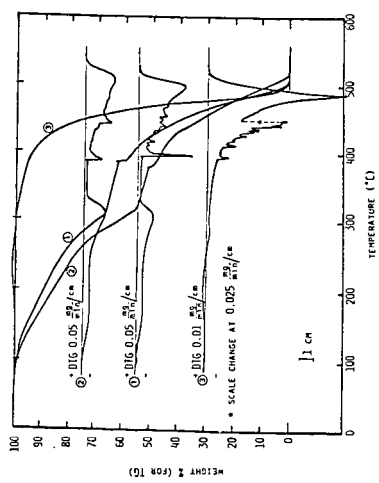


FIGURE 5.- TGA AND DTA CURVES FOR: 1) FUEL OIL (1.8 mg) 2) ASPHALTENE-FREE FRACTION (11.8 mg) AND 3) ASPHALTENES (0.86 mg)

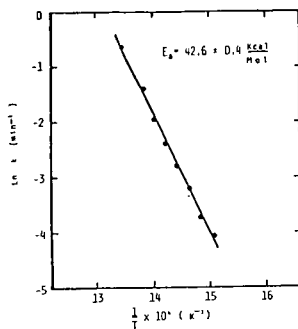


FIGURE 8 .- ARRHENIUS PLOT FOR THE OXIDATION OF THE ASPHALTENES

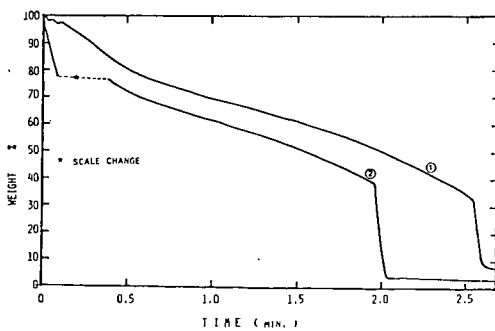


FIGURE 9 .- ISOTHERMIC TGA CURVES FOR ASPHALTENES AT 1).- 470 2).- 480 C.

PARAMAGNETICALLY REDUCED CARBON-13 RELAXATION TIMES
OF HYDROCARBON TYPES: AN AID TO THE QUANTITATIVE
ANALYSES OF SHALE OIL-DERIVED JET FUELS

D. M. Barnhart* and D. A. Netzel

U.S. Department of Energy
Laramie Energy Technology Center
P. O. Box 3395, University Station
Laramie, Wyo. 82071

ABSTRACT

The study includes determining the carbon-13 paramagnetically reduced spin-lattice relaxation times of representative hydrocarbon types, of a model mixture of hydrocarbon types and of an aromatic hydrocarbon added to syncrude JP-4 jet fuel. The paramagnetic relaxation reagent chromium acetylacetonate (CrAcAc) was used in all systems.

The limit of solubility of CrAcAc in 3 ml of jet fuel and 2 ml of CDCl_3 was found to be approximately 0.07 M. Using this concentration, the ^{13}C spin-lattice relaxation times (T_1) of aromatic compounds range from 0.5 to 0.9 seconds, and for n-alkanes the range was found to be 0.9 to 1.8 seconds. A concentration of 0.04 M CrAcAc was used for analytical analysis of average molecular structure parameters of syncrude JP-4 and four other jet fuels. This concentration was below the solubility limit and yet does not appreciably increase the T_1 values or the overall experimental time. The mole percent as determined by NMR of aromatics and alkanes found in syncrude JP-4 jet fuel was found to agree with mass spectral data.

INTRODUCTION

For several years the Department of Defense in cooperation with the Department of Energy has had research programs aimed at characterizing and evaluating liquid hydrocarbon fuels obtained from various fossil sources because the chemical composition of a jet fuel affects jet engine performance, power output, engine life, and operation cost. A number of techniques have been used with some degree of success to characterize hydrocarbon fuels. However, most techniques require a substantial amount of time and require the samples to be fractionated into various hydrocarbon types.

Carbon-13 and proton nuclear magnetic resonance spectroscopy (NMR) can be rapid and can be performed on either the total sample or its fractions. The technique has been used extensively to characterize various fossil fuels in terms of average molecular structure parameters¹⁻³, and thus NMR was chosen to characterize samples of jet fuels.

*Associated Western Universities faculty appointee from Eastern Montana College, Billings, Montana 59101

To use ^{13}C effectively as an analytical technique, the long spin-lattice relaxation times and variable nuclear Overhauser enhancement factor (NOE) for carbon atoms in molecules generally comprising jet fuels must be reduced or eliminated.

Spin-lattice relaxation times can be reduced, thereby reducing the experimental time, by using relaxation reagents⁴⁻⁹. Concurrent with the use of relaxation reagents is the near elimination of the NOE effect which, when present, prevents direct correlation of the area of the resonance peaks with the number of carbon atoms. The effects of relaxation reagents on quantitative analysis of complex mixtures such as petroleum crudes have been conducted^{10,11}. The results of these studies have shown that relaxation reagents are necessary for quantitative analyses if the analyses are to be performed in a reasonable time.

In this investigation, the effects of the relaxation reagent, chromium acetylacetonate (CrAcAc) on the carbon-13 relaxation times of carbon atoms in model compounds, a mixture of several model compounds, and a model compound in jet fuel were measured. Concentration levels of CrAcAc used in the relaxation study were limited to the solubility of CrAcAc in jet fuel. From the knowledge of relaxation times of model compounds in the presence of CrAcAc, optimal instrumental conditions were determined.

EXPERIMENTAL

Nuclear Magnetic Resonance

Carbon-13 spin-lattice relaxation times were determined on a Varian CFT-20 NMR spectrometer, using the standard inversion-recovery pulse sequence, $180^\circ\text{-}\tau\text{-}90^\circ\text{-T}$, where T is the delay time (in seconds) between the pulse sequence and τ is the time (in seconds) between the inversion pulse (180°) and the measuring pulse (90°). Relaxation times were calculated using a nonrectilinear, two-parameter exponential regression technique with the maximum signal amplitude fixed.

A JEOL FX-270 superconducting NMR spectrometer was used to obtain proton and gated proton decoupled carbon-13 spectra used in quantitative analysis of mixtures and jet fuels. Pulse widths of 8 μsec ($15 \mu\text{sec}$ 90°) and 5 μsec ($14 \mu\text{sec} = 90^\circ$) were used for carbon-13 and proton spectra, respectively. Six seconds was used for the pulse delay for carbon-13 spectra and 2.5 seconds for proton spectra. Broadband proton decoupling gated ON during data acquisition was used for carbon-13 spectra to suppress the nuclear Overhauser effect.

Sample Source and Preparation

All hydrocarbon solutions were prepared using reagent-grade compounds dissolved in CDCl_3 . The relaxation measurements were made without vacuum degassing of the samples. The relaxation reagent, chromium acetylacetonate, was purchased from Alpha Products and used as received. Jet fuel samples were received from Wright-Patterson Air Force Base (WPAFB). All jet fuel samples were prepared using a standard

stock solution of 0.1 M CrAcAc in CDCl_3 . Two milliliters of this solution was syringe pipetted into a 5-ml volumetric flask, and fuel was added to the 5-ml level. All samples were then filtered via a syringe and 5- μ Teflon millipore filter into a 10-mm NMR tube.

RESULTS AND DISCUSSION

The carbon-13 spin-lattice relaxation times (T_1) for organic compounds range generally from 5 to 200 seconds. Relaxation times for ipso and bridged carbons of aromatic hydrocarbons are among the highest observed. Two methods are often used to overcome the problem of long relaxation times. One method is to reduce the pulse to a value between 45° and 75° , which in effect reduces the pulse delay time necessary to achieve spin equilibrium. A shorter delay time allows for faster pulsing. However, a pulse less than 90° reduces the signal intensity, and thus more pulses (additional time) will be necessary to achieve the desired S/N ratio. Optimum parameters of pulse Fourier transform NMR are discussed by Becker et al.¹². A second method is the addition of a paramagnetic relaxation reagent to the solution. Depending upon the concentration of the relaxation reagent, relaxation times of the order of 100 seconds can be reduced to a few seconds. Thus, short pulse delay times can be used, which in turn allows for shorter total time to achieve the desired S/N ratio. The disadvantages of using relaxation reagents are signal broadening, difficulties associated with the removal from the solution if recovery of the original solution is necessary, the relatively low solubility of the relaxation reagents in organic solutions, and the lower S/N ratio due to the absence of the NOE effect.

The solubility limit of the relaxation reagent in a given solution dictates the maximum amount of reduction in the observed relaxation time, and this in turn determines the overall experimental time necessary to obtain good S/N ratios for quantitative analysis.

The relaxation reagent, chromium acetylacetonate, is only partially soluble in a mixture of CHCl_3 and jet fuel. To determine the pulse delay time for a 90° pulse (maximum sensitivity) necessary to acquire quantitative results in the shortest possible time, two experiments were conducted: 1) the solubility of CrAcAc in a mixture of CHCl_3 and syncrude JP-4 jet fuel of various ratios was determined and 2) the maximum molar concentration of CrAcAc found for the mixture of CHCl_3 and jet fuel in the first experiment was used to study the reduction effect of CrAcAc on the carbon-13 relaxation times of model compounds of the types which could be found in jet fuels. With this information, a pulse delay time could be determined for a given ratio of CHCl_3 and jet fuel which would give good S/N ratio in the shortest possible time for quantitative determinations. The limit of solubility of CrAcAc in 3 ml of jet fuel and 2 ml of CDCl_3 was found to be approximately 0.07 M.

Relaxation Studies. - Table I lists the ^{13}C spin-lattice relaxation times for (1) the model compounds used in this study, (2) a mixture of several model compounds, and (3) 2,6-dimethylnaphthalene in syncrude JP-4 jet fuel. Also included in the table are the ^{13}C relaxation times of the carbon atoms in n-hexane and in 2,6-dimethylnaphthalene as a function of the molarity of CrAcAc. Carbon-13 chemical shifts for the

model compounds in CDCl_3 with and without the addition of CrAcAc are also listed in Table I.

The relaxation times measured in this study were determined without degassing of the samples. The literature values of the relaxation times for the carbon atoms in the model compounds were, for the most part, determined under more exacting conditions and represent the longest possible relaxation times.

A survey of the data in Table I indicates that CrAcAc at a concentration of about 0.073 M reduces all ^{13}C relaxation times of aromatic compounds to values ranging from 0.5 to 0.9 seconds. For n-alkanes using 0.073 M CrAcAc, the ^{13}C relaxation times range from .9 to 1.8 seconds. CrAcAc has less effect on alkanes than aromatics, which is to be expected because of the type of bonding orbitals associated with the two classes of compounds.

The concentration effects of CrAcAc on the relaxation times of n-hexane and 2,6-dimethylnaphthalene were determined and are shown in Figure 1. For comparison, the ^{13}C relaxation time for benzene¹³ as a function of the molar concentration of CrAcAc is also given in Figure 1. It is seen from both Table I and Figure 1 that all relaxation times for aromatic carbons as well as the substituted alkyl carbons have, in general, the same dependency on the molar concentration of CrAcAc. Thus, it is possible to establish the pulse delay time ($5T_1$) for any given concentration of CrAcAc necessary to give quantitative useful ^{13}C NMR spectra.

Two additional experiments were conducted to determine whether or not the paramagnetically reduced relaxation times are significantly different for 1) a mixture of model compounds and 2) a model compound in syncrude JP-4 jet fuel. Table I lists the ^{13}C relaxation times observed for the model mixture containing n-hexane, 1-ethyl-2-methylbenzene, and 2,6-dimethylnaphthalene in CDCl_3 and containing 0.072 molar CrAcAc. As expected, the relaxation times for the carbon atoms of n-hexane and 2,6-dimethylnaphthalene in the mixture varied little from the values obtained for the individual compounds. However, the T_1 values for 1-ethyl-2-methylbenzene appear to be slightly higher than expected. The differences in T_1 observed (10 to 30 percent) are most likely due to differences in CrAcAc concentration and sample preparation.

The paramagnetically reduced relaxation times for carbon atoms of 2,6-dimethylnaphthalene in syncrude JP-4 jet fuel produced from shale oil differ only slightly (~15 to 20 percent) from values obtained for the pure compound. Crude shale oils contain appreciable amounts of free radicals, and any contribution of the paramagnetic effects of free radicals which may or may not exist in refined jet fuel on the ^{13}C relaxation time of 2,6-dimethylnaphthalene is minimal.

Quantitative Analysis. - Since shale oil-derived jet fuels are complex mixtures of aromatic and aliphatic compounds, conditions established for quantitative NMR were performed on the previously mentioned model mixture of approximate mole fraction ratios of 0.1:0.25:0.65 for 2,6-dimethylnaphthalene, 1-ethyl-2-methylbenzene and n-hexane, respectively.

With accurate weighing, the ^1H and ^{13}C NMR spectral areas could be predicted by direct counting of the various hydrogens and carbons in different site positions for the three types of molecules comprising the mixture. This mixture was also subjected to direct analysis by both ^1H and ^{13}C NMR spectroscopy.

Syncrude JP-4 jet fuel has been extensively studied previously in this laboratory by both NMR and mass-spectral techniques¹⁴ and elsewhere by NMR¹⁵. The structural parameters¹⁴ for this fuel are considered to be fairly well known, and therefore quantitative NMR analysis with and without CrAcAc under the same instrumental conditions was used to confirm the applicability of the method to jet fuel analysis. Table II lists the NMR structural parameters for syncrude JP-4 jet fuel with and without CrAcAc. Also listed are the mass spectral data for comparison. The mass spectral data were obtained using a modified version of the ASTM procedure D2781-71 and are in volume percent; whereas the NMR data are reported in mole percent. For aromatic and alkane hydrocarbons, a nearly 1:1 correspondence exists between mole percent and volume percent¹⁴. The data in Table II show that the jet fuel sample containing CrAcAc gives results that agree closely with mass spectral data. Table III lists the NMR structural parameters for four additional jet fuel samples.

CONCLUSIONS

The limit of solubility of CrAcAc in 3 ml of jet fuel and 2 ml of CDCl_3 was found to be approximately 0.07 M. Using this concentration, the ^{13}C spin-lattice relaxation times (T_1) of aromatic compounds range from 0.5 to 0.9 seconds, and for n-alkanes the range was found to be 0.9 to 1.8 seconds. A concentration of 0.04 M CrAcAc was used for analytical analysis of average molecular structure parameters of syncrude JP-4 and four other jet fuels. This concentration was below the solubility limit and yet does not appreciably increase the T_1 values on the overall experimental time. The mole percent as determined by NMR of aromatics and alkanes found in syncrude JP-4 jet fuel was found to agree with mass spectral data.

REFERENCES

1. Clutter, D. R., Petrakis, L., Stenger, R. L., Jr., and Jenson, R. K., Anal. Chem., 1972, 44, 1395.
2. Cantor, D. M., Anal. Chem., 1978, 50, 1185.
3. Gillet, S., Rubini, P., Delpuech, J., Escalier, J., and Valentin, P., Fuel, 1981, 60, 221.
4. Levy, G. C., and Edlund, U., J. Am. Chem. Soc., 1975, 97, 4482.
5. Gansow, O. A., and Burke, A. R., J. C. S. Chem. Comm. 1972, 456.

6. LaMar, G. N., J. Am. Chem. Soc., 1971, 93, 1040.
7. Barcza, S., and Engstrom, N., J. Am. Chem. Soc., 1972, 94, 1762.
8. Levy, G. C., Edlund, U., and Hexem, J. G., J. Magn. Reson. 1975, 19, 259.
9. Freeman, R., Pachler, K. G. R., and LaMar, G. N., J. Chem. Phys., 1971, 55, 4586.
10. Shoolery, J. H., and Budde, W. L., Anal. Chem., 1976, 48, 1458.
11. Thiault, B., and Mersseman, M., Org. Magn. Resonance, 1976, 8, 28.
12. Becker, E. D., Ferretti, J. A., and Gambhir, P. N., Anal. Chem., 1979, 51, 1413.
13. JEOL Technical Bulletin NBS-11, 1977, 10.
14. Netzel, D. A., and Hunter, P. M., Report of Investigation, DOE/LETC/RI-81-1.
15. Dorn, H. C., Final Progress Report for the Period March 23, 1978 to August 30, 1979, Under Naval Research Laboratory Contract No. N0012-78-0424. Available from National Technical Information Service, U.S. Dept. of Commerce, 5285 Port Royal Circle, Springfield, VA 22161

ACKNOWLEDGMENT

This work was partially supported by contract (MIPR FY1455-81-NO619) with the Air Force Aero Propulsion Laboratory, Wright-Patterson AFB.

DISCLAIMER

Mention of specific brand names or models of equipment is made for information only and does not imply endorsement by the Department of Energy.

TABLE I. - Carbon-13 chemical shifts and spin-lattice relaxation times for model compounds

| Compound | Carbon position | ¹³ C chemical shift (ppm) ^{a, b} | | ¹³ C Spin-lattice relaxation time (sec.) | | | | | | |
|-------------------------|-------------------|--|----------------|---|------------|------------|------------|------------|------------|------------|
| | | with CrAcAc | without CrAcAc | In model mixture | | | | | | |
| n-Hexane | 1 | 14.15 | 14.22 | 0.000 M ^c | 0.210 M | 0.041 M | 0.073 M | 0.121 M | 0.072 M | |
| | 2 | 22.88 | 23.02 | 14.75 ± .69 ^d | 4.54 ± .11 | 2.37 ± .02 | 1.55 ± .04 | 1.04 ± .06 | 1.25 ± .05 | |
| | 3 | 31.86 | 32.00 | 14.78 ± .99 | 4.44 ± .08 | 2.27 ± .04 | 1.68 ± .01 | 0.94 ± .02 | 1.85 ± .16 | |
| n-Dodecane | 1 | 14.14 | | | | | | 0.072 M | | |
| | 2 | 22.83 | | | | | | 1.20 ± .03 | | |
| | 3 | 32.09 | | | | | | 1.19 ± .02 | | |
| | 4 | 29.52 | | | | | | 1.29 ± .02 | | |
| | 5,6 | 29.83 | | | | | | 0.88 ± .02 | | 1.03 ± .02 |
| Tetralin | 1,2 | 136.91 | | | | | | 0.073 M | | |
| | 3,6 | 129.09 | | | | | | 0.94 ± .05 | | |
| | 4,5 | 125.44 | | | | | | 0.81 ± .07 | | |
| | o-CH ₂ | 29.45 | | | | | | 0.75 ± .06 | | |
| | p-CH ₂ | 23.39 | | | | | | 0.74 ± .02 | | |
| 1-Ethyl-2-methylbenzene | 1 | 135.59 | 135.64 | | | | | 0.075 M | | 0.072 M |
| | 2 | 142.21 | 142.33 | | | | | 0.89 ± .02 | | 1.23 ± .08 |
| | 3 | 130.08 | 130.29 | | | | | 0.97 ± .07 | | 1.25 ± .08 |
| | 4 | 126.09 | 126.33 | | | | | 0.93 ± .06 | | 0.07 ± .08 |
| | 5 | 125.70 | 126.02 | | | | | 0.78 ± .05 | | 1.03 ± .03 |
| | 6 | 127.93 | 128.10 | | | | | 0.77 ± .06 | | 1.16 ± .06 |
| | o-CH ₂ | 19.06 | 19.16 | | | | | 0.87 ± .03 | | 1.10 ± .06 |
| 2,6-Dimethylnaphthalene | o-CH ₂ | 26.24 | 26.49 | | | | | 0.87 ± .03 | | 0.87 ± .03 |
| | p-CH ₂ | 14.42 | 14.54 | | | | | 0.78 ± .03 | | 1.14 ± .05 |
| | 1,5 | 127.05 | 127.40 | 0.024 M | 0.045 M | 0.078 M | | 0.072 M | 0.042 M | |
| | 2,6 | 134.34 | 134.41 | 1.59 ± .03 | 1.10 ± .04 | 0.71 ± .03 | | 0.84 ± .02 | 1.12 ± .03 | |
| | 3,7 | 126.58 | 126.52 | 2.47 ± .06 | 1.43 ± .03 | 0.92 ± .03 | | 0.96 ± .08 | 1.31 ± .03 | |
| Acenaphthene | 4,8 | 128.08 | 128.25 | 1.79 ± .05 | 1.10 ± .04 | 0.76 ± .03 | | 0.97 ± .04 | 1.29 ± .04 | |
| | 9,10 | 131.96 | 132.45 | 1.69 ± .02 | 1.07 ± .02 | 0.73 ± .04 | | 0.80 ± .06 | 0.98 ± .04 | |
| | o-CH ₂ | 21.52 | 21.66 | 2.70 ± .06 | 1.45 ± .05 | 0.84 ± .05 | | 0.99 ± .07 | 1.17 ± .05 | |
| | 1,8 | 145.91 | | 1.81 ± .04 | 1.26 ± .02 | 0.81 ± .02 | | 0.88 ± .06 | 1.01 ± .03 | |
| | 2,7 | 119.10 | | | | | | | | |
| Acenaphthalene | 3,6 | 127.72 | | | | | | | | |
| | 4,5 | 123.19 | | | | | | | | |
| | 9 | 139.28 | | 0.000 M | | | | 0.072 M | | |
| | 10 | 131.62 | | 0.75 ± .02 | | | | 0.54 ± .06 | | |
| | o-CH ₂ | 30.27 | | 5.6 | 5.6 | 5.6 | 5.6 | 5.6 | 5.6 | |
| Acenaphthalene | 1,0 | 139.55 | | | | | | 0.075 M | | |
| | 2,7 | 124.02 | | | | | | 0.75 ± .02 | | |
| | 3,6 | 127.57 | | | | | | 0.59 ± .03 | | |
| | 4,5 | 126.08 | | | | | | 0.63 ± .01 | | |
| | 9 | 128.17 | | | | | | 0.65 ± .01 | | |
| | 10 | 127.99 | | | | | | 0.83 ± .05 | | |
| 11,12 | 129.25 | | | | | | 0.74 ± .01 | | | |
| | | | | | | | | 0.70 ± .02 | | |

^aRelative to tetramethylsilane (TMS)

^bIn COCl₂

^cMolarity of CrAcAc

^dH. J. M. Drosell et al., J. C. S. Chem. Comm., 1973, 757.

^eT. D. Alger et al., J. Phys. Chem., 1980, 84, 632.

TABLE II. - Average molecular structure parameters and mole percent aromatics and alkanes for syncrude JP-4 jet fuel with and without CrAcAc

| | Without CrAcAc | With 0.04 M CrAcAc | Mass spectral ^a data |
|---|----------------|--------------------|---------------------------------|
| Hydrogen aromaticity | .037 | .045 | |
| Carbon aromaticity | .108 | .113 | |
| Mole percent aromatics | 12.4 | 11.1 | 11.4 |
| Percent mono- | 12.4 | 8.8 | 11.4 |
| Percent di- | .0 | 2.3 | 0.0 |
| Fraction of substituted and bridged carbons | .03 | .02 | |
| Fraction of unsubstituted carbons | .07 | .09 | |
| Mole percent alkanes | 87.6 | 88.9 | 88.6 |
| Fraction of n-alkanes | .54 | .56 | |
| Fraction of branched alkanes | .46 | .44 | |
| CH ₂ /CH ₃ ratio | 1.9 | 2.1 | |
| Carbon chain length | 9.0 | 8.3 | |
| Total atomic H/C ratio | 2.02 | 2.02 | |
| Aromatic H/C ratio | .69 | .80 | |
| Alkane H/C ratio | 2.18 | 2.17 | |

^aVolume percent

TABLE III. - Average molecular structure parameters and mole percent aromatics and alkanes for NASA jet fuels^a

| | VN-80-71 ERBS-35 | VN-80-72 ERBS-3B | VN-80-73 3B-11.8 | VN-80-74 3B-12.1 |
|---|---------------------|---------------------|---------------------|---------------------|
| Hydrogen aromaticity | .252 | .050 | .144 | .111 |
| Carbon aromaticity | .550 | .190 | .385 | .288 |
| Mole percent aromatics | 82.3 | 19.7 | 45.2 | 33.4 |
| Percent mono- | 69.8 | 15.0 | 34.8 | 25.5 |
| Percent di- | 12.4 | 4.7 | 10.4 | 7.9 |
| Fraction of substituted and bridged carbons | .0 | .0 | .0 | .0 |
| Fraction of unsubstituted carbons | .23 | .10 | .15 | .10 |
| Mole percent alkanes | 17.7 | 80.4 | 54.8 | 66.6 |
| Fraction of n-alkanes | .30 | .46 | .40 | .37 |
| Fraction of branched alkanes | .70 | .54 | .60 | .63 |
| CH ₂ /CH ₃ ratio | .72 | 1.9 | 1.8 | 1.9 |
| Carbon chain length | 11.3 | 10.0 | 10.4 | 7.6 |
| Total atomic H/C ratio | 1.38 | 1.77 | 1.60 | 1.68 |
| Aromatic H/C ratio | .58 | .47 | .60 | .65 |
| Alkane H/C ratio | 2.35 | 2.08 | 2.23 | 2.10 |

^aContains .04 M CrAcAc

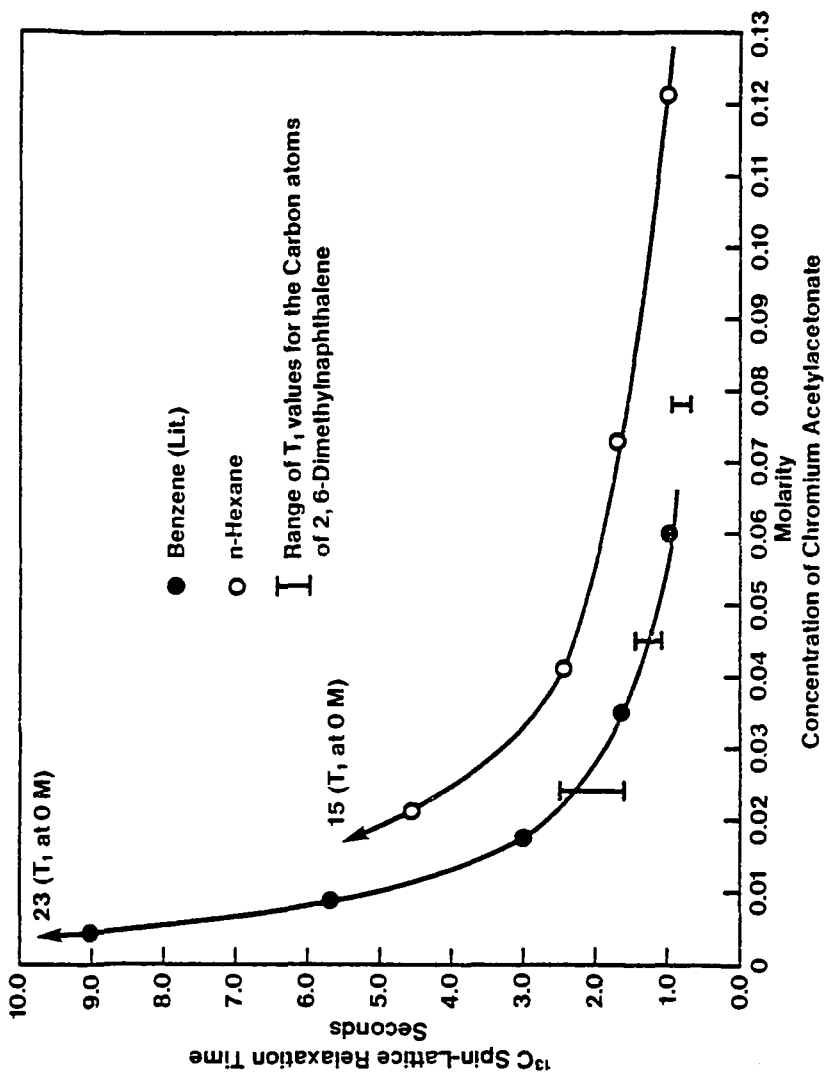


FIGURE 1. - Spin-Lattice Relaxation Times for Hydrocarbons as a Function of the Concentration of Chromium Acetylacetonate